Analyse du comportement de l'abdomen lors d'un choc automobile pour l'amélioration de la biofidélité et de la prédiction des lésions abdominales par le mannequin de choc THOR

Romain Desbats

N° d'ordre NNT : 2016LYSE1070

THÈSE DE DOCTORAT DE L'UNIVERSITÉ DE LYON

opérée au sein de

l'Université Claude Bernard Lyon 1

École Doctorale N° 162

Mécanique - Énergétique - Génie Civil - Acoustique

Spécialité de doctorat : Mécanique

Soutenue publiquement le 23 mai 2016, par :

Romain DESBATS

Analyse du comportement de l'abdomen lors d'un choc automobile pour l'amélioration de la biofidélité et de la prédiction des lésions abdominales par le mannequin de choc THOR

Devant le jury composé de :

M. Éric JACQUELIN	Professeur des Universités	Université Claude Bernard Lyon 1	Président du jury
M. Sébastien LAPORTE	Professeur des Universités	Arts et Métiers ParisTech	Rapporteur
M. Philippe VIOT	Professeur des Universités	Arts et Métiers ParisTech	Rapporteur
M. Xavier TROSSEILLE	Expert biomécanique	LAB PSA Peugeot Citroën - Renault	Examinateur
Mme Sabine COMPIGNE	Technical Manager	Toyota Motor Europe NV / SA	Examinatrice
M. Philippe VEZIN	Directeur de Recherche	IFSTTAR	Directeur de thèse
M. François BERMOND	Chargé de Recherche, HDR	IFSTTAR	Encadrant

Université Claude Bernard — Lyon 1

Président de l'Université	**M. François-Noël Gilly**
Vice-président du Conseil d'Administration	M. le Professeur Hamda Ben Hadid
Vice-président du Conseil des Études et de la Vie Universitaire	M. le Professeur Philippe Lalle
Vice-président du Conseil Scientifique	M. le Professeur Germain Gillet
Directeur Général des Services	M. Alain Helleu

Composantes Santé

Faculté de Médecine Lyon Est – Claude Bernard	Directeur : M. le Professeur J. Etienne
Faculté de Médecine et de Maïeutique Lyon Sud – Charles Mérieux	Directeur : Mme la Professeure C. Burillon
Faculté d'Odontologie	Directeur : M. le Professeur D. Bourgeois
Institut des Sciences Pharmaceutiques et Biologiques	Directeur : Mme la Professeure C. Vinciguerra
Institut des Sciences et Techniques de la Réadaptation	Directeur : M. le Professeur Y. Matillon
Département de formation et Centre de Recherche en Biologie Humaine	Directeur : Mme la Professeure A.-M. Schott

Composantes et Départements de Sciences et Technologie

Faculté des Sciences et Technologies	Directeur : M. F. De Marchi
Département Biologie	Directeur : M. le Professeur F. Fleury
Département Chimie Biochimie	Directeur : Mme Caroline Felix
Département GEP	Directeur : M. Hassan Hammouri
Département Informatique	Directeur : M. le Professeur S. Akkouche
Département Mathématiques	Directeur : M. le Professeur Georges Tomanov
Département Mécanique	Directeur : M. le Professeur H. Ben Hadid
Département Physique	Directeur : M. Jean-Claude Plenet
UFR Sciences et Techniques des Activités Physiques et Sportives	Directeur : M. Y. Vanpoulle
Observatoire des Sciences de l'Univers de Lyon	Directeur : M. B. Guiderdoni
Polytech Lyon	Directeur : M. P. Fournier
École Supérieure de Chimie Physique Electronique	Directeur : M. G. Pignault
Institut Universitaire de Technologie de Lyon 1	Directeur : M. le Professeur C. Viton
École Supérieure du Professorat et de l'Education	Directeur : M. le Professeur A. Mougniotte
Institut de Science Financière et d'Assurances	Directeur : M. N. Leboisne

Analyse du comportement de l'abdomen lors d'un choc automobile pour l'amélioration de la biofidélité et de la prédiction des lésions abdominales par le mannequin de choc THOR

Thèse préparée au Laboratoire de Biomécanique et Mécanique des Chocs
LBMC UMR_T9406 IFSTTAR — Université Claude Bernard Lyon 1
25 Avenue François Mitterrand, Case 24, 69675 Bron Cedex France

Remerciements

Mes premiers remerciements vont à Sabine Compigne, qui après avoir encadré mon stage de fin d'études à Toyota a été à l'origine de ce sujet. Je tiens à la remercier pour pour son encadrement au quotidien pendant ces trois années et son souci du détail qui m'ont permis d'avancer et persévérer.

Je remercie François Bermond pour son suivi et ses conseils tout au long de cette thèse ainsi que Philippe Vezin pour son encadrement pendant ces trois ans.

Je tiens aussi à remercier David Mitton, directeur du LBMC pour son accueil (d'abord dans l'équipe biomécanique des chocs) et ses grandes qualités humaines.

Merci à MM. Sébastien Laporte et Philippe Viot qui ont accepté de rapporter ce travail. Je remercie également MM. Éric Jacquelin et Xavier Trosseille d'être membre du jury de cette thèse.

Le LAB PSA Peugeot Citroën - Renault et le CEESAR ont permis l'utilisation de différents jeux de données, en particuliers les essais charriots IRIS et le modèle éléments finis du banc d'essais, ce pourquoi je les remercie également. Mes remerciements vont également au laboratoire VRTC de la NHTSA qui a aussi fourni des résultats d'essai qui ont été utilisés dans ce travail.

Je suis également reconnaissant envers les chercheurs du LBMC qui ont mis à disposition de ce travail le modèle des capteurs APTS qu'ils ont développé, particulièrement Philippe Beillas pour les discutions intéressante que nous avons eues au sujet de l'abdomen, ainsi qu'envers Yoann Lafon pour ses conseils sur Scilab et Stéphane Nicolle pour les discussions que nous avons eu sur les modèles masse-ressort.

Il me faut aussi remercier Toyota Motor Europe et Toyota Motor Corporation pour avoir financé cette thèse, en particulier M. Mitsutoshi Masuda de Toyota Motor Corporation pour son soutien à ce projet et M. Tjark Kreuzinger de Toyota Motor Europe pour m'avoir accueilli au sein de l'équipe Technical Affairs Planning - Safety. Ainsi que Marco Ammann pour son travail de stage sur la modélisation de l'abdomen prototype et Ernesto Mottola pour ses précieux conseils en simulation numérique.

Les doctorants qui m'ont précédé au LBMC (Doris, Clémentine, Naoual, Yumin, Junfeng, Charles, Pascal, Romain T., Edison) ont été des sources d'inspirations et je leur en suis reconnaissant. Je souhaite également bonne chance à Anicet, Agathe, Léo et Rémy pour la fin de leur thèse. Merci aussi à Jérémy pour son soutien lors de nos soirées passées à rédiger au laboratoire. Merci à Marc pour m'avoir aidé à débloquer mon ordinateur tombé en panne au pires moments.

Merci à Anurag et Fabien pour leur expertise en simulation, à Denis pour le vélo ainsi qu'aux les grimpeurs-yogis, Thomas, Sonia, Bruno et Aurélie.

Je remercie également tout les membres du LBMC et de l'IFSTTAR que je n'ai pas cité et que j'ai pu croiser lors de cette thèse.

Je finirais par remercier mes parents qui m'ont toujours soutenus et encouragés dans la vie et dans mes études.

Résumé en français

Mots-clés : biomécanique des chocs, mannequin, abdomen, THOR, blessures

Les blessures de l'abdomen représentent une faible proportion (5%) des blessures lors d'accidents de la route mais elle augmente fortement pour les blessures sérieuses à sévères (16%). L'abdomen du mannequin THOR (Test device for Human Occupant Restraint), qui va être utilisé dans les futures réglementations de choc frontal, nécessite des améliorations de sa biofidélité et un critère de blessure. Le travail présenté est en trois parties :

Premièrement, les paramètres principaux de la réponse mécanique de l'abdomen du THOR et de Sujets Humain Post Mortem (SHPM) sous chargements impacteur et ceinture furent identifiés à l'aide d'un modèle mécanique simplifié. La comparaison des paramètres mécaniques du THOR et des SHPM a mis en évidence les changements nécessaires pour l'amélioration de la biofidélité de l'abdomen du THOR. Il apparaît que la viscosité équivalente du THOR doit être augmentée d'un facteur 5 et que l'interaction avec la pièce bassin doit être modifiée du fait qu'elle augmentait la rigidité d'un facteur 8. Ces changements furent inclus dans le modèle Éléments Finis (EF) d'un abdomen prototype incluant des capteurs de pression APTS (Abdominal Pressure Twin Sensors) pour caractériser le chargement de l'abdomen.

Deuxièmement, la réponse mécanique du prototype a été évaluée en simulations d'essais chariot, ce qui a montré que l'abdomen prototype a peu d'influence sur la cinématique globale du mannequin mais que la flexion du tronc peut faire augmenter la pression dans les APTS. Cela a mené à des recommandations supplémentaires au niveau de la conception de l'abdomen.

Finalement, en vue de définir un critère de blessure pour l'abdomen, la pression des APTS a été corrélée aux blessures des organes décrites dans les études sur SHPM de la littérature ou prédites par le modèle EF humain THUMS.

Résumé en anglais

Keywords: impact biomechanics, dummy, abdomen, THOR, injury

Abdominal injuries represent a small proportion (5%) of road crash injuries but their proportion increases considerably with regard to serious and severe injuries (16%). The abdomen of the Test device for Human Occupant Restraint (THOR), intended to be used in future frontal impact assessments, needs further developments regarding its biofidelity and injury criterion. The work performed in this thesis project was in three folds:

Firstly, the main parameters of the THOR and Post Mortem Human Subjects (PMHS) abdomen responses under impactor and seatbelt loadings were identified using a lumped element model. The comparison between the THOR and the PMHS mechanical parameters highlighted desired changes for THOR abdomen biofidelity improvement. It was found that THOR material viscosity should be increased by 5 and that interaction with the pelvis flesh should be modified as it increased by 8 the abdomen stiffness. These changes were included in the Finite Element (FE) model of an existing abdomen prototype which is equipped with Abdominal Pressure Twin Sensors (APTS) to quantify the abdomen load.

Secondly, the response of the prototype was evaluated in sled test simulations which showed that the prototype abdomen had little influence on the dummy overall kinematics but that the torso flexion could increase the pressure in the APTS. This led to additional recommendations regarding the abdomen design.

Finally, for the abdominal injury criterion definition, the APTS pressure was correlated with organ injuries as reported in published PMHS tests or as predicted by THUMS human FE model.

Résumé étendu en français

Introduction

Réduire les décès dûs aux accidents de la route est une priorité en Europe et dans le monde. De manière à s'assurer que les véhicules protègent leurs occupants, des essais de choc sont réalisés lors desquels les occupants sont représentés par des mannequins de choc. Les mannequins doivent avoir un comportement mécanique proche des humains, ce qui est appelé biofidélité. Une fois la biofidélité atteinte pour une région du corps, cette région doit être pourvue de moyens de mesure (force, déflection, accélération, pression, . . .) associés à un critère de blessure. Le futur mannequin utilisé pour la réglementation en choc frontal, THOR [1], nécessite l'amélioration de sa biofidélité pour la région abdominale et le développement d'un critère de blessure adapté pour l'abdomen. Le premier objectif de cette thèse est de développer un abdomen biofidèle pour le mannequin THOR pourvu d'un moyen de mesure lié à un critère lésionnel. Le second objectif est l'obtention d'un critère de blessure basé sur les mesures de pression des capteurs APTS [2] insérés dans l'abdomen prototype.

Contexte et revue de la littérature

Le Chapitre 1 présente le contexte de ce travail et expose l'état des connaissance de la littérature au sujet des blessures abdominales et de la réponse mécanique de l'abdomen humain lors d'un choc frontal.

Le nombre de décès sur la route dans l'Union Européenne était de 32 000 en 2010. L'Union Européenne s'est donné pour objectif de réduire ce nombre de 50 % d'ici 2020 comparé au niveau de 2010 selon l'ETSC [3] (ETSC 2015). Réduire le nombre de décès sur la route nécessite plusieurs types d'action comme les politiques publiques, les réglementations, les infrastructures et la performance au choc des véhicules et des dispositifs de protection. Afin d'étudier comment protéger les occupants d'un véhicule en cas de choc automobile, les conditions d'apparition et la sévérité des blessures lors des chocs doivent être prise en compte.

Les études épidémiologiques analysent les bases de données d'accidents de la route de manière à comprendre quelles sont les sources principales de blessures pour les occupants et à analyser leur fréquence et leur sévérité. Klinich et al. 2010 ont montré qu'il y avait 1.5 fois plus de blessures survenant en choc frontal qu'en choc latéral. Le choc frontal est en outre la configuration qui cause le plus de décès (Rudd et al. 2009). Parmi les segments corporels les plus touchés, la part des blessures de l'abdomen croît avec la sévérité des blessures (Elhagediab et Rouhana 1998 ; Lee et Yang 2002 ; Yaguchi et al. 2011). L'abdomen est ainsi une des régions du corps qu'il est important de protéger, tout comme le thorax et la tête, particulièrement pour les occupants arrière sujets au sous-marinage et au mauvais positionnement initial de la ceinture de sécurité (Couturier et al. 2007 ; Martin et al. 2010 ; Frampton et al. 2012).

1. Test device for Human Occupant Restraint
2. Abdominal Pressure Twin Sensors
3. European Transport Safety Council

Toutes les voitures mises en circulation doivent satisfaire à un certain nombre de réglementations où des critères de blessure des occupants sont évalués à l'aide de mannequins de choc. Cependant, aucun critère de blessure pour l'abdomen n'existe à l'heure actuelle dans la réglementation. Le mannequin Hybrid III qui est utilisé dans la réglementation de choc frontal actuelle a été développé dans les années 1970. Il est envisagé qu'il soit remplacé par le mannequin THOR développé par la NHTSA [4] depuis les années 1990. La NHTSA est aussi en train de concevoir une version féminine du mannequin THOR pour laquelle l'abdomen devrait être une des régions améliorées.

(a) Hybrid III (b) THOR

Mannequins Hybrid III et THOR (www.humaneticsatd.com)

Récemment, l'apparition des systèmes de sécurité tels que la ceinture et l'airbag a modifié les causes de blessures abdominales. Le port de la ceinture et la présence d'airbag augmentant, le taux de blessures causées par le volant a décru alors que le taux de blessures causées par la ceinture a augmenté. La source principale de blessures varie selon l'organe considéré. Il a été prouvé que l'usage de la ceinture de sécurité déportait les blessures des organes pleins aux organes creux (Lamielle et al. 2006). Les organes les plus touchés en général sont le foie, la rate et le système digestif (Elhagediab et Rouhana 1998 ; Lamielle et al. 2006 ; Frampton et al. 2012).

La meilleure manière de caractériser le comportement mécanique de l'abdomen humain est de réaliser des essais sur SHPM [5]. Deux types d'essais ont été conçus pour reproduire le choc de l'abdomen avec le volant (essai impacteur) ou son chargement par une ceinture de sécurité. Les essais impacteur considérés sont ceux de Cavanaugh et al. 1986, (impacteur de 32 kg ou 64 kg, vitesse d'impact de 5 m s^{-1} à 13 m s^{-1}), Hardy et al. 2001 (impacteur de 48 kg, vitesse d'impact de 6 m s^{-1}) et Shaw et al. 2004 (impacteur de 64 kg en forme de volant, vitesse d'impact de 4 m s^{-1}). Les études portant sur des essais ceinture sont ceux de Hardy et al. 2001 (vitesse de rétraction maximum de 3 m s^{-1}), Trosseille et al. 2002 (6 m s^{-1} à 12 m s^{-1}), Foster et al. 2006 (8 m s^{-1} à 15 m s^{-1}) et Lamielle et al. 2008 (4 m s^{-1} et 8 m s^{-1}). Les essais sur SHPM mettent en évidence la variabilité de la réponse mécanique de l'abdomen humain du fait de la diversité des dimensions anthropométriques des sujets en question ce qui nécessite de calculer des corridors de réponse comme l'ont fait Lebarbé et al. 2015.

Les seules études présentant un bilan lésionnel cohérent pour une majorité des sujets considérés sont l'étude impacteur de Hardy et al. 2001 ainsi que la condition A de Foster et al. 2006 et l'étude de Lamielle et al. 2008. Le foie est blessé pour tout les sujets de Hardy et al. 2001 sauf un et pour trois des quatre sujets de la condition A de Foster et al. 2006. Lamielle et al. 2008 a décrit des blessures du petit intestin pour la condition MHA (vitesse de chargement de 4 m s^{-1}) et des blessure du petit et du gros intestine pour la condition PRT (vitesse de chargement de 8 m s^{-1}). Un critère de blessure est une fonction mathématique de paramètres physiques mesurés lors de ces essais qui prédit la probabilité d'avoir des blessures d'une gravité (AIS [6]) donnée ou supérieure. Plusieurs variables ont été considérées dans la littérature comme prédicteurs de blessure.

4. National Highway Traffic Safety Administration
5. Sujets Humain Post Mortem
6. Abbreviated Injury Scale

(a) Protocole de Hardy et al. 2001

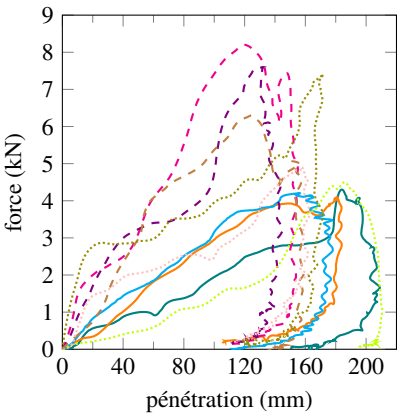

(b) Réponses de Hardy et al. 2001

(c) Protocol de Lamielle et al. 2008

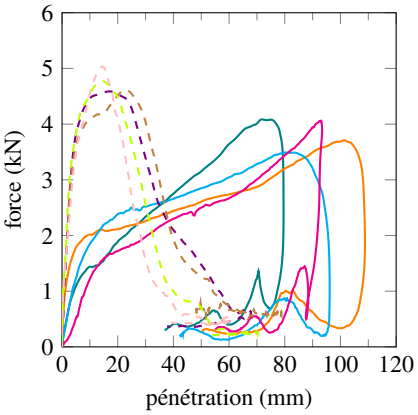

(d) Réponses de Lamielle et al. 2008

Exemples d'essais impacteur et ceinture retenus

La compression de l'abdomen (C), la vitesse de compression (V) et la force exercée sur l'abdomen ont été les plus utilisés. Des combinaisons des ces paramètres ont été proposés comme critères, comme $V_{\max} \cdot C_{\max}$ par Rouhana et al. 1985. D'autres auteurs comme Sparks et al. 2007 ; Kremer et al. 2011 ; Beillas et al. 2012 ont mentionnés des critères de blessures satisfaisant prenant en compte la pression intra-abdominale.

De manière à prévoir le comportement du corps humain lors d'un crash, des modèles numériques élément finis du corps humain ont été développés. Le fait que ces modèles représentent le corps humain de manière précise permet une meilleure compréhension du comportement humain lors d'un choc qu'un mannequin physique. Les améliorations des capacités de calcul et de l'imagerie médicale permettent de générer des modèles avec une représentation des organes de plus en plus détaillée. Ceci peut permettre une prédiction des blessures basée sur des paramètres mécaniques tels que des contraintes, des déformation ou des énergies au niveau de l'organe. Les modèles les plus avancées sont le modèle THUMS [7](Shigeta et al. 2009) et le modèle GHBMC [8] (Gayzik et al. 2012). Ces modèles reproduisent fidèlement la réponse mécanique globale du corps humain sous chargement impacteur ou ceinture, en incluant la dépendance à la vitesse de chargement. Néanmoins, aucune validation du comportement interne de ces modèles n'a été effectuée jusqu'à présent. Des nouvelles méthodes d'observations comme celles détaillées dans Howes et al. 2012 ; Beillas et al. 2013 ; Howes et al. 2015 pourraient fournir des données de référence pour une telle validation.

L'abdomen du mannequin THOR est fait de deux blocs de mousse de raideurs différentes et est

7. Total HUman Model for Safety
8. Global Human Body Models Consortium

instrumenté avec des capteurs de déflection. Plusieurs amélioration à cet abdomen ont été proposées (Onda et al. 2006 ; Hanen et al. 2011). La dernier prototype d'abdomen pour ce mannequin a été développé par l'IFSTTAR et Toyota Motor Europe et décrit dans Compigne et al. 2015. Il inclut dans l'abdomen standard du THOR deux capteurs de pression APTS (décrits dans Beillas et al. 2012) et des masses additionnelles à l'avant de l'abdomen. La biofidélité de ce prototype sous chargement impacteur et ceinture est améliorée comparée à l'abdomen standard. Il pourrait de ce fait être utilisé pour différencier des chargement lésionnels et non lésionnels à partir des mesures de pression des capteurs APTS, pourvu qu'un critère de blessure spécifique soit développé.

Abdomen prototype IFSTTAR / Toyota

Développement et validation du modèle éléments finis de l'abdomen prototype pour le mannequin THOR

Le Chapitre 2 présente des améliorations apportées dans le cadre de cette recherche au modèle éléments finis du mannequin THOR et le développement et la validation du modèle de l'abdomen prototype IFSTTAR / Toyota pour le mannequin.

Un modèle éléments finis du mannequin THOR a été développé depuis 2000 par la NHTSA et d'autres partenaires. Le modèle a été validé de manière globale lors de simulations chariot où sa réponse était en adéquation avec les données d'essai (Panzer et al. 2015). Néanmoins, des améliorations sont possibles pour la validation au niveau des sous-composants tels que l'abdomen haut ou l'abdomen bas. Dans le cadre de ce travail, des améliorations ont été apportées dans la description des propriétés matériau du modèle de mannequin. Les valeurs de contraintes tabulées du matériau du bassin ont été ajustée selon des données fournies par Toyota Motor Corporation. La pièce qui influence le plus la réponse de l'abdomen étant la mousse avant, le modèle matériau de la mousse avant a donc été re-caractérisé à partir d'essais de compression à différentes vitesses de déformation réalisés par Toyota Motor Europe. Un modèle matériau tabulaire prenant en compte la dépendance à la vitesse de déformation a été utilisé.

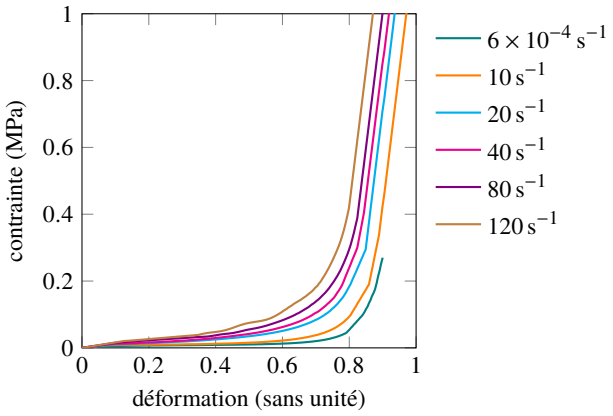

Nouvelles courbes matériau pour la mousse avant de l'abdomen

Le modèle du mannequin amélioré a été validé en utilisant des essais réalisés par le VRTC [9] de la NHTSA reproduisant les essais impacteur de Cavanaugh et al. 1986 et ceinture de Hardy et al. 2001 sur le mannequin. Le modèle du mannequin a été positionné assis comme lors des essais et une simulation appliquant uniquement la gravité a été réalisée afin d'obtenir la géométrie déformée du modèle au niveau du contact avec la table d'essai.

La réponse du modèle sous la condition ceinture de Hardy et al. 2001 reproduit fidèlement les données d'essai. Cette condition corresponds à une pression de 6.6 bar appliquée au dispositif rétractant la ceinture. Pour la condition impacteur de Cavanaugh et al. 1986, (impacteur de 32 kg propulsé à 6.1 $m\,s^{-1}$), la raideur initiale de l'abdomen est fidèlement reproduite par le modèle mais celui-ci prédit légèrement moins de pénétration de l'impacteur dans l'abdomen et montre une force d'interaction bien plus élevée que lors des essais (18 kN au lieu de 10 kN). Ceci est du au fait que l'abdomen est totalement comprimé et que l'impacteur rentre en contact avec la plaque située derrière les mousses de l'abdomen.

Pour la modélisation de l'abdomen prototype IFSTTAR / Toyota, le modèle des capteurs APTS, précédemment développé et validé par l'IFSTTAR a été inséré dans le modèle de l'abdomen du mannequin, puis le maillage des mousses avant et arrière a été raffiné (taille de maille moyenne de 5 mm au lieu de 10 mm à 15 mm précédemment). Les masses additionnelles à l'avant de l'abdomen prototype ont été modélisées par des éléments coques avec des masses nodales rajoutées pour atteindre la masse voulue.

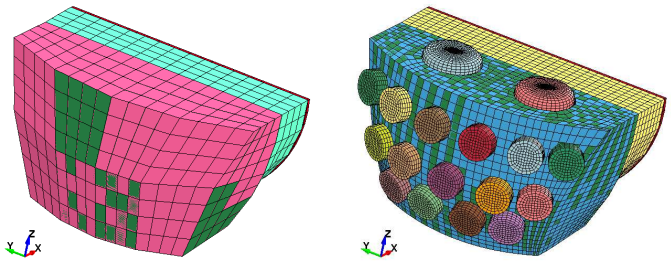

(a) Abdomen standard (b) Abdomen prototype

Modèles des abdomens standard et prototype

La réponse du modèle du mannequin muni de l'abdomen prototype est en adéquation avec les données d'essais pour la condition ceinture de Hardy et al. 2001, bien que la force d'interaction ceinture / mannequin soit légèrement surestimée (5.6 kN au lieu de 4.3 kN). Les valeurs de pression prédites par les APTS sont aussi similaires aux résultats d'essai. Pour la condition impacteur de Cavanaugh et al. 1986, la réponse du modèle reproduit de manière satisfaisante les données d'essais malgré le fait que la simulation se termine avant la fin de l'essai (à 24 ms) dû à des problèmes numériques dans le fluide des capteurs APTS.

Le modèle de l'abdomen prototype IFSTTAR / Toyota développé reproduit donc fidèlement la réponse mécanique du prototype physique, y compris les valeurs de pression mesurées par les APTS. Il peut donc être utilisé pour envisager la conception d'un abdomen prototype plus biofidèle équipé d'une mesure de pression associée à un critère de blessure.

9. Vehicle Research and Test Center

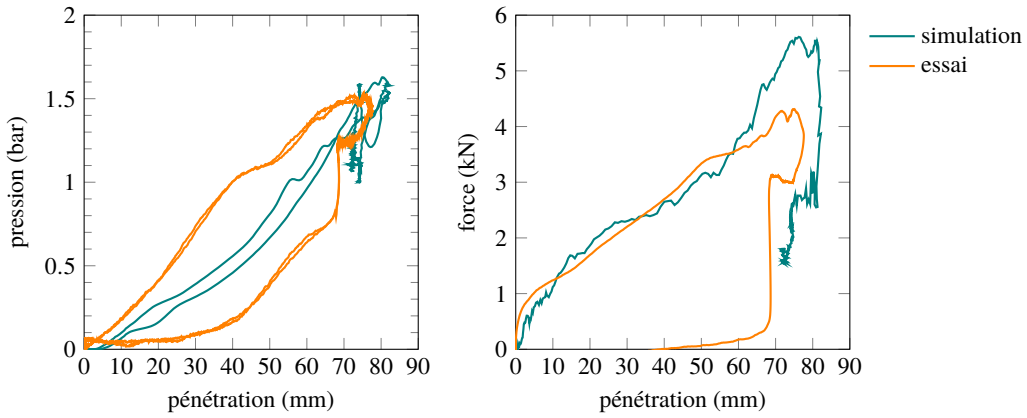

(a) Pression (b) Force

Réponse du modèle du THOR avec abdomen prototype sous chargement ceinture Hardy et al. 2001 6.6 bar

Améliorations de l'abdomen prototype du THOR

Le Chapitre 3 présente les améliorations apportées à l'abdomen prototype afin d'améliorer sa biofidélité. Ces modifications ont été évaluées dans des essais sur l'abdomen isolé ou lors d'essais chariots.

Premièrement, un modèle mécanique simplifié a été appliqué à des résultats d'essais sur SHPM et sur le mannequin THOR. Un modèle adapté de celui proposé par Lamielle et al. 2008 a été utilisé. Ce modèle a été modifié de façon à pouvoir modéliser à la fois un essai ceinture et un essai impacteur. L'étage avant du modèle a été transformé en un modèle de Maxwell avec un ressort et un amortisseur en série.

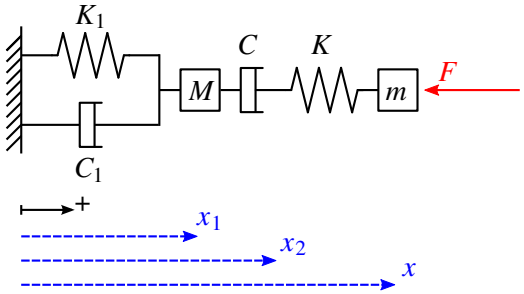

(a) Configuration ceinture

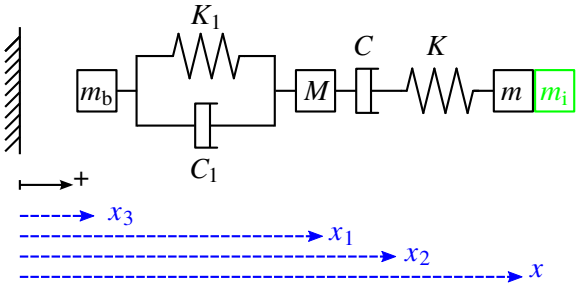

(b) Configuration impacteur

Modèle mécanique simplifié de l'abdomen appliqué à un essai ceinture ou impacteur

Le déplacement de l'avant du modèle est imposé dans le cas ceinture et la vitesse initiale de l'impacteur est imposée dans le cas impacteur. Les équations du mouvement des différents nœuds

du modèle sont résolues avec une méthode de Runge-Kutta d'ordre 4. Les paramètres de ce modèle ont été optimisés avec un critère des moindres carrés afin que la sortie du modèle (la force en fonction du temps) soit conforme à la réponse des essais pour chaque configuration. La justesse de cette optimisation a été évaluée avec des paramètres de corrélation croisée selon Xu et al. 2000. Une étude de sensibilité a ensuite été réalisée de manière à déterminer dans quel intervalle peuvent varier les paramètres optimisés sans changer significativement la réponse du modèle.

Les résultats en terme de conformité de la réponse du modèle aux essais sont positifs. Un modèle mécanique simplifié de ce type peut donc reproduire la réponse de l'abdomen au choc en terme de force et de pénétration de manière satisfaisante, pour le mannequin comme pour les SHPM.

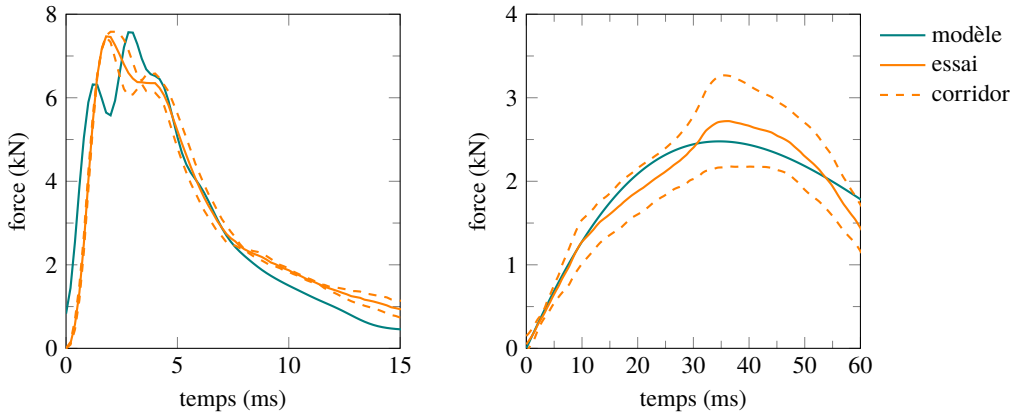

(a) Condition ceinture 2 de Trosseille et al. 2002

(b) Condition impacteur à 6.1 m s^{-1} de Cavanaugh et al. 1986

Réponse du modèle simplifié appliqué aux essais sur SHPM

Les valeurs des paramètres optimisés diffèrent grandement entre les sujets SHPM et le mannequin THOR. Le paramètre de raideur K est plus élevé (8 fois en moyenne) et le coefficient C d'amortissement plus faible (5 fois en moyenne) pour les SHPM. Les paramètres K et C sont ceux qui influent le plus sur la réponse du modèle. Le fait qu'ils soient placés en série implique qu'une valeur élevée de K, par exemple, se traduit par une faible déformation du ressort et par conséquent une réponse peu élastique. Il en va de même pour le comportement visqueux avec le paramètre C. Le comportement du mannequin est donc à la fois trop raide et pas assez visqueux.

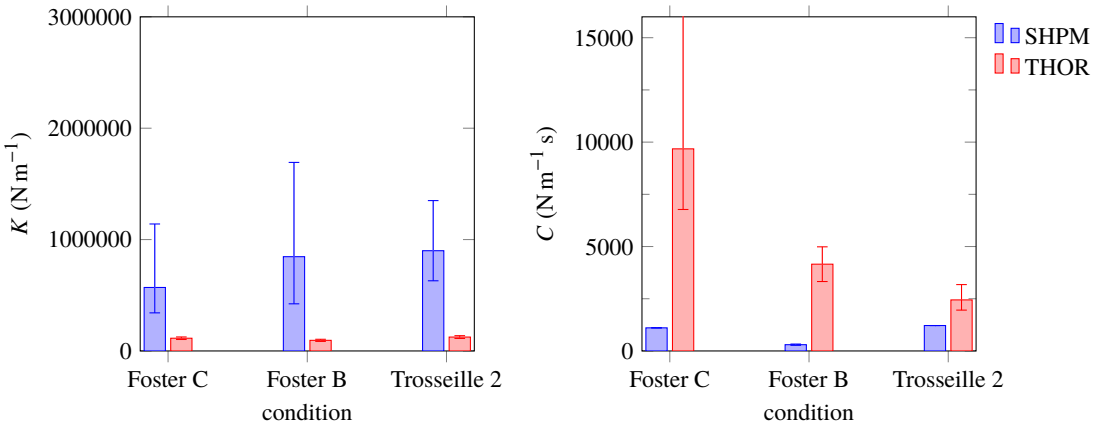

(a) K

(b) C

Paramètres K et C du modèle simplifié pour les configurations ceinture de Trosseille et al. 2002 et Foster et al. 2006

Deuxièmement, le modèle éléments finis de l'abdomen prototype a été amélioré à partir de ces résultats. La biofidélité de l'abdomen prototype a été évaluée par rapport à deux conditions ceinture

supplémentaire : la condition A de Foster et al. 2006 et la condition MHA de Lamielle et al. 2008.

Une première modification fut de diminuer la rigidité de l'abdomen en unifiant les deux blocs de mousse qui le composent. L'abdomen original du THOR est composé d'une mousse avant en matériau Charcoal Polyester, une mousse polyurethane à cellules ouvertes, et d'une mousse arrière en matériau Sponge Rubber Neoprene, une mousse à cellules fermées. Le matériau de la mousse avant a été assignée à la mousse arrière dans le modèle. Cela a amélioré la biofidélité du prototype en créant plus de pénétration lors du chargement de l'abdomen et en réduisant légèrement la force d'impact.

De manière à avoir une meilleure biofidélité pour toutes les conditions de chargement, une modification du modèle matériau des mousses de l'abdomen unifié a été proposée. Un matériau viscoélastique linéaire avec des paramètres basés sur des valeurs de la littérature pour des organes abdominaux humains ajustés a été évalué. Néanmoins, il n'a pas été possible de trouver une combinaison de paramètres apportant une amélioration significative de la biofidélité du prototype.

Troisièmement, le modèle du mannequin équipé de l'abdomen prototype amélioré (blocs unifié) a été utilisé pour reproduire des essais chariots effectués sur SHPM par Luet et al. 2012. Deux configurations de cette étude furent reproduites, l'une d'elle ayant vu les SHPM sousmariner et l'autre les ayant peu vu sousmariner. L'angle entre la ceinture ventrale et la direction horizontale varie entre ces deux configurations ainsi que l'amplitude de la décélération du chariot. Le modèle du mannequin a été positionné en respectant l'angle du bassin du mannequin Hybrid iii lors des essais. Une simulation avec le modèle soumis uniquement à la gravité ayant été réalisée au préalable. Une simulation avec l'abdomen standard et une avec l'abdomen prototype ont été réalisées pour chaque configuration. Le modèle du mannequin présente des résultats comparables aux sujets SHPM pour ce qui est des efforts dans la ceinture thoracique et du déplacement du point H. Néanmoins, il présente moins d'efforts dans la ceinture ventrale et moins de rotation du bassin. L'abdomen prototype provoque plus de déplacement du point H et plus de rotation du bassin que l'abdomen standard. Cela est lié au fait que le mannequin doté de l'abdomen prototype sousmarine plus tôt que le mannequin avec l'abdomen standard (entre 2 ms et 4 ms avant). L'abdomen prototype modifie aussi l'interaction entre l'abdomen haut et l'abdomen bas du mannequin. La force d'interaction augmente significativement, sans que cela puisse être déclaré plus ou moins biofidèle dû au manque de données sur sujets SHPM à ce sujet.

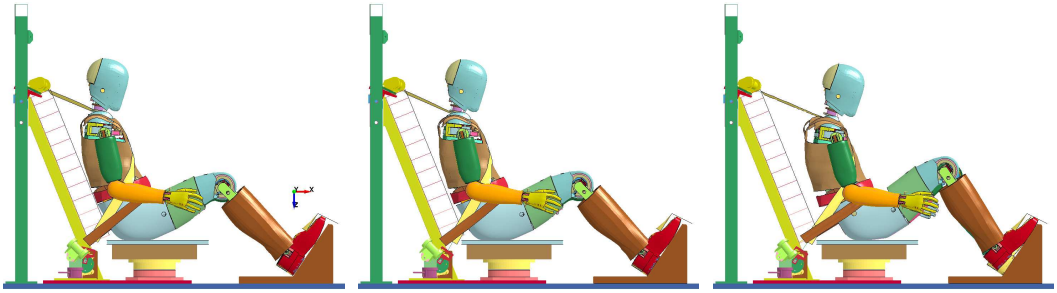

(a) 0 ms (b) 30 ms (c) 60 ms

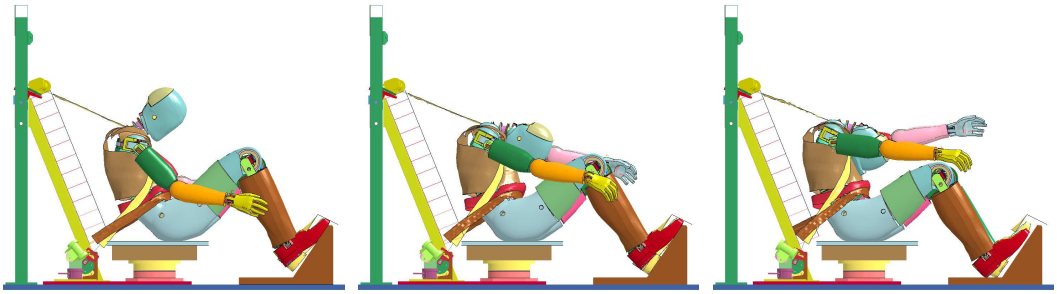

(d) 90 ms (e) 120 ms (f) 150 ms

Résultat d'une simulation chariot

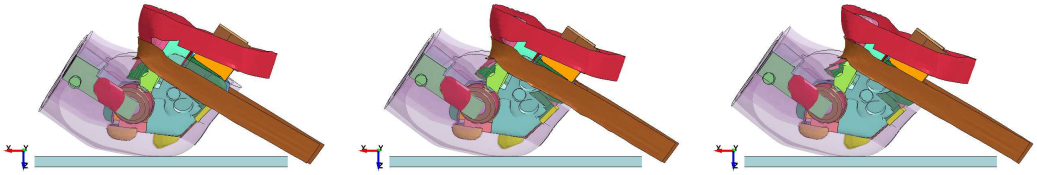

(a) 68 ms (b) 72 ms (c) 76 ms

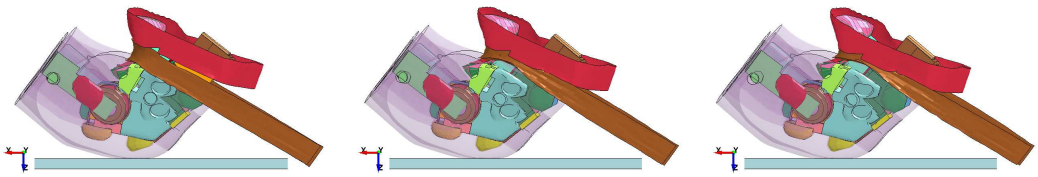

(d) 80 ms (e) 84 ms (f) 88 ms

Sousmarinage pour le mannequin avec abdomen standard

Prédiction des blessures abdominales à l'aide de l'abdomen prototype du THOR

Le Chapitre 4 présente dans un premier temps les essais SHPM reproduits avec le modèle éléments finis du corps humain THUMS en vue d'analyser les paramètres de sollicitation des organes de l'abdomen. Ceci de manière à étudier la pertinence d'un critère lésionnel adapté à chaque organe basé sur les mesures de pression des capteurs APTS de l'abdomen prototype du THOR.

Le modèle THUMS représente un homme moyen (179 cm, 74 kg) et comporte 1300 pièces, 1 800 000 éléments et 630 000 nœuds. Les organes abdominaux sont modélisés par des éléments tétraédriques (volumiques) recouvert d'éléments coques. Leurs modèles matériaux sont des modèles hyper-élastiques à valeurs de contraintes tabulées en fonction de la déformation obtenues à partir d'essais de la littérature sur pièces anatomiques. Parmi tout les essais de la litérature reproduits avec le modèle, seuls trois sont reproduits dans ce chapitre. La condition impacteur de Hardy

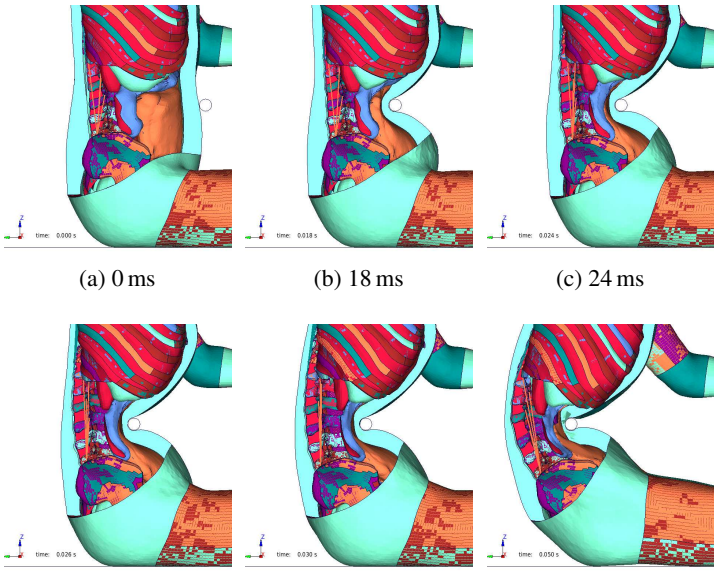

(a) 0 ms (b) 18 ms (c) 24 ms

(d) 26 ms (e) 30 ms (f) 50 ms

Simulation d'un essai impacteur (Hardy et al. 2001 48 kg, 6 m s^{-1}) avec le modèle THUMS

et al. 2001 à 6 m s^{-1} et les deux conditions ceinture de Lamielle et al. 2008. Le modèle THUMS reproduit fidèlement la réponse des SHPM à haute vitesse de chargement (Hardy et al. 2001 6 m s^{-1} et Lamielle et al. 2008 condition PRT) mais présente moins de force d'interaction avec la ceinture que les données d'essai pour la condition MHA de Lamielle et al. 2008 (2.5 kN au lieu de 3.8 kN).

Les résultats des simulations avec le modèle THUMS ont été utilisés pour extraire des données au niveau des différents organes. L'énergie interne de chaque organe a été sélectionnée comme paramètre représentatif de la sévérité du chargement du fait de sa représentation globale de l'organe et de la contribution de la contrainte et de la déformation à l'énergie interne. Les études sur SHPM décrites comme lésionnelles au Chapitre 1 (Hardy et al. 2001 ; Foster et al. 2006 ; Lamielle et al. 2008) ont été reproduites avec le modèle du mannequin THOR équipé de l'abdomen prototype et avec le modèle THUMS. Parmi les trois organes lésés dans les études de la littérature, seules les blessures du foie présentent une tendance en fonction des mesures d'énergie interne. Les blessures du petit intestine et du gros intestin ne sont pas ordonnées par valeurs croissance d'énergie. Les valeurs de pression prédites par les APTS ont ensuite été utilisées pour calculer des mesures de blessures pouvant conduire à l'établissement d'un critère : $P_{\max}$, $\dot{P}_{\max}$ et $\dot{P}_{\max} \cdot P_{\max}$. Les valeurs de la mesure $\dot{P}_{\max}$ ne présentent pas de corrélation avec la sévérité du chargement décrite par les valeurs d'énergie interne, à l'inverse des deux autres critères, cette mesure a donc été éliminée pour l'établissement d'un critère. Un critère lésionnel a donc pu être établi avec les mesures $P_{\max}$ et $\dot{P}_{\max} \cdot P_{\max}$ pour le foie. Une distribution de Weibull a été calculée à partir des valeurs de blessure AIS 3+ et les valeurs seuils $P_{\max} = 1.46$ bar et $\dot{P}_{\max} \cdot P_{\max} = 209$ bar^2 s^{-1} on été établies comme critères pour une probabilité de 50 % de blessure.

Conclusion

Le prototype d'abdomen développé pour le mannequin THOR par l'IFSTTAR et Toyota Motor Europe instrumenté avec les capteurs de pression APTS est un candidat pour la prédiction de lésions. La caractérisation des matériaux composant l'abdomen a été améliorée et validée et la biofidélité de l'abdomen a été améliorée par modélisation éléments finis. L'analyse des blessures issues des études sur SHPM et la mise en parallèle avec le modèle THUMS a permis de définir un critère lésionnel basé sur les valeurs de pression mesurées par les APTS.

Analysis of abdomen behaviour under automotive impact in order to improve the biofidelity and abdominal injury prediction with the THOR dummy

Contents

List of Figures

List of Tables

Introduction

Reducing road fatalities is a priority of the European Union and worldwide. In order to ensure that vehicles are safe for their occupants, regulatory and independent bodies carry crash tests using anthropometric test devices to represent the occupants. These dummies need to have a humanlike behaviour in terms of kinematics as well as mechanical response. Once the biofidelity is achieved for a body region, it has to be equipped with a measurement device recording engineering parameters (force, deflection, acceleration, pressure, . . .) linked to a injury mechanisms identified from field data or laboratory tests on PMHS [1].

Frontal impact is the most common impact case. The current frontal impact dummy, Hybrid III has been designed in the 1970's and is planned to be replaced by the THOR [2] dummy, developed by NHTSA [3]. THOR development started in 1992 and the improvements of the dummy is still ongoing. THOR abdomen has also been modified especially regarding its instrumentation. However, more long-term modifications were also foreseen.

A first objective of this work was to provide, through finite element modelling, the THOR dummy with a biofidelic abdomen equipped with a relevant measuring apparatus regarding loading severity. The APTS [4] sensors were selected as candidate measuring equipment in previous studies performed by IFSTTAR and Toyota Motor Europe. A second objective of this work was to develop a specific injury criterion to those pressure sensors in order to be able to predict the abdominal injury risk with the dummy in a real crash situation.

In order to reach those objectives a first step was to identify the parameters defining the mechanical response of the human and THOR abdomen under dynamic loading to highlight improvement directions for the THOR abdomen biofidelity. A second step was to validate the use of the APTS sensors, included in a recent prototype abdomen developed by IFSTTAR and Toyota Motor Europe, to predict abdominal injuries through direct or derived pressure measure. Finally, a third step was to evaluate the prototype abdomen influence on full dummy kinematics in an environment similar to a vehicle crash.

Chapter 1 of this manuscript presents the context of this work and the literature review about abdominal injuries and the mechanical response of the human abdomen in frontal impact. This includes road safety figures, accidentology studies, regulations as well as a review of PMHS tests, abdomen injury mechanisms and injury criteria. Tools to assess the abdomen protection such as dummies and human body finite element models have also been reviewed.

Chapter 2 describes improvements made to the finite element model of the THOR dummy in order to have a better validation of the dummy model abdomen behaviour under impact. Then the development and validation of the finite element model of the IFSTTAR / Toyota prototype abdomen is described. This includes the description and validation of the APTS sensors model and their inclusion in the THOR abdomen model.

Chapter 3 details modifications to the prototype abdomen model in order to improve its biofidelity.

1. Post Mortem Human Subjects
2. Test device for Human Occupant Restraint
3. National Highway Traffic Safety Administration
4. Abdominal Pressure Twin Sensors

An analysis based on a lumped element model has first been performed to identify global directions for biofidelity improvement. These modifications have then been evaluated in subcomponent tests and sled tests.

Chapter 4 exposes the PMHS tests reproduced with the human body finite element model THUMS [5] in order to analyse the loading parameters of abdominal organs. These loading parameters have been correlated to candidate injury measures based on the pressure measured by the APTS sensors of the THOR dummy abdomen. When linking these injury measures to injuries observed in PMHS tests, an injury criterion could be defined for the liver with two different measures based on pressure.

5. Total HUman Model for Safety

Chapter 1

Context and literature review

Contents

1.1 Frontal impact accidents

The road deaths in the European Union in 2001 were of 55 000. The EU [1] set a target to reduce road fatalities by 50 % by 2010 compared to 2001 levels. Road mortality have been cut by 43 % in the EU leading to 32 000 deaths for the year 2010 according to ETSC [2] (ETSC 2015). This is equivalent to 102 000 less deaths in the EU during this period. In order to keep improving road safety, the commitment has been renewed for 2020 compared to 2010 levels, that is the objective is to have no more than 16 000 road deaths across the EU in 2020. Figure 1.1 shows the results of this policy for the years 2000 to 2014 along with the projection for 2020. This reduction is estimated to saving 182 billion Euro as societal cost.

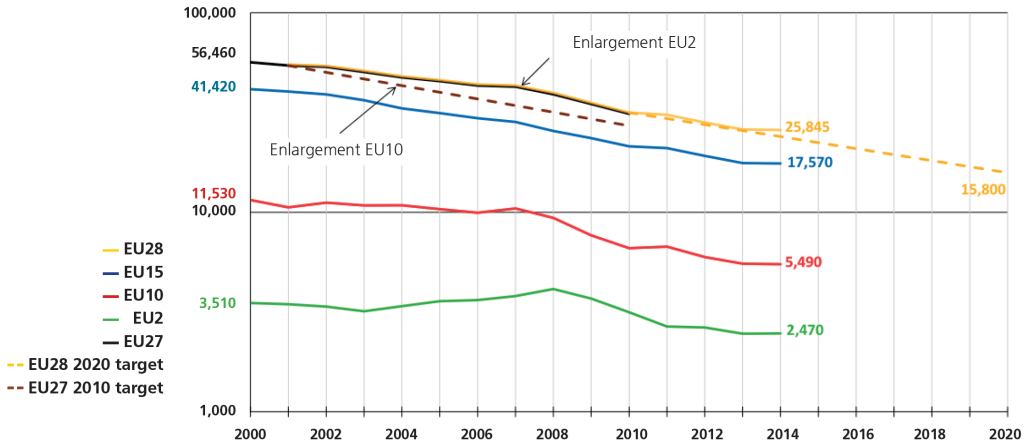

Figure 1.1 – Reduction in road deaths since 2000 in Europe with logarithmic scale (ETSC 2015)
EU15: Austria, Belgium, Denmark, Finland, France, Germany, Greece, Ireland, Italy, Luxembourg, Netherlands, Portugal, Spain, Sweden, United Kingdom
EU10: Cyprus, Czech Republic, Estonia, Hungary, Latvia, Lithuania, Malta, Poland, Slovakia and Slovenia
EU2: Bulgaria and Romania
EU27: EU15 + EU10 + EU2
EU28: EU27 + Croatia

One can also note that the deaths reduction took place despite a constant growth of road traffic as seen on Figure 1.2 according to ETSC 2003. Figure 1.2a presents the fatality rate that is the number of deaths divided by the number of kilometres driven by motor vehicles (in billions) each year in the EU. Figure 1.2b shows the road traffic estimated by the number of kilometres driven by motor vehicles each year in the EU.

Reducing the number of road deaths involves improving many factors such as public policies, regulations, infrastructures and crash performance of vehicles. In order to investigate deeper how to protect the occupants of a vehicle in case of a crash, the occurrence and severity of injuries in case of a crash needs to be considered.

1. European Union
2. European Transport Safety Council

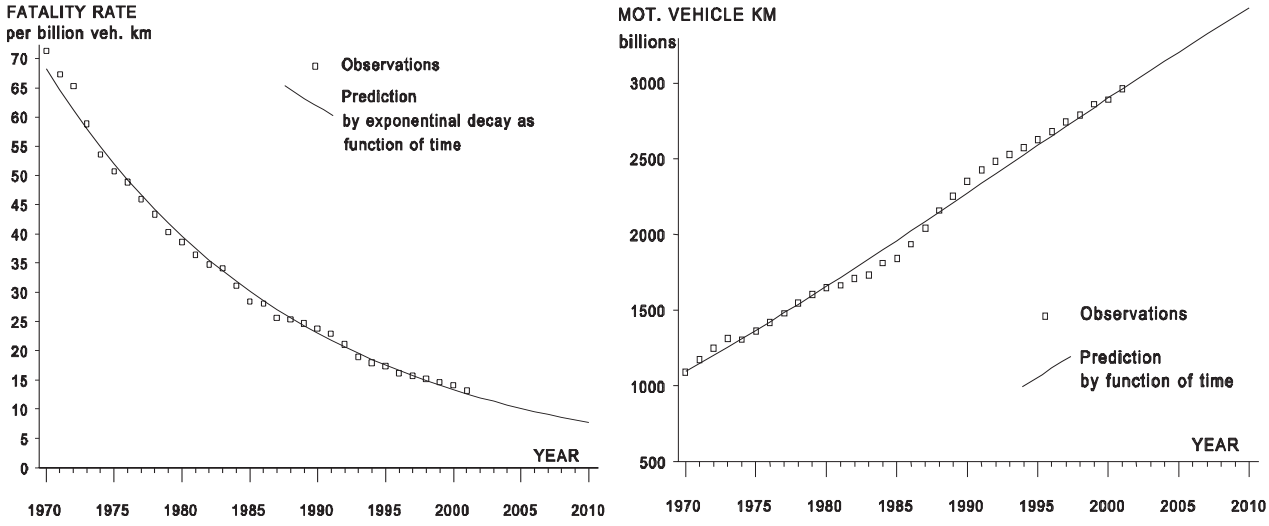

(a) Fatality rate decay

(b) Road traffic growth

Figure 1.2 – Fatality rate and road traffic in Europe (ETSC 2003)

1.1.1 Accidentology

Epidemiological studies analyse car accident databases in order to understand what are the main injury causes to the occupants and to analyse their frequency and severity. Klinich et al. 2010 reported that there is 1.5 times more injuries in frontal impact than in side impact. Rudd et al. 2009 reported that 43 % of occupant fatalities appeared in frontal crashes, making it the impact case creating the more fatalities.

Regarding the abdomen, Elhagediab and Rouhana 1998 demonstrated that the proportion of injuries to the abdomen increases with the injury severity (Table 1.1). This shows that approximately 20 % of the critical injuries are abdominal injuries. Lee and Yang 2002 made similar observations, the abdomen representing the 7th body region in terms of total injuries but the 3rd when looking at the proportion of severe injuries per body region (AIS [3] 3 and more). Yaguchi et al. 2011 also mentioned the abdomen as the 3rd body region in terms of fatalities after the thorax and the head and the 1st by fatality rate (fatalities divided by the sum of all injuries). This puts the abdomen as one of the important body regions to be protected, along with the chest and the head. Martin et al. 2010 described that rear occupants are 1.9 times as likely to sustain abdomen injuries than drivers and 1.5 time than front passengers. Couturier et al. 2007 also stated that rear occupants face a 2.5 time more important abdomen injury risk than front occupants. In each of the two studies, abdomen is the body region that shows the most difference between front and rear occupants for injury risk. There is therefore a benefit for reducing the inequality between car occupants to improve abdomen protection. This has also been highlighted by Frampton et al. 2012, rear occupants sustaining more abdominal injuries (Figure 1.3a) to most of the organs (Figure 1.3b).

3. Abbreviated Injury Scale

	AIS ≥ 3	AIS ≥ 4	AIS ≥ 5
Head	27.8%	35.3%	34.1%
Neck	3.4%	1.8%	2.2%
Chest	37.6%	46.3%	43.3%
Abdomen	8.0%	16.5%	20.5%
Femur	23.2%	0.2%	0.0%
Total	100%	~100%	~100%

Table 1.1 – Injury proportions for body regions depending on injury severity (Elhagediab and Rouhana 1998)

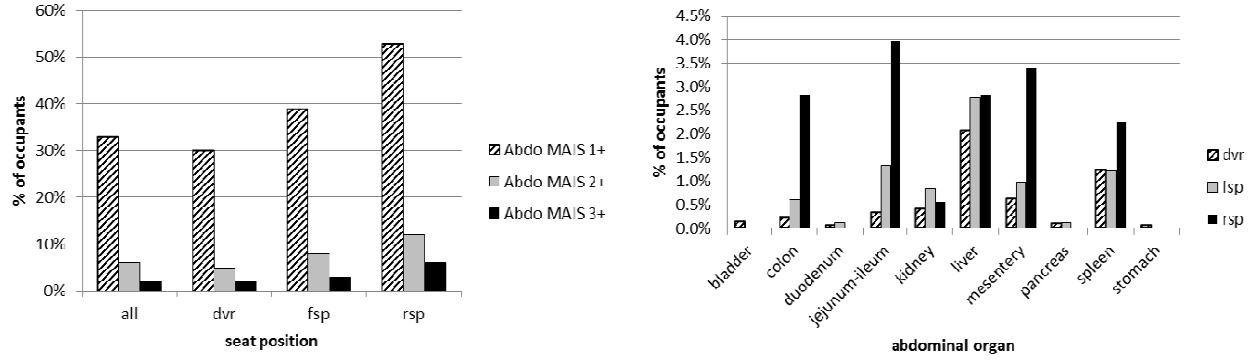

(a) Abdominal injury severity

(b) Abdominal organs injury rates

Figure 1.3 – Abdomen injuries depending on occupant position (Frampton et al. 2012)
dvr: driver, fsp: front seat passenger, rsp: rear seat passenger

1.1.2 Regulation on car passengers protection

In order to be allowed on the market, each car should pass a various number of safety regulations. The two main regulations that are influencing dummy development are the European and the United States regulations. In Europe, UNECE [4] regulations are applicable and regarding frontal impact, UNECE R 94 is used. Until 1998 Global Agreement, the United States were not part of UNECE and followed their own standards. For frontal impact FMVSS [5] 208 is applicable for all passenger cars sold in the United States.

In order to assess occupant protection during car crashes, these regulations perform impact tests with crash test dummies representing the car occupants. Injury criteria are defined in order to link the measurements performed by the dummies to occupant injury risk in the real world. However no injury criteria for the abdomen exists for the moment in regulations. Thorax injury criteria will be presented here as examples.

The frontal impact regulation in Europe consists in a a vehicle impacting a fixed deformable barrier (1 m width and 65 cm height placed 20 cm above the ground) at a 56 km h^{-1} speed with 40 % of the vehicle width overlap on the driver side. Two Hybrid III dummies seating in the front seats are used (UNECE R 94, see UNECE 2013).

The chest deflection and $(V \cdot C)_{\max}$ are used for the thorax. The chest deflection should be less than 50 mm and $(V \cdot C)_{\max}$ should not exceed 1 m s^{-1}. $(V \cdot C)_{\max}$ is computed as the maximum value of the product of compression and rate of chest deflection multiplied by 1.3 (scaling factor). The compression is the deflection divided by the sternum depth of 229 mm.

The United States regulation for frontal impact differs from the European regulation. The test

4. United Nations Economic Commission for Europe
5. Federal Motor Vehicle Safety Standard

consists in the vehicle impacting with full width a rigid barrier at $48\,\mathrm{km\,h^{-1}}$ (FMVSS 208, see NHTSA 2011). Two Hybrid III dummies are seated in the front seats. For the thorax the resultant acceleration should not exceed 60 g's and the chest deflection should not exceed 63 mm. The United States regulation also has a test for the 5th percentile female Hybrid III dummy that is similar to the test case of the European regulation but with a velocity of $40\,\mathrm{km\,h^{-1}}$.

1.1.3 NCAP and Euro NCAP assessment

The NCAP [6] was created by NHTSA in 1978 for cars on the United States market. NCAP goal is to keep on improving the safety of cars by giving rating to each car in the market. The frontal impact test protocol consists in the same test condition as the US [7] regulation with an increased speed of $56\,\mathrm{km\,h^{-1}}$ (NHTSA 2012). It uses the Hybrid III dummy in the driver position and 5th percentile female Hybrid III as passenger and the same injury criteria as the regulation are used with the same tolerance levels.

Euro NCAP [8] is an independent body created in 1997 (Hobbs and McDonough 1998) and backed by the European Commission, European Governments and motoring and consumers organisations. Euro NCAP has more stringent test conditions than the regulation and gives points to assess how good the protection of a body region is. When more than one injury criterion exist, the weakest performance is considered for points attribution. If the value of a criterion is below the higher performance limit, 4 points are given for the body region protection. If the value is above the lower performance limit, 0 points are given. If the value is in between, a linear interpolation is performed to calculate the number of points. Then a score is given to the body region according to Table 1.2. The Euro NCAP frontal impact tests has the same protocol than the European regulation tests, the impact velocity being higher at $64\,\mathrm{km\,h^{-1}}$ (Euro NCAP 2015d). Since 2015, a new test close to the US regulation has also been added with an impact speed of $50\,\mathrm{km\,h^{-1}}$ (Euro NCAP 2015c) with 5th percentile female Hybrid III dummies. This tests includes the assessment of submarining and decreases the car score in case of submarining. Submarining is assessed for driver and rear passenger by a 1 kN drop in any of the two iliac forces within 1 ms and video confirmation. Figure 1.4 shows the principle of the two tests. Table 1.3 shows the values of the $(V \cdot C)_{\max}$ criteria and chest deflection taken from Euro NCAP 2015b.

score	color	points
Good	green	4.000
Adequate	yellow	2.670 to 3.999
Marginal	orange	1.330 to 2.669
Weak	brown	0.001 to 1.329
Poor	red	0.000

Table 1.2 – Euro NCAP scores (Euro NCAP 2015b)

criterion	lower performance limit	higher performance limit	regulation values
deflection (mm)	42	22[a] / 18[b]	50[c] / 63[d]
$(V \cdot C)_{\max}$ ($\mathrm{m\,s^{-1}}$)	1	0.5	1[c]

Table 1.3 – Criteria and limit values for Euro NCAP tests (Euro NCAP 2015b)
[a]Offset-deformable barrier test [b]Full width rigid barrier test [c]European regulation [d]United States regulation

6. New Car Assessment Programme
7. United States
8. European New Car Assessment Programme

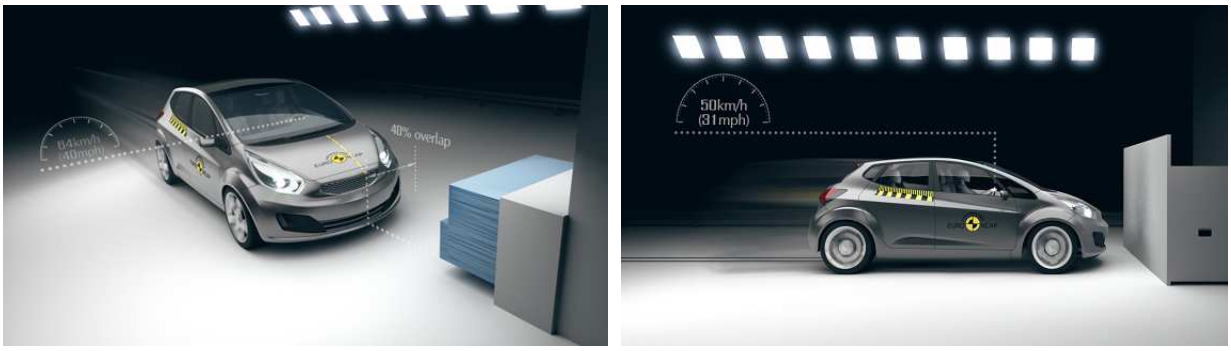

(a) Offset-deformable barrier test (b) Full width rigid barrier test

Figure 1.4 – Euro NCAP frontal tests (www.euroncap.com)

1.1.4 Future trends

The Hybrid III dummy used in the current regulation originates from the 1970's. It is planned to be replaced by the THOR dummy which has been developed by NHTSA since the 1990's. Figure 1.5 shows the two dummies.

NHTSA plans to introduce the THOR 50th percentile dummy in the NCAP program for full frontal tests and a new frontal oblique test condition (NHTSA 2015) for vehicles manufactured from 2019 onwards. On the other hand, in its 2020 roadmap (Euro NCAP 2015a), Euro NCAP describes the THOR mid-sized male dummy as an "enabler" for the "Mobile solution to offset front impact protection". This new test protocol is planned to be defined in 2018 and adopted in 2020. NHTSA is also elaborating a 5th percentile female version of the THOR dummy of which the abdomen would be one of the improved areas.

(a) Hybrid III (b) THOR

Figure 1.5 – Hybrid III and THOR dummies (www.humaneticsatd.com)

1.2 Abdomen response and injury mechanisms

1.2.1 Anatomy of the abdomen

Figure 1.6 shows the planes and directions of the human body. The abdomen is defined as the body region located between the diaphragm on the superior end and the pelvis on the inferior end. Figure 1.7 shows the global location of the abdomen in the human body. The abdomen consists of organs partly protected by skeletal structures and surrounded by muscles and skin. The abdomen can be divided in three parties:

— The upper abdomen or epigastric region is located between the diaphragm and the transpyloric plane
— The mid-abdomen or umbilical region is located between the transpyloric plane and the transtubercular plane
— The lower abdomen or hypograstric / pubic region is located between the transtubercular plane and the pelvis

The transtubercular plane is the transverse plane passing through the iliac tuberosities (see Figure 1.8a). This plane is close to the interspinous plane passing through the anterior superior iliac spines (Figure 1.8b), which can also be used to define the limit mid / lower abdomen. The transpyloric plane is a transverse plane locate halfway between the superior end of sternum (jugular notch) and the inferior end of the pelvis (superior aspect of the pubic symphysis, Figure 1.8b). The location of these planes is reported on Figure 1.7.

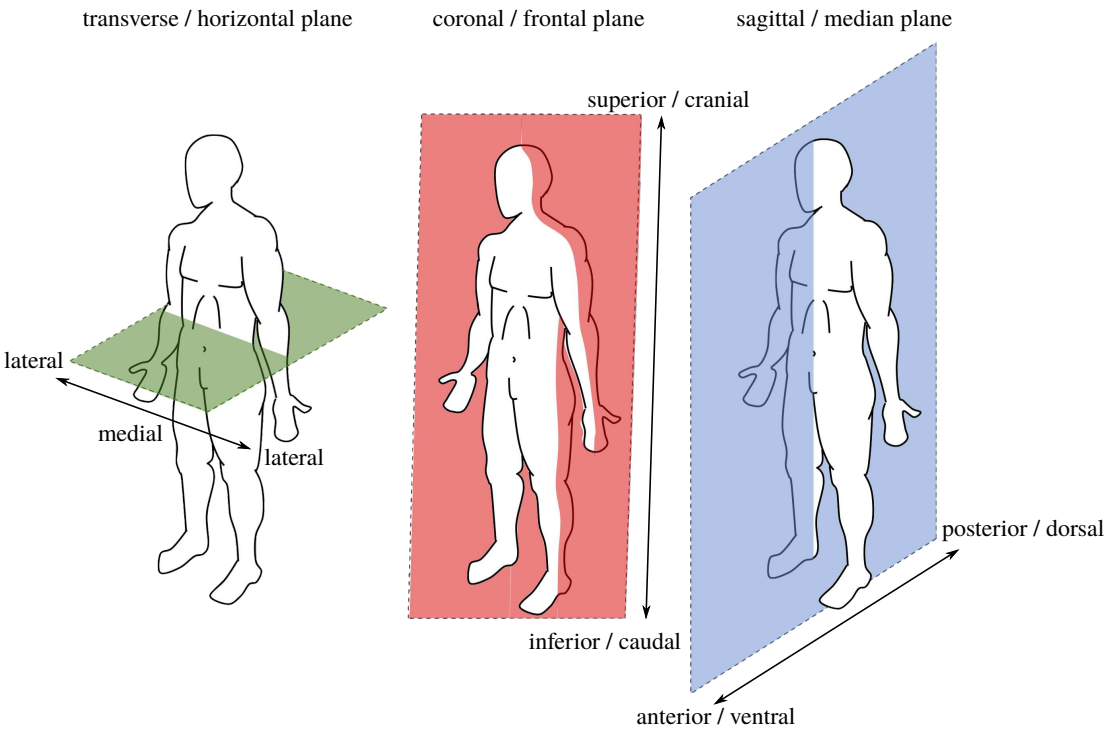

Figure 1.6 – Human planes and body directions (`commons.wikimedia.org`)

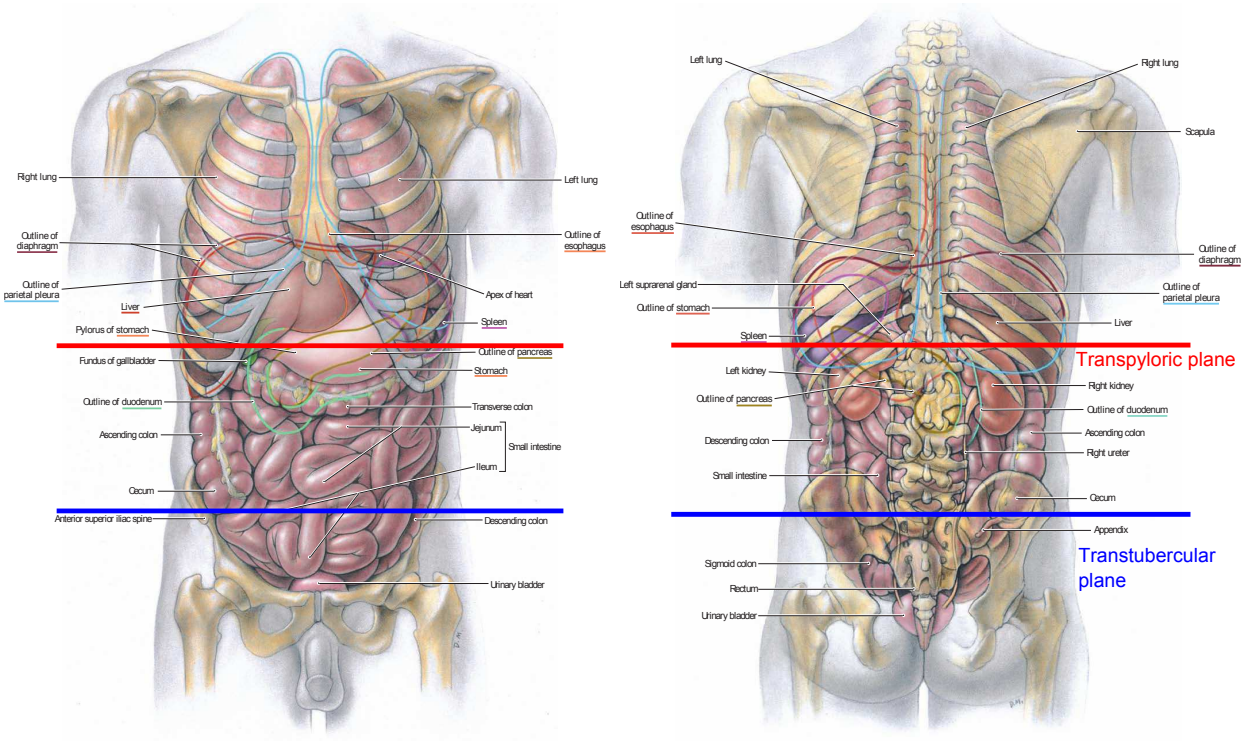

(a) Anterior view (b) Posterior view

Figure 1.7 – Global view of the abdomen (Agur and Dalley 2013)

1.2.1.1 Skeletal system

The abdomen is in relation with three main bony structures. At the inferior end, the pelvis protects the urinary system and includes part of the small intestine. The spine is located at the posterior side of the abdomen. The thoracic and lumbar vertebrae are located in the abdomen zone as well as the sacrum. The sacrum is linked to the hip bones, altogether making the pelvis. Figure 1.8 shows the pelvis, an overview of the spine and the details of a vertebra. At last, the ribcage protects the organs of the upper abdomen.

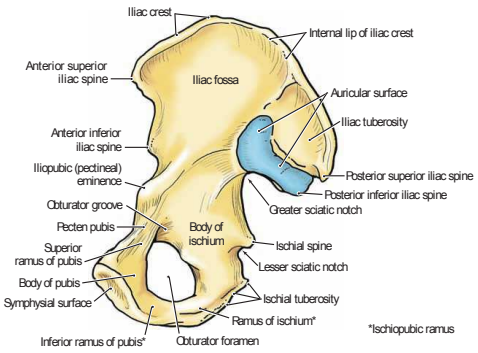

(a) Medial view

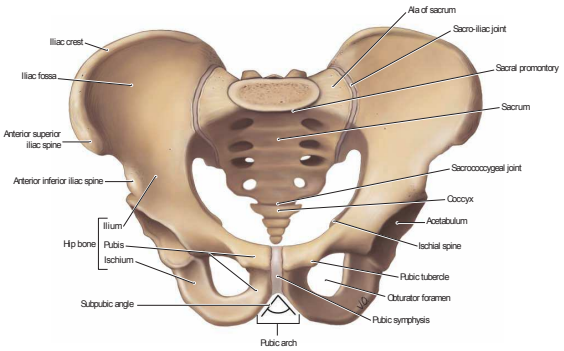

(b) Anterior view

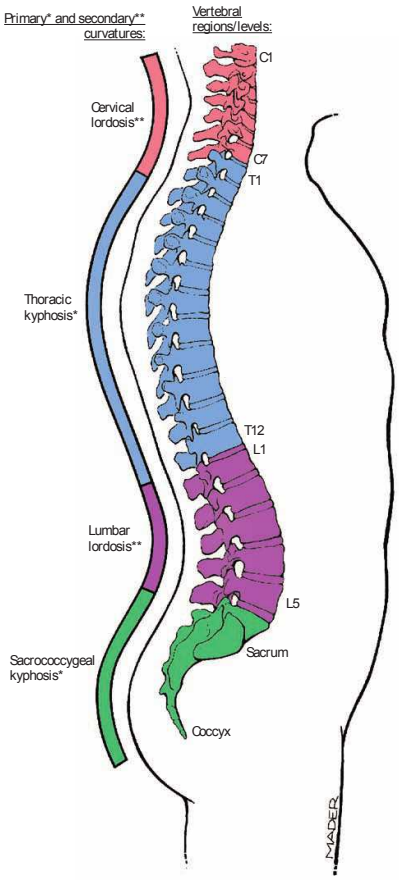

(c) Lateral view of the spine

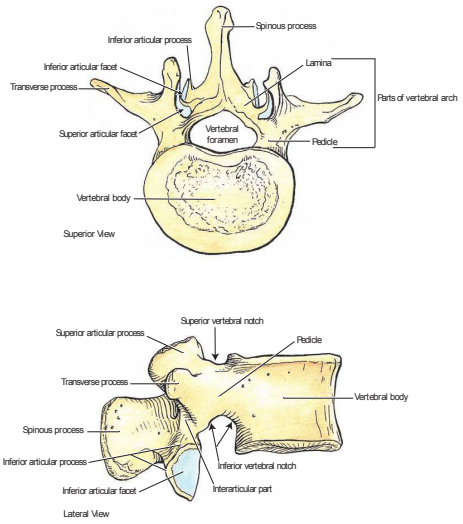

(d) Superior and lateral views of a vertebra

Figure 1.8 – Views of the spine (Agur and Dalley 2013)

1.2.1.2 Muscular system

The organs of the abdomen are surrounded by muscles that keep them compressed in the abdominal cavity. Main muscles include the diaphragm, the rectus abdominis, the external oblique, the internal oblique and the tranversus abdominis. The presence of subcutaneous fat is also important regarding the impact response of the abdomen. The diaphragm is a dome-shaped structure attached to the abdominal wall, the sternum, the ribs and the vertebrae T12 [9], L1 [10] and L2 [11]. The rectus abdominis is a paired muscle located on the anterior side of the abdominal wall. It goes from the pubis to the sternum and costal cartilages. The external oblique is located on the anterior side of the abdominal wall and is linked to the lower ribs and to the iliac crest. The internal oblique lies below the external

9. 12th thoracic vertebra
10. 1st lumbar vertebra
11. 2nd lumbar vertebra

oblique, perpendicular to it. It goes from the costal cartilage to the iliac crest. The tranversus abdominis is located below the internal oblique and goes from the sternum and rib cartilage to the pubis and the iliac crest. Figure 1.9 shows the different layers of muscles in the abdomen region.

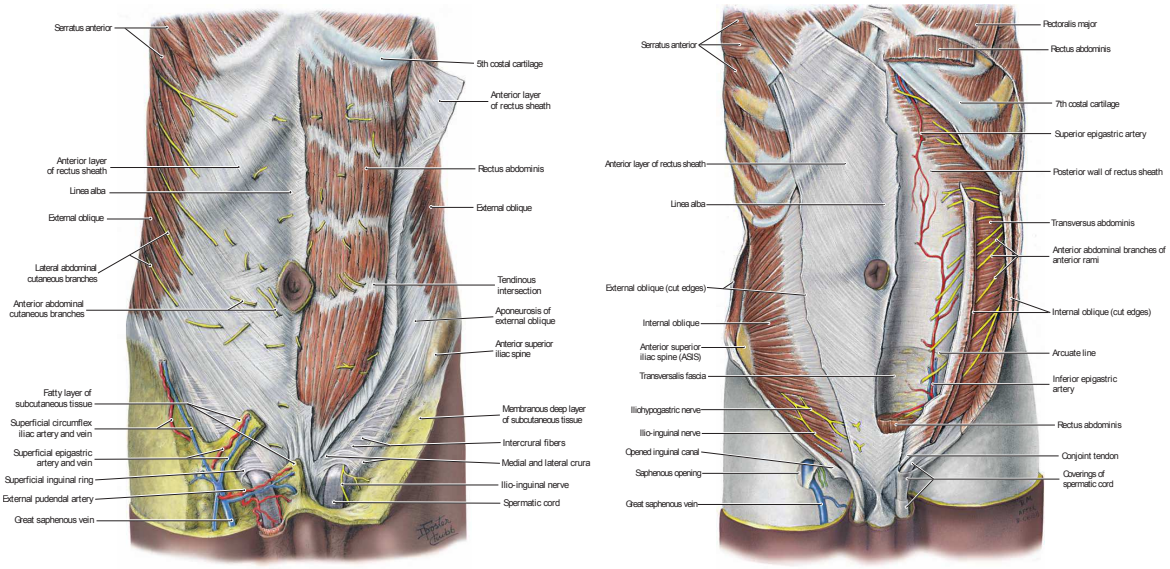

(a) Superficial dissection

(b) Deep dissection

Figure 1.9 – Anterior views of abdominal muscles (Agur and Dalley 2013)

1.2.1.3 Organs

The organs of the abdomen participate to different functions essential to the human body. The liver, gallbladder and pancreas are part of the digestive system as well as the organs that constitute the digestive tract: the stomach, small intestine and the colon (also named large intestine). The digestion takes place first in the stomach, then in the small intestine and at last in the large intestine. The urinary system is composed of the kidneys, the ureters and the urinary bladder. The spleen is an organ that plays a role in the immune system and for blood cells management. Among them, the liver, the pancreas and the two kidneys (together) are vital organs for which a major injury could lead to death. AIS 6 (maximum) is only defined for the liver, compared to AIS 5 (critical) for the pancreas and the kidneys (AAAM 2005).

The organs can also be divided into solid and hollow organs. The solid organs are the liver, the spleen, the kidneys and the pancreas. These organs are located in the upper abdomen and are partially covered by the rib cage. Figures 1.10a to 1.10d show the liver, the kidneys and the spleen. The hollow organs are the gallbladder, the stomach, the small intestine, the colon, the ureters ans the urinary bladder. They are located in the mid and lower abdomen.

The organs are attached by various ligaments and membrane, among them are the peritoneum and the mesentery. The peritoneum covers the most of the abdominal organs and connects them to the abdominal wall. The peritoneal cavity consists of two main region, the greater sac and the lesser sac. The mesentery goes from the posterior wall of the peritoneal cavity and attaches to the intestinal tract. It links the different structures of the small intestine to the peritoneum. Figures 1.10e and 1.10f show the hollow organs and membranes of the abdomen.

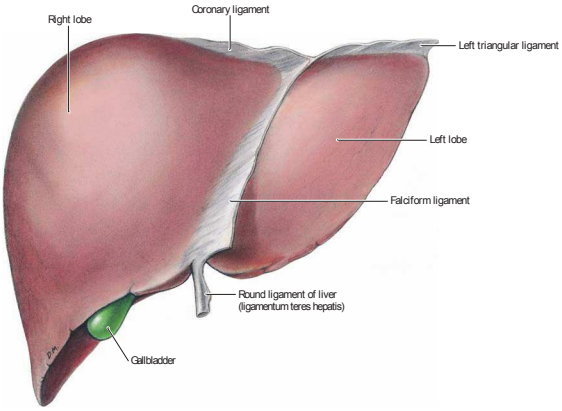

(a) Anterior view of the liver

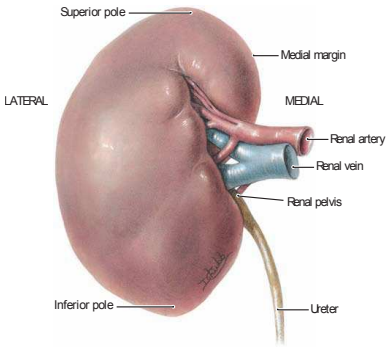

(b) Anterior view of the kidney

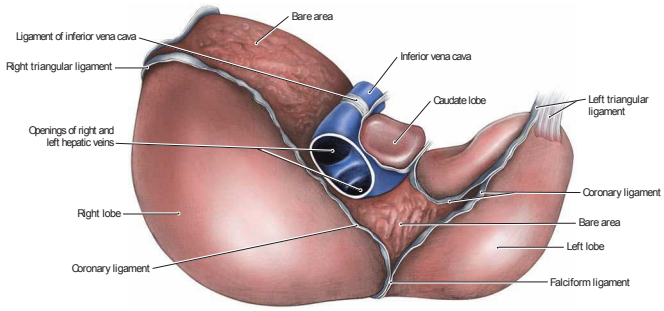

(c) Superior view of the liver

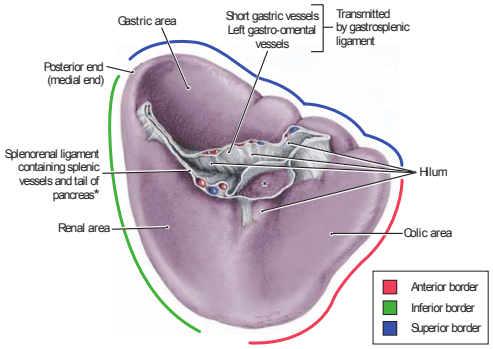

(d) Inferomedial view of the spleen

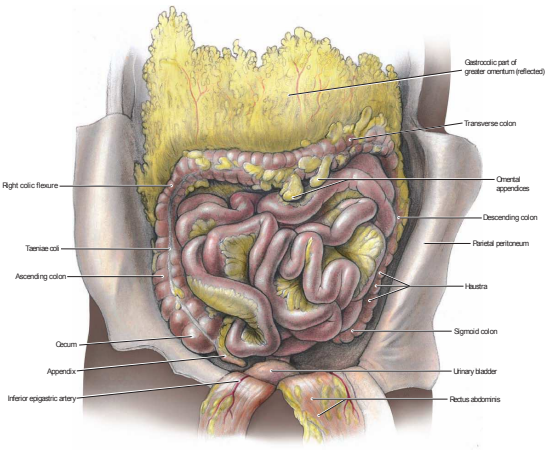

(e) Anterior view of the small intestine and colon

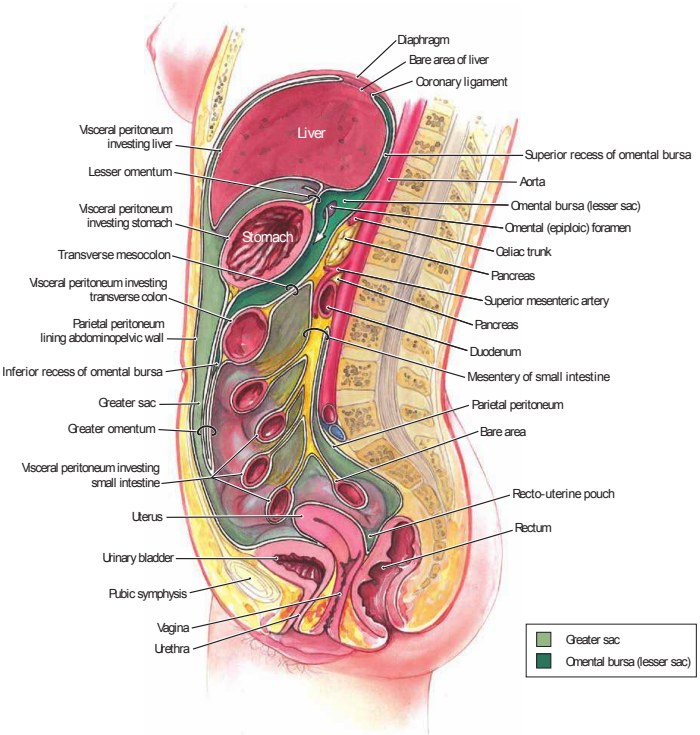

(f) Median section of the abdomen showing mesentery and peritoneum

Figure 1.10 – Solid and hollow organs and membranes of the abdomen (Agur and Dalley 2013)

1.2.2 Accidentology of the abdomen

In order to classify the injuries sustained by car occupants after a crash in a standardised manner, the AIS scale has been developed (AAAM 2005). This system allows to classify any injury by mentioning the body region, the type of anatomical structure, the specific anatomical structure, the level and the AIS score itself. The AIS score describes the severity of the injury. Six levels of increasing severity are defined as mentioned in Table 1.4. The MAIS [12] is the maximum AIS value that a subject sustained to any body part. In order to indicate all the injuries with a minimum AIS of 3 (for instance), the term AIS 3+ is used.

AIS score	description
1	minor
2	moderate
3	serious
4	severe
5	critical
6	maximum

Table 1.4 – Injury severity score (AAAM 2005)

Over the years, seatbelt use and airbag availability modified the sources of injury to the abdomen. This trend has been illustrated for thorax injuries in Kent et al. 2004 and the general statements are valid for the abdomen region. While seatbelt use and airbag availability grew, the proportion of injuries created by the steering wheel decreased whereas the proportion of those created by the seatbelt and the airbag grew. At the end of the 1990's, the seatbelt overtook the steering wheel as main cause of thoracic injuries (Figure 1.11). However results from Kent et al. 2003 clearly show that seatbelt and airbag reduce the probability of injuries (all body regions considered) in frontal crash (Figure 1.12). The principal source of injury vary depending on which organ is considered. Elhagediab and Rouhana 1998 reported that for the abdomen the steering wheel is the main source of injuries for the liver and the spleen but that the seatbelt is the main source of injuries for the digestive system (Table 1.5). Overall 69 % of abdominal injuries are due to the steering wheel and 17 % to the seatbelt. These data represent accidents from 1988 to 1994 so the recent evolution of restraint systems is not included. Klinich et al. 2010 reported more balanced proportions with 50 % AIS 3+ injuries created by the steering wheel and 30 % by the seatbelt for 1998–2008 accidents. They also reported the decrease of abdominal injuries with more recent vehicle model year. The most recent study, Shin et al. 2015 reported that the seatbelt overtook the steering wheel as primary source of abdomen injuries with 64 % of injuries due to the seatbelt and 22 % due to the steering wheel based on 2009–2012 data. This proves that the trend predicted for the thorax in Kent et al. 2004 is also effective for the abdominal region.

	LIVER	SPLEEN	ARTERIES	DIGESTIVE	KIDNEYS	RESPIRATORY	UROGENITAL	TOTAL
BELT	1.63%	2.34%	1.54%	9.62%	1.26%	0.56%	0.00%	**16.95%**
SW	34.31%	13.72%	9.07%	6.68%	0.76%	2.69%	1.49%	**68.72%**
BAG	0.00%	0.13%	0.00%	0.00%	0.00%	0.00%	0.00%	**0.13%**
INTERIOR	3.26%	6.89%	1.37%	0.84%	0.14%	0.77%	0.93%	**14.19%**
TOTAL	**39.20%**	**23.08%**	**11.98%**	**17.13%**	**2.17%**	**4.02%**	**2.41%**	**100.00%**

Table 1.5 – Injury sources for abdominal organs (Elhagediab and Rouhana 1998)
SW: Steering Wheel

Lamielle et al. 2006 described that solid organs were more injured than hollow organs but with close proportions (46 % and 43 %). It has also been demonstrated that the use of a restraint system was shifting the injuries from solid organs to hollow organs for front occupants (Table 1.7). Modern

12. Maximum AIS

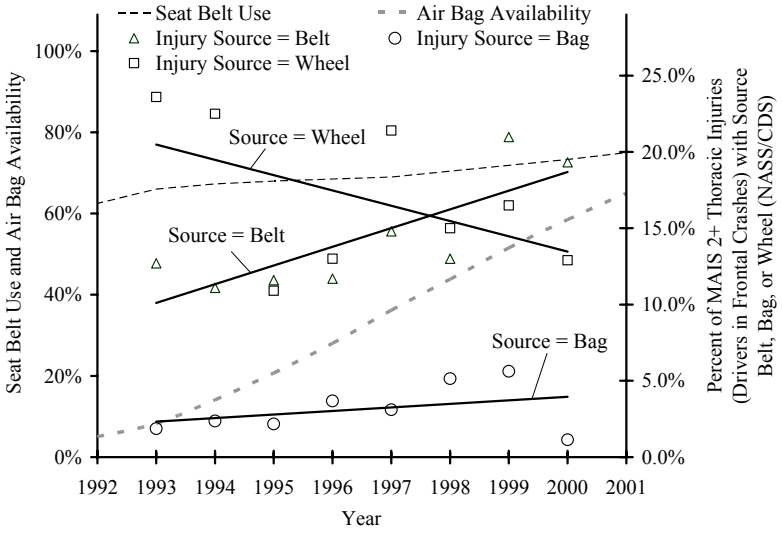

Figure 1.11 – Source of thoracic injuries to drivers in frontal crash compared to seatbelt use and airbag availability trends (Kent et al. 2004)

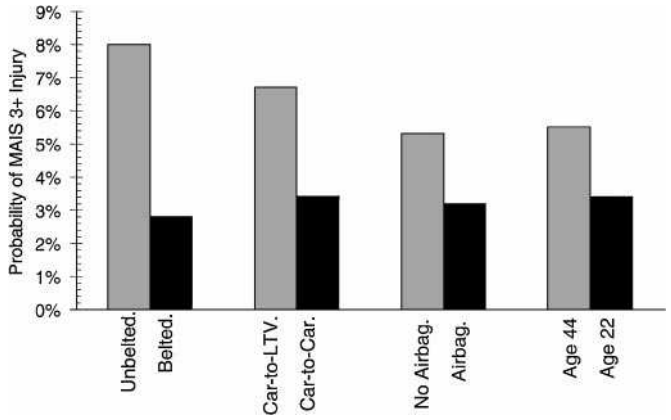

Figure 1.12 – Relative injury probability in frontal crash influenced by seatbelt and airbag use (Kent et al. 2003)

cars equipped with retractable seatbelts, pretensioners and airbags have an injury proportion of 62 % for the hollow organs compared to 38 % for solid organs.

Liver has been described as the most injured abdominal organ in Elhagediab and Rouhana 1998 followed by spleen and the digestive system, base on US data (Table 1.5). Frampton et al. 2012 described similar results but Lamielle et al. 2006 described the spleen as the most injured organ followed by the liver and the jejunum, part of the digestive system based on French data (Table 1.6). The differences in results between these two studies is explained in Lamielle et al. 2006 by the fact that there is more unbelted occupants in the US compared to France. Yoganandan et al. 2000 described the spleen (31 %) and the liver (30 %) as the most injured organs followed by the kidneys (19 %) and the digestive system (11 %). These data included frontal and side impact which explains the presence of kidneys injuries. These results highlight that there is a need to pay particular attention to the hollow organs protection with today's car, and that those injuries are be mainly created by the seatbelt.

	Organs	AIS 3+ Injuries
Solid organs	Liver	101
	Spleen	141
	Kidneys	21
	Pancreas	17
Hollow organs	Duodenum	11
	Jejunum	102
	Colon	47
	Mesentery	82
	Stomach	6
	Bladder	14
	Others	72
	Total solid	280
	Total hollow	262
	Total	634

Table 1.6 – Distribution of abdominal organs injuries (Lamielle et al. 2006)

	%hollow	%solid	%hollow	% solid
Unbelted	23%	77%	23%	77%
SB	63%	38%	58%	42%
RB	55%	45%		
RB+P	50%	50%		
RB+P+AB	62%	38%		

Table 1.7 – Hollow and solid organs injuries depending on the restrain system for front occupants (Lamielle et al. 2006)
SB: Three point static belt
RB: Three point belt plus retractor
RB+P: Three point belt plus retractor and pretensioner
RB+P+AB: Three point belt plus retractor, pretensioner and frontal airbag

1.2.3 Abdomen mechanical response

The mechanical response of the human abdomen can be assessed by different means, either by volunteer tests, animal tests or tests on PMHS. It has been chosen here to review frontal impact PMHS tests given the fact that volunteer test can only give information on very low severity loading and that animal testing can not be considered as a way of assessing adult human response due to the anthropometry mismatch. Two main categories of test have been designed to reproduce the abdomen contact with the steering wheel or the abdomen loading by a seatbelt.

1.2.3.1 Impactor tests

In order to represent the contact of the abdomen with the steering wheel of a car, many studies used an impactor protocol. Figure 1.13 shows the test set-up of the considered studies and Figure 1.14 presents the responses of the subjects in the force-penetration diagram.

The first impactor study on PMHS was done by Cavanaugh et al. 1986, where 12 subjects were tested. The subjects were impacted at the level of the L3 [13] vertebra by a 25 mm diameter rigid bar, their back being unrestrained. The L3 level was chosen because it corresponds to an impact at mid-abdomen level (in terms of height) and prevents interaction with the lower ribcage. The nominal mass assigned to the impactor was either 32 kg or 64 kg. The nominal impact velocity varied from $5\,\mathrm{m\,s^{-1}}$ to $13\,\mathrm{m\,s^{-1}}$.

Impactor test were also conducted in Hardy et al. 2001 with a free back condition. Both the mid-

13. 3rd lumbar vertebra

abdomen (L3 level) and upper abdomen (T11 [14] level) were impacted by a 25 mm diameter impactor having a mass of 48 kg. The subjects were impacted at 6 m s^{-1} (3 subjects at the mid-abdomen level and 2 subjects at the upper abdomen level) and 9 m s^{-1} (3 subjects at the mid-abdomen level and 1 subject at the upper abdomen level).

Shaw et al. 2004 used a steering wheel-like impactor on four subjects. The impactor was inclined at 45° and the subject back was fixed. The impactor diameter was 25 mm and it had a mass of 64 kg. The impact velocity was of 4 m s^{-1}. The impactor was at the level of the T12 vertebra in order to impact the upper abdomen. The impactor penetration in the abdomen was limited to 30 % of the abdomen depth for three subjects and to 50 % for one subject.

(a) Cavanaugh et al. 1986 (picture from Lee and Yang 2001)

(b) Hardy et al. 2001 mid-abdomen

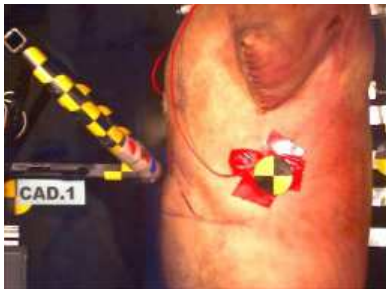

(c) Shaw et al. 2004

Figure 1.13 – Impactor test set-ups from the considered studies

14. 11th thoracic vertebra

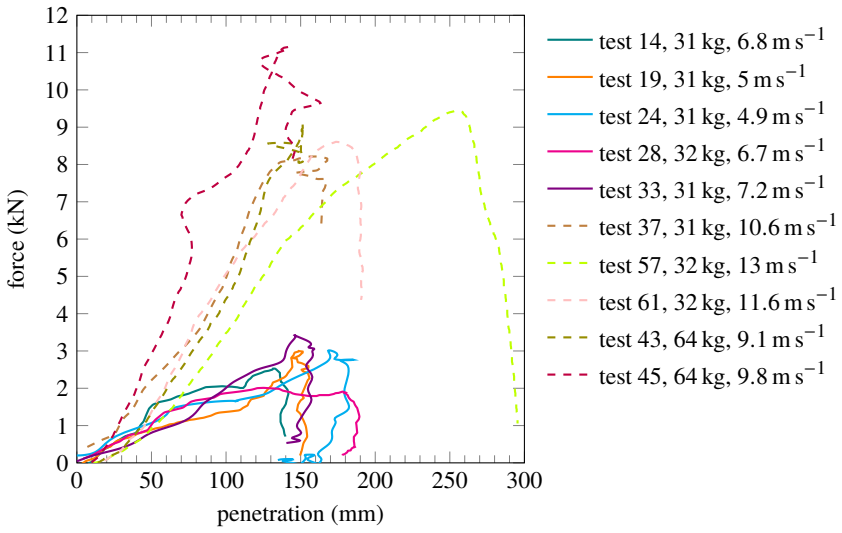

(a) Cavanaugh et al. 1986

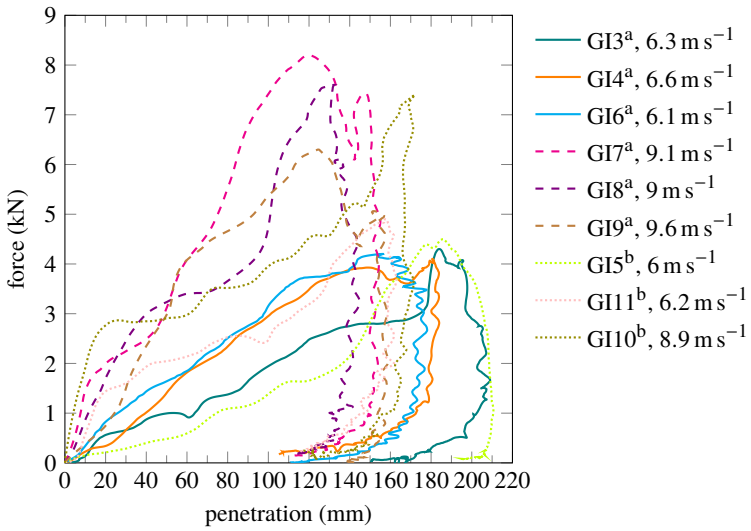

(b) Hardy et al. 2001 (free back condition)

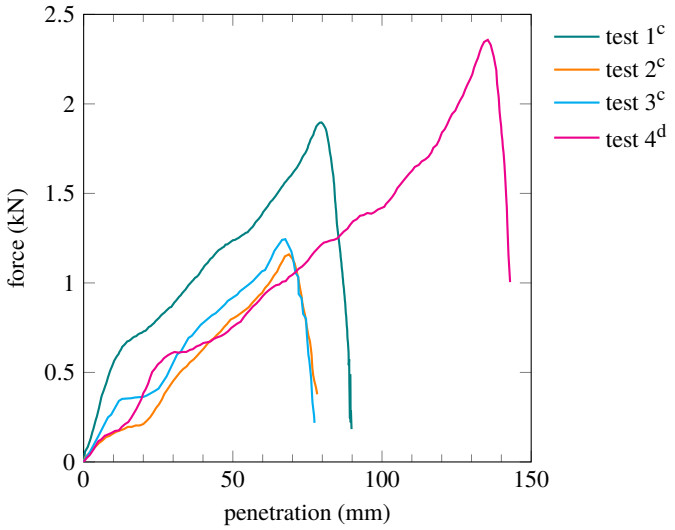

(c) Shaw et al. 2004

Figure 1.14 – Subjects responses under impactor tests for the considered studies

[a]impact at mid-abdomen level

[b]impact at upper abdomen level

[c]Penetration limited to 30 % of torso depth

[d]Penetration limited to 50 % of torso depth

1.2.3.2 Seatbelt tests

In addition to impactor tests, test protocols have also been developed in order to study the behaviour of the abdomen under compression by a seatbelt. Figure 1.15 shows the test set-up of the considered studies and Figure 1.16 presents the responses of the subjects in the force-penetration diagram.

Seatbelt test were performed in Hardy et al. 2001 on three subjects. These tests are the only free back reported tests. The seatbelt was driven by a pneumatic ram with adjusted pressure to produce the desired loading velocity. A peak velocity of $3\,\mathrm{m\,s^{-1}}$ was imposed and a haversine speed-time input condition was obtained. The belt was placed on the mid-abdomen.

In Trosseille et al. 2002, six subjects were tested under a seatbelt loading on the mid-abdomen, the back of the subject being restrained. Two configurations were performed with custom-made pyrotechnic devices:

— *configuration 1* with one pretensioner on one side having 28 kJ of pyrotechnic input and presence of a load limiter of which the limiting force value was not mentioned by the authors.
— *configuration 2* with one pretensioner one each side having 3.2 kJ of pyrotechnic input each.

Three seatbelt retracting conditions were performed in Foster et al. 2006. Two conditions were with one pretensioner retracting the seatbelt (called B and C, the B conditions being of higher energy) and one condition was with two B pretensioners in parallel (called A). Four subjects were tested under the A condition, three under the B condition and one under the C condition (twice). The region loaded was the mid-abdomen.

The study Lamielle et al. 2008 targeted two different velocity ranges aiming to reproduce the conditions of either submarining (retraction velocity around $4\,\mathrm{m\,s^{-1}}$ and penetration around 100 mm) and OOP [15] loading (retraction velocity around $8\,\mathrm{m\,s^{-1}}$ and penetration around 60 mm). The submarining-like series was named MHA and the OOP-like series was named PRT. Eight PMHS were tested, allowing 4 tests of each configuration. The mid-abdomen was loaded either by an hydraulic piston (MHA series) or by pretensioners (PRT series), the subject's back being fixed. In the MHA series, the retraction velocity and the maximum belt displacement were imposed as reported in Table 1.8 with targets in terms of penetration velocity and abdomen compression.

(a) Hardy et al. 2001 (b) Trosseille et al. 2002 (with THOR dummy as demonstrator) (c) Foster et al. 2006 (d) Lamielle et al. 2008

Figure 1.15 – Seatbelt test set-ups from the considered studies

test	penetration velocity ($\mathrm{m\,s^{-1}}$)	penetration (percentage of abdomen depth)
MHA111	4	30
MHA115	5	40
MHA151	4	40
MHA155	5	30

Table 1.8 – Input parameters from Lamielle et al. 2008 MHA tests, according to Lamielle 2008

15. Out Of Position

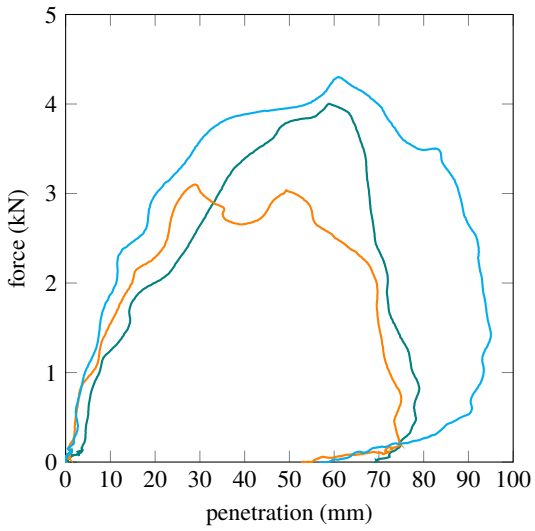

(a) Hardy et al. 2001 responses

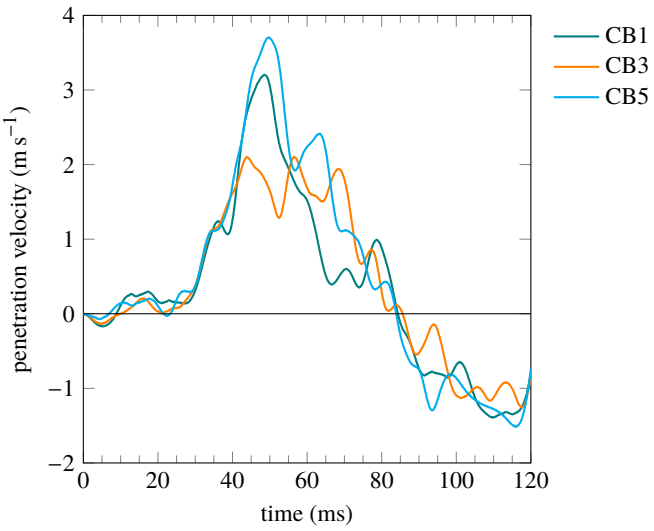

(b) Hardy et al. 2001 input conditions

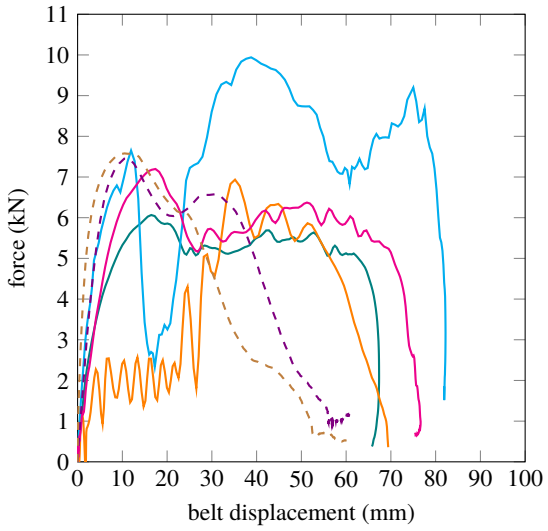

(c) Trosseille et al. 2002 responses

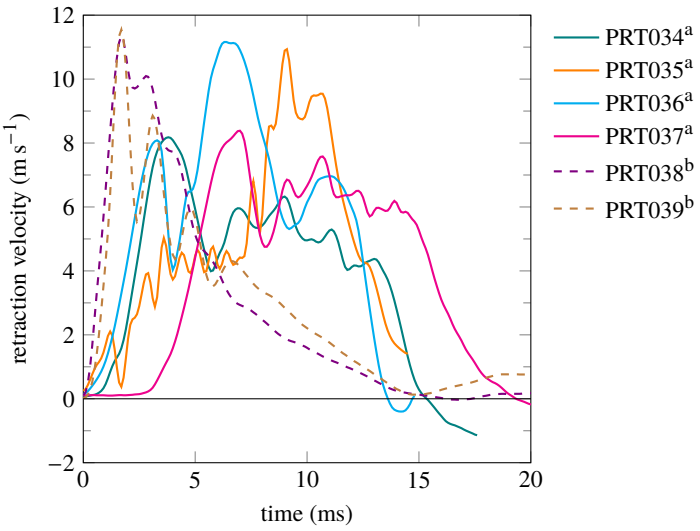

(d) Trosseille et al. 2002 input conditions

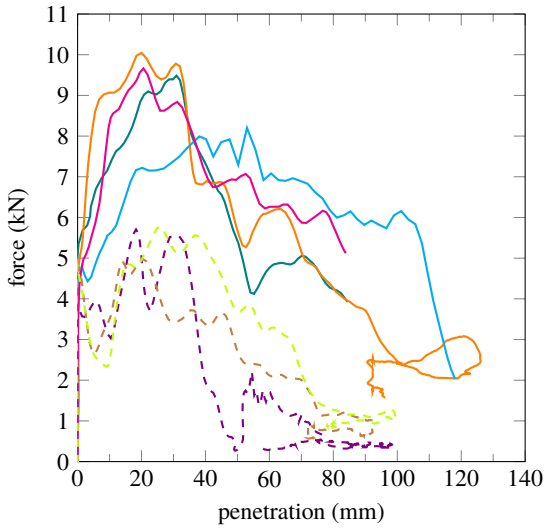

(e) Foster et al. 2006 responses

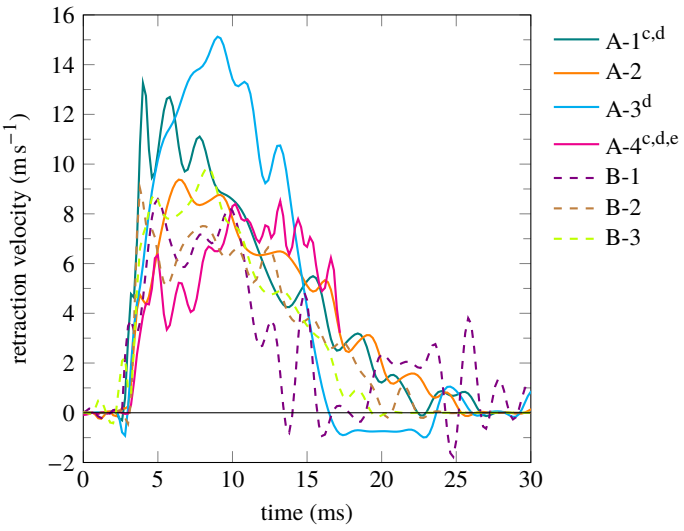

(f) Foster et al. 2006 input conditions

Figure 1.16 – Subjects responses under seatbelt tests for the considered studies

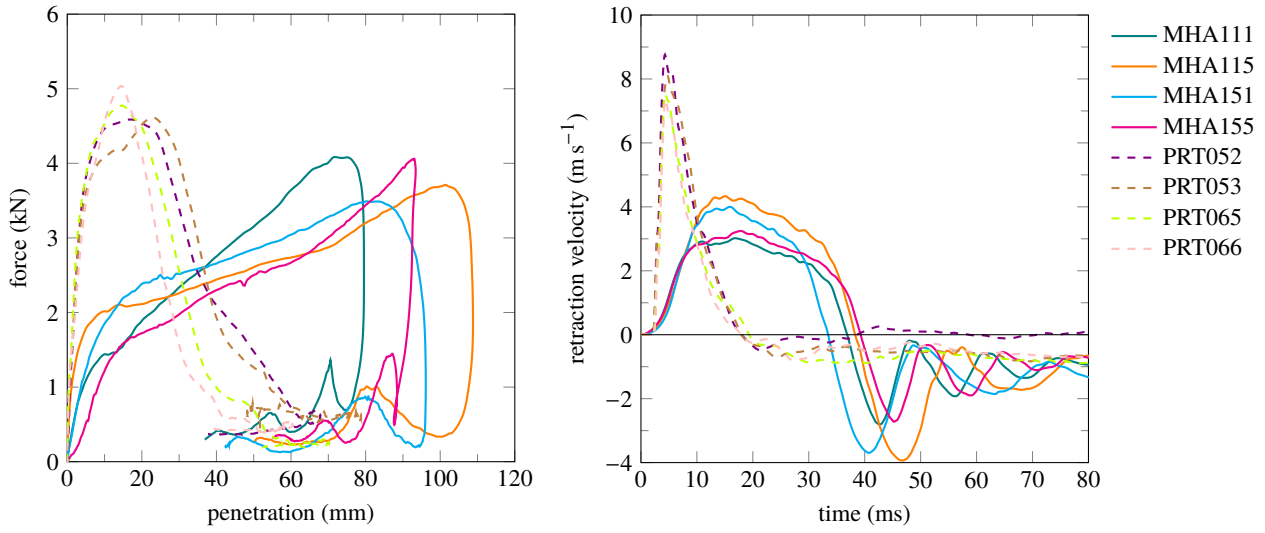

(g) Lamielle et al. 2008 responses

(h) Lamielle et al. 2008 input conditions

Figure 1.16 – Subjects responses under seatbelt tests for the considered studies (continued)

[a] *configuration 1*

[b] *configuration 2*

[c] Penetration values from laser measurement instead of video measurement

[d] Penetration could not be measured until the end of the test

[e] Retraction velocity measurement not available, penetration velocity used instead

For the impactor condition, the results from Hardy et al. 2001 match those from Cavanaugh et al. 1986 in terms of abdomen stiffness for low and high speed impact, although the impactor mass is different. A rate-sensitivity of the abdomen has been highlighted with a stiffer response for a higher impact velocity in both studies.

For seatbelt tests, Trosseille et al. 2002 reported that although the input conditions were believed to be significantly different, no difference was seen in the abdomen response. Differences were however reported in the injury statements. The differences in abdomen loading induces a difference in mechanical response. When the abdomen is loaded with a pretensioner the response shows a high initial force peak at very low penetration which means that the abdomen has very stiff behaviour compared to a loading with a piston or a ram. The rate sensitivity has however also been highlighted, a higher retraction velocity leading to a higher peak force in each case.

A variability of the human response appears from the PMHS test data due to the variety of anthropometric dimensions of the human subjects which leads to the need of developing harmonised response corridors.

1.2.3.3 Biofidelity corridors

The need to provide harmonised references for the evaluation of crash test dummies of numerical human models lead to the development of biofidelity corridors based on PMHS tests. Corridors represent a domain on a graph (usually force / penetration for moment / angle) in which a dummy or model response curve should fit in order to be assessed biofidelic. The borders of the corridor could be either standard deviation values from the average PMHS response or an envelope including all PMHS responses.

Recent harmonised corridors have been developed in Lebarbé et al. 2015. Based on PMHS tests

from the literature mean response data and boundaries are provided. For force and penetration versus time targets, standard deviations values are defined boundaries. For force versus penetration targets, the boundaries are computed as standard deviation ellipses according to the method described in Shaw et al. 2006. Figure 1.17 shows the corridors from Lebarbé et al. 2015.

For the impactor loading case, data from Cavanaugh et al. 1986 have been selected. A first corridor was generated for subjects impacted with a 32 kg mass and a low velocity (average 6.1 m s^{-1}). A second corridor was generated for subjects impacted with either a 32 kg or 64 kg mass and a high velocity (average 10.8 m s^{-1}). The PMHS responses were normalised with the technique described in Mertz 1984 based on subject body mass and abdomen depth before generating the corridors.

For the seatbelt case, the MHA test series from Lamielle et al. 2008 have been used to generate the corridor. This series was chosen because it had been originally designed to represent a submarining phenomenon in terms of abdominal loading. No normalisation was applied and the existing normalisation methods were described as adapted for blunt impacts with an impactor having significant mass but not for belt loadings.

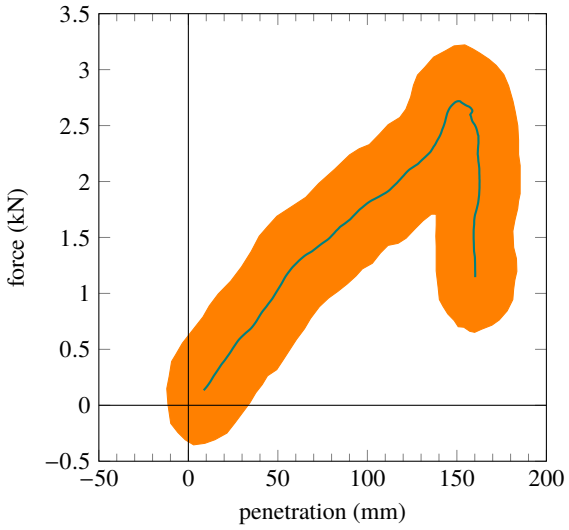

(a) Cavanaugh et al. 1986 low speed condition

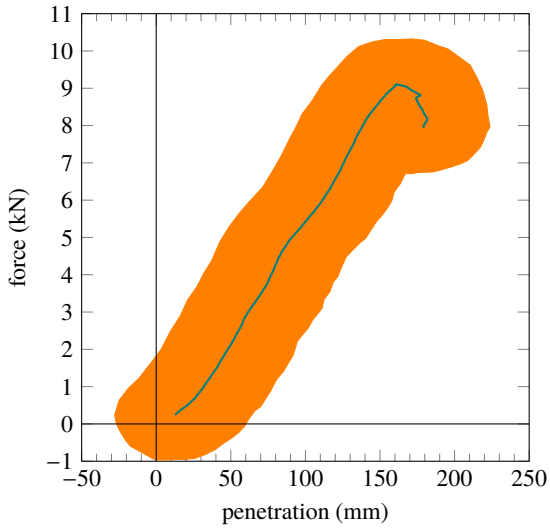

(b) Cavanaugh et al. 1986 high speed condition

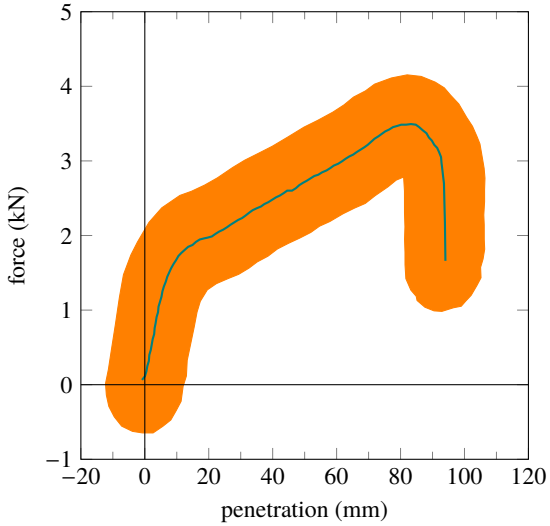

(c) Lamielle et al. 2008 MHA condition

Figure 1.17 – Corridors from Lebarbé et al. 2015

1.2.4 Abdomen injury mechanisms

1.2.4.1 Injury types

The injury types to the abdomen were reported by Lee and Yang 2002 to be mainly contusions (43 % of the total injuries), lacerations (28 %) and abrasions (13 %). When looking at serious to critical, it has however been found that only lacerations were significantly AIS 3+ injuries, along with ruptures and avulsions. Shin et al. 2015 reported that 58 % of the abdomen injuries are contusions and 23 % are lacerations. Contusions were reported to be caused by the steering wheel whereas lacerations were caused by both steering wheel and seatbelt.

Figure 1.18 shows results from Bansal et al. 2009 classifying abdomen injuries types and severity. It appears that AIS 5+ injuries are only liver and spleen lacerations.

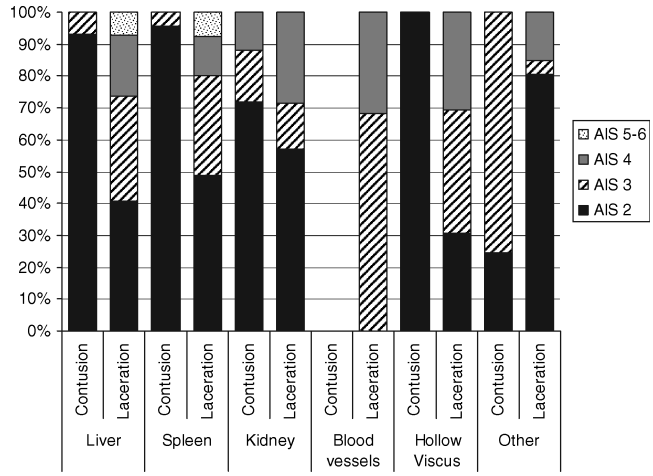

Figure 1.18 – Abdominal injury description and severity (Bansal et al. 2009)
Hollow Viscous includes colon, small intestine, uterus, bladder and stomach
Other includes mesentery, adrenal gland, pancreas, uro-genital organs, skin, omentum and retroperitoneal hemorrhage
Rupture and abdominal organ destruction were included in the laceration category

Regarding PMHS tests, tears and lacerations of liver have been reported in Hardy et al. 2001 impactor tests along with spleen and cecum tears. No other impactor test studies reported injuries. For seatbelt tests, Trosseille et al. 2002 reported a spleen rupture, a mesentery tear and an omentum tear. Foster et al. 2006 reported liver lacerations and tears, lobe transections and disruptions as well as spleen tears. A detailed injury statement has been provided in Lamielle et al. 2008: liver, spleen, pancreas lacerations and tears, mesentery contusions, lacerations and abrasions, colon, jejunum-ileum, duodenum contusions and lacerations. A kidney injury has also been reported.

Injury statements were also reported to be dependent on the subject perfusion method. For instance no organ injuries were reported in Cavanaugh et al. 1986, due to the absence of local vasculature perfusion according to the authors. A perfusion at the organ level has been performed in Lamielle et al. 2008 which can explain the detailled injury statement provided. Detailed injury statements and perfusion conditions can be found in Appendix B.

The only studies presenting a consistent injury statement across a majority of subjects were Hardy et al. 2001 impactor conditions along with Foster et al. 2006 A condition and Lamielle et al. 2008. Tables 1.9, 1.10 and 1.11 show simplified injury statements for those conditions.

region	impact velocity ($m\,s^{-1}$)	liver AIS (injured subjects / number of subjects)
mid-abdomen	6	4 (3 / 3)
	9	4 or 5 (2 / 3)
upper abdomen	6	3 or 4 (2 / 2)
	9	4 or 5 (1 / 1)

Table 1.9 – Simplified injury statement from Hardy et al. 2001 impactor tests, with mention of injuries occurrence

condition	liver AIS (injured subjects / number of subjects)
A	3 (3 / 4)
B	/ (/)

Table 1.10 – Simplified injury statement from Foster et al. 2006, with mention of injury occurrence

con-dition	mesentery AIS (injured subjects / number of subjects)	colon AIS (injured subjects / number of subjects)	jejunum-ileum AIS (injured subjects / number of subjects)
MHA	/	/	2 (3 / 4)
PRT	2 (3 / 4)	3 (3 / 4)	2 (4 / 4)

Table 1.11 – Simplified injury statement from Lamielle et al. 2008, with mention of injury occurrence

1.2.4.2 Abdomen loading types

In a car accident, contusions, lacerations and abrasions can be mostly due to contact between car elements (steering wheel, dashboard) or compression by the seatbelt but ruptures and avulsions can also be due to motion of the organs inside the abdominal cavity as a result of deceleration.

If a car occupant is properly restrained, the seatbelt lies on the pelvic bone which prevents the abdomen from being loaded during the crash. However, a misplacement of the seatbelt, on top of the abdomen instead of on top of pelvis can lead to direct abdomen compression during the crash, especially with the use of seatbelt pretensioners. An other phenomenon leading to direct abdomen loading by the seatbelt is when the seatbelt, although originally positioned on the pelvis, slides over the pelvis to load the abdomen. This phenomenon is called submarining and can happen particularly because of a slouched position of the occupant. Submarining happens when the force acting on the pelvis are not in equilibrium and produce pelvis rotation. These two phenomenons are difficult to identify in the accidentology due to the lack of data on what is happening during a crash. However, they were successfully replicated in sled testing on PMHS. The most recent studies on submarining with PMHS subjects are Luet et al. 2012 and Uriot et al. 2015b.

1.2.4.3 Injury criteria

An injury criteria for blunt abdominal trauma is a mathematical relationship which links the occurrences of an injury observed during tests and physical parameters of those tests. A logistic regression is used to generate risk curves linking the value of the physical parameters and the probability of injury of a specified severity.

Many variables have been considered to be injury predictors. Abdomen compression (C), loading velocity (V), force exerted on the abdomen (F) and intra-abdominal pressure (P) were the most used. Combinations of those parameters have been proposed as injury criteria for the abdomen. Rouhana et al. 1985 proposed $V_{\max} \cdot C_{\max}$ as criterion and called it the Abdominal Injury Criterion. Viano and Lau 1985 proposed $(V \cdot C)_{\max}$, called the Viscous Criterion. Injuries at high compression and low loading velocity have been described in Lau and Viano 1986 as crushing injuries, those with moderate compression and velocity as viscous injuries and those with high velocity and low compression as blast injuries. Kent et al. 2008 conducted a study comparing all the existing criteria to date. The test condition was belt loading on supine porcine subjects. For single parameters,

maximum values of belt force and penetration were reported good injury predictors whereas the velocity was not. Regarding multi-parameters criteria, $V_{\max} \cdot C_{\max}$ and $(V \cdot C)_{\max}$ had similar abilities to predict injuries but newly proposed criteria, $\left(\dot{F} \cdot C\right)_{\max}$ and $F_{\max} \cdot C_{\max}$ had better results, the latter being the best predictor. Kent et al. 2008 also stated that $V_{\max} \cdot C_{\max}$ and $(V \cdot C)_{\max}$ were predicting less accurately injuries than the compression alone, questioning the added value of the loading velocity in the injury criteria, high loading velocity being well correlated with high compression in most studies.

Regarding pressure as an injury criteria, Sparks et al. 2007 investigated pressure-based predictors based on isolated human liver drop tests. In Kremer et al. 2011 where those data have been reprocessed, the best predictors were found to be $\dot{P}_{\max}$, $V_{\max} \cdot C_{\max}$ and $P_{\max}$. Kremer et al. 2011 also performed oblique impact PMHS tests with pressure sensors in the hepatic veins of the liver. $\dot{P}_{\max} \cdot P_{\max}$ and $\dot{P}_{\max}$ were reported to be the best predictors. Based on accident reconstruction with child dummies, Beillas et al. 2012 also reported $P_{\max}$, $\dot{P}_{\max}$ and $\dot{P}_{\max} \cdot P_{\max}$ as satisfactory injury predictors. $\dot{P}_{\max} \cdot P_{\max}$ had been previously proposed in Johannsen et al. 2007.

1.3 Tools for the evaluation of abdomen protection

1.3.1 Computer models

In order to be able to estimate the human body behaviour in case of a car crash, computer models of the human body have been developed. The accuracy of these models to represent the human body allows to get a better understanding of how the human body would behave than a physical test with a dummy. The improvements of computing capabilities and of medical imaging allowed to generate finite element models with more and more detailed organ representation. This bring the advantage to be able to analyse the loading of the internal organs of the body and to analyse the values of engineering parameters such as stresses and strains for local areas of the body. This would allow a precise injury prediction.

In order for these models to be used with the aim of injury prediction, their response needs to be validated. The material properties of the different body segments (organs, bones, cartilages, fat) are obtained from mechanical testing on sampled from PMHS for which there is some variability. The best validation data for the global response of the models are PMHS data. The following paragraphs will present the existing models ad well as their validation cases.

1.3.1.1 Presentation of the different models

This review covers the 50th percentile male models that have been developed until recently. Previous reviews of human body finite element models have been used for this purpose: Yang et al. 2006, Labé 2008, Lamielle 2008 and Luet 2013.

The first model of the human abdomen including different parts for the abdomen cavity is the LAB [16] model as detailed in Lizee et al. 1998. As it can be seen on Figure 1.19c the abdomen was divided in only three solid parts. Further improvements of the model have been mentioned in Luet 2013.

The WSUHAM [17] model is detailed in Lee and Yang 2001. This model is limited to the abdomen region only as it can be seen on Figure 1.19d. It has however been enhanced in Shah et al. 2004 to become a full-body model.

The HUMOS [18] model has been developed as a joint project by the HUMOS consortium. The model has been detailed in Robin 2001 and an improved version, HUMOS 2 in Vezin and Verriest 2005. Figure 1.19e shows the HUMOS 2 model.

A full human body model has been developed by Ford Motor Company and detailed in Ruan et al. 2003. Figure 1.19g shows a full model view as well as an abdomen view of the model.

A full human body model has been developed by Takata company and mentioned in Zhao and Narwani 2005. It gathers together previous models developed by Wayne State University for the thorax, abdomen, shoulder and head-neck regions. This model has been further improved as mentioned in Zhao and Narwani 2007. Figure 1.19i shows the first version of the model.

From this point, highly detailed models of the internal organs of the abdomen have been developed. The first of those models, limited to the abdomen, has been developed in Labé 2008 as seen on Figure 1.19j. The model has been further improved in Chebil 2014.

Then the THUMS model with detailed internal organs have been released and described in Shigeta et al. 2009 (see Figure 1.19o). The previous version of the THUMS model can be seen on Figure 1.19m. This model has been described in Iwamoto et al. 2003.

16. Laboratoire d'Accidentologie et de Biomécanique
17. Wayne State University model of the Human AbdoMen
18. HUman MOdel for Safety

The most recent full body model is the GHBMC [19] model. It has been developed by a consortium of automotive manufacturers and universities. The model has a highly detailed abdominal region as can be seen on Figure 1.19k. The model is detailed in Gayzik et al. 2012.

19. Global Human Body Models Consortium

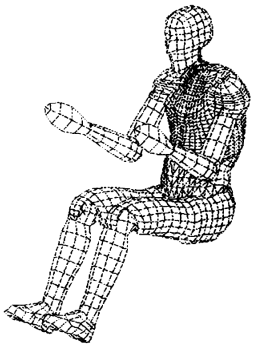

(a) LAB full model (Lizee et al. 1998)

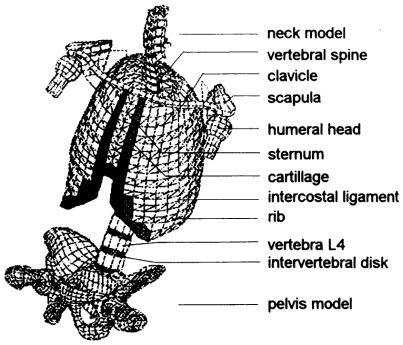

(b) LAB model thorax (Lizee et al. 1998)

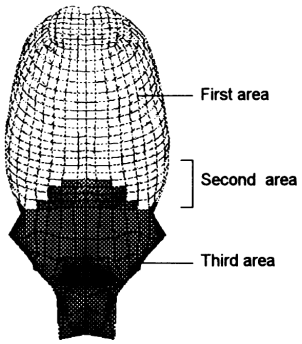

(c) LAB model abdomen (Lizee et al. 1998)

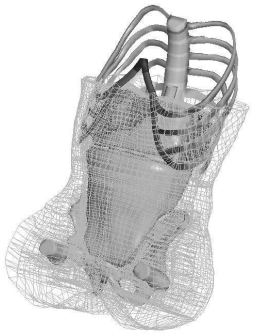

(d) WSUHAM model (Lee and Yang 2001)

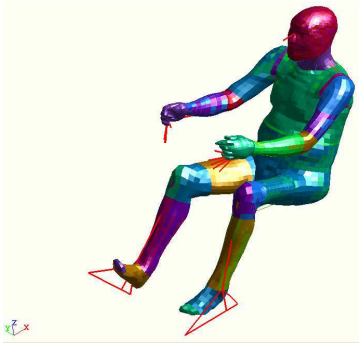

(e) HUMOS 2 full model (Vezin and Verriest 2005)

(f) HUMOS 2 abdomen (picture from Lamielle 2008)

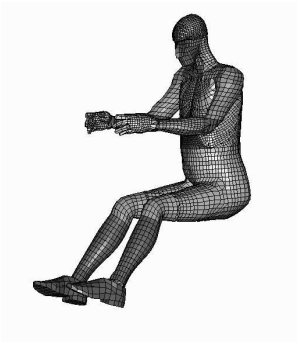

(g) Ford model (Ruan et al. 2003)

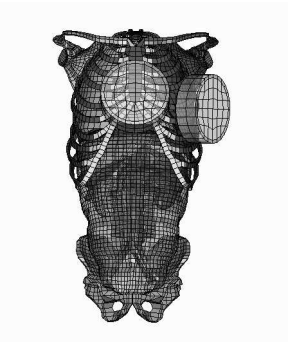

(h) Ford model abdomen (Ruan et al. 2003)

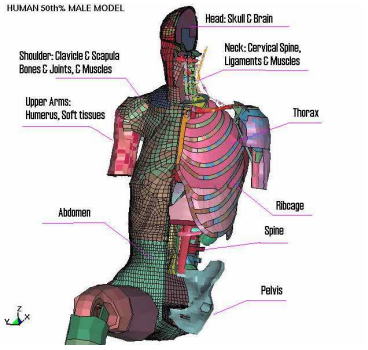

(i) Takata model (Zhao and Narwani 2005)

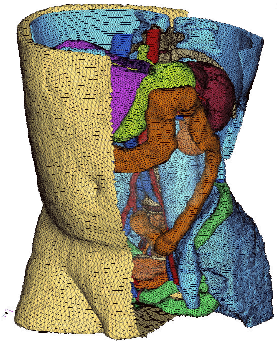

(j) Abdomen model from Labé 2008

(k) GHBMC full model (Gayzik et al. 2012)

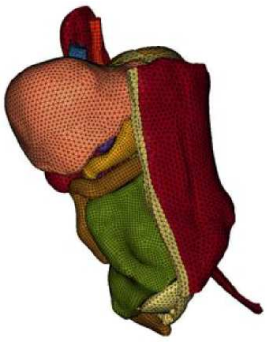

(l) GHBMC model abdomen (Gayzik et al. 2012)

Figure 1.19 – Overview of finite element human body models

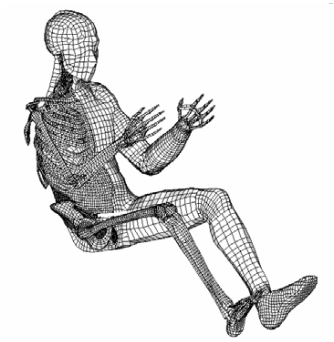

(m) THUMS model from Iwamoto et al. 2003

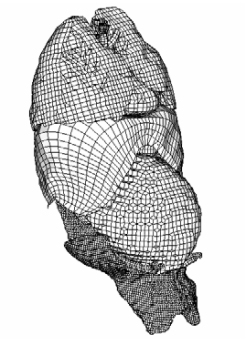

(n) THUMS model abdomen from Iwamoto et al. 2003

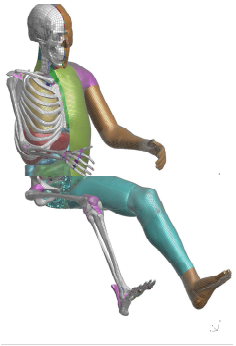

(o) THUMS model from Shigeta et al. 2009

(p) THUMS model abdomen from Shigeta et al. 2009

Figure 1.19 – Overview of finite element human body models (continued)

1.3.1.2 Comparison of the model responses

The above-mentioned models of the human abdomen have been validated against numerous tests described in the literature. Only frontal impacts test conditions will be reported here, according to the conditions described in the previous section.

Figures 1.20 shows the response of the models under the impact test described in Cavanaugh et al. 1986. The corridors from Lebarbé et al. 2015 are overlaid to the model responses. Different impactor masses and impact velocities were used to validate the different models. Figure 1.21 shows the responses if some models under the impactor test described in Hardy et al. 2001. The impactor mass was 48 kg for this test. The corridor defined as standard deviation boundaries versus mean penetration from PMHS tests was plotted.

Data for the validation of the HUMOS model were taken from Haug et al. 2004. The response of the model to a 32 kg 6.1 m s^{-1} can be seen on Figure 1.20a.

The WSUHAM has been validated against impactor tests in Lee and Yang 2001. Four conditions at different impact velocities and impactor masses were performed and can be seen on Figure 1.20.

The validation of the Ford model has been described in Ruan et al. 2005. Three actual impact conditions from Cavanaugh et al. 1986 were performed, simulating tests 24, 41 and 57. The velocities are reported on the plots legends of Figure 1.20. The impactor masses were not exactly 32 kg and 64 kg but those values have been rounded for clarity. Two tests from Hardy et al. 2001 (GI6 and GI8) were also simulated. The mass of the impactor was 48 kg and the velocities values are reported on Figure 1.21.

Impactor validation of the Takata model has been performed in Zhao and Narwani 2005 against the

condition described in Cavanaugh et al. 1986 (Figure 1.20a) and against the condition from Hardy et al. 2001 (Figure 1.21).

The abdomen-only model from Labé 2008 has been subjected to two conditions from Cavanaugh et al. 1986. Two impact velocities were used, corresponding to two different impactor masses. The masses were not exactly 32 kg and 64 kg but the values have been rounded for clarity. The model responses can be seen on Figures 1.20a and 1.20c.

The first version of the THUMS model has been subjected to a 32 kg $10.4\,\mathrm{m\,s^{-1}}$ as seen on Figure 1.20b. This has been reported in Iwamoto et al. 2002. The latest version of the model faced in Shigeta et al. 2009 an impact from Cavanaugh et al. 1986 as reported on Figure 1.20a.

The GHBMC model response has been compared to several impact cases in Beillas and Berthet 2012 under a $6\,\mathrm{m\,s^{-1}}$ impact from Hardy et al. 2001 and is presented on Figure 1.21.

Fewer models have been validated under seatbelt tests than under impactor tests. The reasons for this are the difficulties to reproduce the input conditions of the tests performed on PMHS in the literature and the challenge for the models to show a biofidelic behaviour at rapidly changing strain rates. Figure 1.22 shows the model responses. The corridor defined as standard deviation boundaries versus mean penetration from PMHS tests was plotted with no normalisation, since Lebarbé et al. 2015 reported that no normalisation method was suited to seatbelt loadings.

In Shah et al. 2004, a seatbelt test condition from Hardy et al. 2001 was reproduced on the WSUHAM model. A time-velocity profile from test data (motion of the ram pulling the belt) was applied to the belt of the model. The response of the model can be seen on Figure 1.22a.

The Ford model has been submitted to the configuration from Hardy et al. 2001 as detailed in Ruan et al. 2005. It is presumable that the belt velocity was applied although it is not mentioned. In Rouhana et al. 2010, the force profile (with some modifications) from Foster et al. 2006 A2 test was applied on the belt of the model. The response of the model to those tests can be seen on Figures 1.22a and 1.22b.

Figure 1.22a shows the response of the Takata model to the condition from Hardy et al. 2001 as described in Zhao and Narwani 2005. It is not detailed which quantity from the test data was applied to the seatbelt in the simulation.

The THUMS model has been subjected to the seatbelt A condition test from Foster et al. 2006. The belt was pulled with a maximum velocity of $6.9\,\mathrm{m\,s^{-1}}$. The result of this test is displayed on Figure 1.22b.

All the presented models were correctly representing the stiffness of the PMHS data under impactor loading, including rate-sensitivity. For the low velocity condition from Cavanaugh et al. 1986 (Figure 1.20a), the models tend to predict a stiffness in the higher part of the corridor and to be out of the corridor after a certain penetration. The model from Labé 2008 has a higher stiffness than the corridor bounds. This can be due to the fact that PMHS responses from subject impacted at different velocities were used to create the corridor. For the models submitted to the Hardy et al. 2001 conditions, the models responses are also on the upper part of the corridor for the $6\,\mathrm{m\,s^{-1}}$ condition. This can be explained by the fact that the corridor presented was non normalised and that the PMHS have abdomen depths from 29 cm to 31 cm. The 50th percentile male abdomen depth being 26 cm (Schneider et al. 1989), a normalised comparison in terms of abdomen depth would bring the model and PMHS curves closer.

Under seatbelt loading condition, the model responses are close to the corridors for both conditions (Figure 1.22), except for the Ford model which presents a lower stiffness.

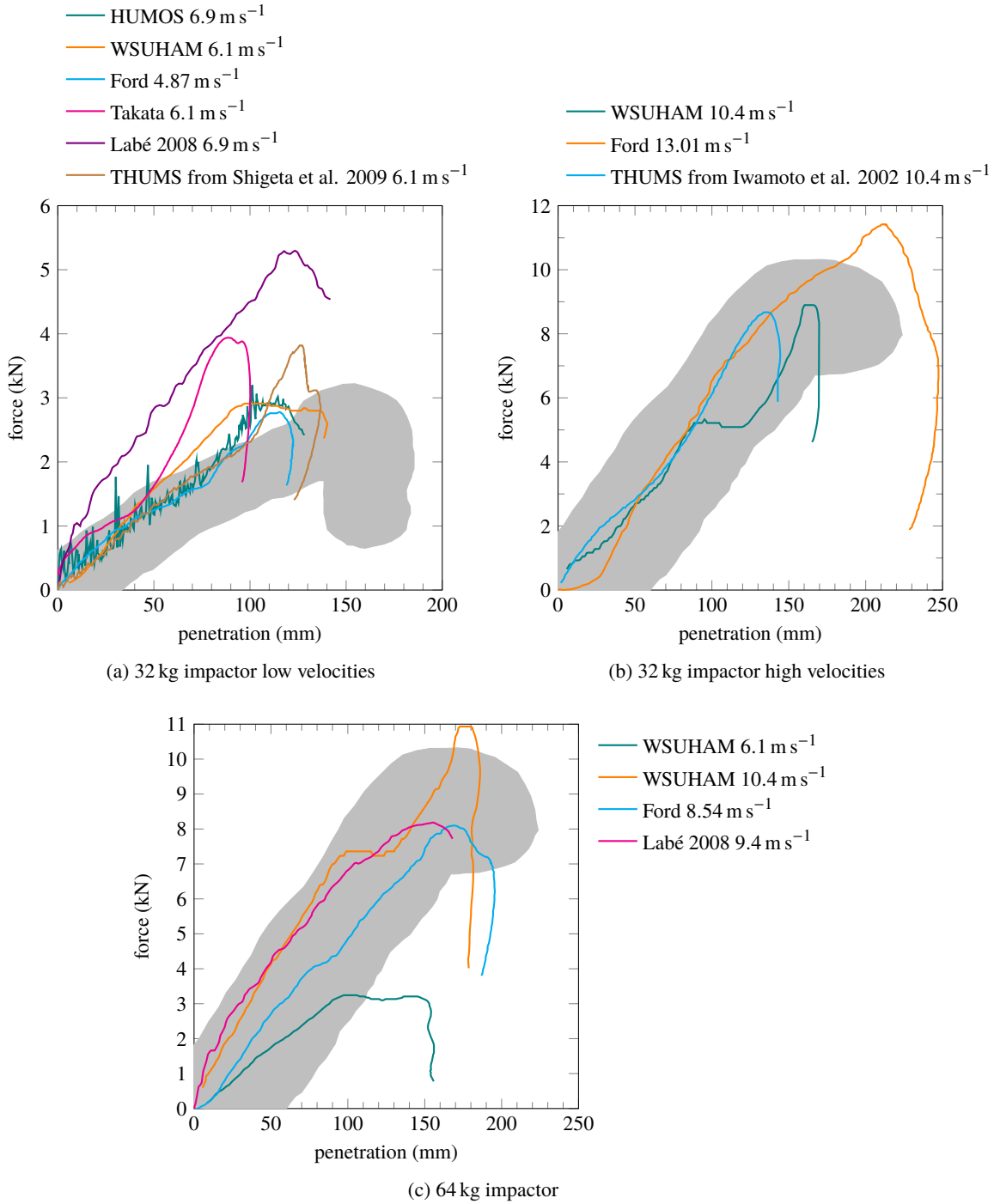

(a) 32 kg impactor low velocities

(b) 32 kg impactor high velocities

(c) 64 kg impactor

Figure 1.20 – Finite element models responses under Cavanaugh et al. 1986 impactor test

The mass of the impactor used in the test is mentioned in each subfigure caption and the impact velocity is specified in the plot legend

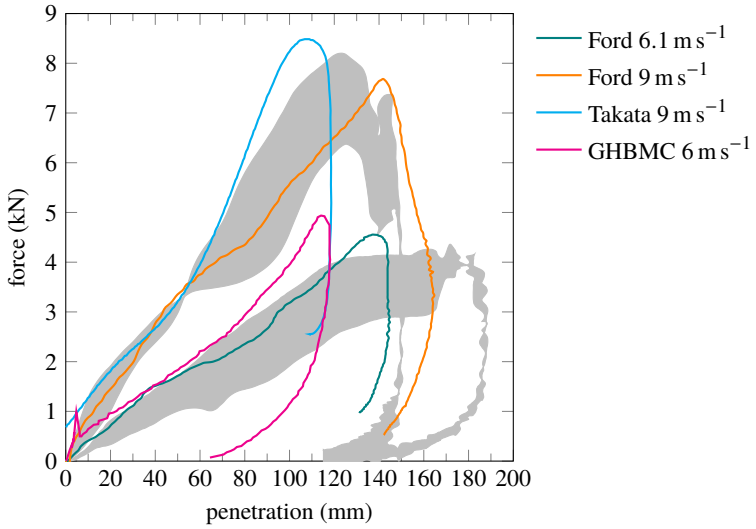

Figure 1.21 – Finite element models responses under Hardy et al. 2001 lower-abdomen impactor test
The impact velocity for each test is specified in the plot legend
Corridors are non-normalised

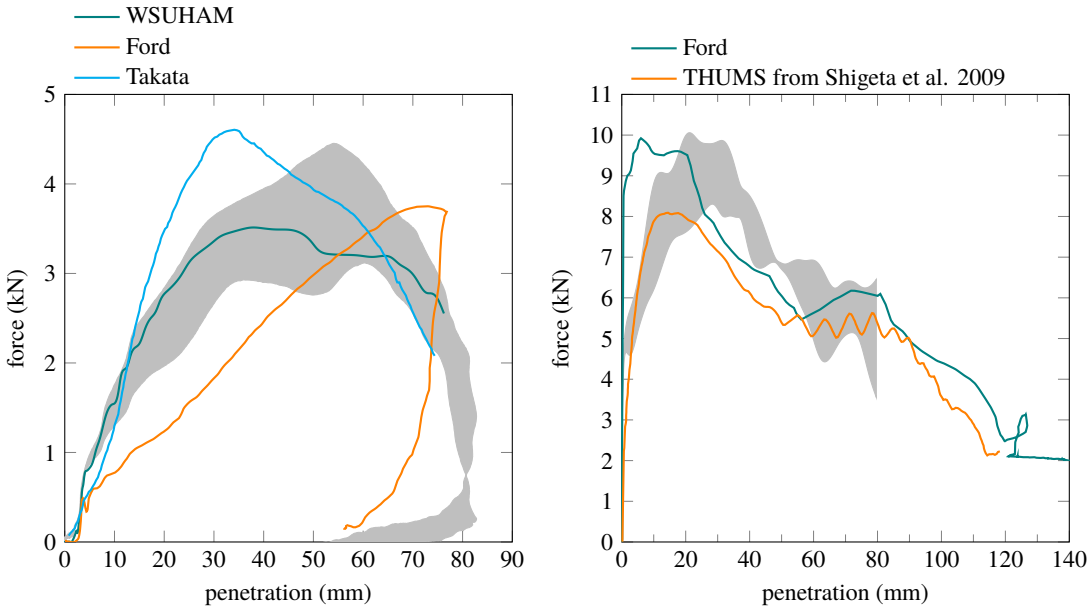

(a) Hardy et al. 2001 seatbelt test

(b) Foster et al. 2006 seatbelt test

Figure 1.22 – Finite element models responses under seatbelt tests
Corridors are non-normalised

1.3.1.3 Injury prediction

So far, finite element human body models have been used for injury prediction by looking at maximum values of local variables such as stress or strain in specified organs. Shigeta et al. 2009 mentioned a 30 % value for first principal strain for solid organs (liver) and 120 % for hollow organs (stomach, intestine) as maximum acceptable value before injury. Figure 1.23a shows injury prediction results for the THUMS model under an impactor test condition (Cavanaugh et al. 1986). However, although most of the intestine properties for the THUMS model were taken from Yamada 1970, the reference strain value used were not documented. First principal strain was also the indicator used in Kitagawa and Yasuki 2013 and was found to be correlated with ribcage deflections only for the spleen. Figure 1.23b shows the strain values for the organs of the THUMS model for a frontal collision simulation. However, no validation of the internal behaviour of finite element models of the human body have been carried on so far. For instance, PMHS tests with markers placed in the organs and imaged by X-ray have been performed in Howes et al. 2012 and Howes et al. 2015. Beillas et al. 2013 performed impact tests on PMHS with an impactor containing an ultrasound probe and another probe was placed on the opposite side of the subject, both linked to an ultrafast data acquisition system and imaging the internal organs. These new experimental protocols allowing to monitor the internal motion of organs during an impact test could give reference data for internal model validation.

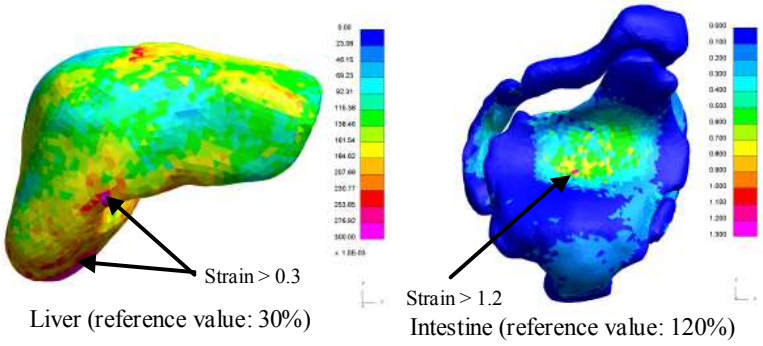

(a) Shigeta et al. 2009

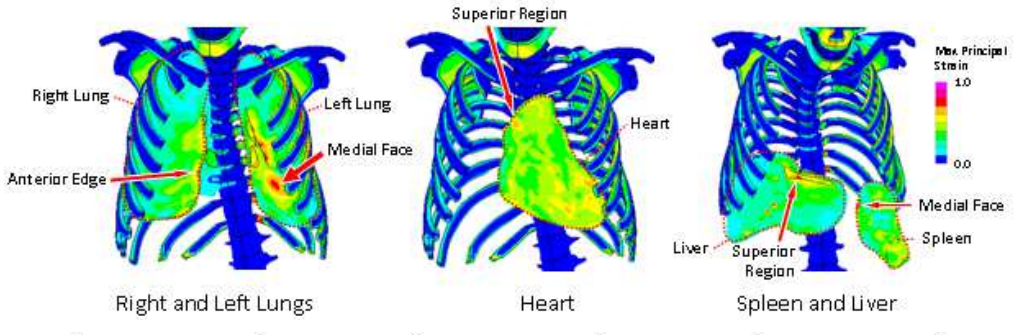

(b) Kitagawa and Yasuki 2013

Figure 1.23 – Injury prediction with the THUMS model

The new generation of human body finite element models with detailed description of the internal structure of the human abdomen is validated against PMHS test data but not yet regarding internal organs displacement or internal organ pressure. However, the fact that these models include a detailed anatomical representation of the abdomen organs as well as specific material data for each organ should allow them to be used for injury prediction on a global scale such as a group of organs or a region of the abdomen.

1.3.2 Crash test dummies

1.3.2.1 Overview of frontal impact dummies

The current regulatory dummy is the Hybrid III, first desbribed in Foster et al. 1977. It was not equipped with an instrumented abdomen. The standard abdomen was made of foam enclosed in a vinyl coating and was not linked to the rest of the body but only inserted in the gap between the thorax and the pelvis. This abdomen can be seen on Figure 1.24a.

The THOR dummy was originally a new torso (Schneider et al. 1992; Haffner et al. 1994) for the Hybrid III dummy called TAD-50M [20]. The TAD-50M has evolved to THOR Alpha (Haffner et al. 2001), then to THOR NT (Shams et al. 2005) and finally to THOR Mod-kit (Ridella and Parent 2011). The abdomen of the THOR dummy is made of two foam block of different stiffnesses and is instrumented with deflection sensors.

Figure 1.24 shows the anatomical difference between the Hybrid III and THOR. For instance, the THOR dummy has one more ribs (seven instead of six) than Hybrid III, representing better the human anatomy consisting of ten ribs.

(a) Hybrid III (b) THOR

Figure 1.24 – Anatomy comparison between Hybrid III and the THOR dummy (Shaw et al. 2004)

1.3.2.2 Previous abdomen concepts

Since the Hybrid III did not have an instrumented abdomen, a frangible abdomen had been proposed in Rouhana et al. 1989 to detect submarining and have an history of the penetration sustained abdomen (Figure 1.25a). A first instrumented abdomen made of elastic foam rubber has been developed in Ishiyama et al. 1994 along with a measurement system called TADAS [21] that measures the contour variation of the abdomen (Figure 1.25b). More recently, Rouhana et al. 2001 designed a rate-sensitive abdomen with improved biofidelity for the Hybrid III. This abdomen consisted in a silicone rubber shell filled with silicone gel. It incorporated a deflection measurement system based on electrical resistance (Figure 1.25c).

The design of an instrumented abdomen for the THOR dummy has been described in Rangarajan et al. 1996 and Rangarajan et al. 1998. This design has been used for the Alpha, NT and Mod-kit versions. It is composed of two foam block attached at the back to a plate, itself attached to the spine

20. Trauma Assessment Device 50th percentile male
21. Toyota Abdominal Deformation Analyzing System

of the dummy. The foam block and the plate are placed inside a fabric bag. Telescopic deflection sensors are attached to the plate brackets and go through the foam blocks. The original sensors were DGSP [22] sensors until the Mod-kit version where IRTRACC [23] sensors were implemented for the same purpose. Figures 1.25d and 1.25e shows the abdomen parts and assembly.

An alternative to the THOR NT dummy called THOR FT has been developed and included a different abdomen design as well as a pelvis modification. This abdomen was made of a single foam block enclosed in a vinyl skin layer and was equipped with IRTRACC sensors. The lower abdomen response of the FT dummy was very similar to the NT response according to Onda et al. 2006. Figure 1.25f shows the THOR FT abdomen and Figures 1.25g and 1.25h compre the pelvis for the two dummy versions.

An abdomen for the THOR dummy designed by GESAC and Toyota Motor Corporation have been mentioned in Hanen et al. 2011 (Figure 1.25i). This abdomen consists in a urethane core moulded around three metal weights (of approximately 250 g) and enclosed in a urethane shell. The total weight of the insert is 3.6 kg. This abdomen proved to have a really stiff response compared to biofidelity corridors.

22. Double Gimbaled String Potentiometer
23. Infra Red Telescoping Rod for the Assessment of Chest Compression

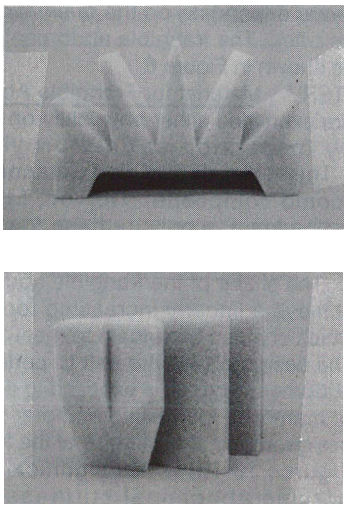

(a) Frangible abdomen for the Hybrid III (Rouhana et al. 1989)

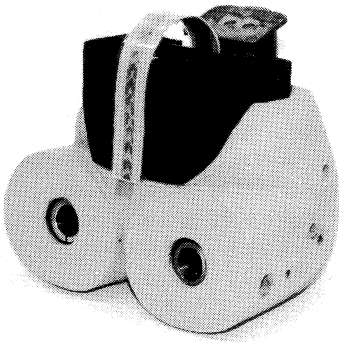

(b) Abdomen from Ishiyama et al. 1994 for the Hybrid III

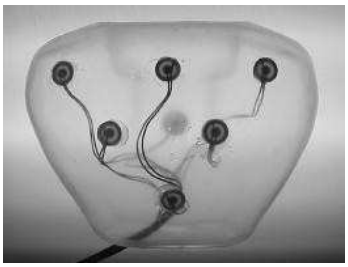

(c) Rate-sensitive abdomen for the Hybrid III (Rouhana et al. 2001)

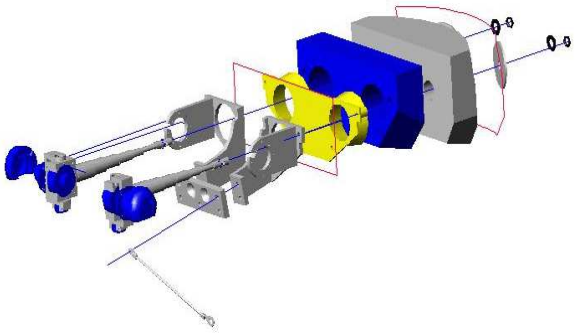

(d) THOR abdomen exploded view (THOR NT Manual, NHTSA / GESAC, Inc. 2005b)

(e) THOR abdomen assembly view (THOR NT Manual, NHTSA / GESAC, Inc. 2005b)

(f) THOR FT abdomen (Onda et al. 2006)

(g) THOR FT pelvis (Onda et al. 2006)

(h) THOR NT pelvis (Onda et al. 2006)

(i) GESAC / Toyota abdomen (Hanen et al. 2011)

(j) IFSTTAR / Toyota prototype abdomen

Figure 1.25 – Abdomen concepts for Hybrid III and THOR dummies

1.3.2.3 IFSTTAR / Toyota prototype abdomen

Based on all the existing dummy abdomen concepts, the need for an abdomen equipped with an omni-directional measurement and with improved biofidelity appears. The abdomen from Rouhana et al. 2001 showed acceptable biofidelity but problems were reported with the measurement system. Furthermore, this abdomen was designed for the Hybrid III dummy, and therefore is not attached to others dummy elements but just inserted between the ribcage and the pelvis.

This led to the development of the last prototype abdomen for the THOR dummy that was developed by IFSTTAR and Toyota Motor Europe and described in Compigne et al. 2015. Figure 1.25j shows the prototype mounted on the dummy. It includes in the standard THOR abdomen two APTS pressure sensors (presented in Beillas et al. 2012) and additional steel masses in order to add 825 g at the front of the abdomen. The biofidelity of IFSTTAR / Toyota prototype abdomen has been evaluated in Compigne et al. 2015 under impactor and seatbelt loading conditions, respectively under Cavanaugh et al. 1986 6.1 m s^{-1} impact and Foster et al. 2006 seatbelt loading with pretensioners (B condition). Figure 1.26 shows the response curves overlaid with the respective PMHS corridors. The prototype has a closer response to the PMHS data under the impactor loading due to a decreased stiffness after the characteristic inflexion in the force-penetration diagram. The biofidelity is also improved under seatbelt loading due to a higher inertia created by the additional masses creating the initial force peak.

The IFSTTAR / Toyota abdomen has therefore an acceptable biofidelity and an adequate measurement system. It can therefore be used for discriminating injurious loadings based on the pressure measurements of the APTS sensors, if a specific injury criteria is developed.

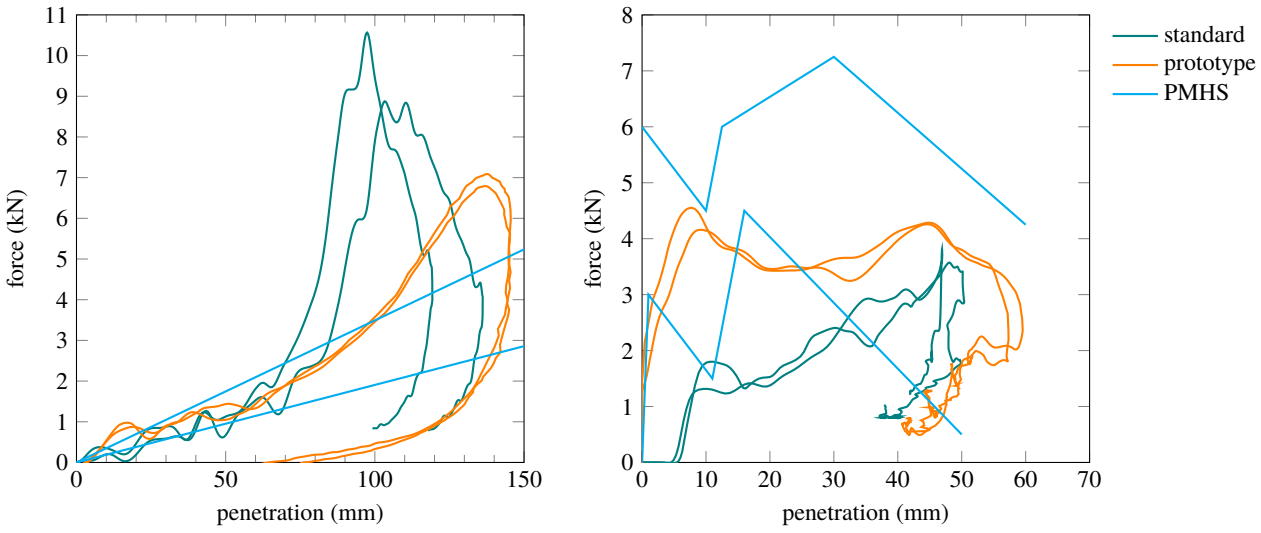

(a) Cavanaugh et al. 1986 impactor condition

(b) Foster et al. 2006 B seatbelt condition

Figure 1.26 – Biofidelity evaluation of IFSTTAR / Toyota prototype abdomen (Compigne et al. 2015)

1.4 Conclusion and objectives of this thesis

There is a global need to decrease the number of road fatalities, frontal impact being the most common crash case. The abdomen is a crucial region regarding serious to critical injuries, especially for rear passengers and in case of submarining. However, no injury criterion for the abdomen is applied in the regulation or by consumers organisations. The THOR dummy is planned to become the future dummy used in regulation and consumers tests but the biofidelity of its abdomen needs to be improved and its sensors measurement needs to be linked to an injury risk. The recent abdomen prototype developed by IFSTTAR and Toyota has shown better biofidelity than the standard abdomen and has the ability to estimate omni-directional loading severity thanks to APTS sensors. Furthermore, recently developed finite element models of the human body having a highly detailed geometry of the abdominal organs will allow for injury prediction on a regional level based on engineering parameters obtained from impact simulations.

The aim of this work is to improve the biofidelity of the IFSTTAR / Toyota prototype through finite element modelling, to evaluate its influence on the global dummy behaviour and to develop an injury criteria based on abdominal sensors pressure measurements.

Chapter 2

THOR abdomen prototype finite element model development and validation

Contents

2.1 Introduction

A finite element model of the THOR dummy has been developed by NHTSA. The validation of this model under impact conditions needs to be confirmed, especially for the abdomen region with regards to loading velocity dependency. The validation regarding test data should be assessed for both impactor and seatbelt loading cases. In order to be able to reproduce a variety of test configurations, the prototype abdomen described in Compigne et al. 2015 should also be available as a finite element model, including the APTS sensors, and validated against test data. Recently performed tests from NHTSA's VRTC [1] on this prototype abdomen provide data for validation. Once the validation versus test data will be assessed, the prototype abdomen model could be used to propose design changes or material modifications in order to improve its biofidelity.

2.2 Finite element model of the THOR abdomen

A finite element model of the THOR dummy under LS-DYNA has been developed since 2000 by NHTSA and other partners. The version 2.0.5 model of the Mod-kit dummy was used. The model is described in THOR FE [2] Manual (Panzer et al. 2015). The model has been built using CAD [3] drawings of the dummy. It contains 469 parts, approximately 460 000 elements and 237 000 nodes. Rigid and deformable material properties derived from impact test data are used. Figure 2.1a shows a global view of the dummy model.

Figure 2.1b shows the upper and lower abdomen of the dummy model. Both abdomens consist in a front and a rear foam block, linked to a plate attached to the dummy spine. Tables 2.1 shows the properties of the main deformable parts of the dummy abdomen and pelvis. According to GESAC, Inc. 1999, the front foam material is an open cell charcoal polyester and the rear foam material is a closed cell sponge rubber. Figure 2.2 shows the material curves associated with the upper and lower abdomen parts for different strain rates. These curves are used for hyperelastic material models that allow strain rate dependency (`MAT_057: LOW_DENSITY_FOAM` and `MAT_083: FU_CHANG_FOAM`, detailed in Appendix C).

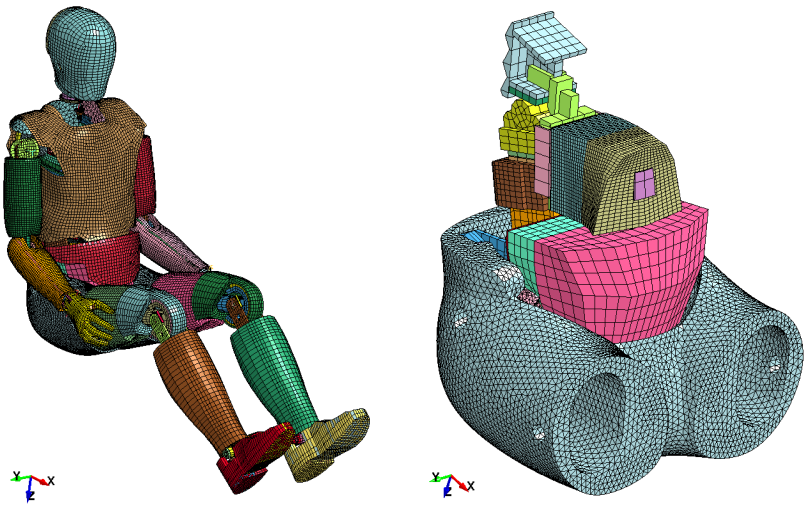

(a) Global view (b) Upper and lower abdomen

Figure 2.1 – THOR finite element model

1. Vehicle Research and Test Center
2. Finite Element
3. Computer-Aided Design

part	type	material model	density (kg m^{-3})	mass (g)
pelvis foam	volumetric	hyperelastic compressible (`MAT_083`)	199	2154
pelvis skin	shell	elastic (`MAT_001`)	940	1790
upper rear foam	volumetric	hyperelastic compressible (`MAT_083`)	1500	808
upper front foam	volumetric	hyperelastic compressible (`MAT_083`)	1500	764
lower rear foam	volumetric	hyperelastic compressible (`MAT_057`)	140	132
lower front foam	volumetric	hyperelastic compressible (`MAT_057`)	150	288
lower jacket	shell	hyperelastic incompressible (`MAT_181`)	160	46

Table 2.1 – THOR abdomen model parts list

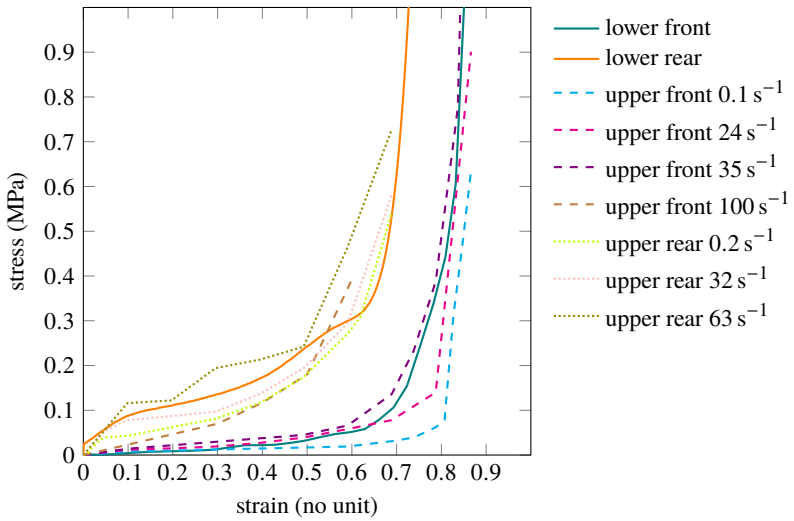

Figure 2.2 – Material curves for the foam parts of THOR abdomen

2.2.1 Evaluation

The component-level response of the dummy has been evaluated in THOR FE Manual (Panzer et al. 2015) according the the procedures detailed in THOR Certification Manual (NHTSA / GESAC, Inc. 2005a) and sled tests performed at 11 m s^{-1}with a 16 *g*'s deceleration peak (protocol from Untaroiu et al. 2009). For the global evaluation, the belt forces, landmarks trajectories and kinematics, neck load cells signals and femur forces were in fair adequation with the test data.

However, regarding the component level evaluation, the upper and lower abdomen responses showed margin for improvement. Figure 2.3a shows the upper abdomen validation under a 8 m s^{-1} impact with a 18 kg wheel shaped impactor according to Nusholtz and Kaiker 1994 and Figure 2.3b shows the lower abdomen validation under a 6.1 m s^{-1} impact with a 32 kg impactor according to Cavanaugh et al. 1986. The response of the FE model shows a higher force response than the test data for both abdomen regions. This is believed to be due to imprecisions in the material characterisation for the abdomen foams and the pelvis.

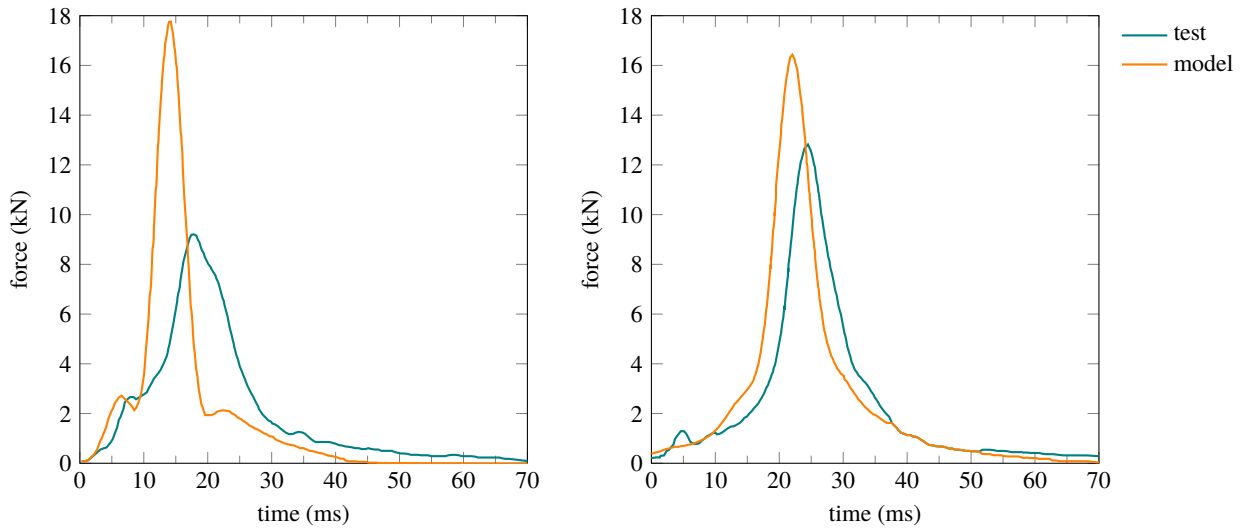

(a) Upper abdomen (b) Lower abdomen

Figure 2.3 – THOR finite element model abdomen validation (THOR FE Manual, Panzer et al. 2015)

2.2.2 Improvements

Improvements to the material properties of the THOR dummy model were performed as part of this work. The stress values of the pelvis material curves were multiplied by 0.16 according to tests performed by Toyota Motor Corporation and the front foam material properties have been re-characterised as part of this work to introduce material strain rate effect, the front foam being the part that influences the most the lower abdomen response. Drop tests were performed on cubic foam samples by by Toyota Motor Europe at strain rates from $6 \times 10^{-4}\,\mathrm{s}^{-1}$ to $120\,\mathrm{s}^{-1}$. The original material model was a simplified hyperelastic foam model (`MAT_057: LOW_DENSITY_FOAM`) and was replaced by a rate dependent hyperelastic foam model (`MAT_083: FU_CHANG_FOAM`) with new tabulated curves for different strain rates as seen on Figure 2.4.

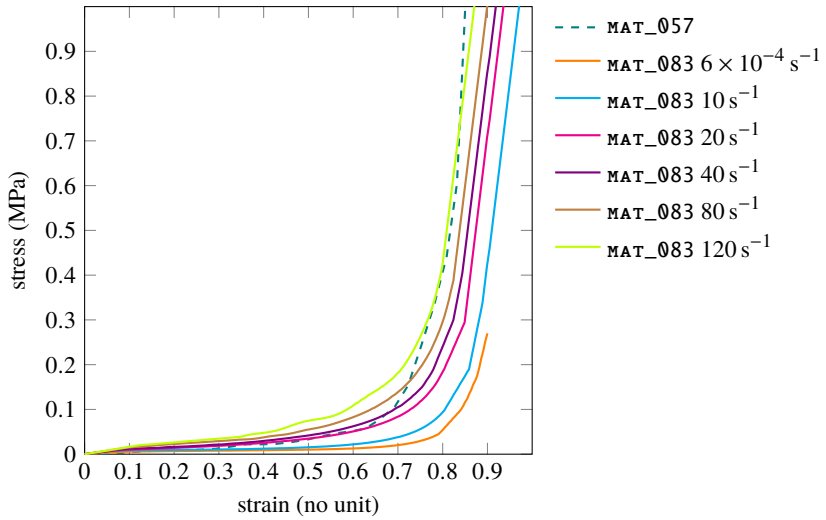

Figure 2.4 – New material curves for the front foam part of the lower abdomen

The modified dummy model has been validated using tests performed by NHTSA's VRTC and provided for this project. Two conditions were performed: a seatbelt loading reproducing the PMHS tests from Hardy et al. 2001 and an impactor loading reproducing the PMHS tests from Cavanaugh et al. 1986. For the seatbelt condition, the belt was pulled at the back of the dummy

by a pneumatic system, the dummy back being free. Figure2.5 shows the two different set-ups. Three different pressures were applied to the belt retraction system: 4.5 bar, 5.5 bar and 6.6 bar. The 6.6 bar condition corresponds to the loading applied to PMHS in Hardy et al. 2001. Figure 2.6a shows the different belt retraction profiles. For the impactor case, a 32 kg mass (diameter 25 mm) stroke the dummy with an initial velocity of 6.1 m s^{-1}.

In the simulations, the dummy was positioned seated according to the physical test and gravity was applied for 500 ms in order to obtain the initial geometry for the simulations. Initial stresses and strains resulting from the gravity deformation were not taken into account. Figure 2.7 shows the positioning and gravity deformation process. A fixed timestep of 4×10^{-4} ms was achieved through mass scaling.

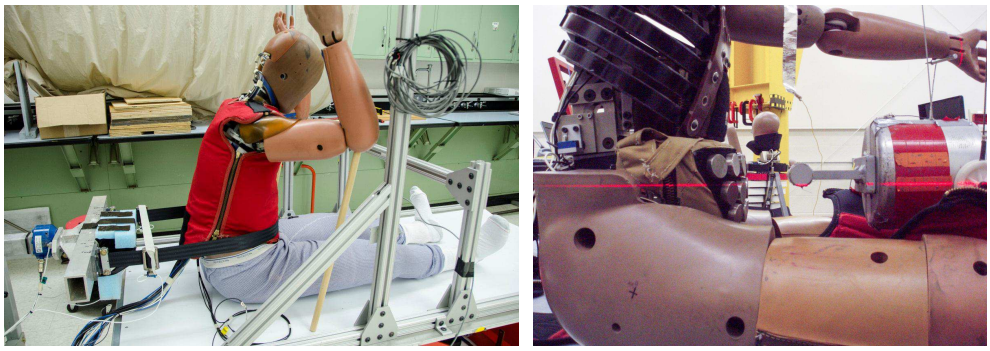

(a) Seatbelt (b) Impactor

Figure 2.5 – Test set-ups from VRTC

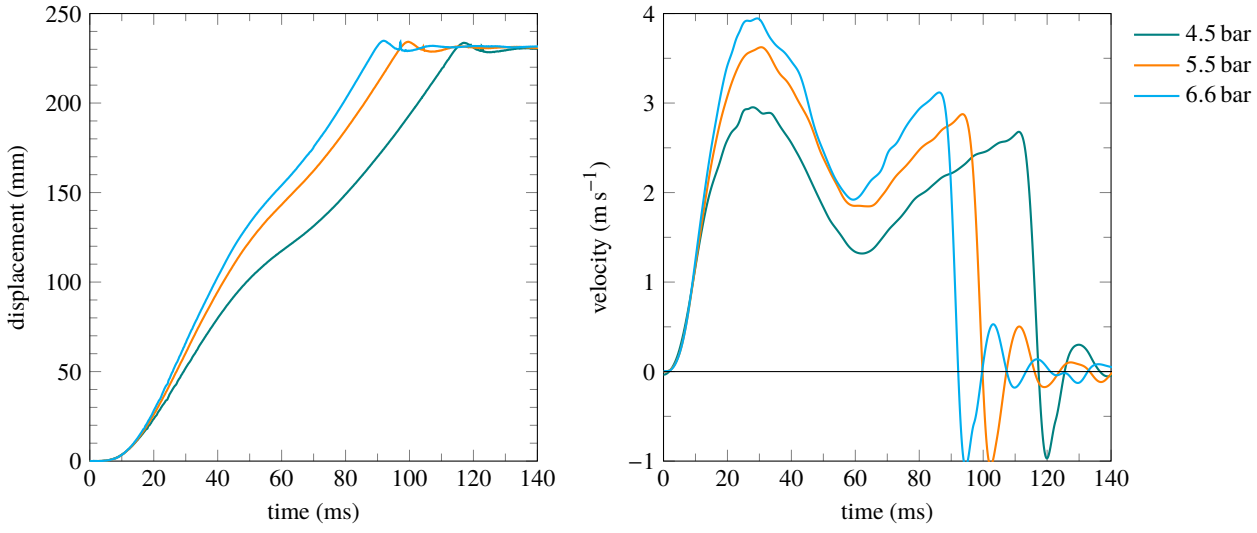

(a) Belt retraction (b) Belt retraction velocity

Figure 2.6 – Belt retraction velocity profiles from VRTC test data

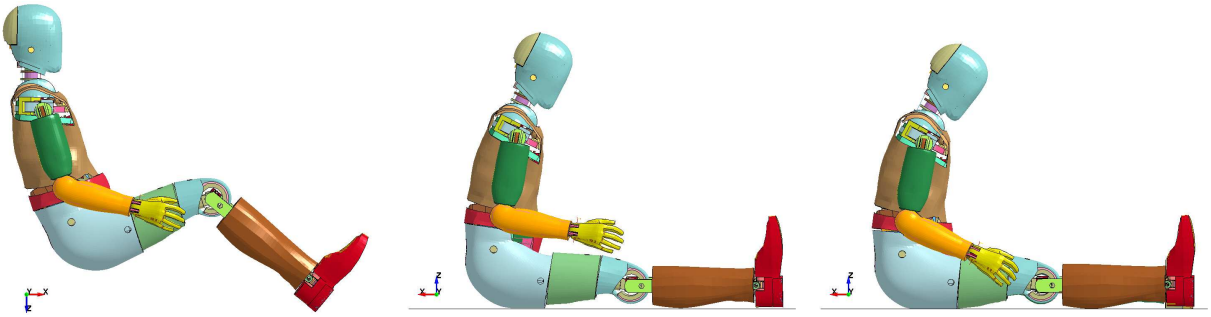

(a) Initial model (b) Before gravity deformation (c) After gravity deformation

Figure 2.7 – Positioning and gravity deformation

2.2.2.1 Seatbelt condition

The seatbelt conditions having a similar input profile, the dummy model response will be considered under the 6.6 bar condition since the standard dummy abdomen has only been tested under this condition. The results are presented on Figure 2.8. The belt retraction over time from test data was applied to the model, the back of the dummy being unrestrained. This condition corresponds to a 6.6 bar pressure applied to the belt retraction system. The model predicts well the response from test data, although there is a second force peak from the test data, that is not entirely reproduced by the simulation. But the second peak in the simulation is due to the seatbelt almost sliding over the pelvis, which is not the same phenomenon as in the test. Figure 2.9 shows the deformed shape of the model for different simulation times.

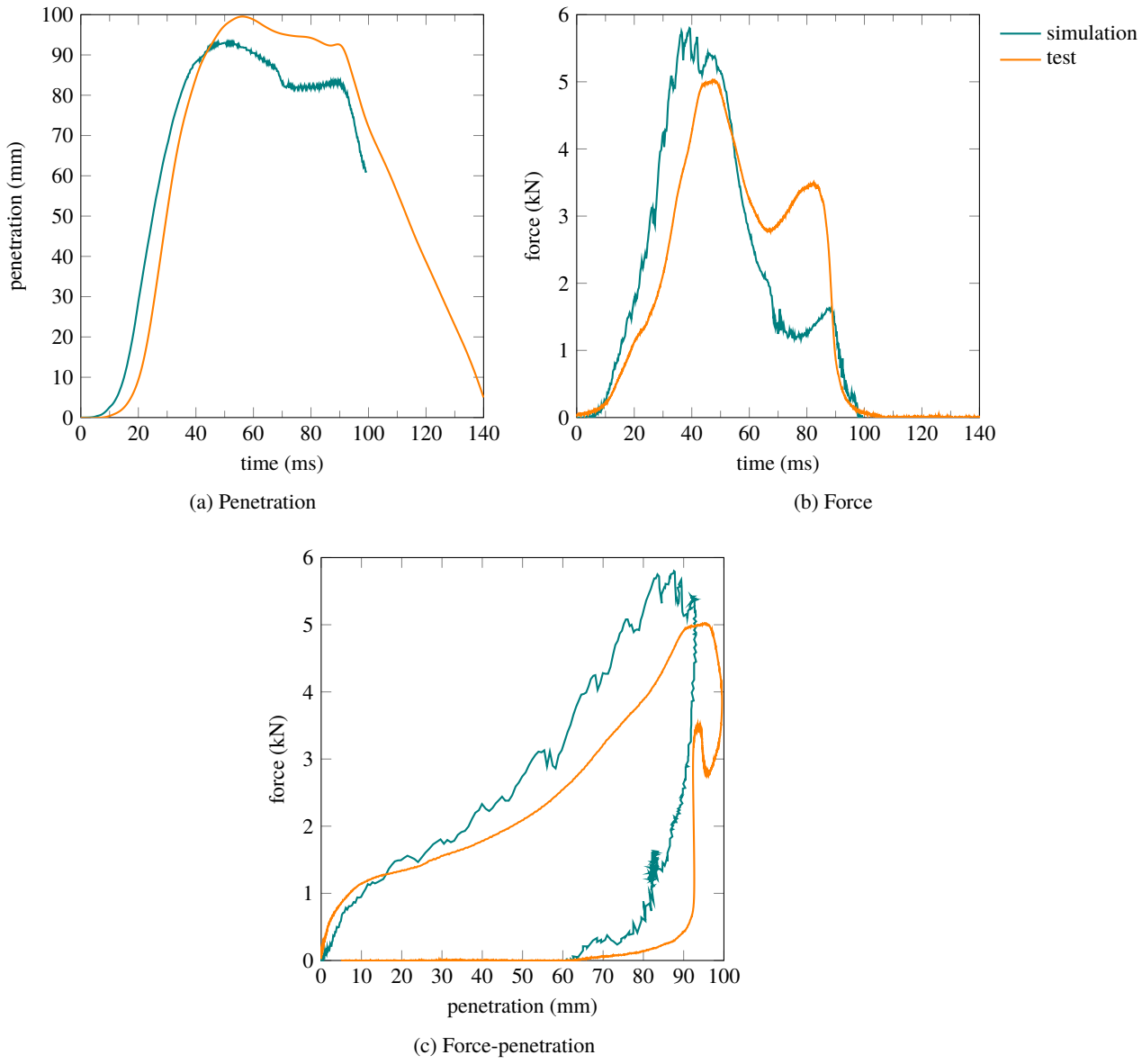

(a) Penetration

(b) Force

(c) Force-penetration

Figure 2.8 – THOR Mod-Kit response under Hardy et al. 2001 6.6 bar seatbelt loading

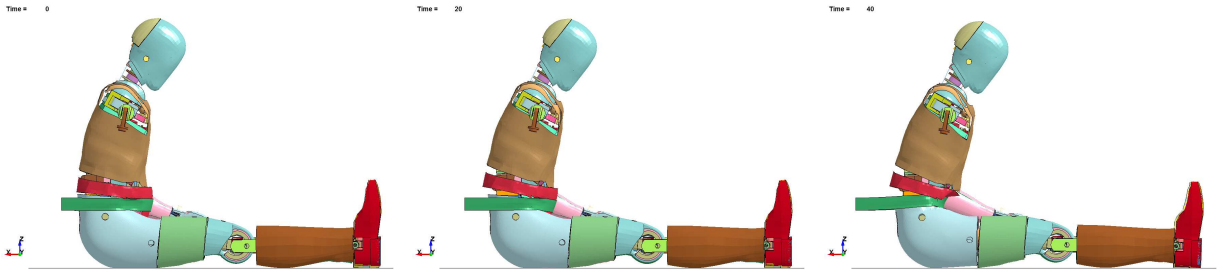

(a) 0 ms (b) 20 ms (c) 40 ms

(d) 60 ms (e) 80 ms (f) 98 ms

Figure 2.9 – THOR Mod-Kit deformed shape under Hardy et al. 2001 6.6 bar seatbelt loading
The right arm of the dummy has been blanked

2.2.2.2 Impactor condition

The dummy model response under impactor condition can be seen on Figure 2.10. The test data were not available over time, only as force / penetration graph. The force from the simulation was filtered at CFC [4] 180, the same way as the test data, which reduced the observed force peak. However the simulation results show a too high force and less penetration compared to the test data. The higher peak force is due to the abdomen foams being fully compressed and the impactor contacting the abdomen plate as it can been seen on Figure 2.10c. Here the test on the physical dummy is not properly reproduced by yhe model in terms of dummy behaviour. Figure 2.11 shows the model deformed shape along the simulation.

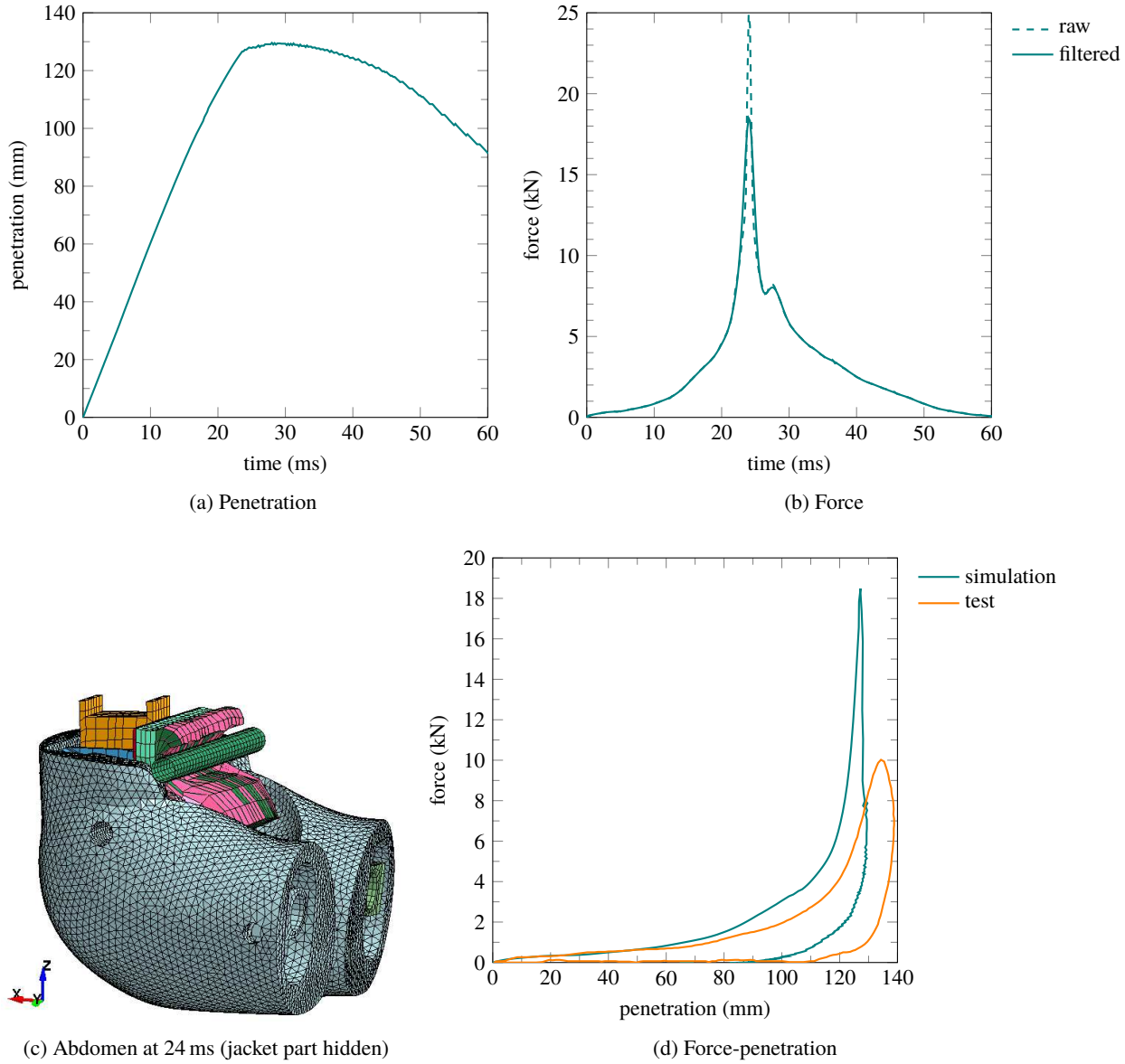

(a) Penetration

(b) Force

(c) Abdomen at 24 ms (jacket part hidden)

(d) Force-penetration

Figure 2.10 – THOR Mod-Kit response under impactor loading

4. Channel Frequency Class

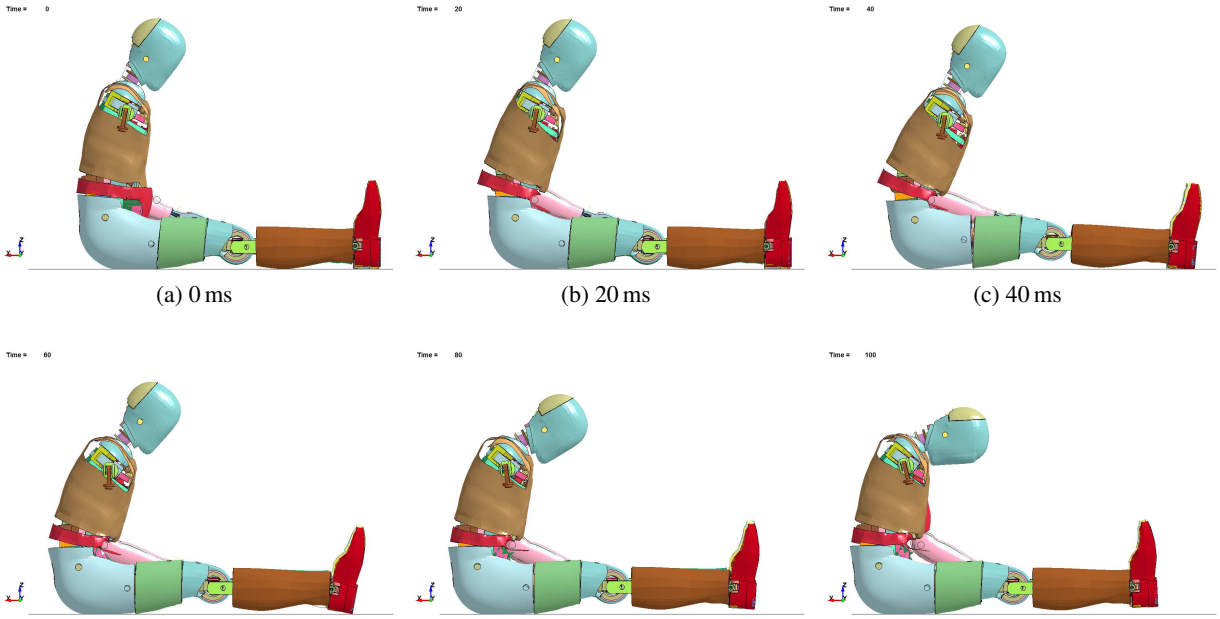

(a) 0 ms (b) 20 ms (c) 40 ms

(d) 60 ms (e) 80 ms (f) 100 ms

Figure 2.11 – THOR Mod-Kit deformed shape under impactor loading
The right arm of the dummy has been blanked

2.3 Development of prototype abdomen finite element model

2.3.1 Prototype description

The prototype abdomen developed for the THOR dummy by IFSTTAR and Toyota Motor Europe is a modification of the dummy standard abdomen. DGSP sensors were removed and replaced by two APTS sensors placed in vertical position thanks to holes drilled in the front foam part as described in Compigne et al. 2015. The APTS sensors (presented in Beillas et al. 2012) consist in a 50 mm diameter polyurethane bladder filled with paraffin oil and equipped with a pressure sensor. In order to increase the initial inertia response of the abdomen, 825 g of additional mass were added through the attachment of fifteen steel cylinders attached to the fabric bag of the dummy abdomen by a Velcro layer. Figure 2.12 shows the APTS sensors and the prototype abdomen.

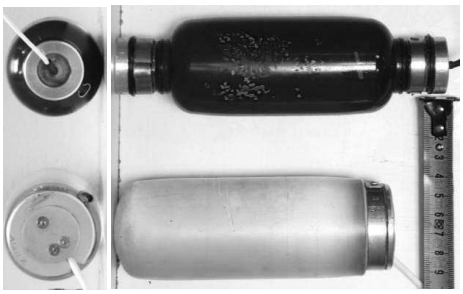

(a) APTS sensors (Beillas et al. 2012)

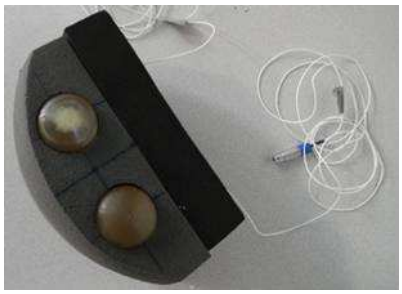

(b) Prototype abdomen

(c) Abdomen with additional masses

Figure 2.12 – IFSTTAR / Toyota Motor Europe prototype abdomen

2.3.2 Model development

The model of the standard dummy was modified to include the model of the prototype abdomen. The APTS polyurethane bladders were modelled as an elastic material with an 3.25 MPa Young's modulus and a 0.38 Poisson's ratio. The APTS fluid is modelled with a solid material but includes an equation of state with only one coefficient which gives a relationship between the pressure in the material (P) and the current volume of the material (V) as described by Equation 2.1. This modelling method for this kind of structure have been described in Soni and Beillas 2015. C_1 is equal to 0.5 GPa in the model. A viscosity coefficient of 785 Pa s is also defined. The fifteen steel cylinders were modelled by shell elements and each of them is rigidly linked to shell elements of the front foam coat. The front and rear foams meshes have been refined as shown on Figure 2.13 in order to have a element size of around 5 mm instead of between 10 mm and 15 mm previously. Table 2.2 gives a list of the prototype abdomen model parts.

The APTS sensors FE model provided by IFSTTAR had been previously validated under compression by a 50 mm diameter impactor with a 1 m s^{-1} velocity until 50 % compression (25 mm). However, in simulation the sensors are compressed more than 50 %. Figure 2.14 shows that the model predicts perfectly the sensors response in terms of pressure measurement but predicts a force a bit lower than the test data. This is probably due to the fact that the fluid (little compressibility) was modelled with a compressible material.

The APTS model was inserted in the front foam part of the THOR model prior to applying gravity for 500 ms to the full dummy. The abdomen internal plate served as reference to position the new abdomen. Care has been taken that the APTS do not penetrate neither the pelvis parts nor the upper abdomen before applying gravity. The vertical position of the APTS in the abdomen has therefore been adjusted in order not to penetrate the pelvis and the dummy torso has been rotated in order not to have initial penetrations between the upper abdomen and the APTS.

$$P = C_1 \cdot \frac{V_0 - V}{V} \tag{2.1}$$

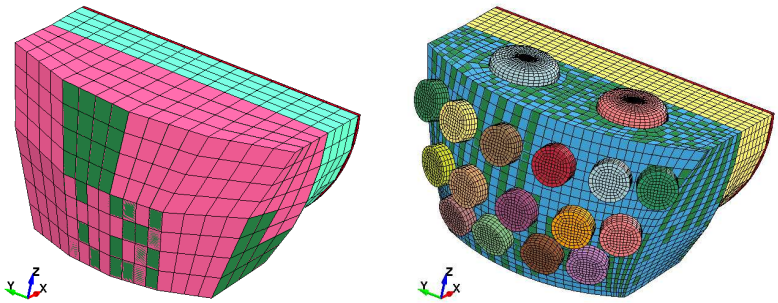

(a) Standard abdomen (b) Prototype abdomen

Figure 2.13 – Standard and prototype abdomen models

part	type	material model	density (kg m^{-3})	mass (g)
APTS right bladder	volumetric	elastic (MAT_001)	1400	119
APTS left bladder				
APTS right fluid	volumetric	equation of state (MAT_009)	865	148
APTS left fluid				
APTS right cap	volumetric	rigid (MAT_020)	2700	45
APTS left cap				
15 steel cylinders	shell	rigid (MAT_020)	2700	825 for the 15 cylinders using added mass

Table 2.2 – Prototype abdomen model parts list

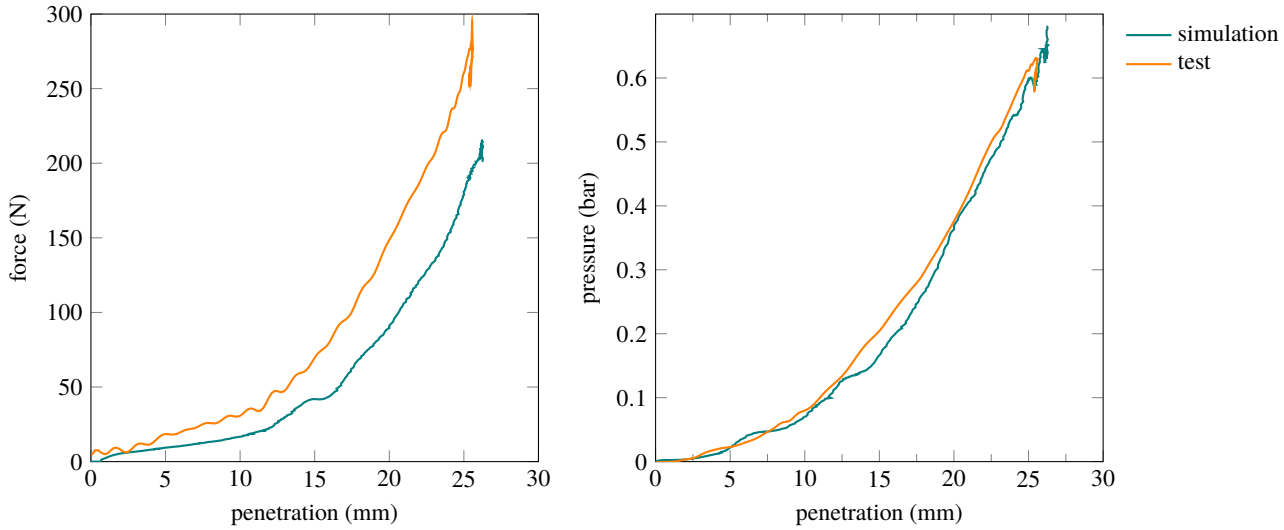

(a) Force-penetration

(b) Pressure-penetration

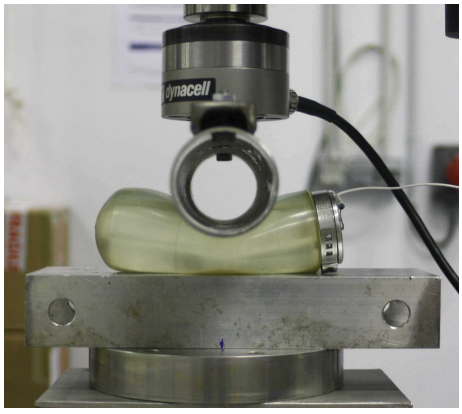

(c) Compression test

Figure 2.14 – APTS compression test

Force and pressure signals from simulation were filtered with a CFC 180 filter

2.3.3 Evaluation

The abdomen model of the prototype abdomen was evaluated versus test on the physical dummy performed under the conditions described in Section 2.2.2.

2.3.3.1 Seatbelt simulations

Figure 2.15 shows the results of simulation for the 6.6 bar pressure condition. In addition to the force and penetration results, Figure 2.15c compares the pressure measured in the APTS sensors and the simulation prediction. Two curves for the same case (test or simulation) represent the left and right sensor response. The model reproduces well the test data in terms of shape although the penetration and force peak values are slightly overestimated. The force unloading response is also not well reproduced

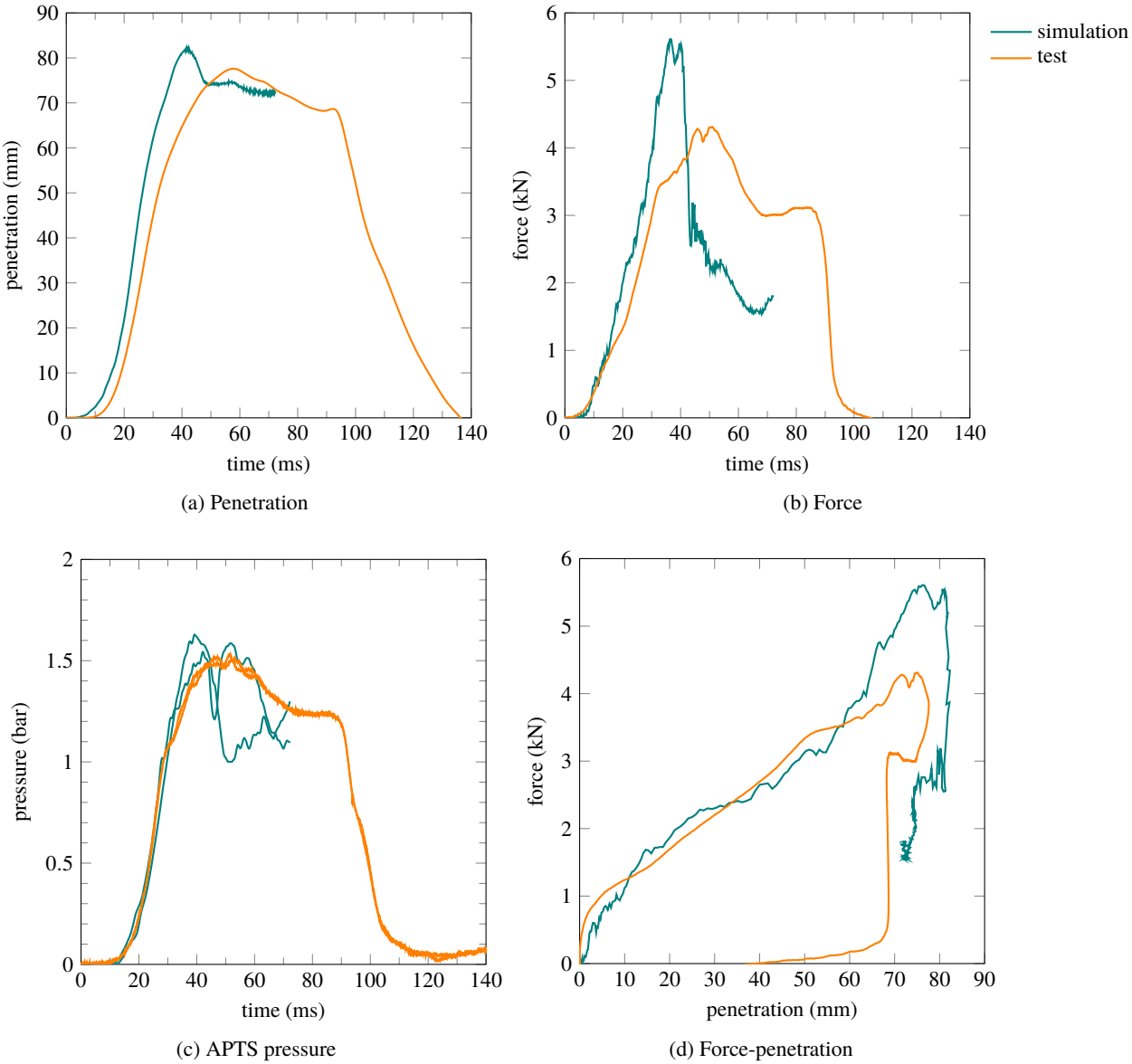

(a) Penetration

(b) Force

(c) APTS pressure

(d) Force-penetration

Figure 2.15 – THOR dummy with prototype abdomen response under Hardy et al. 2001 6.6 bar seatbelt loading

Pressure signals filtered with CFC 180 filter

2.3.3.2 Impactor simulations

Impactor simulations with a 6.1 m s^{-1} velocity created negative volumes in the APTS fluid, leading to an early termination. A maximum termination time of 24 ms could be reached. The results of the simulation of impactor test are presented on Figure 2.16. Although the simulation terminates early, there is a good adequation between the test and simulation results, except from pressure which is lower in the simulation. The early oscillations in the force signal are due to the contact between rigid parts: the impactor and the added masses in front of the abdomen. Although separated from each other by the jacket, the contact between rigid parts with a high initial velocity creates oscillations due to the high stiffness of the virtual springs used to compute the contact force.

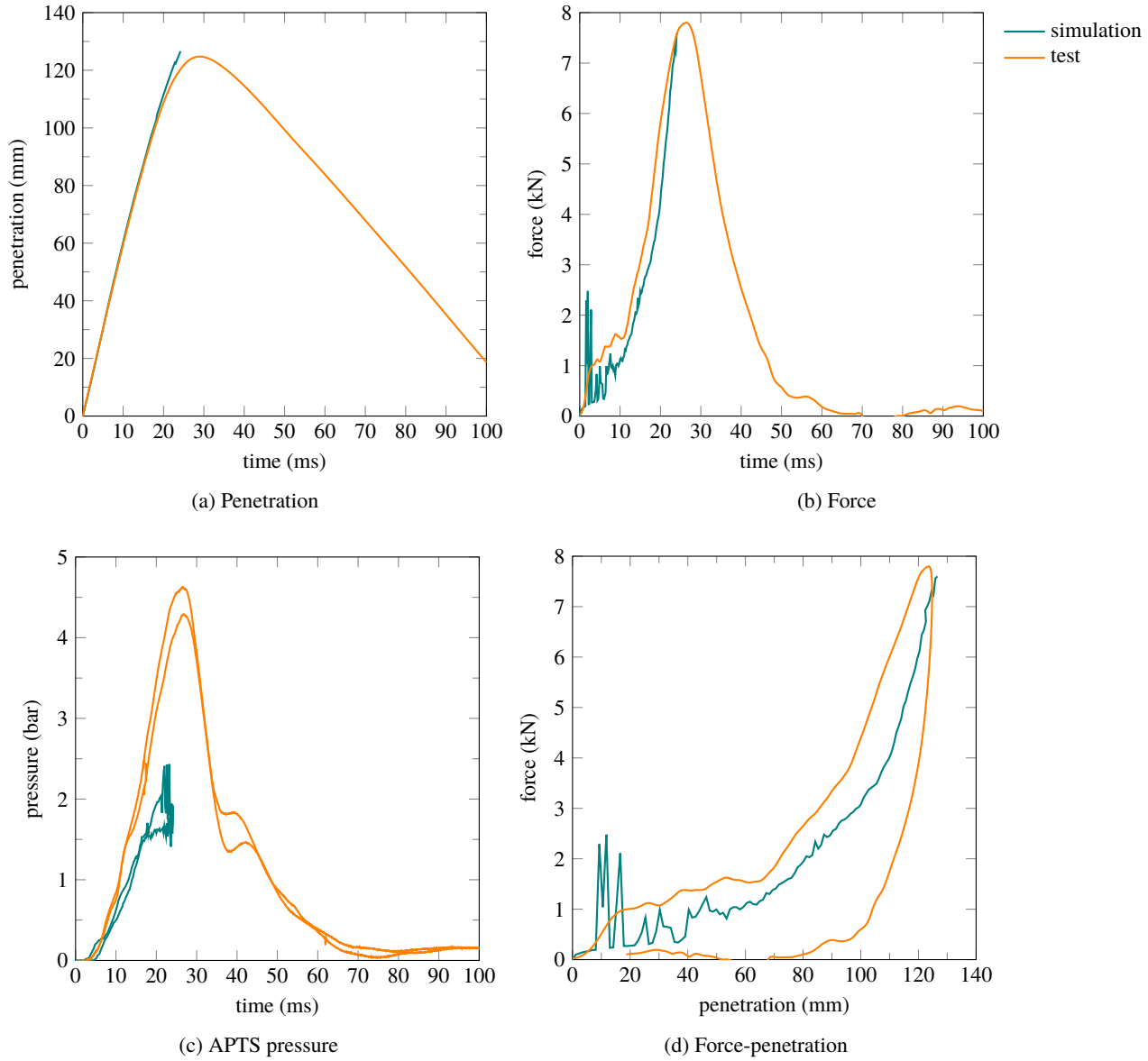

(a) Penetration

(b) Force

(c) APTS pressure

(d) Force-penetration

Figure 2.16 – THOR dummy with prototype abdomen response under impactor loading

2.4 Conclusion

The finite element model of the THOR dummy provided by NHTSA has been improved in order to have a model response correlating better with the test data. Based on these improvements, the abdomen prototype finite element model has been included in the dummy finite element model. This new model allows to reproduce the prototype abdomen response under seatbelt and impactor test. The simulation results do not match perfectly the test data, it appears that the model reproduces better a loading of the abdomen by a seatbelt compared to an impactor loading. This is true for the standard abdomen response and for the prototype abdomen pressure prediction. The seatbelt loading being a more frequent case of abdomen loading considering a car crash, this test case is a better candidate for injury prediction with the dummy model.

Chapter 3

THOR abdomen prototype improvements

Contents

3.1 Introduction

The finite element model of the THOR dummy with the IFSTTAR / Toyota prototype abdomen have been developed in the previous chapter. The aim of this chapter is to analyse the mechanical behaviour of the dummy abdomen under impact in order to draw ways of improvement. This has been done in subcomponent tests (loading of the dummy abdomen only) with a simplified mechanical model and with the prototype FE model. Sled test simulations have also been performed with the dummy FE model in order to study the influence of the prototype abdomen on the dummy kinematics in a loading case representative of a crash.

3.2 Subcomponent tests

3.2.1 Lumped element model

A simplified model of the human abdomen was built to reproduce dynamic loading tests on the human abdomen and on the THOR dummy abdomen. The aim of this lumped element model is to determine the main characteristics of the human abdomen response under impact and to improve the biofidelity of the THOR dummy abdomen.

3.2.1.1 Previous models

A lumped element model was proposed in Trosseille et al. 2002 where the abdomen was approximated by a spring in parallel with a damper to simulate a seatbelt test (see Figure 3.1a). This was representing the contribution of a static and a dynamic force to the abdomen response. The abdomen force was computed from the test penetration and penetration velocity data with the relationship $F = K \cdot x + C \cdot \dot{x}$. The parameters were identified from test data using an analytical method.

Trosseille et al. 2002 also developed a lumped element model applied to the THOR dummy. A mass M was added at the front of the model used for the PMHS subjects and a non-linear spring was used giving an $F = K_0 \cdot \dfrac{L}{L - x} \cdot x$ contribution, L being the thickness of the foam layers of the dummy abdomen. The parameters identified for the PMHS subjects were on average $K = 12\,850\,\mathrm{N\,m^{-1}}$ for the stiffness contribution and $C = 765\,\mathrm{N\,m^{-1}\,s}$ for the damping contribution. For the THOR dummy, L was set to 0.12 m and the average parameters were $M = 0.15\,\mathrm{kg}$, $K_0 = 11\,225\,\mathrm{N\,m^{-1}}$ and $C = 193\,\mathrm{N\,m^{-1}\,s}$. Figure 3.2 shows the validation of the model versus THOR and PMHS data.

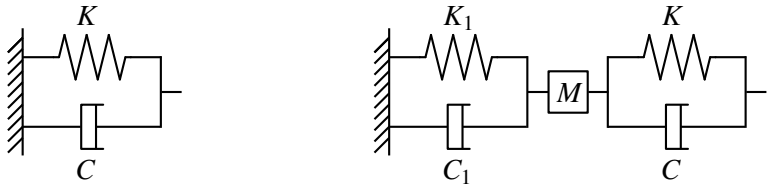

(a) Trosseille et al. 2002 (b) Lamielle et al. 2008

Figure 3.1 – Previous lumped element models for the abdomen

In Lamielle et al. 2008 seatbelt tests, the use of force sensors between the back of the subject and the testing apparatus allowed a more detailed modelling consisting in two spring / damper models in series with a mass in between (see Figure 3.1b). The model parameters were identified from

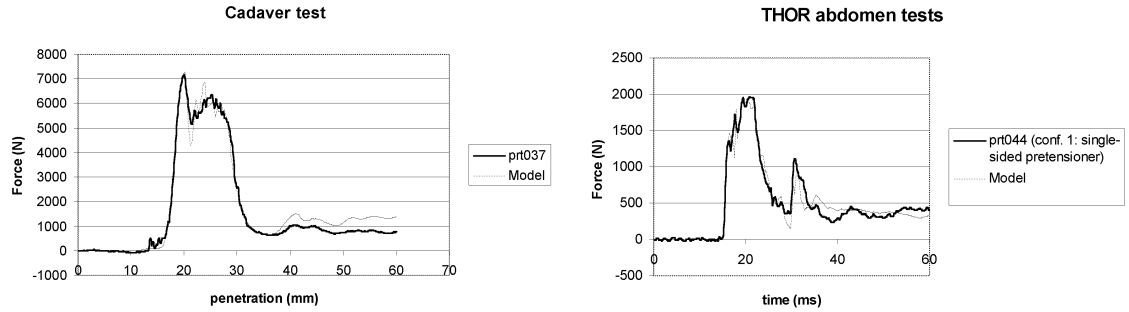

(a) Versus PMHS (b) Versus THOR

Figure 3.2 – Validation of model from Trosseille et al. 2002

test data with a similar method as in Trosseille et al. 2002. Then the resolution of the model was performed with a 4th order Runge-Kutta method having the abdomen force from test data imposed. The belt displacement and velocity were then compared to test data.

The parameter K_1 was identified first in a F_{back} versus x_1 diagram by fitting a cubic curve ($F_{\text{back}} = K_1 \cdot x_1^3$) through the point $\left(\left(x_1^{\max}\right)^3 ; F_{\text{back}}\left(\left(x_1^{\max}\right)^3\right)\right)$. The measured F_{back} data had been scaled before with a factor comprised between 0.8 and 1.2 in order to have a force equal to zero after the unloading . C_1 was then determined for each test fitting a cubic curve in a $F_{\text{back}} - K_1 \cdot x_1^3$ versus $\dot{x}_1$ diagram. However, the determination of K_1 does not take into account the contribution of C_1 to F_{back}. The parameters K and C were determined in a similar way for each test. The same remark can be expressed that the determination of K does not take into account the contribution of C to the force F.

The average parameters found for the first block of the model representing the part of the abdomen between the front wall and the centre of gravity were $K = 13\,000\,\text{kN m}^{-3}$ and $C = 665\,\text{N m}^{-1}\,\text{s}$. The mass representing the abdomen was chosen as $M = 14\,\text{kg}$. The second block was showing much more stiffness with $K_1 = 800\,000\,\text{kN m}^{-3}$ and $C_1 = 3940\,\text{N m}^{-3}\,\text{s}^3$. The components K, K_1 and C_1 were non linear components with a cubic relationship, for instance $F = K \cdot x^3$. Similarly, $F = K_1 \cdot x^3$ and $F = C_1 \cdot \dot{x}^3$ in the other components. But $F = C \cdot \dot{x}$ for the C component. Figure 3.3 shows the validation of those models versus PMHS data.

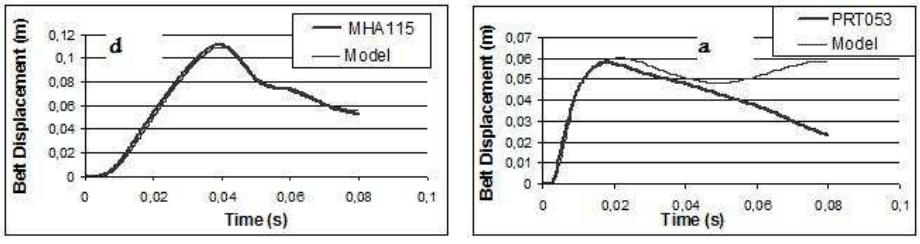

(a) Versus MHA data (b) Versus PRT data

Figure 3.3 – Validation of model from Lamielle et al. 2008

A thorax model for an impactor test was developed in Lobdell et al. 1973, consisting of a mass representing the impactor (m_1), a mass representing the sternum, the ribs and the thoracic content (m_2) and a mass representing the spine (m_3). These masses are linked by the spring k_{12} representing the thorax skin and a block of springs and dampers representing the ribcage and the thoracic content. The components are linear except k_{23} that is bi-linear in order to match the target corridors for large deflections and c_{23} that has different damping values for tension and compression in order to model force decay. The initial velocity of the impactor was applied as input condition of the model. Figure 3.4a shows the models. The resolution of the system's equations was performed until the

force in spring k_{12} became tensile. The model parameters has been estimated arbitrary for some of them and determined from curve fitting load-deflection data for the others.

This model was used in Kent et al. 2004 to simulate an impactor test. The initial velocity of the impactor was applied as input condition. To simulate a belt loading the displacement-time curve was applied to a simplified version of the model with the impactor mass removed and m_3 being fixed as seen on Figure 3.4b. The coefficients of the original model were used.

An other simplified version of the model from Lobdell et al. 1973 has been used in Parent et al. 2013 for thoracic impactor loading. The behaviour of k_{23} and c_{23} is the same as in the original model and the viscoelastic branch was removed. The input condition is the initial velocity of the impactor. The model parameters were optimised the sum of the normalised distances between the model response and target point in the force-deflection diagram as objective function. The initial values of the parameters were selected as the best among random values between 0.1 and 10 time the original values from Lobdell et al. 1973.

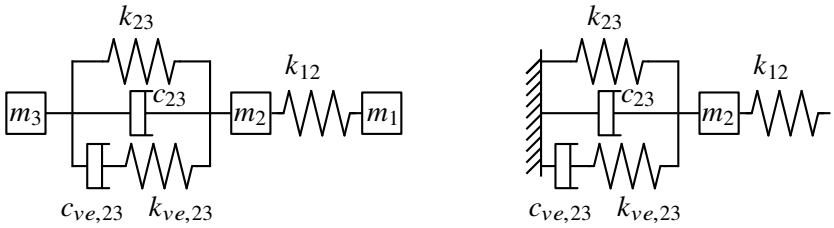

(a) Lobdell et al. 1973 (b) Kent et al. 2004

Figure 3.4 – Simplified thorax models

3.2.1.2 Proposed model

In order to be able to reproduce the PMHS or dummy response with the same model for both seatbelt and impactor case, a new model needed to be developed. The two stages of the model are meant to represent the deformable behaviour of the organs on one hand and the one of the flesh and skin in the other hand. Each stage of this model consists of a spring and a damper in order to represent a visco-elastic behaviour.

This model was built modifying the model from Lamielle et al. 2008. First, linear elements were used instead of components with a cubic relationship. A mass has been added at the front of the model to represent the flesh and skin mass. In order to be able to represent an impactor as well as a seatbelt loading case, a mass has been added at the back of the model to represent the global subject mass. This mass is fixed to model a seatbelt loading and let free to model an impactor test. More important, a modification of the structure of the model needed to be done in order to represent both seatbelt and impactor loading cases. Indeed, the original model from Lamielle et al. 2008 can model a seatbelt test but not an impactor test. Since the extremity of the model has a non-zero initial velocity, the fact of having a damper in parallel creates a non-zero initial reaction force. This is in contradiction with the test data. Therefore, it was chosen to transform the front stage of the model into a spring in series with a damper (Maxwell model), in order to have a similar front stage as the model from Lobdell et al. 1973. Figure 3.5 shows the models for seatbelt and impactor loading cases.

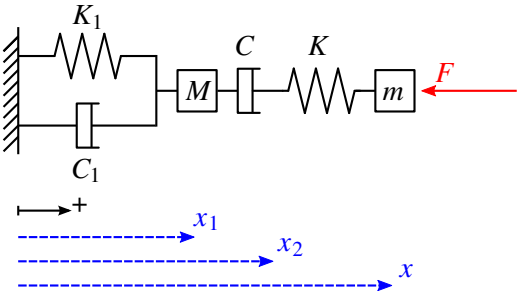

(a) Seatbelt

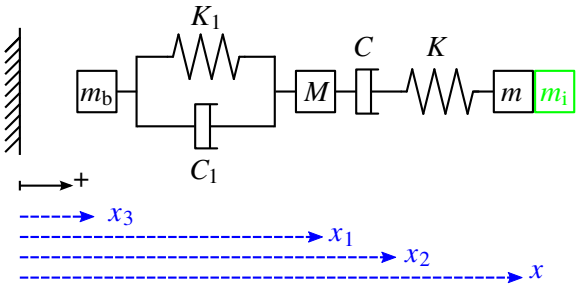

(b) Impactor

Figure 3.5 – Simplified abdomen model for seatbelt and impactor loading cases

3.2.1.2.1 Resolution for seatbelt case

The variables of the simplified model can be seen on Figure 3.5a. x, $\dot{x}$ and $\ddot{x}$ are the input conditions ($\dot{x} = \frac{\mathrm{d}x}{\mathrm{d}t}$ and $\ddot{x} = \frac{\mathrm{d}^2x}{\mathrm{d}t^2}$). They are taken from the test data and imposed to the model.

Equations 3.1a, and 3.1b are obtained by isolating the mass M and the point where x_2 is measured, respectively. These are two coupled differential equations where the unknowns are x_1 and x_2. x_2 is used to compute F from Equation 3.2 (obtained from isolating the mass m) and x_1 is used to compute the force between the back of the subject and the test bench as shown on Equation 3.3.

$$-M \cdot \ddot{x}_1 = K_1 \cdot x_1 + C_1 \cdot \dot{x}_1 - C \cdot (\dot{x}_2 - \dot{x}_1) \tag{3.1a}$$

$$0 = -K \cdot (x - x_2) + C \cdot (\dot{x}_2 - \dot{x}_1) \tag{3.1b}$$

$$F = m \cdot \ddot{x} + K \cdot (x - x_2) \tag{3.2}$$

$$F_{\text{back}} = K_1 \cdot x_1 + C_1 \cdot \dot{x}_1 \tag{3.3}$$

The system of Equations 3.1a and 3.1b has to be solved numerically. This is done by programming a 4th order Runge-Kutta resolution in Scilab. The system is transformed into $\dot{u} = f(u)$ by setting $u = \begin{pmatrix} u_1 = x_1 \\ u_2 = \dot{x}_1 \\ u_3 = x_2 \end{pmatrix}$. This leads to Equation 3.4, the system of three equations to be solved.

$$\begin{cases} \dot{u}_1 = u_2 \\ \dot{u}_2 = -\dfrac{K_1}{M} \cdot u_1 - \dfrac{C_1}{M} \cdot u_2 + \dfrac{K}{M} \cdot (x - u_3) \\ \dot{u}_3 = \dfrac{K}{C} \cdot (x - u_3) + u_2 \end{cases} \tag{3.4}$$

3.2.1.2.2 Resolution for impactor case

The variables of the simplified model can be seen on Figure 3.5b. The model is solved by imposing the initial impactor velocity, $v_0 = \dot{x}(t = 0)$. Equations 3.5a to 3.5d give the equations of motion of the simplified model. The interaction force between the impactor and the subject is computed according to Equation 3.6.

$$-(m + m_\mathrm{i}) \cdot \ddot{x} = K \cdot (x - x_2) \tag{3.5a}$$

$$0 = -K \cdot (x - x_2) + C \cdot (\dot{x}_2 - \dot{x}_1) \tag{3.5b}$$

$$-M \cdot \ddot{x}_1 = -C \cdot (\dot{x}_2 - \dot{x}_1) + K_1 \cdot (x_1 - x_3) + C_1 \cdot (\dot{x}_1 - \dot{x}_3) \tag{3.5c}$$

$$-m_\mathrm{b} \cdot \ddot{x}_3 = -K_1 \cdot (x_1 - x_3) - C_1 \cdot (\dot{x}_1 - \dot{x}_3) \tag{3.5d}$$

$$F = (m + m_\mathrm{i}) \cdot \ddot{x} \tag{3.6}$$

The four variables for resolution are x, x_1, x_2 and x_3. They are changed to a single u variable as detailed on Equation 3.7 with $\dot{u}_1 = u_2$, $\dot{u}_3 = u_4$ and $\dot{u}_5 = u_6$. The system to solve is written in Equation 3.8.

$$u = \begin{pmatrix} u_1 & u_2 & u_3 & u_4 & u_5 & u_6 & u_7 \end{pmatrix} = \begin{pmatrix} x & \dot{x} & x_1 & \dot{x}_1 & x_3 & \dot{x}_3 & x_2 \end{pmatrix} \tag{3.7}$$

$$\begin{cases} \dot{u}_1 = u_2 \\ \dot{u}_2 = -\dfrac{K}{m + m_\mathrm{i}} \cdot (u_1 - u_7) \\ \dot{u}_3 = u_4 \\ \dot{u}_4 = \dfrac{K}{M} \cdot (u_1 - u_7) - \dfrac{K_1}{M} \cdot (u_3 - u_5) - \dfrac{C_1}{M} \cdot (u_4 - u_6) \\ \dot{u}_5 = u_6 \\ \dot{u}_6 = \dfrac{K_1}{m_\mathrm{b}} \cdot (u_3 - u_5) + \dfrac{C_1}{m_\mathrm{b}} \cdot (u_4 - u_6) \\ \dot{u}_7 = \dfrac{K}{C} \cdot (u_1 - u_7) + u_4 \end{cases} \tag{3.8}$$

3.2.1.3 Test data

All test data available in the literature on the THOR dummy were concerning the NT version. Therefore, although the Mod-kit is the last version of the dummy, this lumped element model study will be based on the NT version data.

3.2.1.3.1 Seatbelt

The seatbelt tests selected from the literature and applied to the lumped element model are taken from Trosseille et al. 2002 and Foster et al. 2006 for the PMHS tests. For the THOR dummy, tests from Compigne et al. 2015 (replication of tests from Foster et al. 2006) and Trosseille et al. 2002 were selected. These are fixed-back tests where the belt is placed on the abdomen at the umbilicus level and retracted toward the back of the subject thanks to pretensioners. Three conditions from the literature are common to PMHS subjects and the dummy: B and C conditions from Foster et al. 2006 (different pretensioners) and configuration 2 from Trosseille et al. 2002. These conditions were selected to be reproduced with the developed lumped element model.

The average penetration across all the tests for a given condition was applied to the model. The average force was compared to the model response. The average penetration was differentiated to

obtain velocity and then differentiated a second time to determine acceleration. The three signals were filtered with a CFC filter which filtering frequency was adjusted according to a FFT [1] analysis in order to avoid noise that would distort the model computations. Average penetration, velocity and acceleration were applied to the model and the average force was compared to the model response. Figure 3.6 shows those input conditions applied to the lumped element model overlaid together. It can be seen that all the input conditions do not have the same time duration and for some of them the data is not available over the full time range of the test.

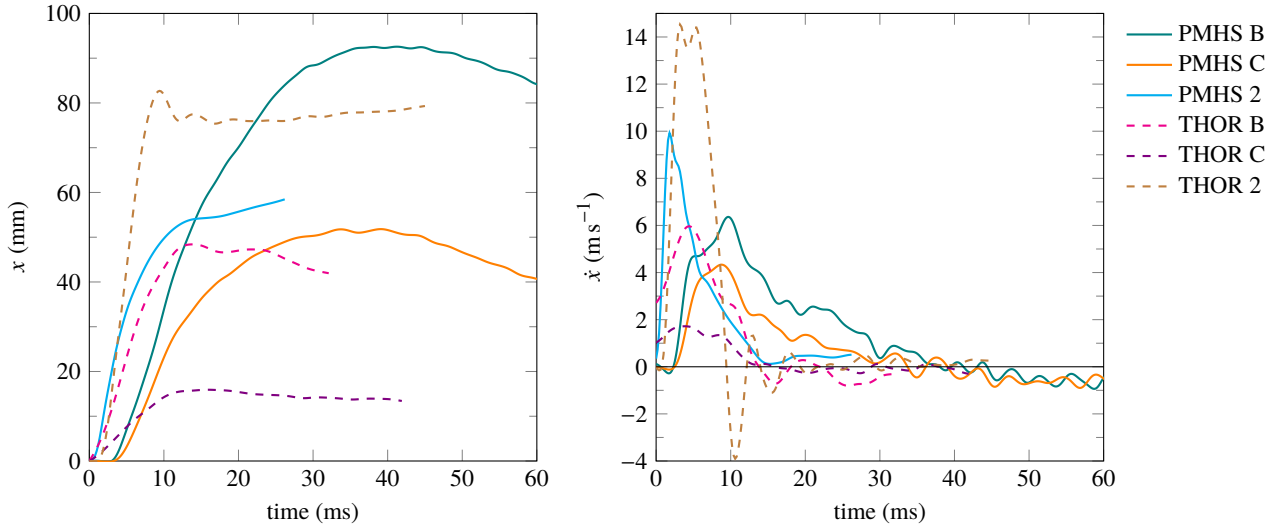

(a) Abdomen penetration

(b) Abdomen penetration velocity

Figure 3.6 – Input conditions for seatbelt loading conditions
B: Foster et al. 2006 B condition
C: Foster et al. 2006 C condition
2: Trosseille et al. 2002 configuration 2

3.2.1.3.2 Impactor

Four impactor conditions were applied to the model. For the PMHS subjects, two conditions were taken from Cavanaugh et al. 1986. The tests with a 64 kg mass from Cavanaugh et al. 1986 were excluded. For the THOR dummy two conditions were taken from Compigne et al. 2015. There is only one common configuration for the PMHS and the dummy, the 6 m s^{-1} (nominal velocity) 32 kg test condition. For each configuration, the penetration data from the different tests were averaged and the corresponding initial velocity was taken as input condition v_0. Table 3.1 shows the considered input velocities.

condition		v_0 (m s^{-1})	m_i (kg)	kinetic energy (J)
PMHS	Cavanaugh et al. 1986 6.1 m s^{-1}	6.1	32	595
	Cavanaugh et al. 1986 10 m s^{-1}	10	32	1600
THOR	Compigne et al. 2015 3 m s^{-1}	3.0	32	141
	Compigne et al. 2015 6.1 m s^{-1}	6.3	32	628

Table 3.1 – Initial impact velocity values

3.2.1.4 Non-linear stiffness

Cubic non-linear elements as used in Lamielle et al. 2008 have little effect on small x values but great effect on higher x values due to the nature of the cubic relation. Proper non-linear components

1. Fast Fourier Transform

would include more than one parameter in order to amplify differently low and high x values. It was therefore chosen to use only linear components, if they are sufficient, not to add more parameters to the model.

However, it was not possible to fit the THOR dummy impactor test data with linear elements only. It was therefore chosen to replace the element K by a non-linear spring with a strain dependency as seen on Equation 3.9. The nonlinear stiffness browses successively two regimes of compression and is characterised by three parameters: a linear stiffness K_0; a compression limit d; and a power p (imposed as an integer number). For low compression values, when $(x - x_2) \ll d$, the term between curly brackets in Equation 3.9 reduces to unity and the response of the spring is linear, $F_{\text{spring}} = K_0 \cdot (x - x_2)$. At moderate to high compression, a stiffening sets in and the restore force becomes higher than the K_0 linear contribution.

$$F_{\text{spring}} = K_0 \cdot (x - x_2) \cdot \left(1 + \left(\frac{|x - x_2|}{d}\right)^p\right) \tag{3.9}$$

Figure 3.7 highlights the differences between a linear relationship, a cubic relationship and the chosen non-linear power law. It appears that the power law amplifies the low x values linearly and has a non-linear response for higher x values. The parameter values of the different components are arbitrary in order to have a sensible display.

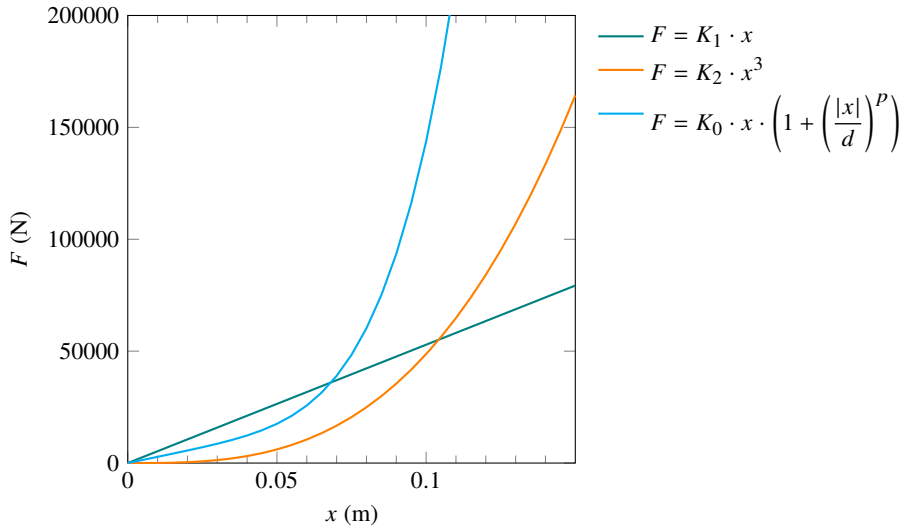

Figure 3.7 – Comparison between linear and non-linear components
$K_1 = 528\,800\,\text{N m}^{-1}$; $K_2 = 48\,680\,000\,\text{N m}^{-3}$
$K_0 = 278\,200\,\text{N m}^{-1}$; $d = 0.07\,\text{m}$; $p = 4$
Parameters values are arbitrary

3.2.1.5 Determination of model parameters

3.2.1.5.1 Masses determination

According to the abdomen representation described above, the masses of the model applied to PMHS subjects have been estimated by measuring the mass of the THUMS model abdomen. The abdomen was isolated from the rest of the model by drawing a three dimensions box between L1 and L5 [2] lumbar vertebrae. The abdomen was divided in three zones as shown on Figure 3.8. The *abdomen content* part is meant to represent the organs that will move during the impact. It will correspond to the mass M in the simplified model. The *front flesh* part represents the tissues that

2. 5th lumbar vertebra

create the initial inertia of the abdomen when subjected to seatbelt loading. This corresponds to the mass m. The calculated masses on the THUMS model (from the selected parts densities) are $M = 5.7\,\text{kg}$ and $m = 0.92\,\text{kg}$.

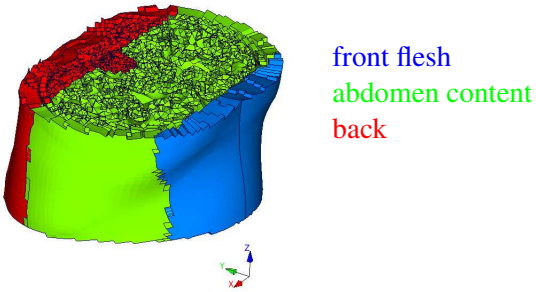

Figure 3.8 – Masses repartition of the THUMS abdomen

Therefore, for all the PMHS subjects, $M = 6\,\text{kg}$ and $m = 1\,\text{kg}$ were used. The mass m_{back} was computed as $m_{\text{back}} = BM - M - m$ where BM is the average body mass of the PMHS subjects of the considered test condition. The masses for the THOR dummy have been measured on the dummy FE model described in Chapter 2. The part densities were taken from GESAC, Inc. 1999. The mass of the two foam blocks of the abdomen was approximately 0.3 kg. Therefore M was set to 0.2 kg and m was set to 0.1 kg. The mass m_{back} was computed as $m_{\text{back}} = 78.3\,\text{kg} - M - m = 78\,\text{kg}$ since the total mass of the dummy is equal to 78.3 kg according to GESAC, Inc. 2016.

3.2.1.5.2 Optimisation loop

The response of the model for a specific loading condition is computed with a Scilab program. Based on manually adjusted initial values, the parameter values are optimised for each test configuration with the Scilab `optim` function until the model response (the force signal) matches the test data, minimising the criteria $f = \sum_{i=1}^{N} \left(F_{\text{model}}(i) - F_{\text{test}}(i)\right)^2$ with N the number of data points. The goodness of fit is then estimated by calculating cross-correlation coefficients and the variation range of the parameters is determined.

3.2.1.5.3 Goodness of fit assessment

The assessment of the goodness of fit between the model response with the optimised parameters and the reference test data is obtained by calculating amplitude ratio, shape factor and phase shift as described in Xu et al. 2000. Equations 3.10a to 3.10c define the three ratios with $x(t)$ being the signal to compare to the reference $y(t)$ and $\|x\| = \int_{-\infty}^{+\infty} x^2(t) \cdot \mathrm{d}t$ is the norm of x. The integrals of digital signals are computed as: $\int_{-\infty}^{+\infty} x(t) \cdot \mathrm{d}t = \sum_{i=1}^{N-1} T \cdot \frac{x_{i-1} + x_i}{2}$ with T the sampling rate and N the number of data points (numerical integration by trapezoidal rule). A perfect fit between the two signals would lead to an amplitude ratio and a shape factor of 1 and a phase shift of 0 ms.

$$\text{amplitude ratio} = \frac{\|x\|}{\|y\|} \tag{3.10a}$$

$$\text{shape factor} = \frac{\int_{-\infty}^{+\infty} x(t) \cdot y(t) \cdot \mathrm{d}t}{\sqrt{\|x\| \cdot \|y\|}} \tag{3.10b}$$

$$\text{phase shift} = h \text{ so that } \frac{\int_{-\infty}^{+\infty} x(t) \cdot y(t+h) \cdot \mathrm{d}t}{\sqrt{\|x\| \cdot \|y\|}} \text{ is minimal} \tag{3.10c}$$

3.2.1.5.4 Sensitivity analysis

In order to compare the model parameters for different conditions, it was necessary to estimate the range in which the optimised parameters can vary without significantly changing the model response result. The optimised values of the model parameters (spring stiffnesses and damping parameters) and the masses values were subjected to variations by steps of 10% of their value, ranging from 0.1 to 2 times the initial value. For each parameter value the three correlation coefficients mentioned above between the model response and the test data were computed. The percentage of variation of the three coefficients was computed at each step. A variation of one of the coefficients exceeding 10% of the coefficient value computed with the optimised parameter was considered as the limit of the range of variation of the parameter. An exception was made for the phase shift coefficient. In order to avoid the artefacts due to small phase values, the value of phase shift used in these computations was divided by 10 ms and the coefficient $1 - \frac{\text{phase shift}}{10\,\text{ms}}$ was considered instead of the phase shift in ms, in order to have a coefficient equal to 1 in case of a perfect fit.

3.2.1.6 Results

3.2.1.6.1 Model fit to test data

Figures 3.9 and 3.10 show the model response fit to the test data under seatbelt and impactor loading respectively, for the common conditions between PMHS subjects and the dummy. This model response is obtained with the optimised mechanical parameters values reported in Tables 3.2 and 3.3, respectively. Non-normalised data have been used for the PMHS penetration and force response. The standard deviation corridors are indicated for the PMHS force data. The goodness of fit coefficients are reported at the bottom of each subfigure. Force-penetration graphs of those results are presented in Figure D.1 (in Appendix).

For the seatbelt conditions, the initial negative slope of the model force response for some tests is an artefact due to the negative slope in the $\dot{x}$ data (see Figure 3.6b). This may be a consequence of the filtering of penetration data to compute the input velocity. The THOR dummy response shows sharp peaks and an abrupt initial slope that the model can not fit exactly, regardless of the potential time offset in the force signal from test data. For the impactor conditions, the non linearity of the dummy response can be seen on Figures 3.10c and 3.10d, where the slope of the force-time signal changes around 10 ms, and on Figures D.1b and D.1d (in Appendix). Comparing Figures D.1b end D.1d for the PMHS data, it appears that the model predicts a higher penetration than measured in the test data.

For both seatbelt and impactor case the model allows to fit the test data, the response being mainly in the standard deviation corridors for the PMHS, the amplitude and shape ratios stay between 0.8 and 1.1 and the phase shift between ±1.2 ms. This means that this model is suitable to analyse the human and dummy abdomen response.

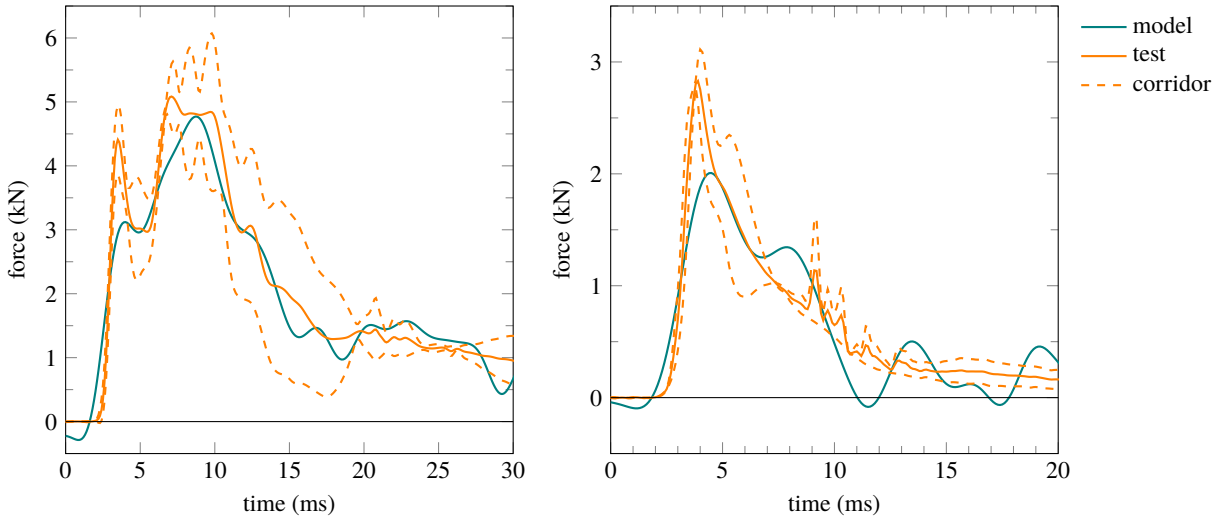

(a) PMHS B
amplitude=0.86, shape=0.99, phase=0.05 ms

(b) PMHS C
amplitude=0.87, shape=0.95, phase=−0.1 ms

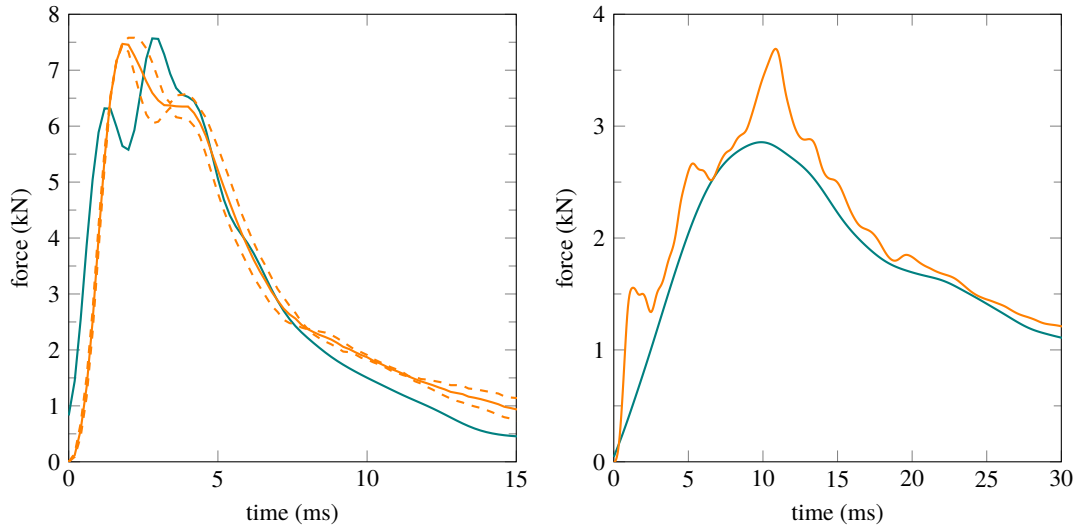

(c) PMHS 2
amplitude=1.01, shape=0.98, phase=0.3 ms

(d) THOR B
amplitude=0.80, shape=0.99, phase=−0.05 ms

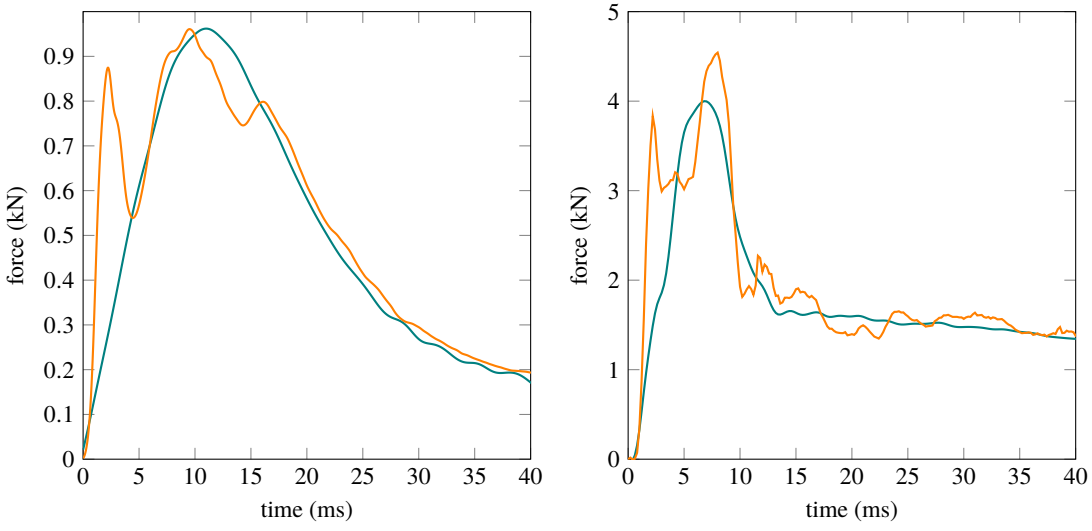

(e) THOR C
amplitude=0.93, shape=0.97, phase=−1.2 ms

(f) THOR 2
amplitude=0.86, shape=0.97, phase=−0.1 ms

Figure 3.9 – Fit of the model response to test data for seatbelt case
B: B condition from Foster et al. 2006
C: C condition from Foster et al. 2006
2: configuration 2 from Trosseille et al. 2002

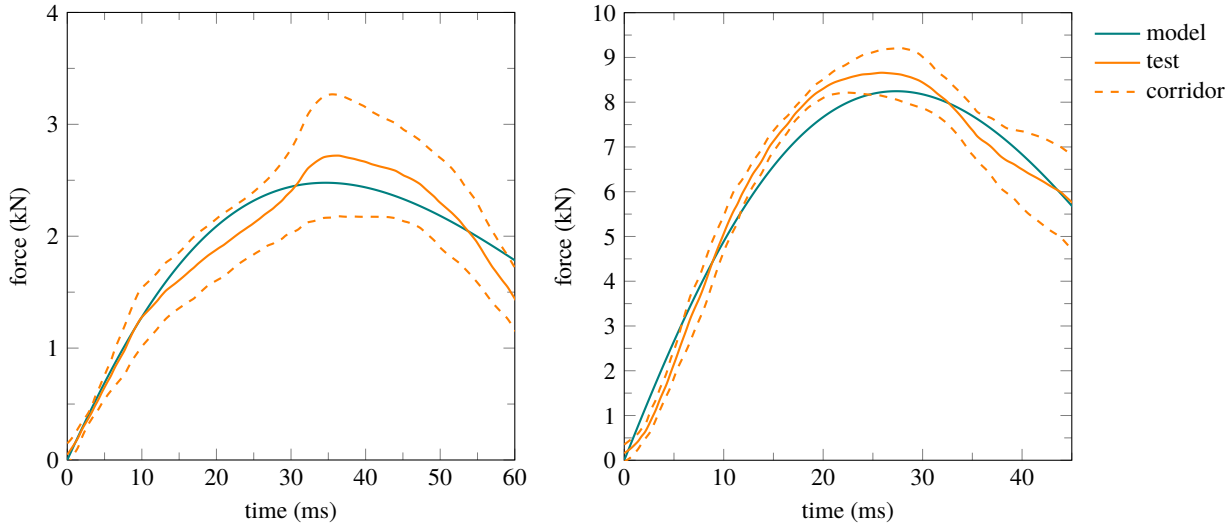

(a) PMHS 6.1
amplitude=0.95, shape=1.00, phase=0 ms

(b) PMHS 10
amplitude=1.00, shape=1.00, phase=0 ms

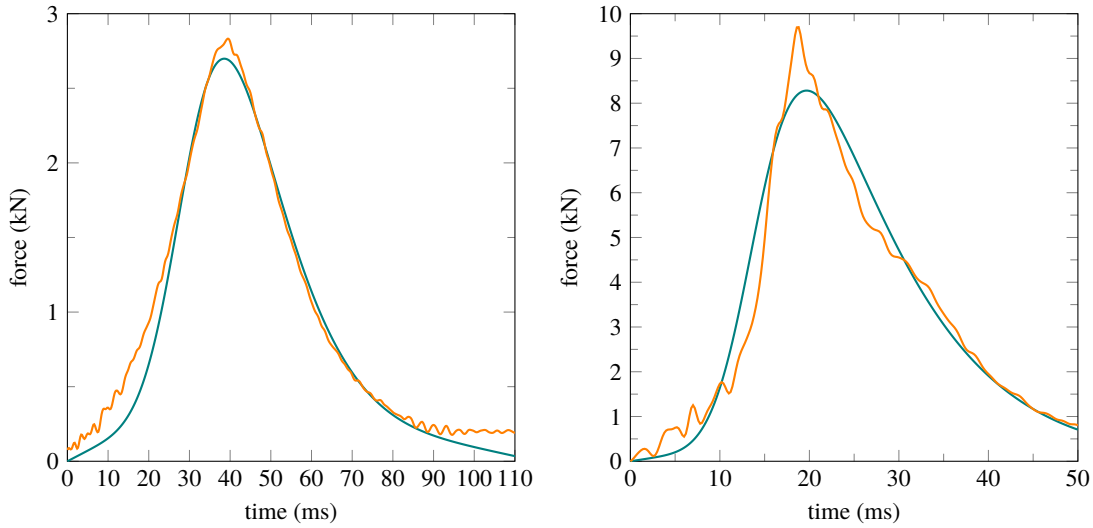

(c) THOR 3
amplitude=0.94, shape=0.99, phase=−1 ms

(d) THOR 6.1
amplitude=1.04, shape=0.99, phase=0.4 ms

Figure 3.10 – Fit of the model response to test data for impactor case
PMHS 6.1: 32 kg 6.1 m s^{-1} condition from Cavanaugh et al. 1986
PMHS 10: 32 kg 10 m s^{-1} condition from Cavanaugh et al. 1986
THOR 3: 32 kg 3 m s^{-1} condition from Compigne et al. 2015
THOR 6.1: 32 kg 6.1 m s^{-1} condition from Compigne et al. 2015

3.2.1.6.2 Parameters values

Figure 3.11 shows the parameters identified for each common PMHS / dummy condition along with their range of variation for the seatbelt and impactor cases, respectively. The numerical values are reported in Tables 3.2 and 3.3.

For the seatbelt case, the first thing to be noticed on Figure 3.11a is that the K values for the PMHS subjects are much higher than for the THOR dummy. The C values are higher for the dummy than for the PMHS subjects (Figure 3.11c), except for configuration 2 from Trosseille et al. 2002 where they are equal. The C_1 values (Figure 3.11g) are higher for the dummy compared to the PMHS, except for the configuration 2 from Trosseille et al. 2002, but since ranges of variation overlap for most of the test conditions, it is concluded that the values are the same for the PMHS and the

PMHS	Trosseille et al. 2002 configuration 2						
		K (N m^{-1})	C (N m^{-1} s)	K_1 (N m^{-1})	C_1 (N m^{-1} s)	M (kg)	m (kg)
	superior limit	1350054	1217	210787	3282	10.2	1
	optimised value	**900036**	**1217**	**105393**	**2344**	**6**	**0.5**
	inferior limit	630025	1217	10539	1641	1.8	0.05
	Foster et al. 2006 B condition						
		K (N m^{-1})	C (N m^{-1} s)	K_1 (N m^{-1})	C_1 (N m^{-1} s)	M (kg)	m (kg)
	superior limit	1140043	1107	76428	1527	9.6	1.6
	optimised value	**570021**	**1107**	**38214**	**1175**	**6**	**1**
	inferior limit	342013	1107	3821	940	3	0.3
	Foster et al. 2006 C condition						
		K (N m^{-1})	C (N m^{-1} s)	K_1 (N m^{-1})	C_1 (N m^{-1} s)	M (kg)	m (kg)
	superior limit	1692911	330	77983	1608	12	1.1
	optimised value	**846456**	**300**	**38992**	**804**	**6**	**1**
	inferior limit	423228	270	3899	80	1.2	0.9
THOR	Trosseille et al. 2002 configuration 2						
		K (N m^{-1})	C (N m^{-1} s)	K_1 (N m^{-1})	C_1 (N m^{-1} s)	M (kg)	m (kg)
	superior limit	137326	3178	43387	428	0.4	0.2
	optimised value	**124841**	**2445**	**39443**	**389**	**0.2**	**0.1**
	inferior limit	112357	1956	35499	350	0.02	0.01
	Foster et al. 2006 B condition						
		K (N m^{-1})	C (N m^{-1} s)	K_1 (N m^{-1})	C_1 (N m^{-1} s)	M (kg)	m (kg)
	superior limit	125792	19356	62396	1000	0.4	0.2
	optimised value	**114357**	**9678**	**51997**	**910**	**0.2**	**0.1**
	inferior limit	102921	6774	41597	819	0.02	0.01
	Foster et al. 2006 C condition						
		K (N m^{-1})	C (N m^{-1} s)	K_1 (N m^{-1})	C_1 (N m^{-1} s)	M (kg)	m (kg)
	superior limit	104873	4986	55076	2317	0.4	0.2
	optimised value	**95339**	**4155**	**27538**	**2106**	**0.2**	**0.1**
	inferior limit	85805	3324	2754	1896	0.02	0.01

Table 3.2 – Identified parameters for seatbelt loading conditions including sensitivity analysis (parameters value range which keeps goodness of fit parameters within ±10 % range)

PMHS	Cavanaugh et al. 1986 32 kg 6.1 m s^{-1} condition							
		K (N m^{-1})	C (N m^{-1} s)	K_1 (N m^{-1})	C_1 (N m^{-1} s)	M (kg)	m (kg)	m_b (kg)
	superior limit	31179	2244	3949	1189	9	2	110
	optimised value	**23984**	**1726**	**1974**	**991**	**6**	**1**	**55**
	inferior limit	21585	1381	197	793	3	0.1	33
	Cavanaugh et al. 1986 32 kg 10 m s^{-1} condition							
		K (N m^{-1})	C (N m^{-1} s)	K_1 (N m^{-1})	C_1 (N m^{-1} s)	M (kg)	m (kg)	m_b (kg)
	superior limit	66570	25217	4149	2746	10.8	2	154
	optimised value	**55475**	**12609**	**2075**	**2288**	**6**	**1**	**77**
	inferior limit	49928	6304	207	1830	1.2	0.1	53.9

THOR	Compigne et al. 2015 32 kg 3 m s^{-1} condition								
		K_0 (N m^{-1})	d (mm)	p (no unit)	C (N m^{-1} s)	K_1 (N m^{-1})	C_1 (N m^{-1} s)	M (kg)	m (kg)	m_b (kg)
	superior limit	5284	52	4	11588	32005	3326	0.4	0.2	101.4
	optimised value	**4804**	**52**	**4**	**6817**	**16002**	**2772**	**0.2**	**0.1**	**78**
	inferior limit	4323	52	4	4772	1600	2217	0.02	0.01	62.4
	Compigne et al. 2015 32 kg 6.1 m s^{-1} condition									
		K_0 (N m^{-1})	d (mm)	p (no unit)	C (N m^{-1} s)	K_1 (N m^{-1})	C_1 (N m^{-1} s)	M (kg)	m (kg)	m_b (kg)
	superior limit	6911	42	4	9514	31955	3519	0.4	0.2	109.2
	optimised value	**4936**	**42**	**4**	**6796**	**15977**	**3199**	**0.2**	**0.1**	**78**
	inferior limit	3949	42	4	5437	1598	2879	0.02	0.01	62.4

Table 3.3 – Identified parameters for impactor loading conditions including sensitivity analysis (parameters value range which keeps goodness of fit parameters within ±10 % range)

dummy. Additionally, the K_1 values presented on Figure 3.11e are similar between the PMHS and the dummy, but large ranges of variation exist for all of the conditions. This high range of variation of the parameter K_1 is due to the fact that x_1 is significantly lower than x for most of the conditions. Therefore, a given variation of K_1 would have less effect on the abdomen force than the same variation of K. Regarding the results for configuration 2 from Trosseille et al. 2002, the fact that C is equal for the PMHS and the dummy and that C_1 is lower for the dummy, can be explained by the fact that the penetration velocity is the highest for this condition (Figure 3.6b).

For the impactor case, since a non-linear spring was needed to fit the THOR test conditions, the effective stiffness of these conditions is compared to the K values of the other conditions on Figure 3.11b. The effective stiffness for the non-linear spring is computed as $K_{\text{eff}} = \dfrac{F_{\text{spring}}}{x - x_2}$ with F_{spring} taken from Equation 3.9, the force given by the spring. K_{eff} is plotted against the relevant elongation, $x - x_2$. For a linear spring (PMHS case), $K_{\text{eff}} = K$. For clarity, only optimised values are plotted, without range of variation. The K_{eff} values for the THOR dummy are lower than the K values of the PMHS subjects on most of the penetration range. The C values are higher for the THOR dummy compared to the PMHS subjects (Figure 3.11d) except for the $10\,\text{m}\,\text{s}^{-1}$ condition where the PMHS have a higher C value than the other conditions. The same trend is noted for the C_1 parameter (Figure 3.11h), although there is a large range of variation for the $10\,\text{m}\,\text{s}^{-1}$ condition. The K_1 values presented on Figure 3.11f seem higher for the dummy compared to the PMHS, but due to relatively large ranges of variation of this parameter it can take the same values for all the conditions. The same observation can be made for the high range of variation of K_1 in the seatbelt case. The fact that the $10\,\text{m}\,\text{s}^{-1}$ condition has a higher C value compared to the other PMHS condition can be due to the fact that this is the highest velocity of the test conditions.

It stands out that the second stage of the model contributes less to the global penetration response of the model since the displacement and velocity of the second stage, (x_1 and $\dot{x}_1$ for seatbelt, $x_1 - x_3$ and $\dot{x}_1 - \dot{x}_3$ for impactor), are lower than those of the front stage ($x - x_1$ and $\dot{x} - \dot{x}_1$). This leads to focussing on the K and C parameters for the analysis.

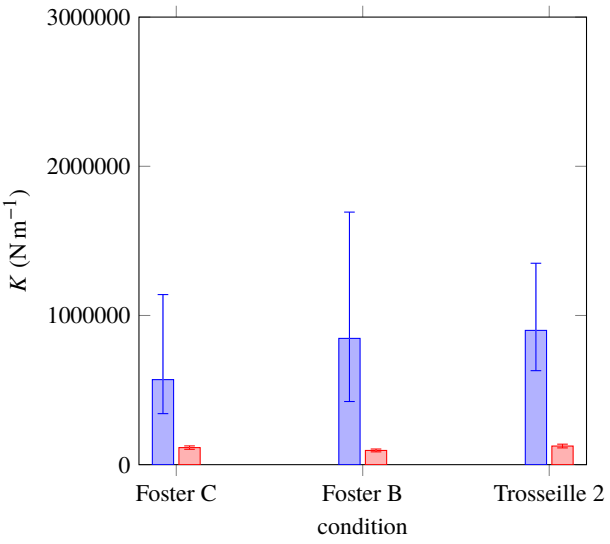

(a) K for seatbelt

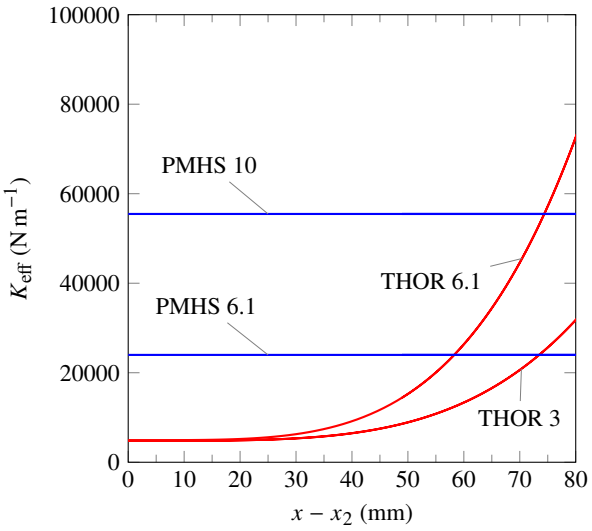

(b) K_{eff} for impactor

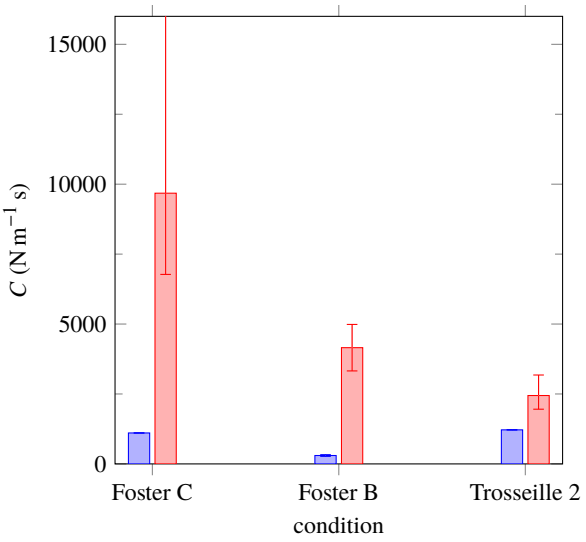

(c) C for seatbelt

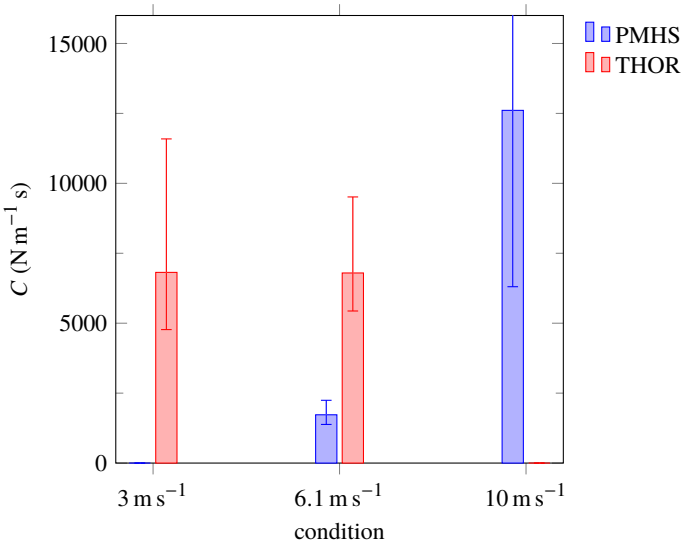

(d) C for impactor

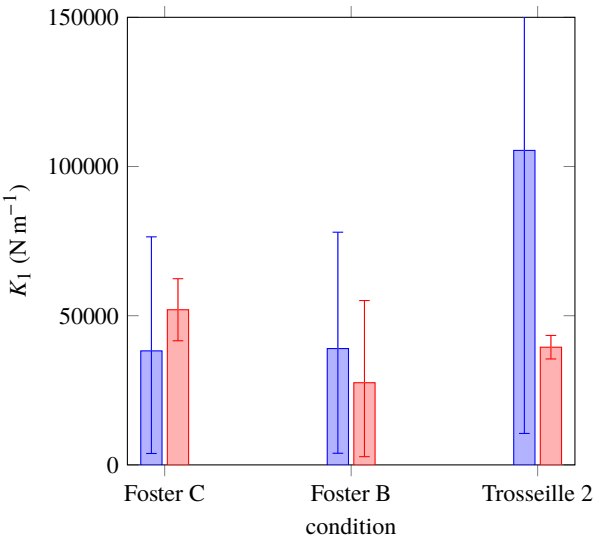

(e) K_1 for seatbelt

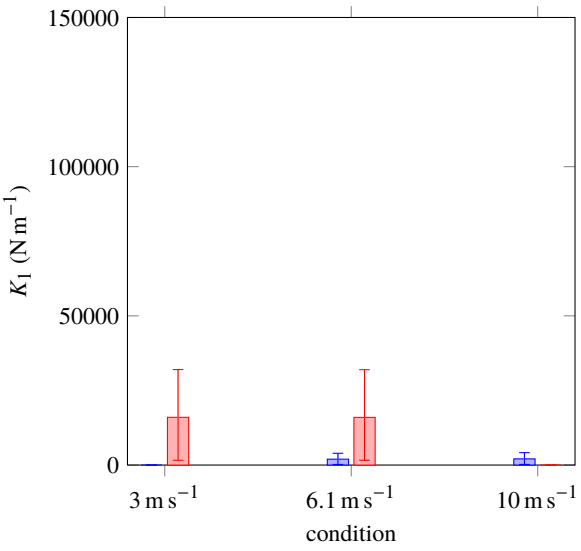

(f) K_1 for impactor

Figure 3.11 – Identified model parameters for seatbelt and impactor common loading conditions to PMHS and THOR

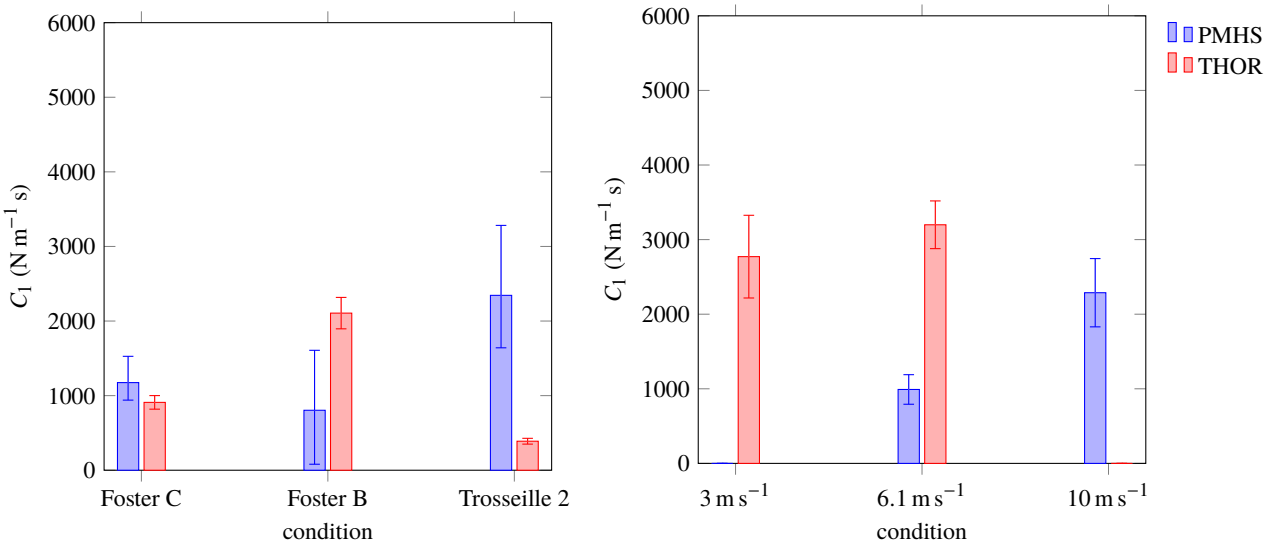

(g) C_1 for seatbelt (h) C_1 for impactor

Figure 3.11 – Identified model parameters for seatbelt and impactor common loading conditions to PMHS and THOR (continued)
B: B condition from Foster et al. 2006
C: C condition from Foster et al. 2006
2: configuration 2 from Trosseille et al. 2002
PMHS 6.1: 32 kg 6.1 m s^{-1} condition from Cavanaugh et al. 1986
PMHS 10: 32 kg 10 m s^{-1} condition from Cavanaugh et al. 1986
THOR 3: 32 kg 3 m s^{-1} condition from Compigne et al. 2015
THOR 6.1: 32 kg 6.1 m s^{-1} condition from Compigne et al. 2015

In order to understand the meaning of the parameters value comparison, one has to note that the influence of the parameters is not the same whether they are placed in series or in parallel in the model. For instance, a spring in parallel will have no effect when its stiffness is equal to 0, whereas a spring in series has no effect when its value tends toward infinity. It is the same for damping parameters. This explains the important range of variation toward high values for K and C concerning PMHS and THOR respectively. A high value for such a component in series means it deforms little. Therefore a higher value means it deforms even less, which does not necessarily change the global result.

The model in series has a characteristic time $\tau = {}^{C}/_{K}$. The model behaviour is elastic for times inferior to τ and viscous for times superior to τ. The characteristic times have been computed with the optimised K and C values. It can be concluded that the penetration response of the abdomen is mainly caused by the instantaneous deformation of the spring K for the THOR dummy and by the long-term deformation of the damper C for the PMHS. For the seatbelt case, this is highlighted by Figures D.2a and D.2b (in Appendix), which show the prominence of the spring and damper responses on the abdominal penetration of the dummy and the PMHS, respectively. The PMHS characteristic time being low (less than 3 ms) compared to the loading duration, the PMHS response is mainly viscous. On the opposite, the dummy characteristic times are between 20 ms and 80 ms, higher than the loading duration, therefore the response is mainly elastic. Figures D.3a and D.3b (in appendix) show the same phenomenon for the impactor case. It is difficult, however, to compare the characteristic times with a non linear spring in the dummy case.

These findings correlate with the test data reported in Compigne et al. 2015. For the impactor case the dummy force response was higher than the PMHS responses and for the seatbelt case the dummy force response was lower than the PMHS responses. This is explained by the previous findings.

An impactor loading creates high abdomen penetration, therefore the dummy force response is higher than the PMHS one due to the higher influence of K (the spring non-linearity enhances this phenomenon since high penetration increases the spring force contribution). On the other hand, a seatbelt loading creates less penetration (compared to the impactor loading) and a sharp velocity peak, therefore the dummy force response is lower than the PMHS one due to the lower influence of C.

This spring-driven behaviour of the dummy and the damper-driven behaviour of the PMHS highlighted by the model are due to the nature of the constitutive material of the human subjects and the dummy. The human abdomen is made of soft tissues that include a large proportion of water, therefore causing a viscous behaviour whereas the dummy abdomen is made of foam and therefore has an elastic behaviour, although not linear and strain rate dependent. The influence of the dummy spine and pelvis (more important than for the human) explains the need for a non-linear spring in the impactor case. The optimised values of the parameter of the non-linear spring (42 mm and 52 mm) represent the level of compression after which the non-linearity appears. This corresponds to the depth the abdomen foam has to be compressed before the pelvis is involved (measured at approximately 45 mm on the dummy).

3.2.1.7 Guidelines for improving the THOR dummy

Although there are differences in the model parameters values between the seatbelt and impactor case, the results show that the THOR dummy abdomen is more elastically and less viscously deformable compared to the human abdomen. This behaviour is mainly explained by the first stage of the model, i.e. related to parameters K and C since the second stage contributes less to the response as explained above.

Based on these observations, some improvements can be applied to the dummy at the material and structural levels. The material properties of the lower abdomen foam should be modified to favour the viscous behaviour instead of the elastic behaviour. The need of a non-linear spring for the dummy model at high penetrations, whilst it was not necessary for the PMHS, means that stiffer parts (such as the pelvis) contribute in a non-biofidelic way more to the response than soft parts. This confirms the design changes of this region implemented on THOR Mod Kit, which shortened the pelvis flesh at antero-superior iliac spines by around 20 mm. Furthermore, the difference in moving mass between the dummy abdomen and the PMHS has an influence and therefore the dummy abdomen mass should be increased.

3.2.2 Finite element improvement of the prototype abdomen

In this section, the biofidelity of the IFSTTAR / Toyota prototype abdomen has been assessed versus PMHS tests. The finite element model previously presented and validated in Chapter 2 has been used for this purpose. Seatbelt and impactor loadings from PMHS tests were simulated with the dummy model. The 4.5 bar seatbelt condition from VRTC (since this condition is the closest to the PMHS condition from Hardy et al. 2001) and the 6.1 $\mathrm{m\,s^{-1}}$ impactor condition from Cavanaugh et al. 1986 were at first considered since test results for the prototype abdomen exist for these configurations, as described in Chapter 2. Additional seatbelt conditions A from Foster et al. 2006 and MHA from Lamielle et al. 2008 were also added. Their belt retraction displacement and velocity profiles can be seen on Figure 3.12. In the following paragraphs, the PMHS corridor is overlaid on the THOR model responses in order to assess its biofidelity. The force-penetration corridor has been plotted as the average force plus or minus one standard deviation versus the average penetration.

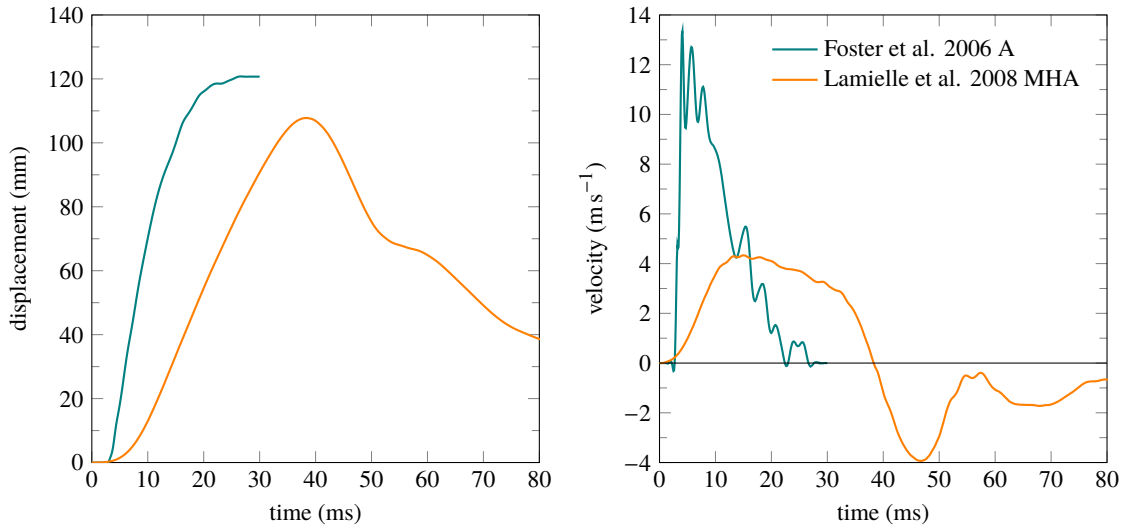

(a) Belt retraction

(b) Belt retraction velocity

Figure 3.12 – Additional conditions for THOR FE model improvements

3.2.2.1 Prototype abdomen response

The original dummy abdomen response has been overlaid with a modified version of the model (detailed in next paragraph) on Figures 3.13 to 3.16. The first thing to be seen is that the overall behaviour of the original dummy abdomen is too stiff: not enough penetration for Hardy et al. 2001 condition (Figure 3.13), too much force for Lamielle et al. 2008 condition (Figure 3.15) and Cavanaugh et al. 1986 condition (Figure 3.16). Only the condition from Foster et al. 2006 (Figure 3.14) shows a different behaviour, the original dummy response showing less force and less penetration compared to the PMHS data. This seems to indicate a rate-sensitivity effect not reproduced by the dummy. Moreover, unlike the condition from Hardy et al. 2001 and the MHA condition from Lamielle et al. 2008, the condition from Foster et al. 2006 is a pretensioner condition, where the seatbelt is pulled back by pretensioners and not by a hydraulic or pneumatic device. Such conditions are not well reproduced in FE simulation where the belt retraction over time is imposed. This explains that the sharp force peak occurring before the penetration peak can not be well fitted by dummy or human model.

3.2.2.2 Unified front an rear abdomen foams

Therefore, the first improvement to the prototype abdomen was to decrease its stiffness by setting the front foam material for both foam blocks, front and rear. In the original dummy, the front foam block is made of a soft Charcoal Polyester (open cell polyurethane foam) foam and the rear foam block is made of a stiff Sponge Rubber Neoprene (closed cell foam), according to GESAC, Inc. 1999.

Figure 3.13 shows the model response before and after the foams unification for the condition replicating 4.5 bar VRTC test. It stands out that the modification had the effect of increasing the penetration to the level of the PMHS response. The force magnitude stayed the same with a slightly modified profile, still staying in the PMHS corridor. The biofidelity is therefore increased, even if the force-penetration response shows a lower stiffness than the original model and than the PMHS response. This trend has been confirmed by replicating the A condition from Foster et al. 2006 and the MHA condition from Lamielle et al. 2008 as seen on Figure 3.14 and Figure 3.15 respectively. The same conclusion as from the VRTC test can be drawn, that is improved biofidelity.

3.2.2.2.1 Hardy et al. 2001 seatbelt condition

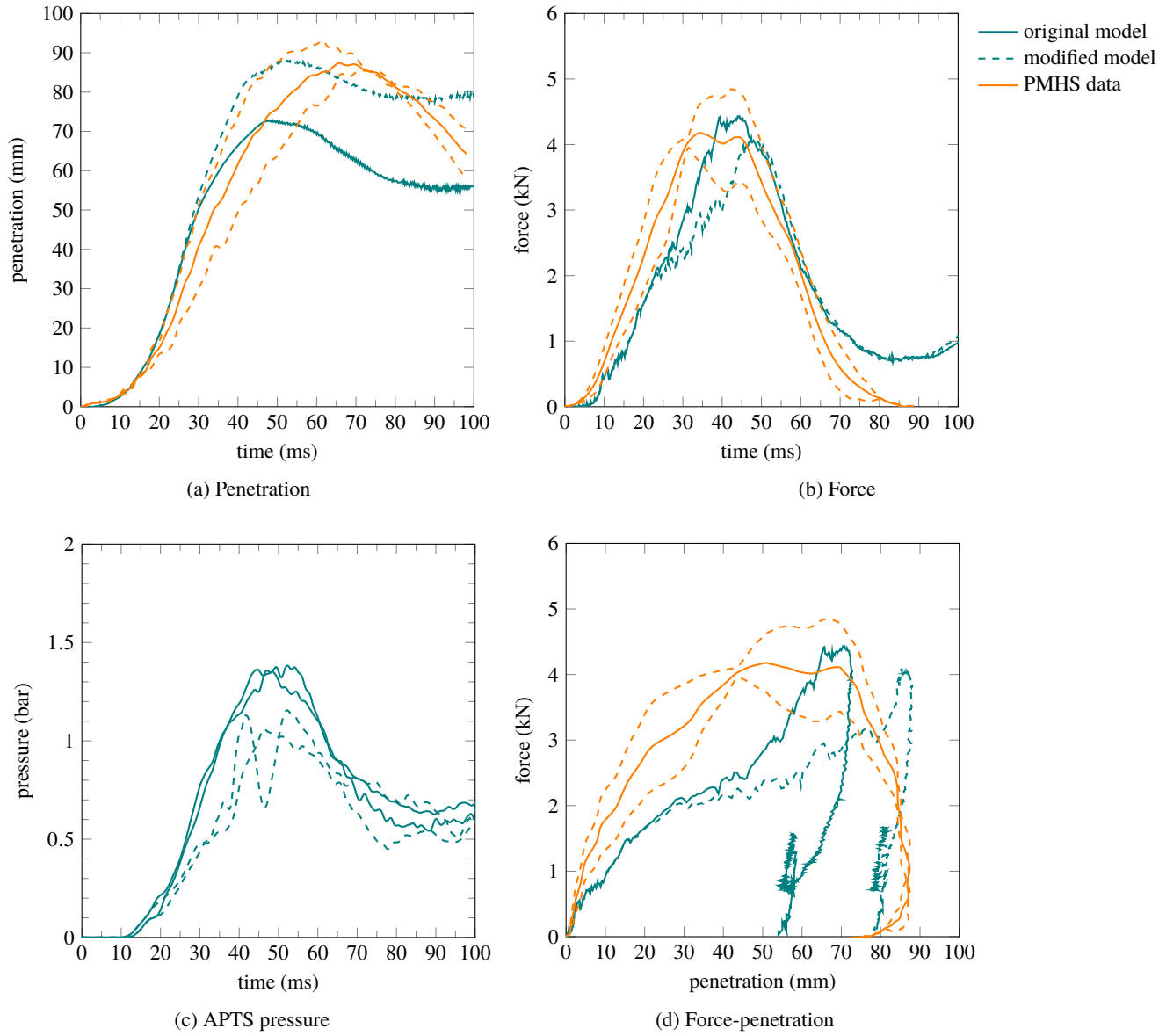

(a) Penetration

(b) Force

(c) APTS pressure

(d) Force-penetration

Figure 3.13 – THOR dummy with unified abdomen foams response under Hardy et al. 2001 4.5 bar seatbelt loading

Pressure signals filtered with CFC 180 filter

3.2.2.2.2 Foster et al. 2006 seatbelt condition

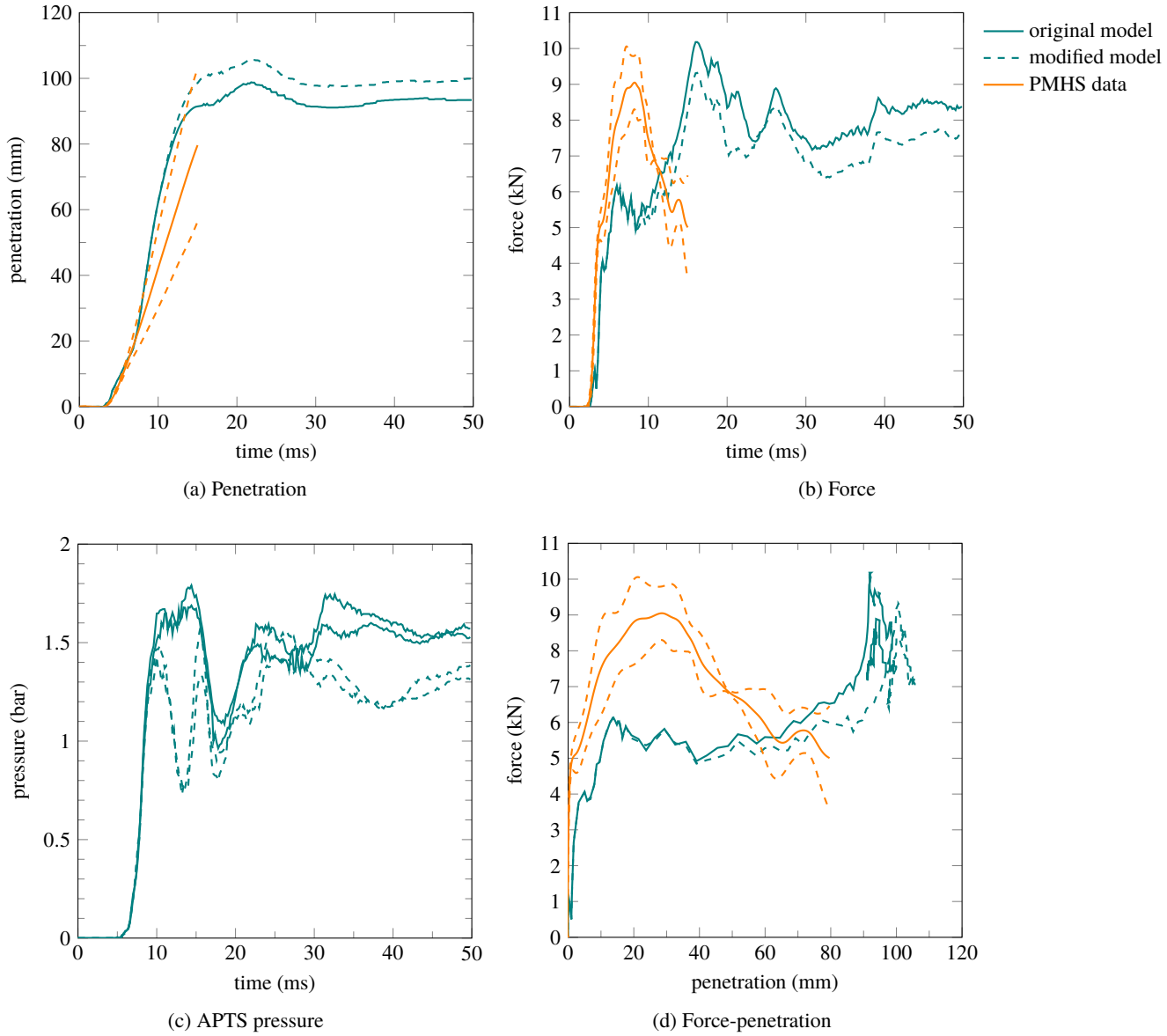

(a) Penetration

(b) Force

(c) APTS pressure

(d) Force-penetration

Figure 3.14 – THOR dummy with unified abdomen foams response under Foster et al. 2006 A condition seatbelt loading

3.2.2.2.3 Lamielle et al. 2008 seatbelt condition

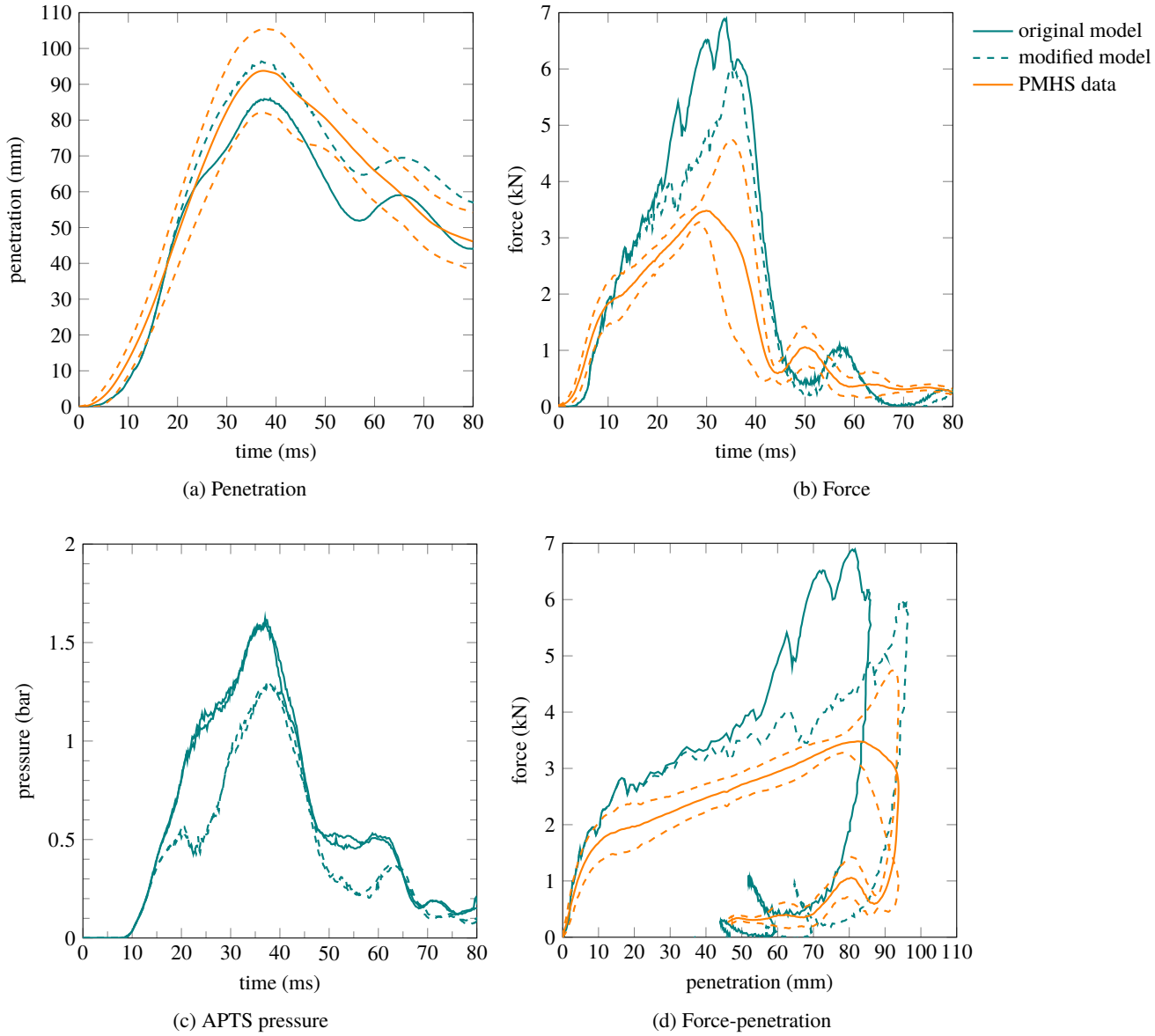

(a) Penetration

(b) Force

(c) APTS pressure

(d) Force-penetration

Figure 3.15 – THOR dummy with unified abdomen foams response under Lamielle et al. 2008 MHA condition seatbelt loading

3.2.2.2.4 Impactor simulations

The model with unified foams has been compared to the original model for the impactor case as well. As seen on Figure 3.16, the modification decreased the abdomen stiffness, bringing the dummy response closer to the PMHS response. However, the abdomen bottoms out at 120 mm, leading to a force rise toward extremely high values. It seems that no material change could solve this problem, since the dummy stiffness is correct until bottoming out.

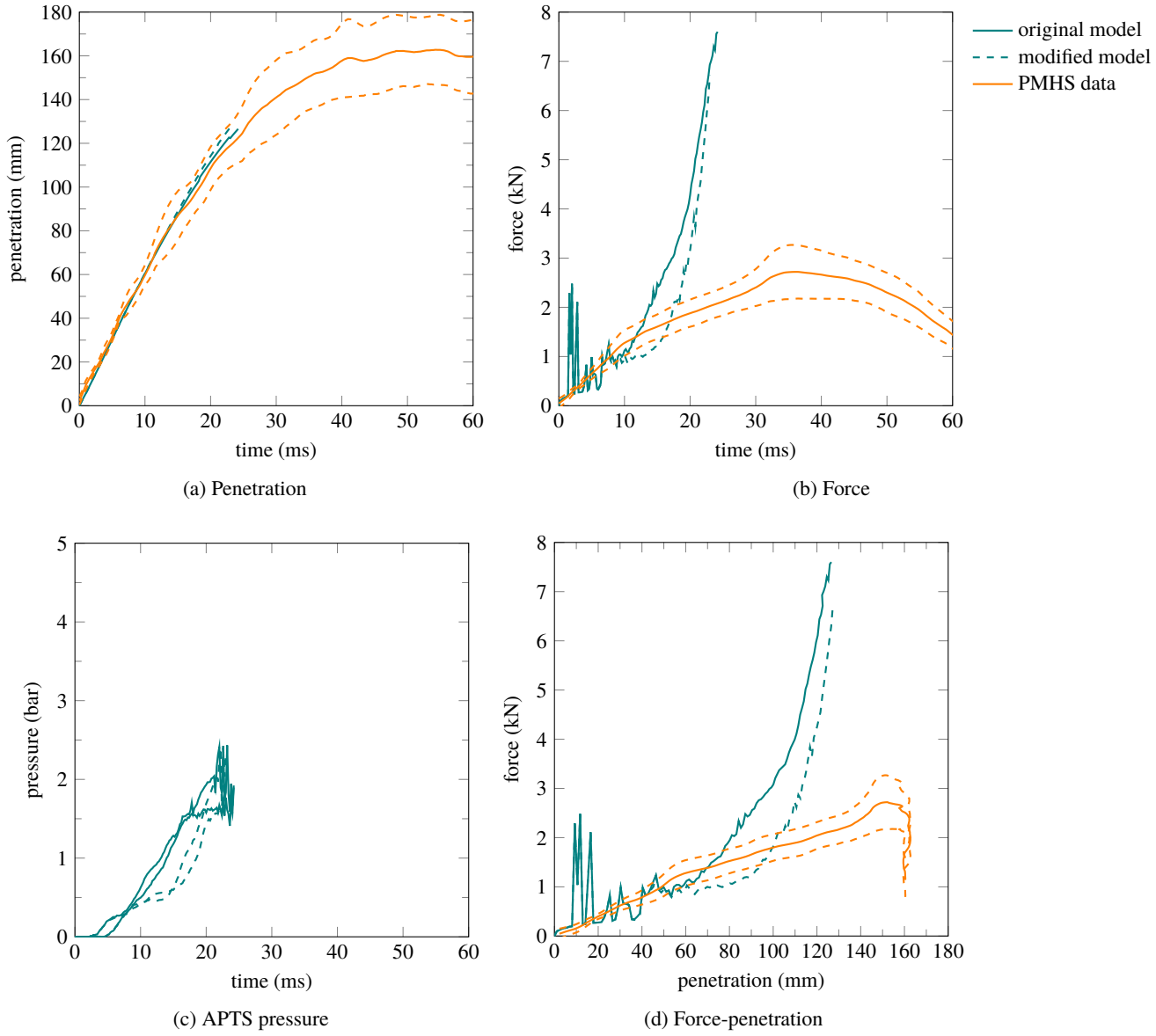

(a) Penetration

(b) Force

(c) APTS pressure

(d) Force-penetration

Figure 3.16 – THOR dummy with unified abdomen foams response under impactor loading

3.2.2.3 Change of abdomen material

Given the fact that unifying the two abdomen blocks was not enough for the dummy abdomen to achieve biofidelity, a material change was needed. A viscoelastic material model was implemented for the two deformable parts of the lower abdomen (front foam and rear foam). `MAT_006: VISCOELASTIC` was chosen due to the relatively low number of input parameter needed to represent such a behaviour and the presence of literature data for human tissue modelling for this material model. The viscous behaviour is described by a relaxation function based on a Generalized Maxwell Model as described on Figure 3.17. The deviatoric part of the stress tensor is computed with a

relaxation function in including two shear moduli (Equation 3.11c) and the volumetric part of the stress tensor is computed with the bulk modulus (Equation 3.11d), according to LS-DYNA Theory Manual (Hallquist 2006).

$$\text{Total stress: } \sigma_{ij} = s_{ij} + \pi \cdot \delta ij \tag{3.11a}$$

$$\text{Deviatoric stress: } s_{ij} = 2 \int_0^t G\left(t-\tau\right) \cdot \frac{\partial \varepsilon_{ij}\left(\tau\right)}{\partial \tau} \cdot \mathrm{d}\tau \text{ with } \varepsilon \text{ the deviatoric strain} \tag{3.11b}$$

$$\text{With: } G\left(t\right) = G_\infty + \left(G_0 - G_\infty\right) \cdot \mathrm{e}^{-\beta \cdot t} \tag{3.11c}$$

$$\text{Volumetric stress: } \pi \cdot \delta_{ij} = K \cdot \ln\left(V\right) \cdot \delta_{ij} \text{ with } V \text{ the volume} \tag{3.11d}$$

Therefore the four input parameters are:

— K: bulk modulus
— G_0: short-time shear modulus
— G_∞: long-time shear modulus
— β: decay constant

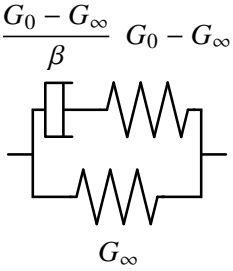

Figure 3.17 – Viscoelastic material model principle

Table 3.4 describes the viscoelastic material properties used in the human FE models from the literature.

study	organ	density (kg m^{-3})	K (MPa)	G_0 (MPa)	G_∞ (MPa)	β (ms^{-1})
Lizee et al. 1998	abdominal organs	1100	0.166	0.036	0.027	1
Ruan et al. 2003	liver, kidneys, spleen	1100	2.8	0.23	0.044	NA
	abdomen	1150	0.15	0.015	0.005	NA
	flesh	1100	1.33	0.14	0.04	NA
Kimpara et al. 2005	upper abdomen	1100	0.65	0.067	0.022	NA
	lower abdomen	1350	0.15	0.015	0.005	NA
Arnoux et al. 2008	liver, kidneys	1000	0.166	0.045	0.036	1
	spleen, stomach	1000	0.25	0.054	0.04	1
	intestines	1000	0.001	0.036	0.027	1
	abdominal flesh	1000	0.01	0.045	0.036	1
version	modification	density (kg m^{-3})	K (MPa)	G_0 (MPa)	G_∞ (MPa)	β (ms^{-1})
"liver"	human liver properties	100	0.166	0.045	0.036	1
"foam"	fit foam response	100	0.03	0.00844	0.00675	1
high G_0	G_0 mult. by 10 / "liver"	100	0.302	0.45	0.036	1
low G_∞	G_∞ div. by 10 / high G_0	100	0.302	0.45	0.0036	1

Table 3.4 – Viscoelastic material properties from the literature and for different simulation versions

3.2.2.3.1 Hardy et al. 2001 seatbelt condition

In order to make adjustment of the viscoelastic model parameters for the abdomen, Hardy et al. 2001 configuration was selected as reference condition. The liver properties of the HUMOS model (reported in Arnoux et al. 2008) were first chosen to be implemented for the dummy abdomen (apart from the density which has been kept the same as the foam material, 100 kg m^{-3}). Then, in order to

match the foam material response with the viscoelastic material, the three coefficients K, G_0 and G_∞ have been divided by 5.5. In order to improve the biofidelity and match the PMHS corridor, the initial stiffness had to be increased. This was achieved when G_0 was multiplied by 10 compared to the model with the "liver" parameters. However, despite the fact that K was kept as low as possible (this is limited by the need of having a positive Poisson's ratio, that is $\nu = \frac{3K - 2G_0}{2\,(3K + 2G_0)} > 0$), the overall behaviour was too stiff, resulting in a too low penetration. It was then chosen to divide G_∞ by 10. This resulted in an increased penetration and a suitable response in terms of biofidelity although the peak penetration is lower than the PMHS data. These results show that the K modulus was influencing the global stiffness, the G_0 modulus the short-term stiffness and G_∞ the long-term stiffness as expected. Table 3.4 shows the parameters values for all those cases and Figure 3.18 shows the result of those simulations for the 4.5 bar condition.

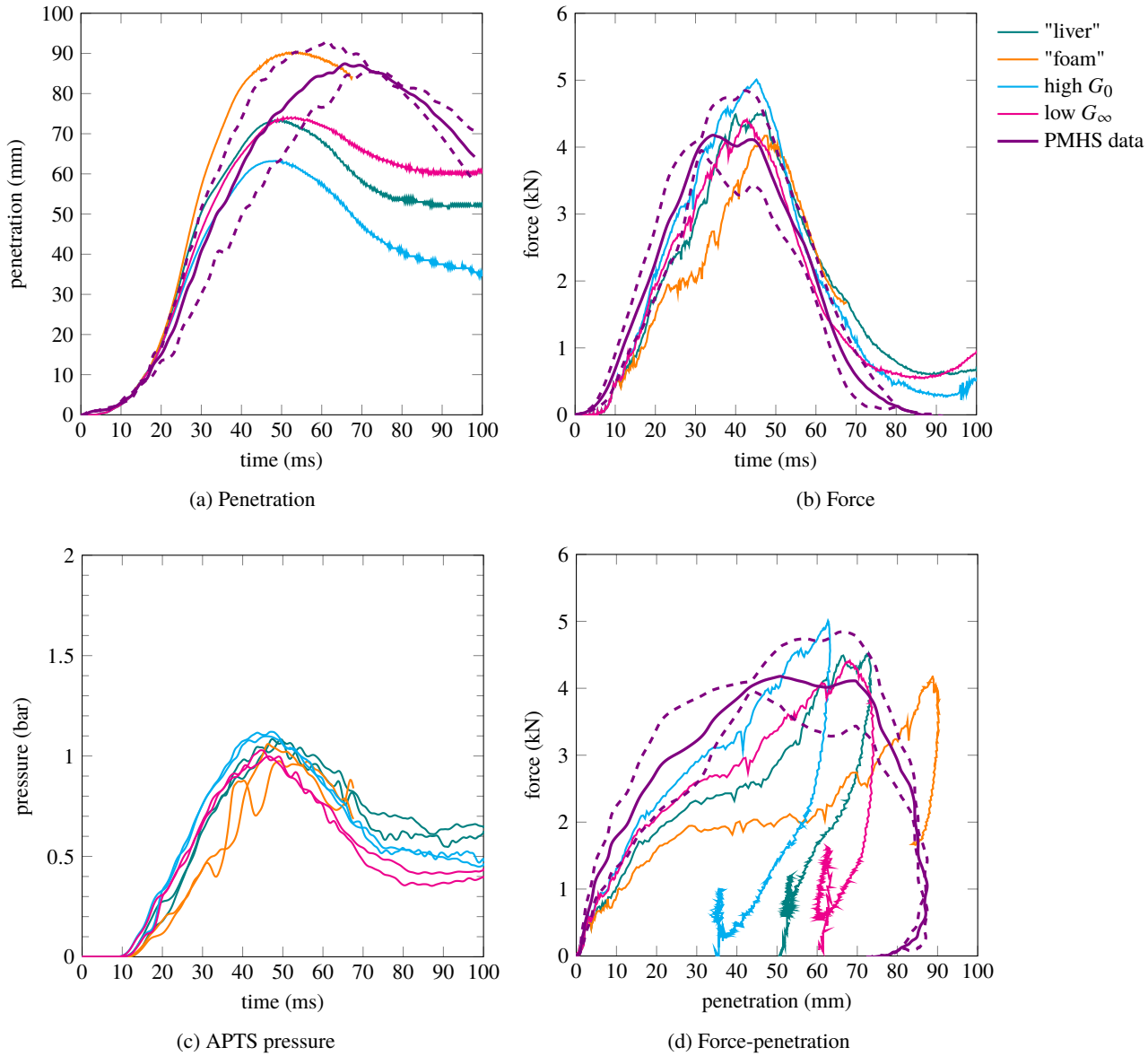

(a) Penetration

(b) Force

(c) APTS pressure

(d) Force-penetration

Figure 3.18 – THOR dummy with viscoelastic material for abdomen foams response under Hardy et al. 2001 4.5 bar seatbelt loading

Pressure signals filtered with CFC 180 filter

3.2.2.3.2 Foster et al. 2006 seatbelt condition

Figure 3.19 presents the results of the simulation with the viscoelastic material for the A condition from Foster et al. 2006. It appears that the modified material improves the abdomen response, with a good response in terms of penetration and a force magnitude close to the PMHS value although the peak time is different. As mentioned previously, this pretensioner condition is not perfectly reproduced by FE simulation which could explain those differences.

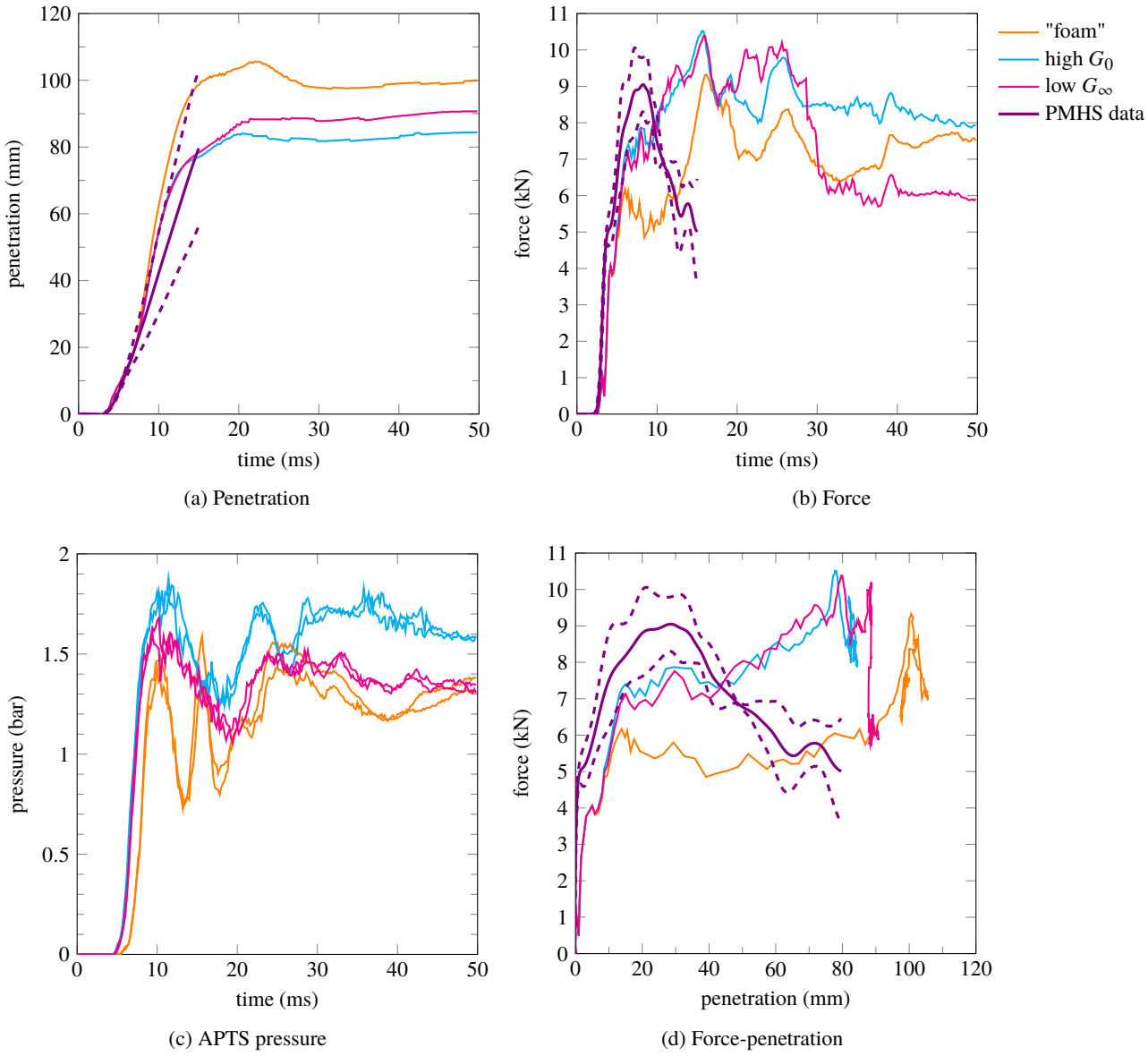

(a) Penetration

(b) Force

(c) APTS pressure

(d) Force-penetration

Figure 3.19 – THOR dummy with viscoelastic material for abdomen foams response under Foster et al. 2006 A condition seatbelt loading

3.2.2.3.3 Lamielle et al. 2008 seatbelt condition

The MHA condition from Lamielle et al. 2008 was selected as a biofidelity corridor for dummy abdomen in Lebarbé et al. 2015. Figure 3.20 shows the model response to the foam material modifications under this condition. On the opposite of Hardy et al. 2001 4.5 bar condition, the original foam properties of the abdomen gave the most biofidelic response and the modified versions had the effect of increasing the interaction force between the dummy and the seatbelt and lowering the penetration.

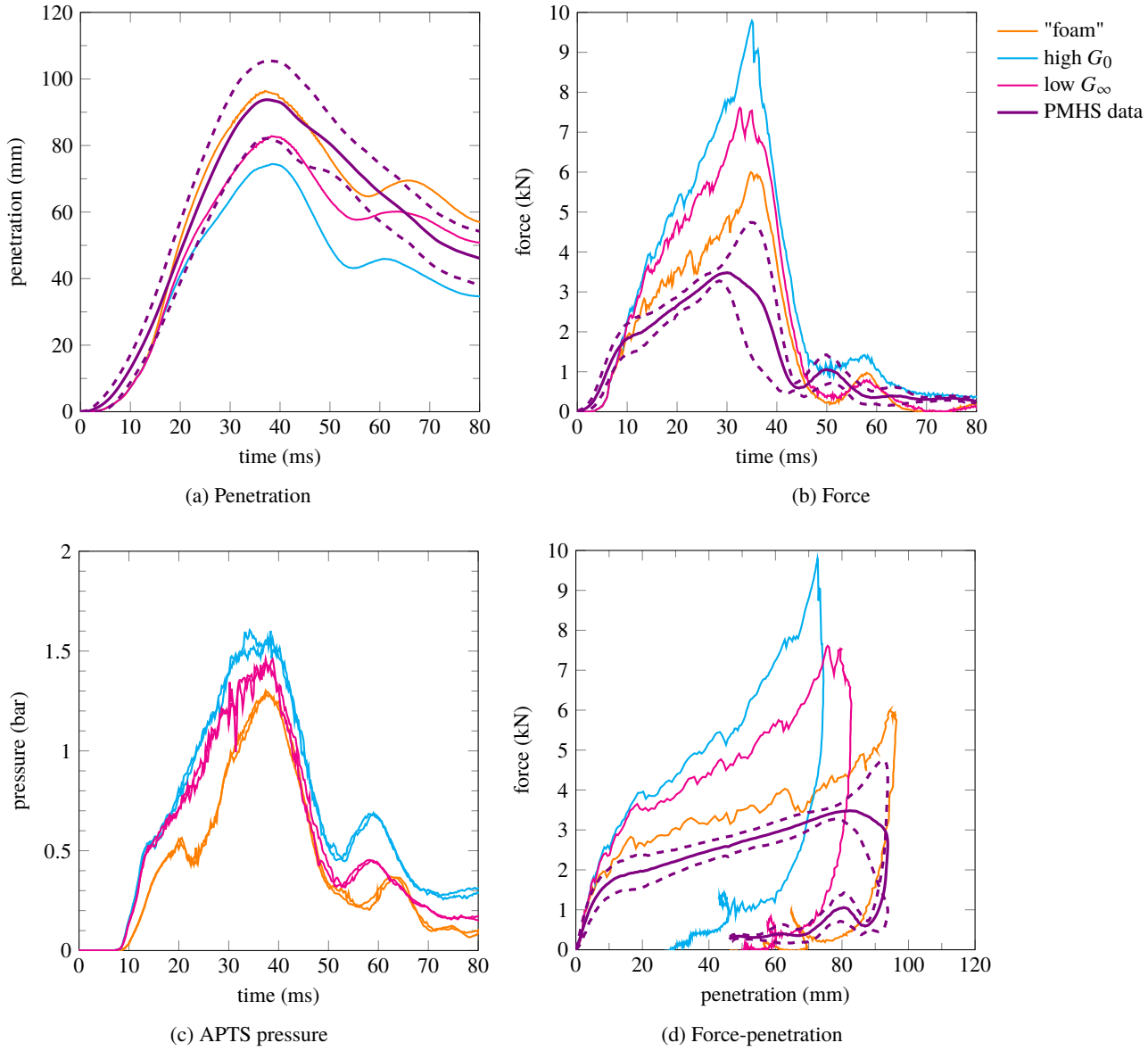

(a) Penetration

(b) Force

(c) APTS pressure

(d) Force-penetration

Figure 3.20 – THOR dummy with viscoelastic material for abdomen foams response under Lamielle et al. 2008 MHA condition seatbelt loading

3.2.2.4 Conclusion for subcomponents tests

The dummy FE model is a reliable tool to reproduce the physical dummy response under impact, including APTS pressure sensors. However, the original dummy abdomen response needs to be improved in order to have the same response as the biofidelity reference, that is PMHS subjects. Having a unified abdomen with no more distinction between the front and rear part helps to have a more biofidelic response. A change in material toward a material with a higher initial stiffness

compared to the long term stiffness allows to reproduce the PMHS response for a given condition. The modified material model fitted the human response for Hardy et al. 2001 condition and for Foster et al. 2006 condition but did not give a biofidelic result for an other condition (Lamielle et al. 2008). Given the fact that Lebarbé et al. 2015 selected Lamielle et al. 2008 MHA condition as reference condition for biofidelity targets, the abdomen with the modified material properties will not be used for the following step that is studying the influence of the dummy kinematics on the APTS pressure reading during sled tests. The prototype abdomen model with unified foam will be used since it shows good agreement with the biofidelity reference as defined by Lebarbé et al. 2015.

3.3 Sled tests

3.3.1 Test conditions

Three deceleration conditions were performed in Luet et al. 2012. The PMHS subject was seated in a rigid seat with vehicle foam covering the back rest and the feet maintained in a footrest. The subject was maintained with a two-point shoulder belt and a two-point lap belt in order to avoid the lifting of the lap belt by the shoulder belt that happens with a three-point belt. Retractors were placed on either extremities of the lap belt and at the top extremity of the shoulder belt. Three PMHS were tested for each condition. The configurations 1 and 2 were reproduced with the THOR dummy model. The lap belt angle from horizontal, the deceleration magnitude and the belt length wrapped in the retractors varied between the two configurations. Table 3.5 shows the parameters of the two configurations. Figure 3.21a shows the test set-up and Figure 3.21b shows the two deceleration profiles used. All PMHS submarined in configuration 1 whereas only one out of three submarined in configuration 2.

configuration	deceleration ($m\,s^{-2}$)	velocity change ($km\,h^{-1}$)	lap belt angle (°)	wrapped belt length (cm)
1	121	40	MS631: 36.5 MS632: 40 MS633: 35	80
2	154	50	MS634: 49.5 MS635: 48 MS636: 49	60

Table 3.5 – Configurations from Luet et al. 2012

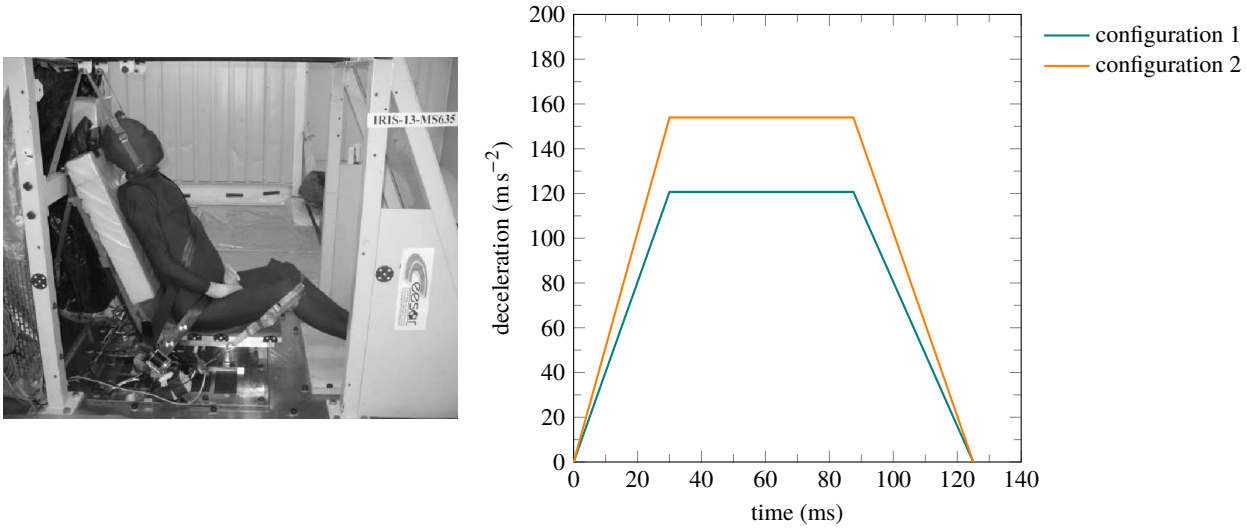

(a) Test set-up

(b) Sled decelerations

Figure 3.21 – Sled test set-up and decelerations from Luet et al. 2012

These tests have been reproduced with the FE model of the THOR dummy. The sled model with configurations parameters were provided by LAB. The model was detailed in Luet 2013. Figure 3.22a shows the differences in the FE simulation set-up for the two configurations. The deceleration profiles from Figure 3.21b were imposed to the sled floor and seat along the x direction. The dummy model was positioned with a 23° pelvis angle from horizontal as described by Luet et al. 2012 for test performed with the Hybrid III dummy. The pelvis angle for the dummy is defined as the tilt sensor angle (shown on Figure 3.22b) plus 10°. The hip, knee and ankle joints were then positioned in order to have the model feet placed flat on the footrest. This gave femur and tibia angles close to the values reported from Luet et al. 2012 for Hybrid III (24° and 47° respectively).

The dummy model was then placed tangent both to the seat and seatback. Gravity was then applied for 500 ms in order to allow the dummy pelvis to deform and have a realistic contact surface with the seat. A fixed timestep of 4×10^{-4} ms was imposed by mass scaling.

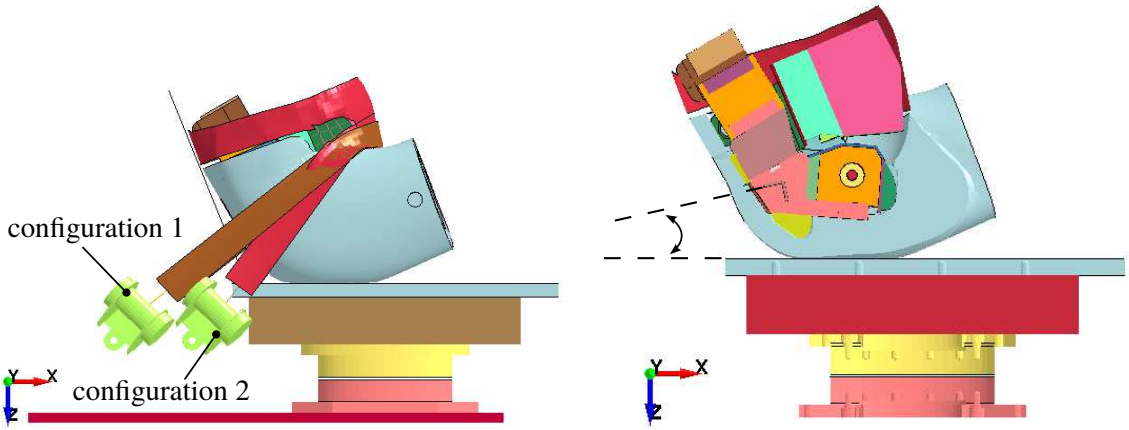

(a) Lap belt inclination for the two configurations (b) Tilt sensor angle (cross section)

Figure 3.22 – Lap belt angle for the two configurations from Luet et al. 2012

Simulations were performed with the dummy model including both the standard THOR abdomen and the IFSTTAR / Toyota prototype abdomen model with the modifications described in Section 3.2.2. This will allow to analyse the potential influence of the prototype abdomen on he dummy kinematics and on the interaction with the upper abdomen. The biofidelity of the dummy versus PMHS tests will also be assessed, particularly in terms of submarining.

3.3.2 Kinematics and global response

Figure 3.23 shows the global motion of the dummy model for a typical simulation. Trajectories of the model landmarks are presented on Figure 3.24 for all configurations. The trajectories are relative to the seat and presented for the dummy model only since the trajectories are not available for PMHS tests from Luet et al. 2012. The trajectories are presented in the lateral plane (x, z) and the top plane (x, y). The trajectories of the knee, ankle and hip point were averaged for the lateral plane trajectories between the left and right landmark due to their similarities. The hip point is the center of the hip joint. The y and z coordinates have been inverted in order to have the (x, y) corresponding to the top view and to show a positive upward vertical axis which is not the case in the model. A hip point movement along the x direction can be seen, going forward first and then backward-left relative to the seat. The knee joint center moves forward and then backward along an oblique line in the (x, z) plane while the ankle joint center moves little, the feet being maintained in overshoes. Both the shoulder and the sternum go forward-downward as a result of sled deceleration first and have a backward motion when the sled reached a constant velocity. The shoulders and sternum also move left along the simulation, the right shoulder being restrained unlike the left shoulder. For all the trajectories, no appreciable difference can be seen between the dummy with the standard or the prototype abdomen. The changes induces by the prototype abdomen are not significant enough to generate a change of such global data as landmark trajectories.

Figures 3.25 and 3.26 compare the global response parameters between the standard abdomen and the prototype abdomen for configuration 1 and configuration 2, respectively. The dashed lines represent the PMHS data, the dotted line the THOR test data and the solid lines the THOR model data. Force signals from simulation were filtered with a CFC 60 filter according to the processing mentioned in Luet et al. 2012. The dummy model global kinematics response shows less shoulder and lap belt forces than the test data from the THOR dummy. The difference is significant mostly for configuration 2 and lap belt force. It is therefore difficult to declare that the dummy model has

a validated global behaviour in sled test. For the dummy validation case under sled test detailed in THOR FE Manual (Panzer et al. 2015), the dummy model showed more belt forces than the test data (2 times as much for lap belt force). The configuration used for the model validation was however different, with the dummy knees restrained (protocol from Untaroiu et al. 2009). No information on pelvis rotation was provided, however the dummy model reproduces correctly the pelvis acceleration. However, in this study, despite the differences compared to test data, the dummy model can still be used to assess the differences induced by the prototype abdomen on the dummy behaviour.

The belt forces are of similar magnitudes between the dummy model with the standard or the prototype abdomen. However, the model with prototype abdomen shows more hip point displacement and more pelvis rotation around the y axis. This can be due to the fact that the prototype abdomen submarines earlier, therefore leading to less restraint from the lap belt and increased hip point displacement and pelvis rotation (see Table 3.6 for submarining times).

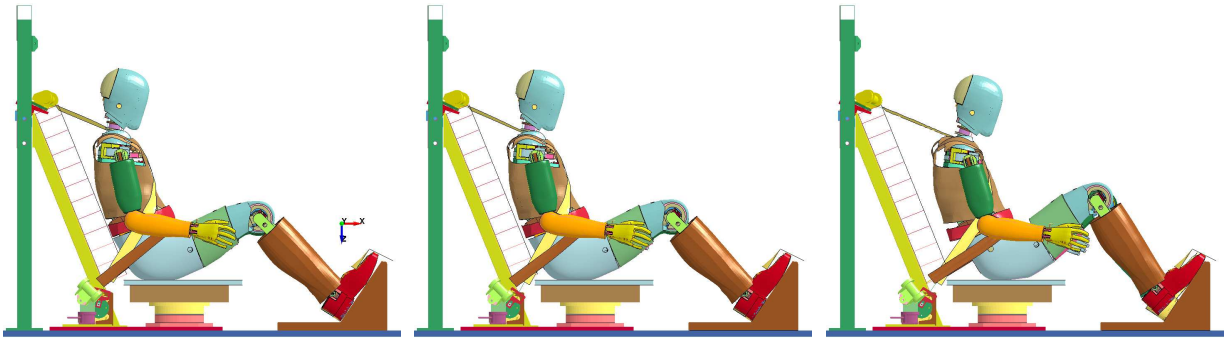

(a) 0 ms (b) 30 ms (c) 60 ms

(d) 90 ms (e) 120 ms (f) 150 ms

Figure 3.23 – Motion of standard abdomen dummy under configuration 1 relative to seat

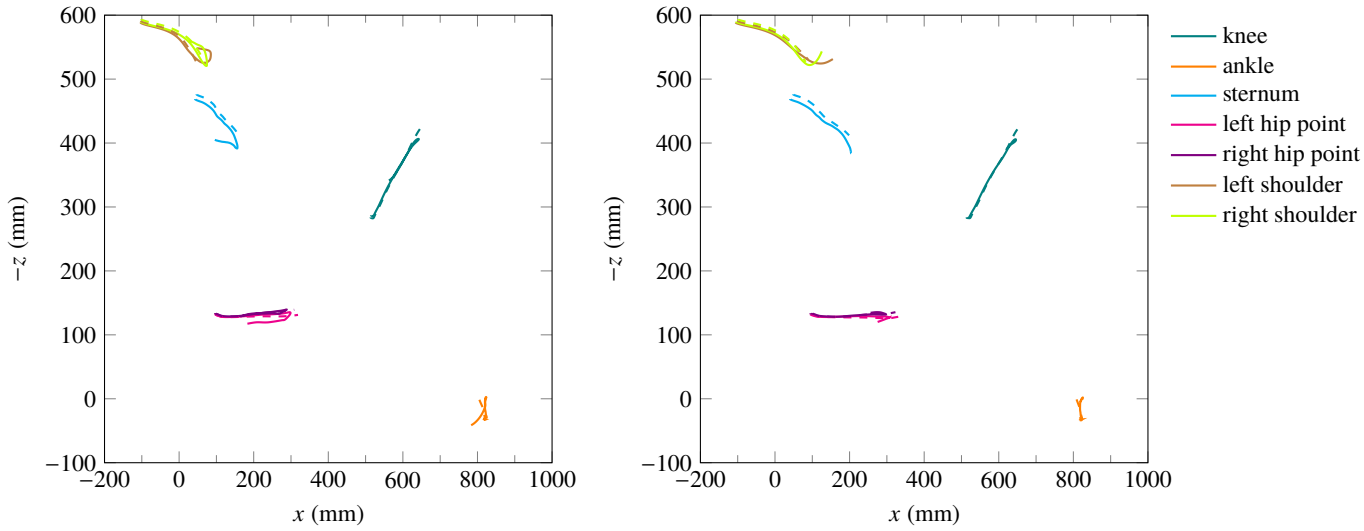

(a) Configuration 1 lateral plane

(b) Configuration 2 lateral plane

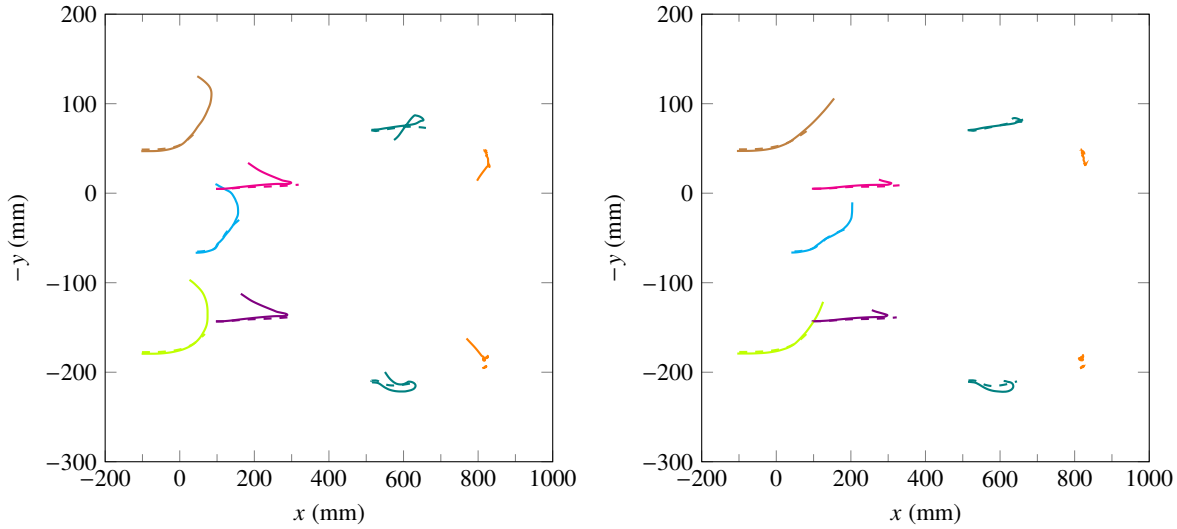

(c) Configuration 1 top plane

(d) Configuration 2 top plane

Figure 3.24 – THOR model landmarks trajectories relative to seat
Solid lines: standard abdomen
Dashed lines: prototype abdomen

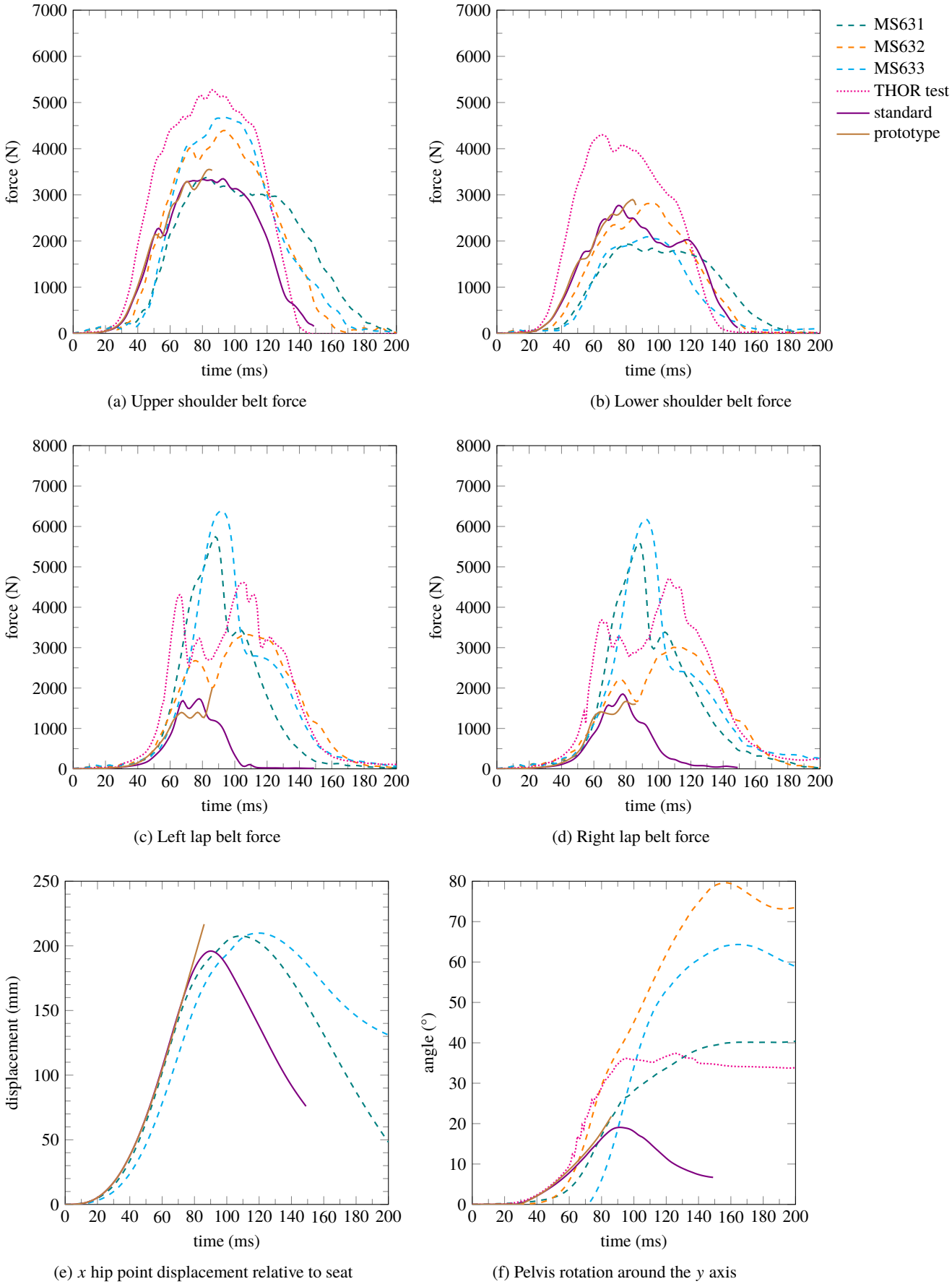

(a) Upper shoulder belt force

(b) Lower shoulder belt force

(c) Left lap belt force

(d) Right lap belt force

(e) x hip point displacement relative to seat

(f) Pelvis rotation around the y axis

Figure 3.25 – THOR model response compared to PMHS data from Luet et al. 2012 configuration 1

Force signals filtered with CFC 60 filter

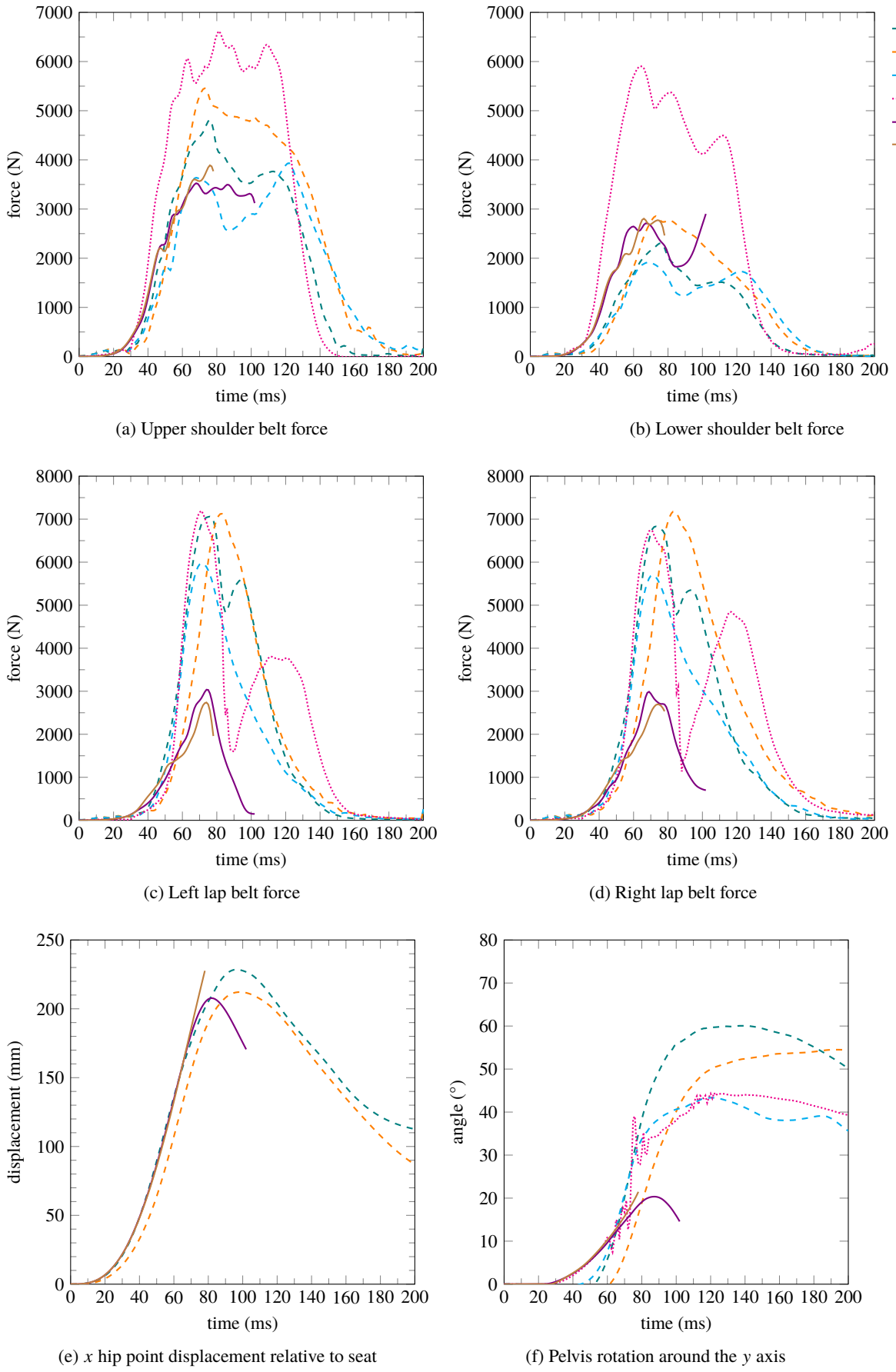

(a) Upper shoulder belt force

(b) Lower shoulder belt force

(c) Left lap belt force

(d) Right lap belt force

(e) x hip point displacement relative to seat

(f) Pelvis rotation around the y axis

Figure 3.26 – THOR model response compared to PMHS data from Luet et al. 2012 configuration 2

Force signals filtered with CFC 60 filter

3.3.3 Submarining

Submarining happens with the dummy model in all conditions, as it happened on tests with the physical dummy performed by LAB. Submarining can be identified from the animation results of the simulation when the lap belt goes over the pelvis flesh, as seen on Figure 3.27. Since the lap belt is not in direct contact with the pelvis bone, it is difficult to estimate submarining based on pelvis bone observation. However, the lap belt stops loading the pelvis bone before going over the pelvis flesh. No particular drop can be noticed in the lap belt forces but the comparison between the belt / pelvis and the belt / abdomen forces can highlight the submarining phenomenon. Figure 3.28b clearly shows for the standard abdomen in configuration 1 that the abdomen force becomes higher than the pelvis force after approximately 80 ms, before the lap belt leaves the left pelvis crest at 84 ms, the belt staying on the right crest until the end of the simulation. The same mechanism is highlighted for configuration 2 for the standard abdomen on Figure 3.28c although the pelvis and abdomen forces stay with the same magnitude after the lap belt leaves the left crest at 82 ms. For the prototype abdomen, submarining times are 82 ms for configuration 1 and 78 ms for configuration 2. Table 3.6 recapitulates the submarining times for all the configurations. The abdomen force also becomes higher than the pelvis force around submarining time but with a very high rise as described in the previous paragraph.

The fact that the lap belt goes over the pelvis only on the left side can be due to the non-symmetrical set-up of the sled test. The shoulder belt restraining the torso from the left shoulder to the right side of the trunk could be a reason. The fact that the right leg is slightly higher in the initial configuration than the left leg could also make the pelvis rotate around the x avis and create submarining on the left side.

As said previously all PMHS submarined in configuration 1 and one out of three did in configuration 2. The dummy model submarined in all the configurations, whatever with which abdomen it was equipped. The THOR dummy model shows here more tendency to submarine than the PMHS. In sled tests performed on a real car seat with the same protocol as Luet et al. 2012, Uriot et al. 2015a reported that the THOR dummy was always submarining when the PMHS were doing so. Furthermore, in a configuration where no PMHS submarined, Uriot et al. 2015a reported that the THOR dummy potentially submarined since a decrease was observed in the left ASIS [3], which matches the behaviour observed in this study with the dummy model where the lap belt goes over the pelvis only on the left side. Uriot et al. 2015a reported that the THOR predicted better submarining than the Hybrid III dummy with a better prediction of submarining time.

configuration	dummy model submarining time (ms)		PMHS submarining time (ms)
1	standard abdomen prototype abdomen	82–84 80–82	MS631: 92–97 MS632: 80–87 MS633: 96–106
2	standard abdomen prototype abdomen	80–82 76–78	MS634: 80–87 MS635: NA* MS636: NA

Table 3.6 – Dummy model submarining time for all configurations compared with PMHS results from Luet et al. 2012

*Not Applicable

3. Anterior Superior Iliac Spine

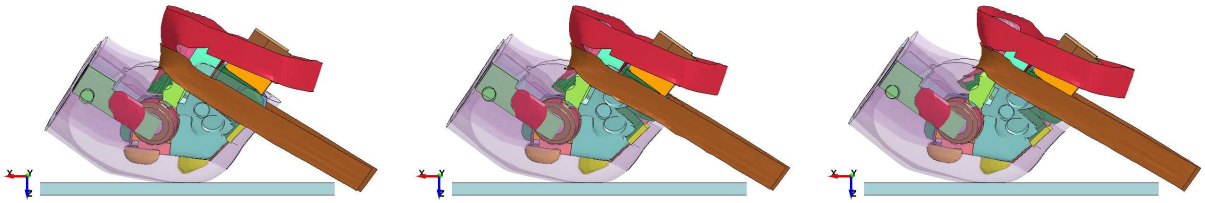

(a) 68 ms (b) 72 ms (c) 76 ms

(d) 80 ms (e) 84 ms (f) 88 ms

Figure 3.27 – Submarining phenomenon for standard abdomen dummy under configuration 1
The pelvis part has been set to transparent

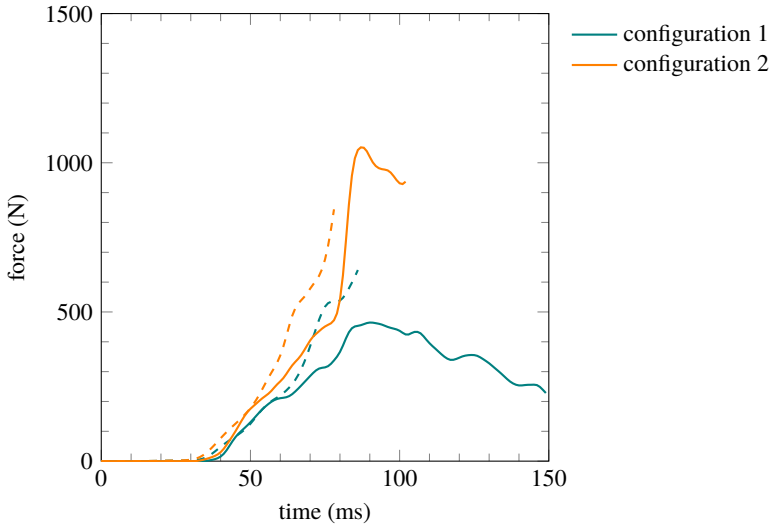

(a) Upper / lower abdomen interaction force

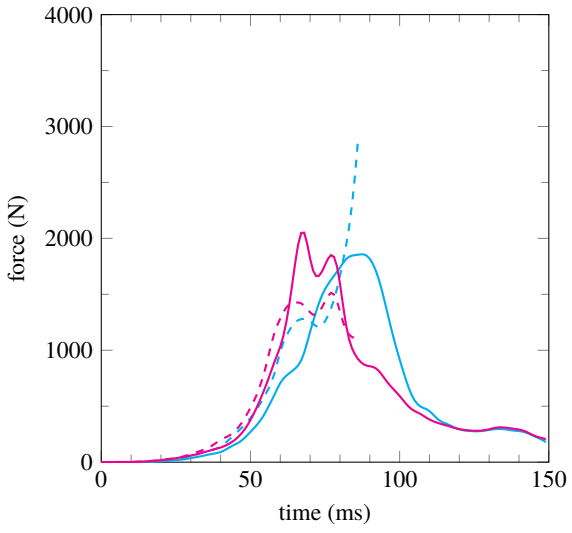

(b) Abdomen and pelvis force versus belt force for configuration 1

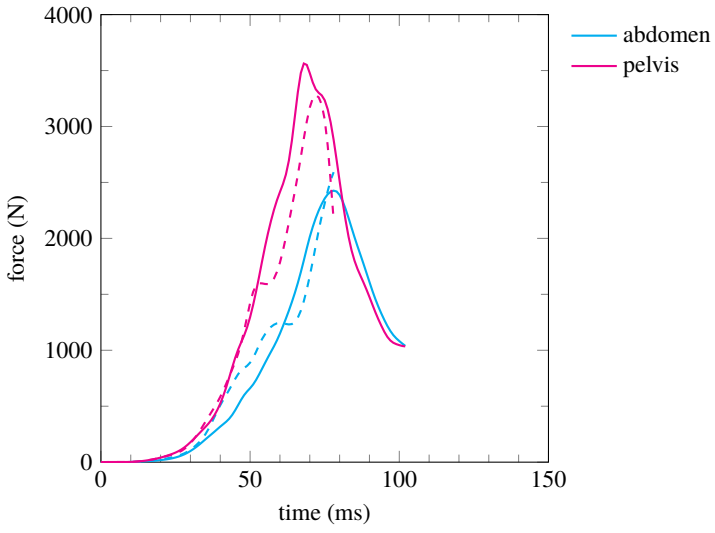

(c) Abdomen and pelvis force versus belt force for configuration 2

Figure 3.28 – Abdomen and pelvis force versus belt force
Solid lines: standard abdomen
Dashed lines: prototype abdomen
Pressure signals filtered with CFC 180 filter

3.3.4 Upper / lower abdomen interaction

Figure 3.28a compares the force data that allows to investigate if the change from standard to prototype abdomen modifies the interaction with the upper abdomen. The interaction force between the lower and upper abdomen have been computed separately from other contact forces. The model with prototype abdomen shows a higher interaction force with the upper abdomen for both configurations. This is due to the fact that, the abdomen being compressed vertically, the presence of the APTS sensors increase the abdomen stiffness in this direction. Figures 3.28b and 3.28c show the interaction forces between the lap belt and the dummy abdomen and between the lap belt and the dummy pelvis, for configuration 1 and 2 respectively. Belt / pelvis and belt / abdomen forces are higher in configuration 2 compared to configuration 1, which is explained by the fact that configuration 2 has more kinetic energy than configuration 1 which creates more forces for belt to restrain the dummy (also seen on Figures 3.25 and 3.26). Comparing the two abdomens, while the pelvis force is slightly lower for the prototype compared to the standard, the abdomen force increases for the prototype much above the force level of the standard abdomen. This is probably due the presence of the APTS in the abdomen which contact the abdomen back plate. The APTS being less compressible than the abdomen foam material, this creates a high reaction force.

Figure 3.29 shows the evolution of pressure in the APTS sensors as a function of time and other variables along with the identification of submarining event. It appears from Figure 3.29c that the sudden pressure increase before submarining is not linked to the compression of the abdomen by the seatbelt (pressure increase with the same level of belt / abdomen force) but to the interaction of the upper and lower abdomen, the upper abdomen compressing the lower abdomen as a result of torso flexion as it can be seen on Figure 3.29d, the pressure increase being almost linearly linked to the upper / liver abdomen interaction force. This pressure increase due to torso flexion only could potentially not be representative of an injury mechanism so the magnitude of pressure increase due to this phenomenon (between 0.6 bar and 0.8 bar) should potentially be substracted from the pressure value used for injury prediction.

Since the simulations terminate early for the prototype abdomen (86 ms and 78 ms for configurations 1 and 2 respectively), the evolution of the APTS pressure after submarining happened can not be analysed. It is likely that the pressure in the sensors would continue increasing after submarining.

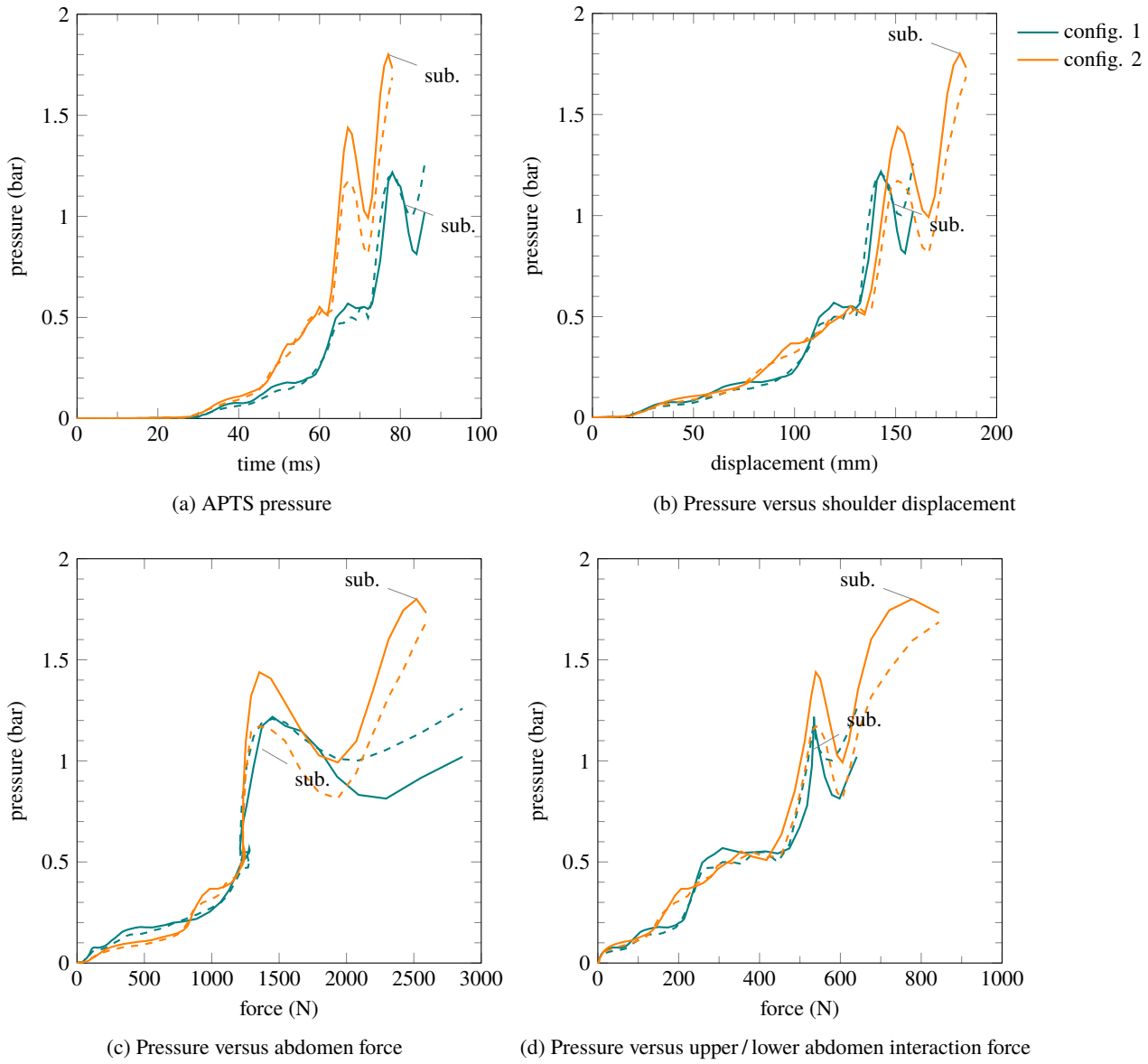

(a) APTS pressure

(b) Pressure versus shoulder displacement

(c) Pressure versus abdomen force

(d) Pressure versus upper / lower abdomen interaction force

Figure 3.29 – APTS pressure analysis with indication of submarining event
Solid lines: right pressure
Dashed lines: left pressure

3.3.5 Conclusion on the influence of the prototype abdomen

The integration of the IFSTTAR / Toyota prototype abdomen in the THOR dummy had no influence on the global dummy kinematics in terms of landmarks trajectories and restraint belt forces. However, due to the increased abdomen mass (plus 1.3 kg), the prototype abdomen model induces more hip point displacement and more pelvis rotation, which leads to an earlier submarining of 2 ms to 4 ms, which is low compared to the variability between PMHS for submarining time. Furthermore, increased pelvis rotation with the prototype abdomen goes toward more biofidelity compared to PMHS responses. The APTS sensors included in the prototype abdomen also creates more force when the lower abdomen interacts with the upper abdomen. However, since no PMHS reference exist for the internal interaction of organs between the different part of the abdomen, it is not possible to estimate if either the prototype of the standard abdomen is more biofidelic in that perspective. Furthermore, a part of pressure increase can be linked to torso flexion, which could be a bias not representing an injurious loading of the abdomen. However, due to the absence of PMHS reference concerning injury mechanisms created by torso flexion, it is difficult to estimate the bias introduced

by this pressure increase in injury prediction. There is potentially a paradox with the dummy model showing less pelvis rotation than the PMHS but submarining more easily. This is likely to be due to the pelvis part design which "hooks" less the seatbelt compared to a human pelvis. Therefore the fact that the pelvis rotation of the prototype abdomen is closer to the PMHS response increases the submarining ability, which goes against the PMHS observations. This should be balanced compared to the observations from Uriot et al. 2006 who stated that the THOR NT pelvis hooks more the seatbelt than the PMHS pelvis. The belt / pelvis angle at submarining time was higher for the dummy compared to the human subjects in an isolated pelvis set-up. However, the results from Uriot et al. 2006 are based on the NT version of the dummy, whereas in this study the Mod-kit version was used. Since the pelvis flesh was significantly modified between the two versions, new test data based on the Mod-kit version would be needed.

3.4 Conclusion

The lumped element model analysis showed that the THOR dummy abdomen was more elastically and less viscously deformable than the human abdomen. Material and design changes of the abdomen that would allow a more biofidelic response were implemented in the FE model of the prototype abdomen. The unification of the two foam layers of the abdomen improved the biofidelity. A material change for the unified foam block toward a visco-elastic material with an increased viscous contribution proved to be able to improve the biofidelity for some loading conditions. However, although the prototype abdomen has little influence on the global kinematics of the dummy in sled tests, more hip point displacement and more pelvis rotation can be seen. The interaction force between the upper and lower abdomen is also increased by the prototype abdomen presence. Nevertheless, it is difficult to know if the influence of such interaction on the APTS pressure reading represents a risk of injury. The fact that no biofidelity reference exists for this phenomenon adds to this difficulty. Further design changes would also be needed to have a biofidelic submarining behaviour, that is to say a more pelvis rotation and no submarining when it is not observed with PMHS.

Chapter 4

Abdominal injury assessment using THOR prototype abdomen

Contents

4.1 Introduction

Impactor or seatbelt loading tests on PMHS provide global response data in terms of force and penetration as well as injury outcomes but do not allow to estimate the loading severity for a specified organ. Human finite element models allow to reproduce these loadings while looking at detailed engineering parameters at the organ level. In order to find an injury criterion applicable to the IFSTTAR / Toyota prototype abdomen, PMHS studies were reproduced with the THUMS finite element human model. The injury outcomes from the PMHS studies in parallel with the organ loading parameters from the model would allow to set a threshold for the pressure measured by the APTS in the prototype abdomen in order to define an injury criterion.

4.2 Reproduction of PMHS tests with the THUMS model

4.2.1 Presentation of the THUMS model

The THUMS model is a full body human finite element model developed under LS-DYNA by Toyota Motor Corporation and Toyota Central R & D Labs., Inc.. The last commercial version of the model is version 4.0 as described in Shigeta et al. 2009. This model have proportions close to an average adult male (size 179 cm, weight 74 kg according to THUMS Manual (Toyota Motor Corporation 2011). The thorax and abdomen of the version 4.0 model have been created using CT [1] scans from a 39 year-old subject (size 173 cm, weight 77 kg). The scans were from the University of Michigan database. The model is available in two different positions. The model in the pedestrian (standing) position was directly build from the scans. The model in car occupant position was derived from the pedestrian model. Figure 4.1 shows the two commercial models. Models specifically positioned to reproduce PMHS tests from the literature received from Toyota Motor Corporation have been used for impactor and seatbelt simulations.

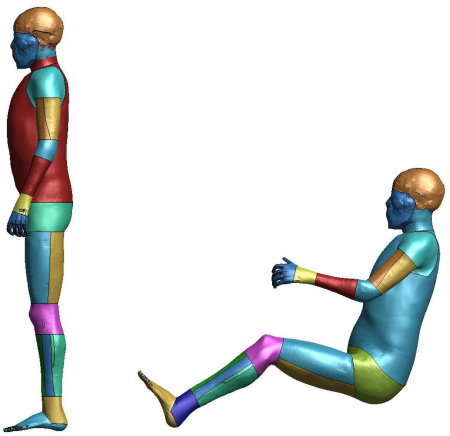

Figure 4.1 – Pedestrian and occupant versions of the THUMS model (THUMS Manual, Toyota Motor Corporation 2011)

The model has approximately 1300 parts, 1 800 000 elements and 630 000 nodes. Table 4.1 shows the different anatomical regions of the model along with the number of parts of those regions.

The abdomen of the model can be seen on Figures 4.2a and 4.2b. The properties of the main parts such as type and number of elements, density and material law are detailed in Table 4.2. Each volumetric part is coated by a shell part for contact purposes or to represent the capsule of the organs if they have one. The hollow organs are modelled as compressible with a simplified hyperelastic material model (`MAT_057: LOW_DENSITY_FOAM`) whereas the solid organs are modelled as

1. Computed Tomography

number	body region	number of parts
1	Lower Extremity - Right	129
2	Lower Extremity - Left	129
3	Abdomen and Pelvis	48
4	Internal Organs	60
5	Upper Extremity - Right	97
6	Upper Extremity - Left	97
7	Neck	156
8	Head	236
9	Thorax	321

Table 4.1 – Body regions of the THUMS pedestrian model (THUMS Manual, Toyota Motor Corporation 2011)

incompressible with a hyperelastic rubber material model (`MAT_181: SIMPLIFIED_RUBBER`), according to Shigeta et al. 2009. Those material models are detailed in Appendix C. The mechanical response of those models is based on an engineering stress / strain curve from uniaxial test data. The curves can be seen on Figures 4.2c and 4.2d. The liver data was obtained from Tamura et al. 2002 and the small and large intestine data was obtained from Yamada 1970.

part	type	number of elements*	material model	density ($kg\,m^{-3}$)	mass (kg)
thoracic fat	volumetric	43000	hyperelastic incompressible (`MAT_181`)	1100	0.985
abdominal fat	volumetric	84000	hyperelastic incompressible (`MAT_181`)	1100	2.276
liver	volumetric	59000	hyperelastic incompressible (`MAT_181`)	100	0.179
liver coat	shell	6500	orthotropic membrane (`MAT_034`)	900	0.147
pancreas	volumetric	1500	hyperelastic incompressible (`MAT_181`)	100	0.00291
pancreas coat	shell	600	orthotropic membrane (`MAT_034`)	900	0.0132
spleen	volumetric	1800	hyperelastic incompressible (`MAT_181`)	100	0.0588
spleen coat	shell	2900	orthotropic membrane (`MAT_034`)	900	0.0744
right kidney	volumetric	6100	hyperelastic incompressible (`MAT_181`)	100	0.0186
left kidney		6300			0.0191
right kidney coat	shell	1200	orthotropic membrane (`MAT_034`)	900	0.0334
left kidney coat		1200			0.0339
stomach	volumetric	6100	hyperelastic incompressible (`MAT_181`)	100	0.0161
stomach coat	shell	1400	orthotropic membrane (`MAT_034`)	900	0.0335
small intestine	volumetric	68000	hyperelastic compressible (`MAT_057`)	499	1.18
small intestine coat	shell	9600	orthotropic membrane (`MAT_034`)	1000	0.245
large intestine	volumetric	39000	hyperelastic compressible (`MAT_057`)	708	0.54
large intestine coat	shell	7000	orthotropic membrane (`MAT_034`)	1000	0.161
bladder	volumetric	4400	elastic fluid (`MAT_001`)	1000	0.118
bladder coat	shell	1500	orthotropic membrane (`MAT_034`)	1000	0.0314
left flesh	volumetric	42000	hyperelastic incompressible (`MAT_181`)	1100	7.09
right flesh					
left flesh coat	shell	8300	orthotropic membrane (`MAT_034`)	1000	0.248
right flesh coat					

Table 4.2 – Properties of the main parts of the THUMS abdomen
*Approximate number

Three main contacts are defined in the model. All the parts in the contact are checked for penetration with all the others. The skin contact (Figure 4.3a) contains 34 parts and represents the outer surface of the body. It prevents the regions of the model of penetrating the others. The body contact (Figure 4.3b) is made of 201 parts and manly includes bones connecting tissues. The organs contact (Figures 4.3c and 4.3d), made of 18 parts includes the shell parts covering the organs and shell parts surrounding the organs such as the pleura or the peritoneum parts. Contacts create a non-penetration condition between the parts they include. The other way to create non-penetration condition between parts used in the model is to have the parts sharing the same nodes at their interface. This technique is used to link together the different part sets mentioned above in the different contacts.

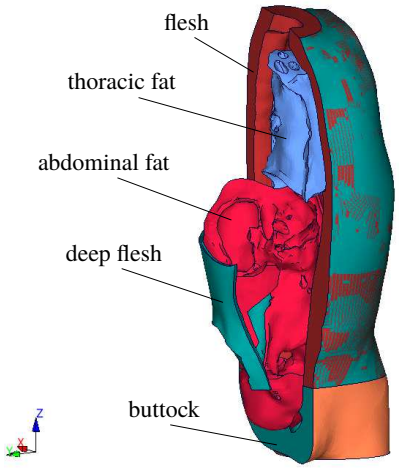

(a) Flesh and fat tissues

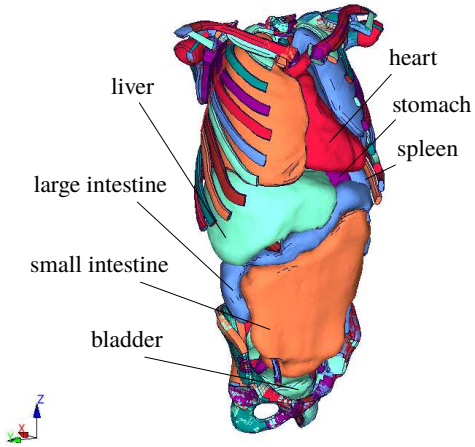

(b) Organs[a]

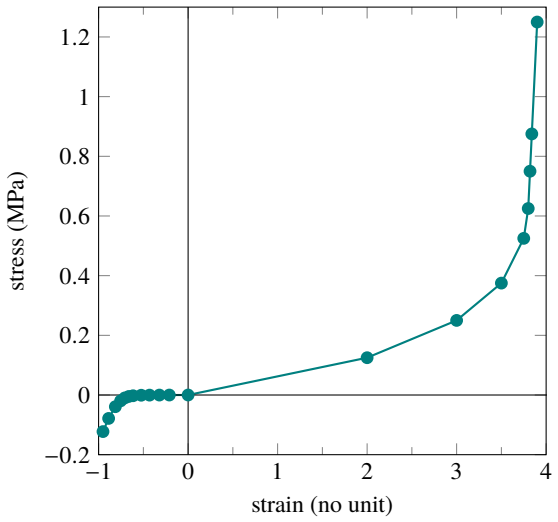

(c) Liver material curve[b]

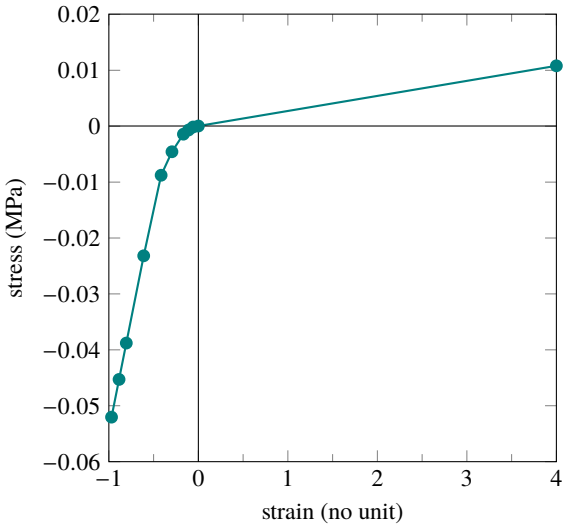

(d) Intestines material curve[b]

Figure 4.2 – Partial view and material curves of the main parts of the THUMS abdomen

[a]Flesh and fat parts have been hidden as well as pleurae, sternum, ribs cartilage and intercostal parts. Kidneys and pancreas can not be seen

[b]Positive and negative values represents the tension and compression characteristics, respectively

The simulations performed with the THUMS model were run using a fixed timestep of 4×10^{-4} ms achieved with mass scaling (as advised by Toyota Motor Corporation) and no gravity was applied.

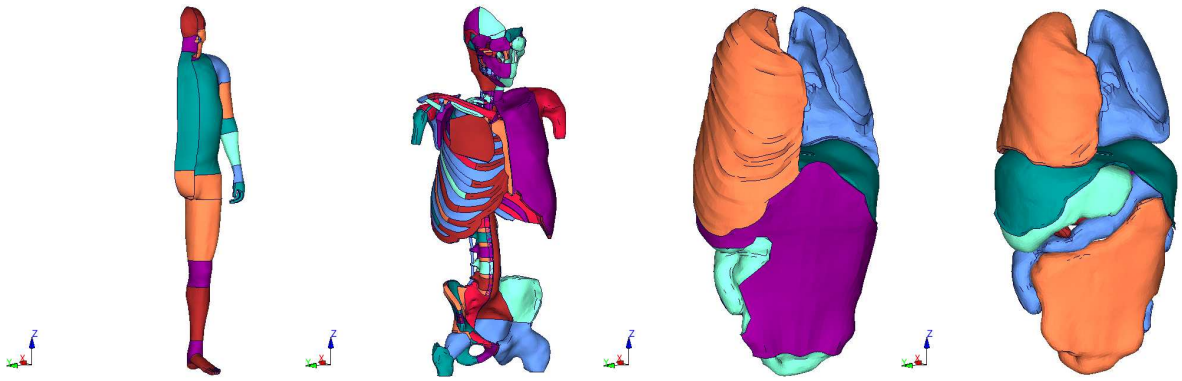

(a) Skin contact[a] (b) Body contact[a] (c) Organs contact (d) Organs contact (partial view)[b]

Figure 4.3 – Main contacts in the THUMS model (scale is not consistent across the pictures)
[a]Shell part on the right hand side of the model have been hidden for clarity
[b]Shell parts surrounding the organs have been hidden

4.2.2 Impactor simulations

Impactor tests from the literature were selected to be reproduced in simulation. Only results from Hardy et al. 2001 mid-abdomen 6 m s^{-1} will be presented here. Other configurations (Cavanaugh et al. 1986 and Hardy et al. 2001 upper abdomen) will not be presented. The model used was a model positioned for impactor test configuration by Toyota Motor Corporation, as used in Shigeta et al. 2009. The mass of the impactor was adjusted to 48 kg and its velocity was set to 6 m s^{-1}. The differences between the model and tests from Hardy et al. 2001 are the position of the legs, which are not straight and supported by the floor surface. The position of the arms is also different since in the model they are not hung to a hook above the subject. It has been chosen to keep the model that way, as no major influence on the response was forecasted.

To reproduce the mid-abdomen loading case from Hardy et al. 2001, the position of the impactor aligned with the L3 vertebra. The penetration was measured as the difference between y-coordinate of a node in the median plane of the impactor and a node on the back of the subject in line with the impactor node as seen on Figure 4.4b. The force is taken as the the y component of the contact force between the impactor as master part and the abdomen.

Figure 4.5c shows the simulation response in terms of force and penetration although slightly less penetration is predicted by the model. The response is in good agreement with the PMHS data from Hardy et al. 2001. However the response matchs better the test data when considering abdominal compression instead of penetration as shown on Figure 4.5d. The compression is the penetration of the impactor into the abdomen divided by the initial abdominal depth of the subject. This is to take into account the disparity between the abdominal depth of the THUMS model and those of the test subjects from Hardy et al. 2001 as shown on Table 4.3. The abdominal depth of the model is the difference between the y axis coordinates of the nodes shown on Figure 4.4b in the initial state of the simulation. Figure 4.6 shows the deformed shape of the model.

subject	gender	age (years)	stature (cm)	mass (kg)	abdomen depth (mm)
THUMS model	NA	NA	178	73	260
GI3	M	87	173	73	307
GI4	F	93	165	58	292
GI6	M	85	165	91	307

Table 4.3 – Abdominal depths of the THUMS model and subjects from Hardy et al. 2001

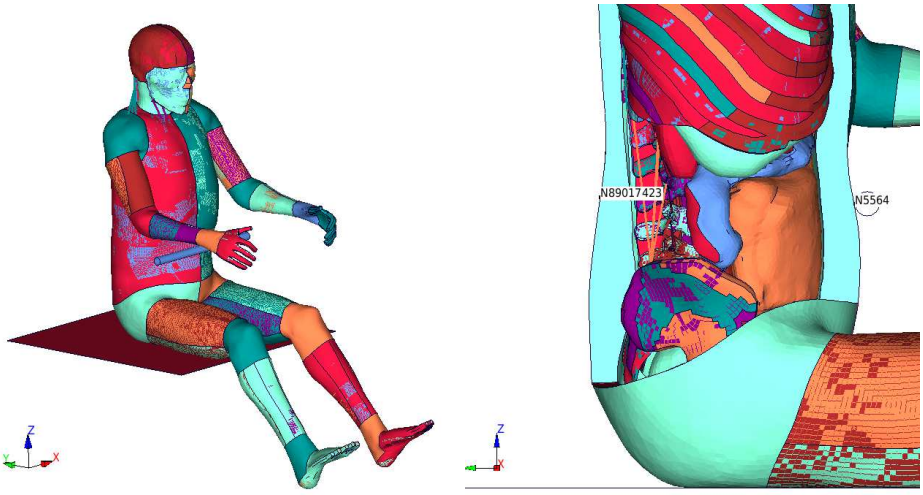

(a) Mid-abdomen impactor simulation

(b) Penetration measurement for impactor simulation

Figure 4.4 – Mid-abdomen impactor simulation setup and penetration measurement

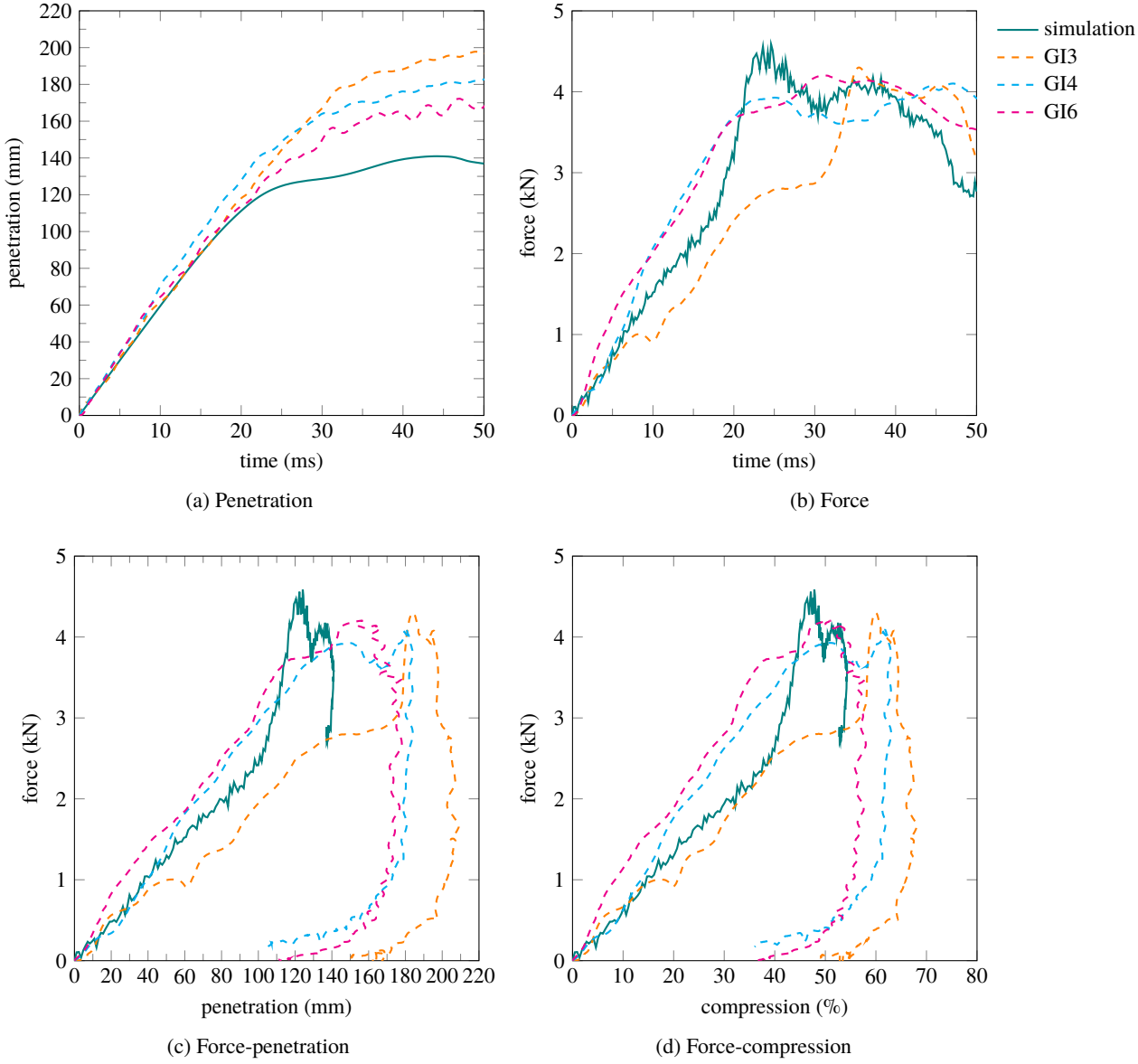

(a) Penetration

(b) Force

(c) Force-penetration

(d) Force-compression

Figure 4.5 – Mid-abdomen impactor 6 m s^{-1} simulation response versus PMHS from Hardy et al. 2001

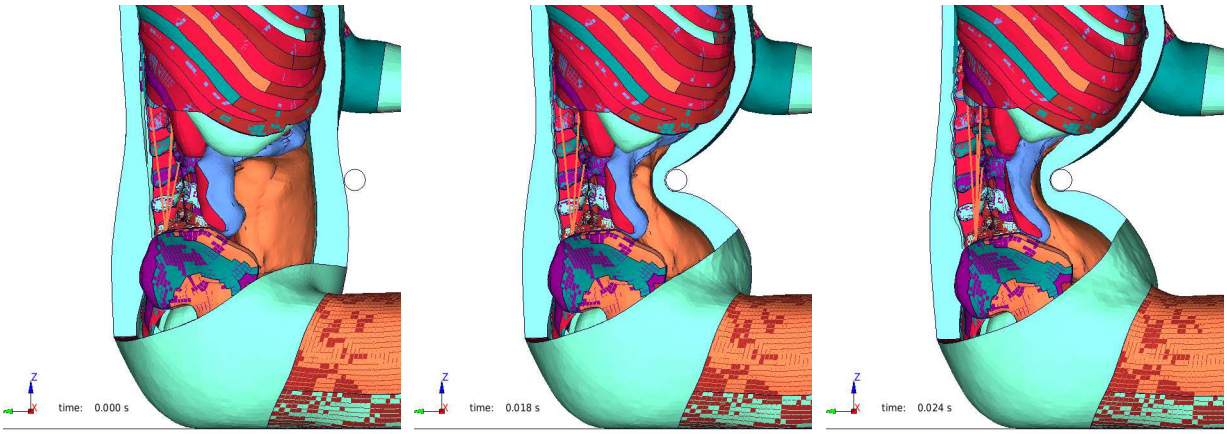

(a) 0 ms (b) 18 ms (c) 24 ms

(d) 26 ms (e) 30 ms (f) 50 ms

Figure 4.6 – Mid-abdomen impactor 6 m s^{-1} simulation deformed shape

4.2.3 Seatbelt simulations

Seatbelt tests from Foster et al. 2006 and Lamielle et al. 2008 were reproduced in simulation. Toyota Motor Corporation provided the model used in Shigeta et al. 2009. Due to chapter length considerations, only the two conditions from Lamielle et al. 2008 will be presented here.

4.2.3.1 Lamielle et al. 2008 MHA condition

For Lamielle et al. 2008 MHA tests the belt was pulled by an hydraulic jack with the objective of reaching a constant speed. Two target retraction velocities of $4\,\mathrm{m\,s^{-1}}$ (MHA111 and MHA151) and $5\,\mathrm{m\,s^{-1}}$ (MHA115 and MHA155) were used. Figure 4.7 shows the belt retraction, velocity and displacement profile of the MHA tests. Table 4.4 shows the characteristics of the PMHS subjects.

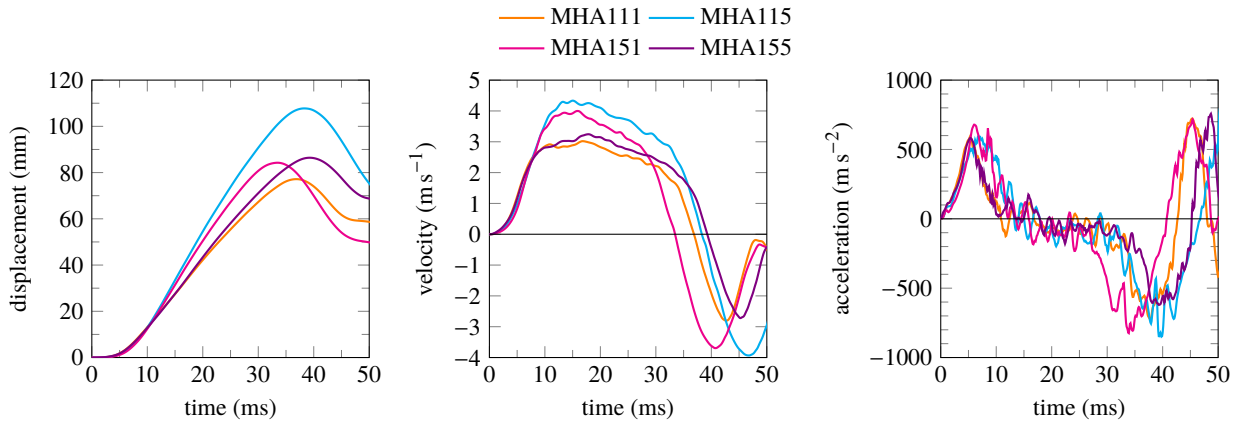

(a) Seatbelt retraction (b) Velocity (c) Acceleration

Figure 4.7 – Input conditions from Lamielle et al. 2008 MHA series

subject	gender	age (years)	stature (cm)	mass (kg)	abdomen depth (mm)
THUMS model	NA	NA	178	73	252
MHA111	M	74	175	77	287
MHA115	M	82	180	78	268
MHA151	M	88	166	69	249
MHA155	M	88	169	60	234

Table 4.4 – Abdominal depths of the THUMS model and subjects from Lamielle et al. 2008 MHA condition

In order to reproduce the PMHS test condition, it has been chosen to impose the belt retraction profile over time. All tests from the MHA condition were simulated and the THUMS model showed a lower force level than the PMHS data. Therefore, the test with the highest retraction velocity of all, MHA115, will be used as reference since it gave the highest force level of all the simulated cases.

Figure 4.8 shows the response of the model along with the PMHS curves. Penetration is in good agreement with the PMHS data, which is expected. The force magnitude is lower than the test data but the shape exactly the same the test responses.

Figure 4.8d compares the force between the back of the subject and the test bench, for the test data as well as for the simulation. The back force predicted by the simulation is lower than the test data, in the same proportions as the abdomen force. An other difference is that the simulated back force is phase-shifted compared to the test data. That is the back force from the simulation starts rising approximately 15 ms after the force from PMHS tests. This could be explained by how the

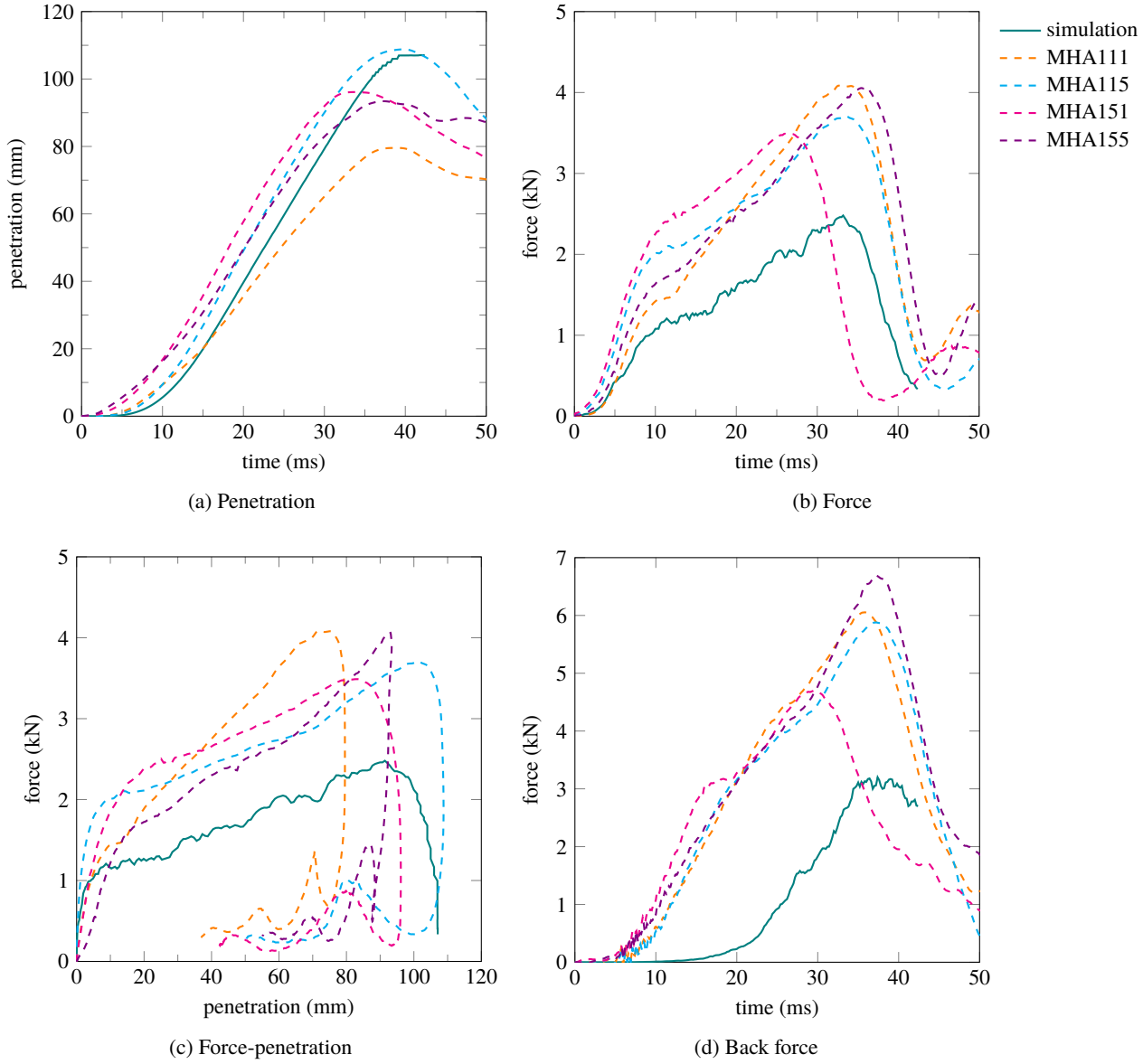

(a) Penetration

(b) Force

(c) Force-penetration

(d) Back force

Figure 4.8 – Simulation results of Lamielle et al. 2008 MHA115 condition

subject is positionned against the seatback in both cases. In the simulation, the model has been translated until its back became tangent to the seatback plane. The coupling between the subject and the seatback is therefore weak before the simulation starts. It is likely that in the PMHS set-up, the subject back is already deformed against the seatback before the test starts, therefore creating a stronger coupling.

Figure 4.9 compares the deformed shape of the simulation and images from the relevant PMHS test. In the PMHS test, the belt penetrates into the abdomen of the subject before the test starts. This initial penetration is due to the pre-tension of 20 N applied to the belt (10 N in each strand as mentioned in Lamielle et al. 2008). This applies to the PRT condition too where the initial penetration seems more important (see Figure 4.14d).

Figure 4.10 shows the deformation of the seatbelt during the simulation and Figure 4.11a superimposes the belt deformed shapes along the simulation with the umbilicus point as fixed reference point. According to Figure 4.11b, the peak of belt penetration into the abdomen is the same as the peak seatbelt retraction.

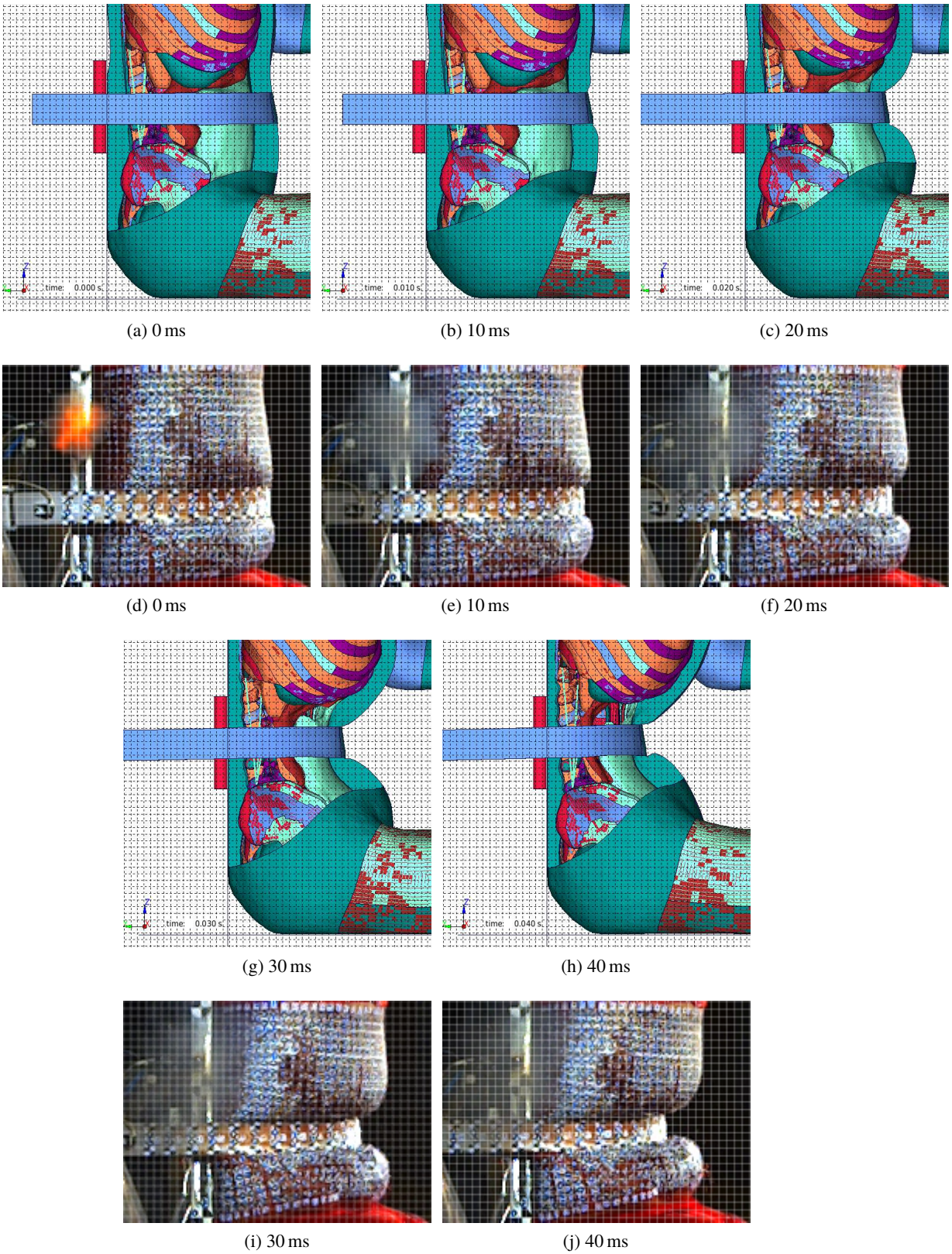

(a) 0 ms (b) 10 ms (c) 20 ms

(d) 0 ms (e) 10 ms (f) 20 ms

(g) 30 ms (h) 40 ms

(i) 30 ms (j) 40 ms

Figure 4.9 – MHA condition seatbelt simulation deformed shape compared with MHA115 PMHS images

The grid size is 10 mm

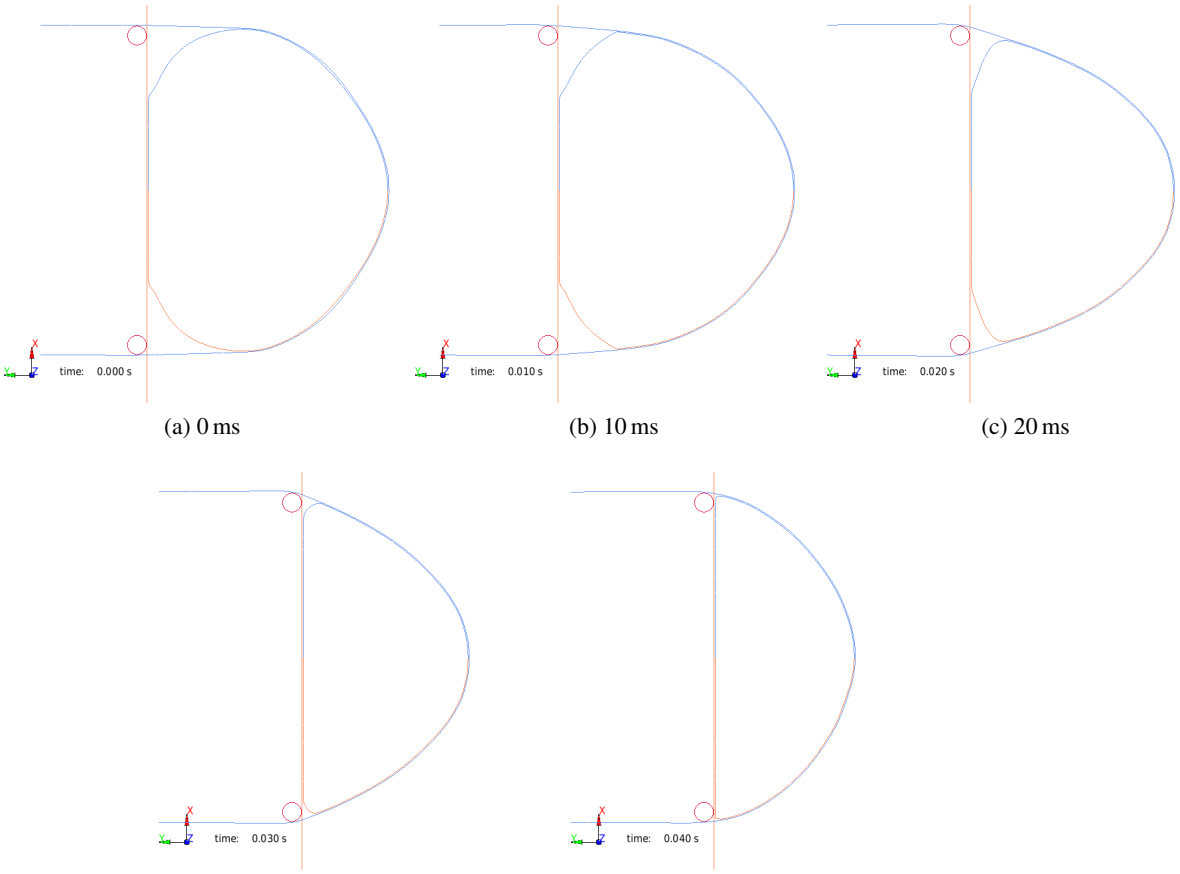

(a) 0 ms (b) 10 ms (c) 20 ms

(d) 30 ms (e) 40 ms

Figure 4.10 – Seatbelt deformation for MHA condition

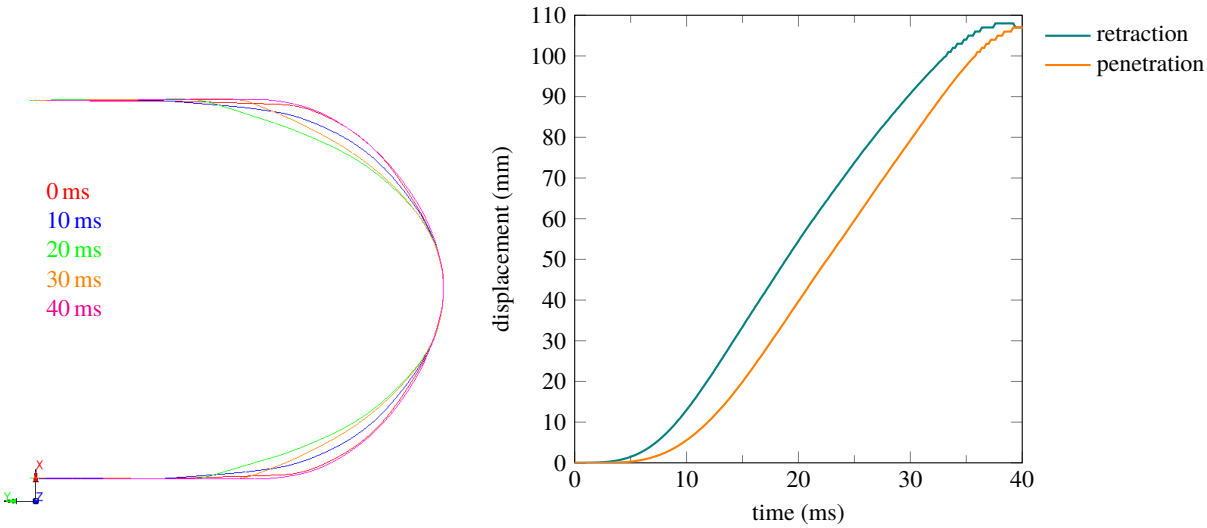

(a) Seatbelt deformation (b) Belt retraction and abdomen penetration

Figure 4.11 – Belt retraction and seatbelt deformation for MHA115 simulation

4.2.3.2 Lamielle et al. 2008 PRT condition

It has been chosen to impose the belt retraction profile over time from test data in order to simulate PMHS tests. All tests from the PRT condition were simulated. The THUMS model showed a lower penetration level than the PMHS data. Therefore, the test with the highest penetration of all, PRT052, will be presented here and used in this chapter since it results is the closest to PMHS data. Figure 4.12 shows the retraction conditions for the PRT tests and Table 4.4 shows the characteristics of the PMHS subjects.

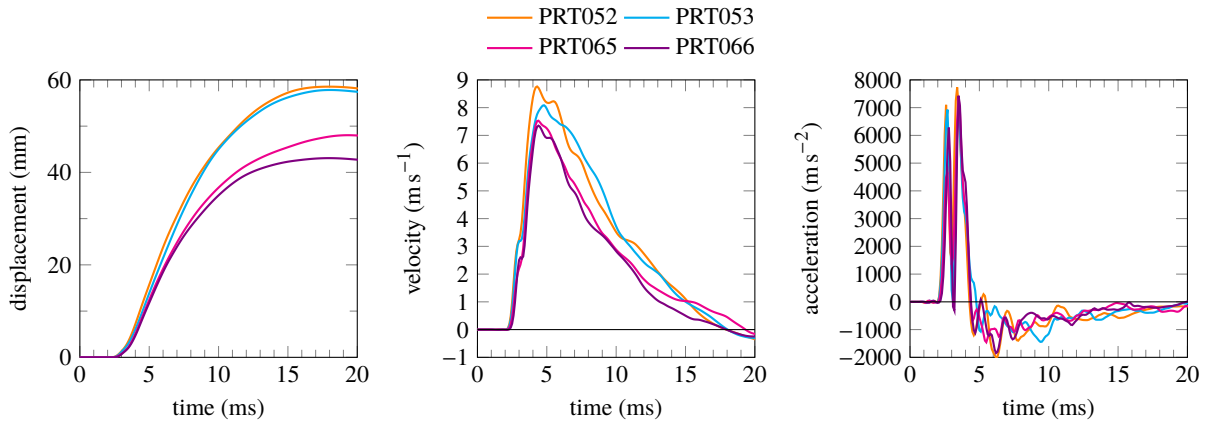

(a) Seatbelt retraction (b) Velocity (c) Acceleration

Figure 4.12 – Input conditions from Lamielle et al. 2008 PRT series

subject	gender	age (years)	stature (cm)	mass (kg)	abdomen depth (mm)
THUMS model	NA	NA	178	73	252
PRT052	M	72	162	54	222
PRT053	M	85	153	56	254
PRT065	M	88	172	72	243
PRT066	M	82	172	77	258

Table 4.5 – Abdominal depths of the THUMS model and subjects from Lamielle et al. 2008 PRT condition

As it can be seen on Figure 4.13a, the penetration response of the model goes lower than the test data after the initial loading phase. The peak belt retraction imposed in the simulation is 60 mm but the simulation gives a maximum abdomen penetration of 56 mm where 68 mm were expected. The interaction force between the belt and the abdomen (Figure 4.13b) has a magnitude comparable to test data but the profile over time of the force signal does not match the test data. The force in the simulation drops approximately 8 ms earlier compared to the PMHS results.

Regarding the back force comparison, the force magnitude in the simulation is much lower than in the test. A phase shift is observed in the back force, it can be explained the same way as for the MHA condition.

Figure 4.14 compares the deformed shape of the simulation and images from the relevant PMHS test. The fact that the model shows less penetration of the belt into the abdomen can be seen on the different pictures. It has been mentioned in Lamielle 2008 that for PRT tests (unlike the MHA tests), the belt retraction profile was different than the displacement of the umbilicus point of the abdomen. The umbilicus displacement was, after the initial period of the loading, higher than the belt retraction. This was believed to be the result of the lateral deformation of the abdomen causing more penetration of the belt into the abdomen compared to the belt retraction (the abdomen being incompressible). This also highlights the effect of the abdomen mass at higher velocities. However, this is not the case in our simulations. Figure 4.16b shows higher belt retraction than penetration all

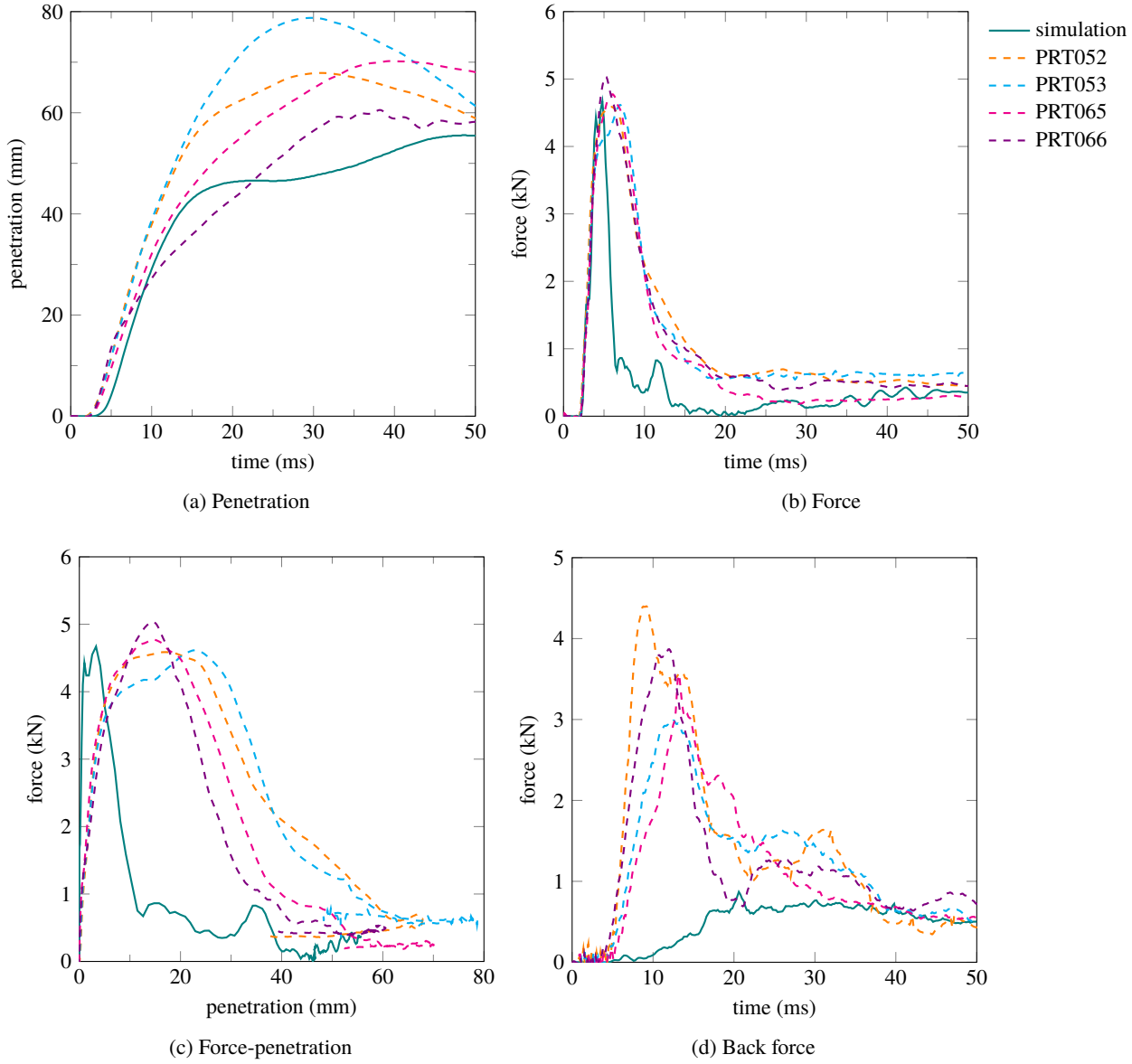

(a) Penetration

(b) Force

(c) Force-penetration

(d) Back force

Figure 4.13 – Simulation results of Lamielle et al. 2008 PRT052 condition

along the simulation, which could suggest that the mass effects that are observed in the PMHS data are not reproduced in the simulation. The incompressibility of the abdomen creates only very little lateral seatbelt deformation in the simulation (see Figures 4.15 and 4.16a).

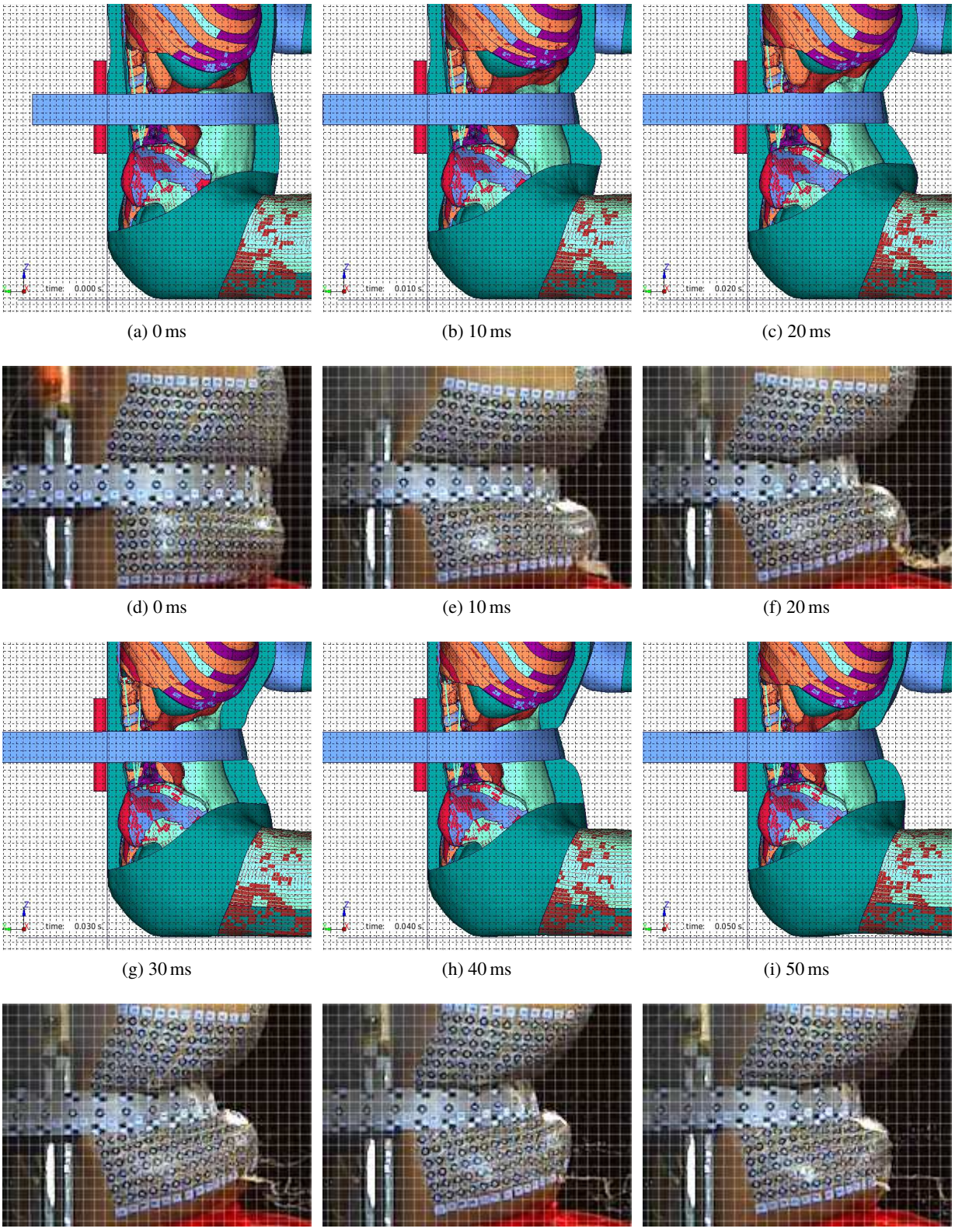

(a) 0 ms (b) 10 ms (c) 20 ms

(d) 0 ms (e) 10 ms (f) 20 ms

(g) 30 ms (h) 40 ms (i) 50 ms

(j) 30 ms (k) 40 ms (l) 50 ms

Figure 4.14 – PRT condition seatbelt simulation deformed shape compared with PRT052 PMHS images

The grid size is 10 mm

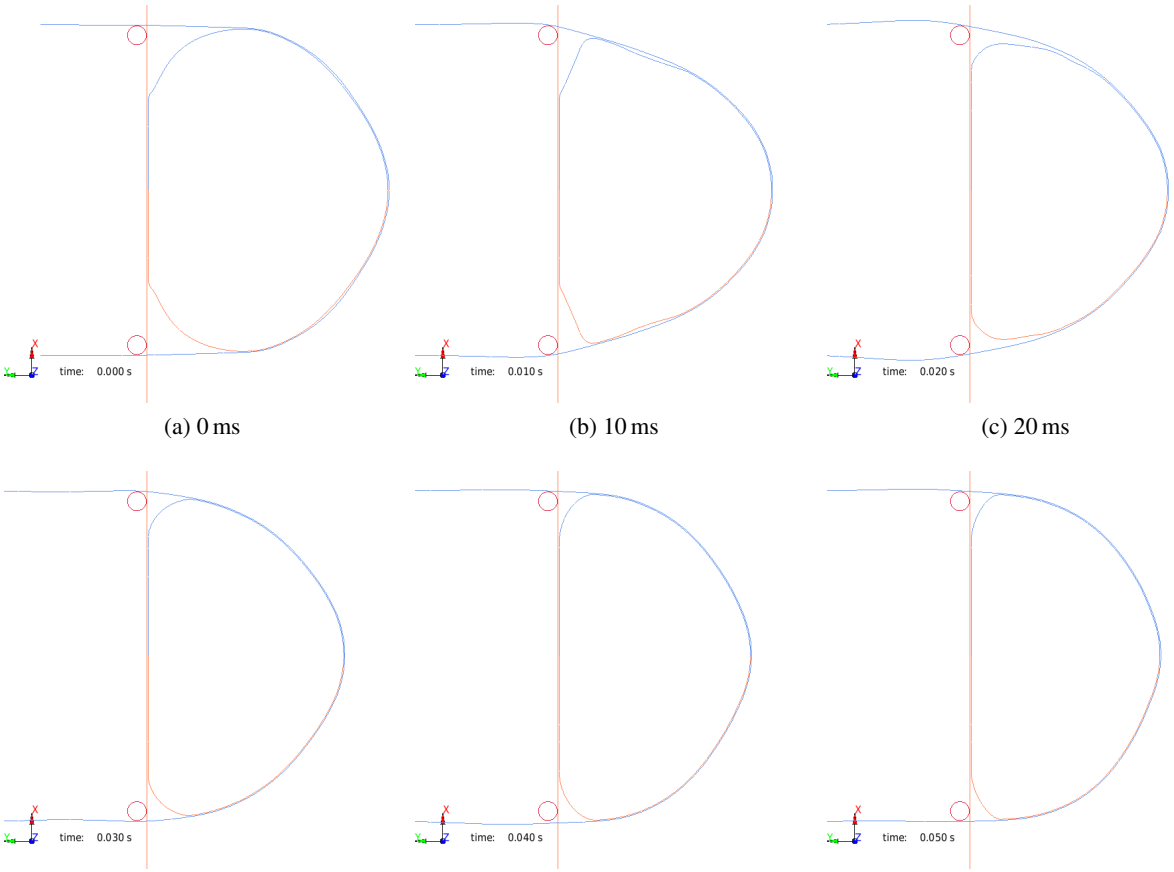

(a) 0 ms (b) 10 ms (c) 20 ms

(d) 30 ms (e) 40 ms (f) 50 ms

Figure 4.15 – Seatbelt deformation for PRT condition

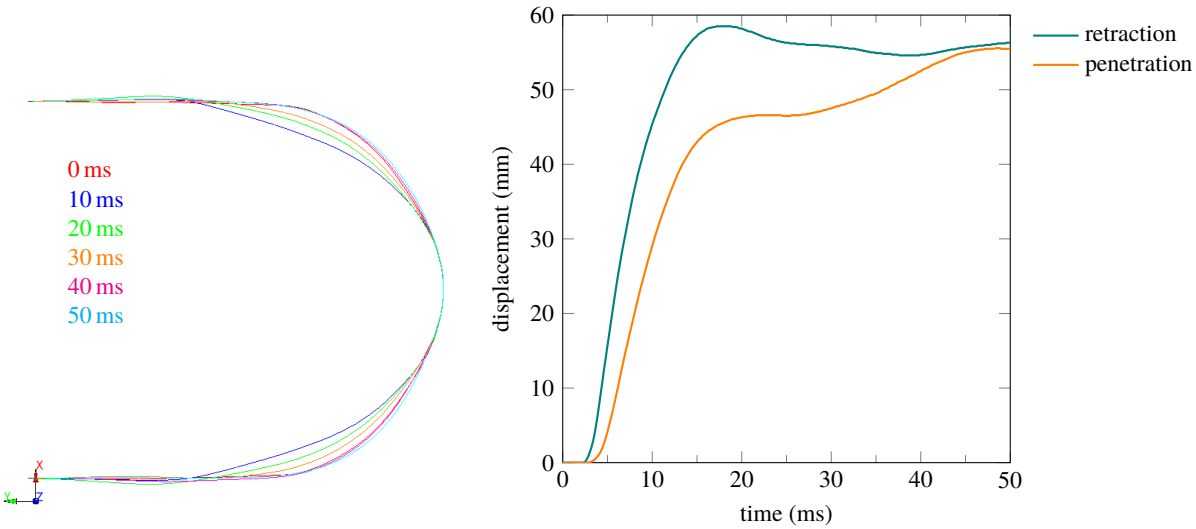

(a) Seatbelt deformation (b) Belt retraction and abdomen penetration

Figure 4.16 – Belt retraction and seatbelt deformation for PRT052 simulation

4.2.4 Conclusion on simulations with the THUMS model

Among the PMHS load cases reproduced with the THUMS model, only the impactor case from Hardy et al. 2001 at $6\,\mathrm{m\,s^{-1}}$ and the seatbelt cases from Lamielle et al. 2008 were presented here. The model response in terms of force and penetration is in good agreement with the tests data for most of the cases. For the MHA condition from Lamielle et al. 2008, the force level is however below the PMHS level probably due to the relatively low loading velocity for this condition compared to the other PMHS conditions. The rate-sensitivity of the THUMS model is therefore more adapted for highly dynamic loadings for which it had been initially validated in Shigeta et al. 2009.

Due to its detailed anatomical representation of the human body, the THUMS model could also be seen as a suitable tool for injury prediction under the confirmation that engineering parameter values extracted from the model are correlated to injury severity reported for the PMHS. This will be addressed in the following section.

4.3 Injury criteria using APTS pressure

It has been reported in Chapter 1, Section 1.2.4 that the only injurious study for impactor loading was Hardy et al. 2001 with liver injuries occurring in all the conditions. No injuries were reported in Cavanaugh et al. 1986, which is questionable given the fact that the impact velocities were similar to those of Hardy et al. 2001. Therefore, Cavanaugh et al. 1986 will not be considered for injury analysis.

Regarding seatbelt loading, Hardy et al. 2001 and Trosseille et al. 2002 did not report consistent injuries across all the subjects. Foster et al. 2006 reported liver injuries for the A condition and no injuries for the B condition. Lamielle et al. 2008 reported small intestine injuries for the MHA condition and small and large intestine injuries for the PRT condition. Mesentery injuries will be considered as small intestines injury since the mesentery is attached to the small intestine.

Given the scarcity of injury occurrence for a specific organ across all the different studies, all injuries reported in PMHS studies will be considered, which means injuries with AIS 2 or above. In practice, only the small intestine injuries from Lamielle et al. 2008 are AIS 2 injuries, all the other considered injuries are AIS 3 or above.

4.3.1 Internal energy as an injury measure for THUMS

Internal energy computed at the part level in the FE model has been chosen as an injury indicator for organs. The internal energy for a part is the sum of the internal energies of all the part's elements. Equation 4.1 defines the internal energy as mentioned in LS-DYNA Theory Manual (Hallquist 2006) for an element. Internal energy for an element is an incremental sum over time which includes the sum over the space direction of the product stress / incremental strain / volume. Therefore the internal energy represents both stress and strain states. Due to the important geometry variability between the PMHS subjects and the THUMS model, a global measure at the organ level is appropriate to estimate the injury risk to an organ.

$$e^{n+1} = e^n - \frac{1}{2} \cdot \triangle v \cdot \left(p^n + p^{n+1} + q^{n-\frac{1}{2}} + q^{n+\frac{1}{2}}\right) + v^{n+\frac{1}{2}} \cdot s_{ij}^{n+\frac{1}{2}} \cdot \triangle \varepsilon_{ij}^{n+\frac{1}{2}}$$

$$\text{With: } \begin{cases} e \text{ the element internal energy} \\ v \text{ the element volume} \\ q \text{ the bulk viscosity} \\ p \text{ the pressure} \\ s_{ij} \text{ the deviatoric stress components} \\ \varepsilon_{ij} \text{ the strain components} \\ n \text{ the timestep} \\ \triangle v = v^{n+1} - v^n \\ v^{n+\frac{1}{2}} = \frac{1}{2} \cdot \left(v^n + v^{n+1}\right) \end{cases} \tag{4.1}$$

4.3.2 Correlation between internal energy values from THUMS and PMHS injuries

In order to determine if engineering parameters from the THUMS model can be used for injury prediction, the maximum values of internal energy for each organ are compared to the injury outcome from PMHS studies on Figure 4.17. It stands out that the organs internal energy values are correlated with the injury outcome only for the liver. The small and large intestine present a negative correlation between injuries and internal energy. However, the liver is the organ with the lowest energy values among the three injured organs. This is explained by the fact by the liver is not

directly loaded by the seatbelt or the impactor at the mid-abdomen level in the model. However, in a PMHS test the liver position can vary due to anthropometric differences and it is likely that the abdominal organs shift in the inferior direction when considering PMHS compared to healthy subject due to the post-mortem lack of muscles tension. Howes et al. 2013 reported that markers placed on the liver of a post-mortem subject had a displacement of between 55 mm and 111 mm in the superior direction when the subject was placed from head up to head down. This explains why liver injuries are seen in PMHS studies while the loading parameters of the FE model have relatively low values. The injury observed to the liver in PMHS tests could also be due to an indirect loadings such as pressure increase in the liver due to the loading of an other region of the abdomen.

The fact that no correlation appear for injuries to the small and large intestine is due to the fact that such injuries were only observed in one study, Lamielle et al. 2008. This study is the only considered study to have perfused the PMHS subjects at the organ level in addition to the arteries (see Table B.3 in Appendix), therefore allowing to see contusions in those organs. Furthermore, Howes et al. 2015 reported that in order to detect jejunum injuries, the presence of fluid or air in the loaded portion of the organ was necessary. There could therefore have been a variety of different conditions in the literature studies which did not lead to detect injuries.

The evaluation of injury measures based on the THOR APTS pressures measurements will be undertaken based on the liver data only.

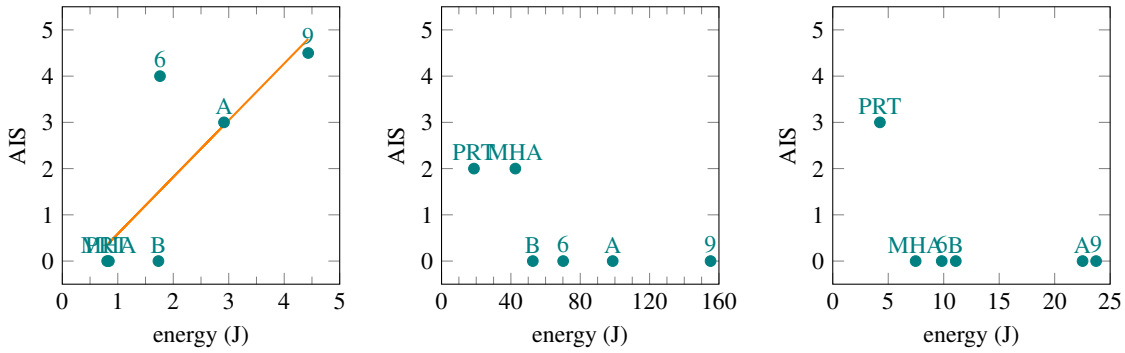

(a) Liver (b) Small intestine (c) Large intestine

Figure 4.17 – THUMS internal energies maximum values and AIS values
6: Hardy et al. 2001 6 m s^{-1} condition
9: Hardy et al. 2001 9 m s^{-1} condition
A: Foster et al. 2006 A condition
B: Foster et al. 2006 B condition
MHA: Lamielle et al. 2008 MHA condition
PRT: Lamielle et al. 2008 PRT condition

4.3.3 Selection of an injury measure based on pressure values from THOR

In order to assess if the pressure measurements from the THOR APTS sensors are representative of a particular organ injury mechanism or if it can be used as a global injury indicator, the pressure values will be compared to the internal organ energy from THUMS simulations. Due to the symmetrical nature of the different loadings, it has been chosen to average the left and right APTS pressures for a given loading case. The internal energy of the liver, small intestine and large intestine was extracted from the simulation results for each condition.

The improved prototype dummy abdomen described in Chapter 3, with the unified foam blocks have been used for APTS pressure assessment.

Figures 4.18 and 4.19 compare the APTS pressures from THOR simulations with the organs internal energy from THUMS simulations for impactor and seatbelt loading cases. What stands out is that

internal energies of the organs are always ranked in the same way. This means that the organs internal energies in the THUMS represent well the loading severity. Indeed, for seatbelt case, the internal energy ranking follows the ranking of maximum penetration velocity of the seatbelt in the abdomen or maximum abdomen compression (see Table B.2, in Appendix). In order of severity, the conditions are: Foster et al. 2006 A and B, Lamielle et al. 2008 PRT. However, Lamielle et al. 2008 MHA condition has the lowest penetration velocity values but shows higher internal energies than the PRT condition. This is due to the fact the MHA condition is the only non-pretensioner condition, having a slower velocity increase and higher abdomen compression than the PRT condition. The pressure measurement from the APTS follows the same ranking, although with close value for the two Foster et al. 2006 condition and Lamielle et al. 2008 MHA condition, with the presence of a phase shift.

Candidate injury measures based on pressure measurements have been computed from THOR simulations. The considered measures are $P_{\max}$, $\dot{P}_{\max}$ (both reported in Kremer et al. 2011 and Beillas et al. 2012) and $\dot{P}_{\max} \cdot P_{\max}$ (reported in Johannsen et al. 2007 and Beillas et al. 2012). The value of those measures are reported in Table 4.6 and Figure 4.20 shows the correlation between the injury measures and organ internal energies from THUMS simulations for the liver only, following the conclusions from the previous section. A linear regression has been performed for each data series. The measure best correlated with the energy levels is $\dot{P}_{\max} \cdot P_{\max}$ with a R^2 value of 0.44, followed by the $P_{\max}$ measure. The measure $\dot{P}_{\max}$ does not correlate with the energy levels, the R^2 value being of 0.14 and the p-value of 0.47. The measures that correlate with the internal energies from the THUMS model for each of the three injured organs are judged suitable to investigate the link between their values and the injury outcome.

condition	measure			internal energy		
	$P_{\max}$ (bar)	$\dot{P}_{\max}$ (bar s^{-1})	$\dot{P}_{\max} \cdot P_{\max}$ (bar^2 s^{-1})	liver (J)	small intestine (J)	large intestine (J)
A	1.5	299	448	2.9	99	23
B	1.1	153	176	1.7	53	11
MHA	1.3	47	61	0.8	43	7
PRT	0.7	181	131	0.8	19	4
6	2.1	103	216	1.8	70	10
9	1.9	146	273	4.4	155	24

Table 4.6 – Injury measures and internal energy peak values
6: Hardy et al. 2001 6 m s^{-1} condition
9: Hardy et al. 2001 9 m s^{-1} condition
A: Foster et al. 2006 A condition
B: Foster et al. 2006 B condition
MHA: Lamielle et al. 2008 MHA condition
PRT: Lamielle et al. 2008 PRT condition

This page was intentionally left blank.

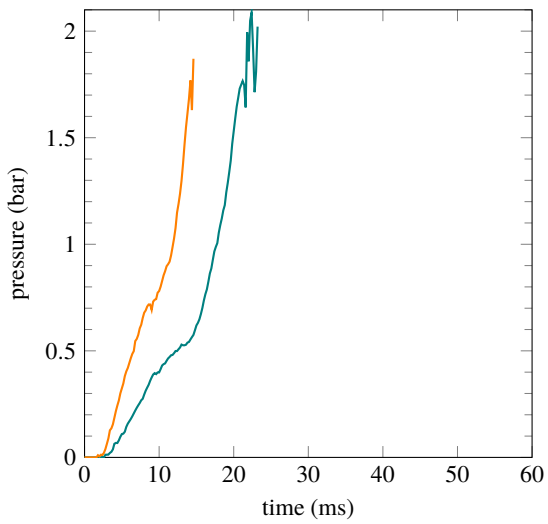

(a) THOR APTS pressure

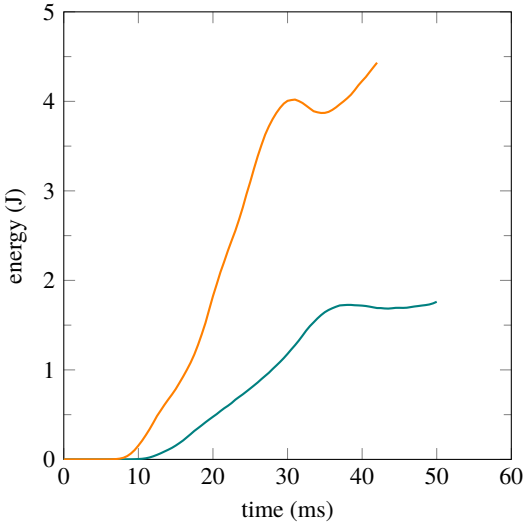

(b) THUMS liver internal energy

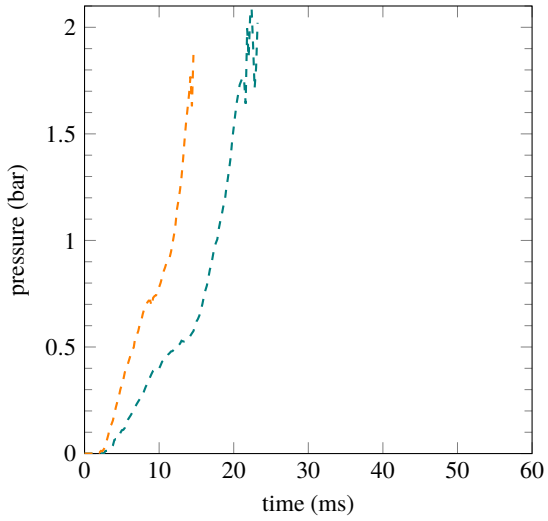

(c) THOR APTS pressure

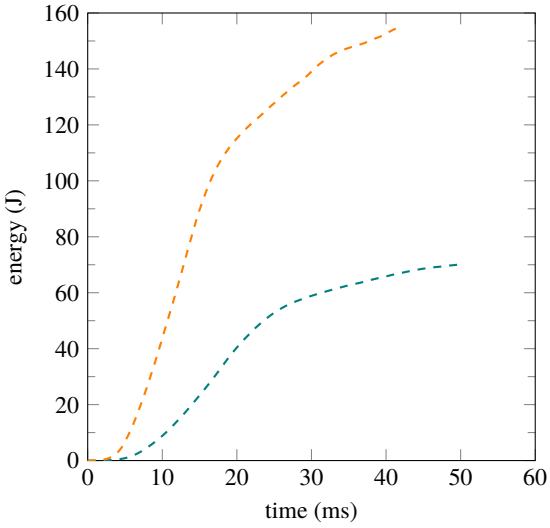

(d) THUMS small intestine internal energy

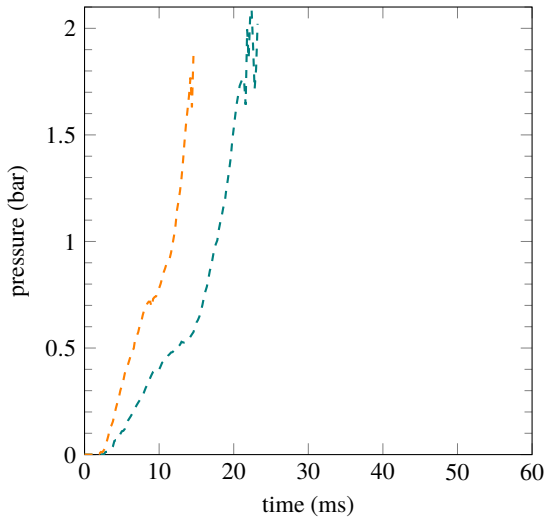

(e) THOR APTS pressure

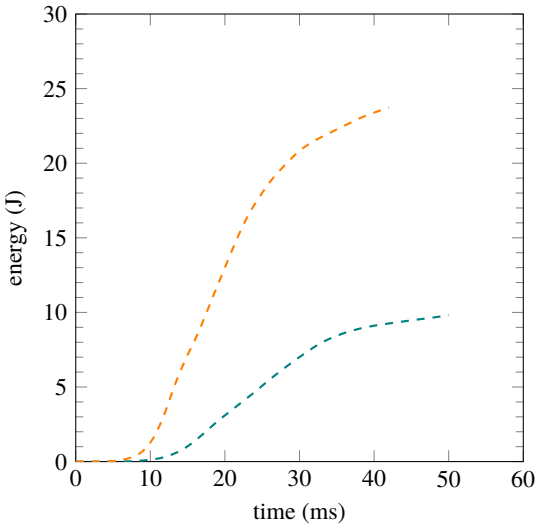

(f) THUMS large intestine internal energy

Figure 4.18 – THOR APTS pressure and THUMS internal energies for impactor case
Solid lines: injurious loading
Dashed lines: non injurious loading

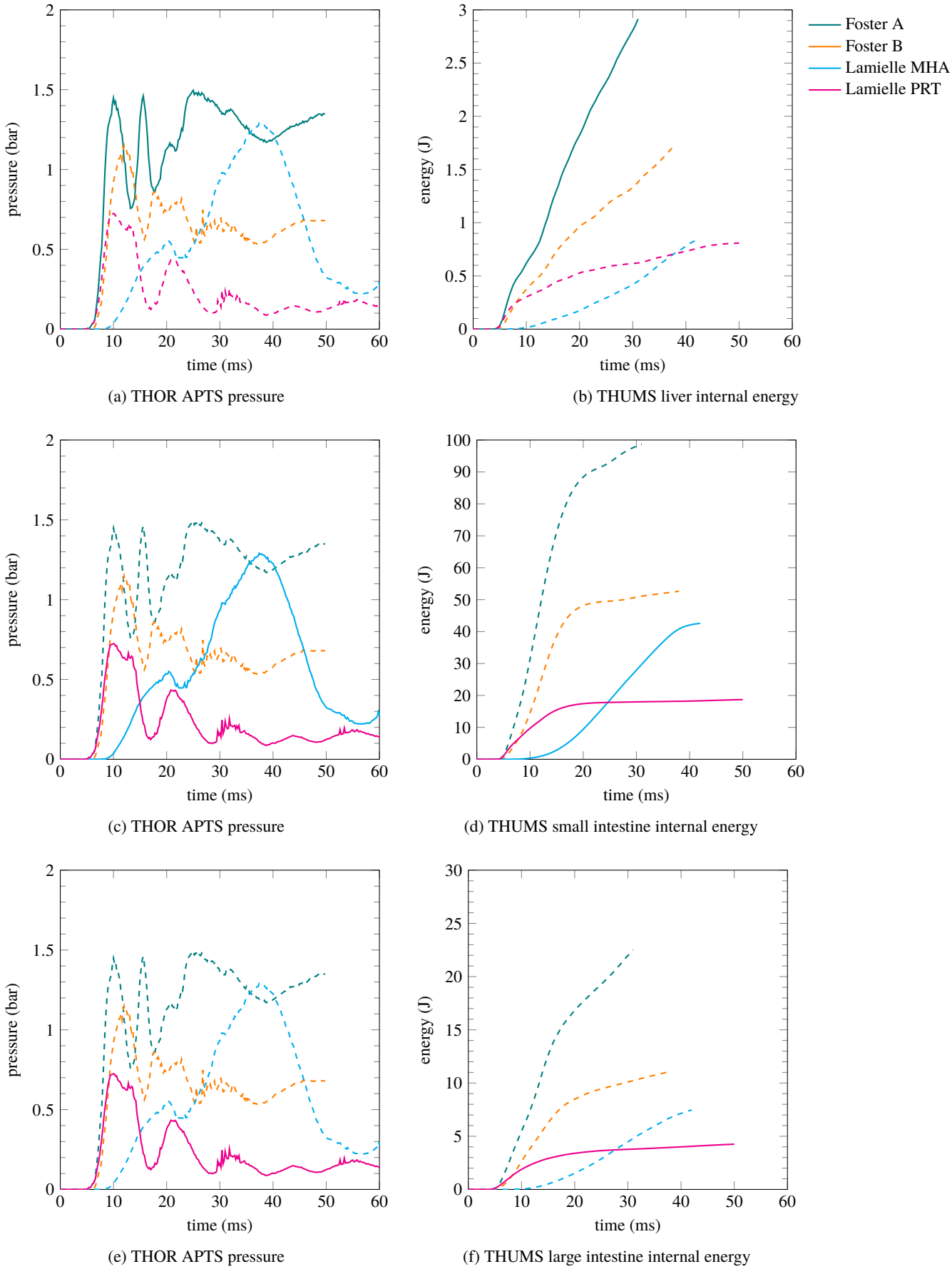

(a) THOR APTS pressure

(b) THUMS liver internal energy

(c) THOR APTS pressure

(d) THUMS small intestine internal energy

(e) THOR APTS pressure

(f) THUMS large intestine internal energy

Figure 4.19 – THOR APTS pressure and THUMS internal energies for seatbelt case
Solid lines: injurious loading
Dashed lines: non injurious loading

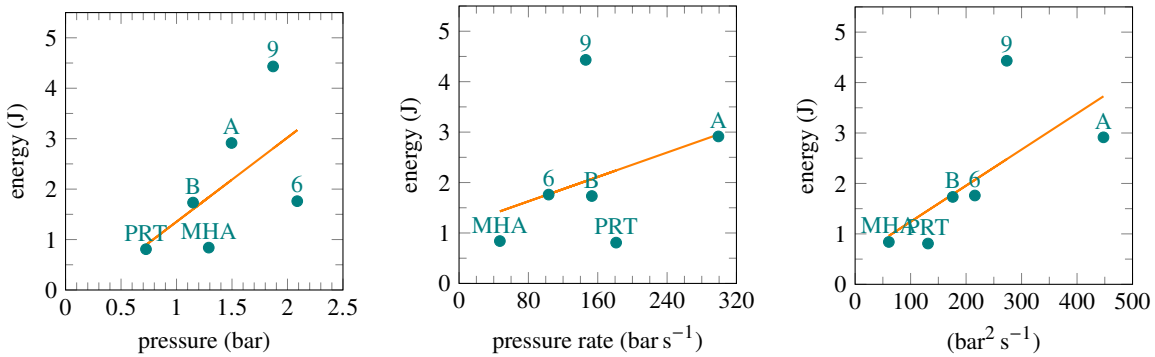

(a) P_{max}
$R^2 = 0.36$
p-value: 0.21

(b) $\dot{P}_{max}$
$R^2 = 0.14$
p-value: 0.47

(c) $\dot{P}_{max} \cdot P_{max}$
$R^2 = 0.48$
p-value: 0.13

Figure 4.20 – THOR injury measures and THUMS internal energies maximum values for the liver
6: Hardy et al. 2001 6 m s^{-1} condition
9: Hardy et al. 2001 9 m s^{-1} condition
A: Foster et al. 2006 A condition
B: Foster et al. 2006 B condition
MHA: Lamielle et al. 2008 MHA condition
PRT: Lamielle et al. 2008 PRT condition

4.3.4 Injury criteria based on pressure

The selected injury measures based on the pressure measured by the APTS are P_{max} and $\dot{P}_{max} \cdot P_{max}$. Figure 4.21 presents the injury AIS 3+ values plotted versus the candidate measures values for the liver. Only the liver injury values present a profile that can be fitted by an injury risk curve, due to the lack of correlation between injuries and other parameters for the intestines as explained earlier. A Weibull distribution was used with a survival model as desbribed in Kent et al. 2008. The distribution states that the probability of injury $p(I)$ is linked to the the probability of "surviving" $p(S)$ by the relation $p(I) = 1 - p(S)$. The Weibull distribution uses a scale (η) and a shape factor (φ) in order to express $p(S)$ as in Equation 4.2 where x is the injury criterion. A Scilab program using the `optim` function was used to fit the Weibull function by adjusting the parameters η and φ. Table 4.7 shows the values of the scale and shape factor for the generated distributions along with the 50 % injury threshold, the x value so that $p(I) = 0.5$. In this case, the threshold values are very close to the scale factor values since the criteria values do not overlap for the injurious and non injurious conditions which gives a neat distinction by the Weibull function. Criteria values of $P_{max} = 1.46$ bar and $\dot{P}_{max} \cdot P_{max} = 209$ bar^2 s^{-1} represent a 50 % injury threshold.

$$p(S) = e^{-\left(\frac{x}{\eta}\right)^{\varphi}} \tag{4.2}$$

criterion	η	φ (no unit)	50 % injury threshold
P_{max}	1.46 bar	170	1.46 bar
$\dot{P}_{max} \cdot P_{max}$	209 bar^2 s^{-1}	120	209 bar^2 s^{-1}

Table 4.7 – Injury criteria values for AIS 3+ liver injuries

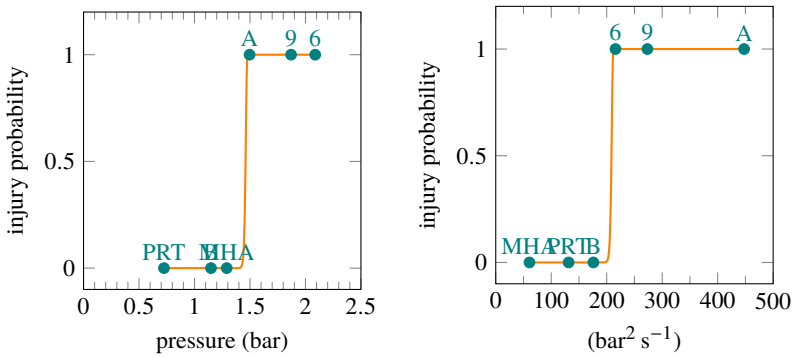

(a) P_{max} (b) $\dot{P}_{max} \cdot P_{max}$

Figure 4.21 – Candidate injury criteria for the liver
6: Hardy et al. 2001 6 m s^{-1} condition
9: Hardy et al. 2001 9 m s^{-1} condition
A: Foster et al. 2006 A condition
B: Foster et al. 2006 B condition
MHA: Lamielle et al. 2008 MHA condition
PRT: Lamielle et al. 2008 PRT condition

4.3.5 Conclusion on injury criteria

Organs internal energy from THUMS simulations have been used to assess the relevance of pressure injury measures. The only organ for which pressure measures lead to a link with injuries is the liver. No injury criteria could be defined for the small and large intestines due to the fact that injuries were not ranked in the same order as the considered injury measures. For the liver, the injury measure $\dot{P}_{max}$ was rejected due to lack of correlation with the organ internal energy from THUMS. The most significant injury measure was $\dot{P}_{max} \cdot P_{max}$ followed by P_{max}.

The distinction between the liver and the small and large intestines is that the liver is a solid organ and the intestines are hollow organs. In this study the attempt was made to find a single injury criterion for all types of organs, in order to have a reliable criterion to use with the dummy abdomen measurements. But since the nature of the organs are different, different injury criteria could be considered for both types of organs if more injurious data for hollow organs were available. The fact that only six loading conditions from the literature presented consistent injury statements across a majority of subjects also reduces the statistical strength of the injury criteria.

4.4 Conclusion

The validation of the THUMS model has been assessed for a wide range of loading conditions (six in total). The internal energy of the THUMS organs was extracted in order to assess the loading severity of each organ (liver, small intestine, large intestine) injured in PMHS tests from the literature. The correlation between energy and injuries was successful for the liver only. Candidate pressure measures with the THOR prototype abdomen have been selected for injury prediction for the liver based on the correlation with injury levels. The measures $P_{\max}$ and $\dot{P}_{\max} \cdot P_{\max}$ have then been linked to the the injuries from PMHS studies and criteria could be defined for the liver. $P_{\max} = 1.46\,\text{bar}$ and $\dot{P}_{\max} \cdot P_{\max} = 209\,\text{bar}^2\,\text{s}^{-1}$ represent a 50 % liver injury risk. No criteria could be defined for the other injured organs in PMHS studies, the small intestine and the large intestine. This is due to difficulties in assessing injuries for those organs in PMHS tests. The fact that the proposed injury criteria are based on only six conditions (three injurious and three non-injurious) is a limit of the statistical significance of the criteria.

Conclusion

A first objective of this work was to improve the biofidelity of the THOR dummy prototype abdomen developed by IFSTTAR and Toyota Motor Europe. This has been done by unifying the front foam blocks and a material change for the abdomen has been considered. A second objective was to develop a specific injury criterion based on the APTS sensors pressure measurements. A first step has been to asses the influence of the dummy torso flexion on the APTS reading during sled tests. In a second step, using local engineering parameters from the THUMS model at the organ level allowed to select suitable injury measures based on pressure and to link them with organ injuries from PMHS tests.

Chapter 1 showed that there is a global need to decrease the number of road fatalities, frontal impact being the most common crash case. The abdomen is a crucial region regarding serious to critical injuries, especially for rear passengers and in case of submarining. However, no injury criterion for the abdomen is applied currently. The biofidelity of the THOR dummy abdomen needs to be improved and its sensors measurement needs to be linked to an injury risk. The recent abdomen prototype developed by IFSTTAR and Toyota has shown better biofidelity than the standard abdomen and is equipped with APTS sensors that are candidates for providing pressures measurements for injury prediction. Recently developed finite element models of the human body having a highly detailed geometry of the abdominal organs could also help for injury prediction based on engineering parameters obtained from impact simulations.

In Chapter 2, the finite element model of the THOR dummy has been improved in order to have a model response correlating better with the test data. Based on these improvements, the abdomen prototype finite element model has been included in the dummy finite element model. This new model allows to reproduce the prototype abdomen response under seatbelt and impactor test.

Chapter 3 presented the use of a lumped element model which showed that the THOR dummy abdomen was more elastically and less viscously deformable than the human abdomen. Material and design changes of the abdomen that would allow a more biofidelic response were implemented in the FE model of the prototype abdomen. The unification of the two foam layers of the abdomen improved the biofidelity. A material change for the unified foam block toward a visco-elastic material with an increased viscous contribution proved to be able to improve the biofidelity for some loading conditions. However, the prototype abdomen influences the dummy behaviour in sled tests, showing more hip point displacement and more pelvis rotation. The interaction force between the upper and lower abdomen is also increased by the prototype abdomen presence but no biofidelity reference exist for this phenomenon. Only static spine stiffness assessments have been performed in Luet et al. 2012 which does not provide information on the abdomen behaviour during such loading. Further design changes would be needed to overcome these issues and have a really biofidelic submarining behaviour.

The validation of the THUMS model has been assessed in Chapter 4 for a wide range of loading conditions (six in total). The internal energy of the THUMS organs was extracted in order to assess the loading severity of each organ (liver, small intestine, large intestine) injured in PMHS tests from the literature. Based on these internal energy values, candidate pressure measures from the THOR prototype abdomen have been selected for injury prediction. The measures $P_{\max}$ and $\dot{P}_{\max} \cdot P_{\max}$ have then been linked to the the injuries from PMHS studies and a criterion could be defined for the

liver. $P_{max} = 1.46\,bar$ and $\dot{P}_{max} \cdot P_{max} = 209\,bar^2\,s^{-1}$ represent a 50 % liver AIS 3+ injury risk. No criteria could be defined for the other injured organs in PMHS studies, the small intestine and the large intestine. This is due to difficulties in assessing injuries for those organs in PMHS tests.

The findings of this work being mainly based on simulation results, this implies limitations. The THOR finite element model abdomen validation has been improved during this work by implementation of more detailed material characteristics. However the validation of the model in sled tests is limited regarding pelvis rotation and lap belt forces which raises the question on the correct reproduction of the physical dummy submarining phenomenon.

Other limitations of this work is the fact that all conclusions based on PMHS results do not represent a healthy car passenger. The lack of muscle tension may modify the mechanical response under impact. This lack of tension will also affect the position of the organs in the body, the organs having a tendency to go down in the abdominal cavity without tension, resulting in a larger abdomen depth for PMHS compared to healthy subjects. Therefore the use of a finite element model of the human body such as THUMS with an average healthy male geometry to reproduce PMHS tests is not an exact reproduction of the test. The use of PMHS subject also questions the validity of injury statements, since the organs are not in their physiological state and that there is a dependency on the perfusion method.

More generally, the use of crash test dummies is also not perfectly representative of the real behaviour of car occupants during a crash. Dummies being a passive device, their pre-crash position is not representative of an active human occupant. It seems that this limit will always be inherent to dummies. Therefore, the development of active human body models representative of the human passenger reactions would allow to perform virtual crash tests in the future in order to assess a car's safety.

Bibliography

Agur, A. and A. Dalley (2013). *Grant's Atlas of Anatomy*. Thirteenth Edition. ISBN 978-1-60831-756-1. Lippincott Williams & Wilkins.

Arnoux, P.-J., T. Serre, N. Cheynel, L. Thollon, M. Behr, P. Baque, and C. Brunet (2008). « Liver injuries in frontal crash situations a coupled numerical-experimental approach ». *Computer Methods in Biomechanics and Biomedical Engineering* 11.2, pp. 189–203.

Association for the Advancement of Automotive Medicine (AAAM) (1990). *The Abbreviated Injury Scale*.

– (2005). *The Abbreviated Injury Scale*.

Bansal, V., C. Conroy, G. Tomiaga, and R. Coimbra (2009). « The Utility of Seat Belt Signs to Predict Intra-Abdominal Injury Following Motor Vehicle Crashes ». *Traffic Injury Prevention* 10, pp. 567–567.

Beillas, P. and F. Berthet (2012). « Performance of a 50th Percentile Abdominal Model for Impact: Effects of Size and Mass ». *Journal of Biomechanics* 45(S1), S83.

Beillas, P., F. Alonzo, M.-C. Chevalier, P. Lesire, F. Leopold, X. Trosseille, and H. Johannsen (2012). « Abdominal Twin Pressure Sensors for the Assessment of Abdominal Injuries in Q Dummies: In-Dummy Evaluation and Performance in Accident Reconstructions ». *Stapp Car Crash Journal* 56. number 2012-10, pp. 387–410.

Beillas, P., C. Helfenstein, F. Rongieras, J.-L. Gennisson, and M. Tanter (2013). « A new method to assess the deformations of internal organs of the abdomen during impact ». *Computer Methods in Biomechanics and Biomedical Engineering* 16.S1, pp. 202–203.

Cavanaugh, J., G. Nyquist, S. Goldberg, and A. King (1986). « Lower Abdominal Tolerance and Response ». In: *30th Stapp Car Crash Conference Proceedings*. number 861878. San Diego (USA).

Chang, F., Y. Song, D. Lu, and C. DeSilva (1998). « Unified Constitutive Equations of Foam Materials ». *Journal of Engineering Materials and Technology* 120.3, pp. 212–217.

Chebil, O. (2014). « Interactions et mobilité des organes abdominaux sous sollicitations dynamiques : Approche expérimentale et numérique ». in French. PhD thesis. Université Aix-Marseille.

Compigne, S., M. Masuda, G. Hanen, P. Vezin, and F. Bermond (2015). « Proposal for a Modified THOR Lower Abdomen Including Abdominal Pressure Twin Sensors ». In: *24th International Technical Conference on the Enhanced Safety of Vehicles (ESV)*. number 15-0216. Gothenburg (Sweden).

Couturier, S., J. Faure, R. Satué, J. Huguet, and J. Hordonneau (2007). « Procedure to Assess Submarining in Frontal Impact ». In: *20th International Technical Conference on the Enhanced Safety of Vehicles (ESV)*. number 07-0481. Lyon (France).

DuBois, P. (2003). « A simplified approach to the simulation of rubber-like materials under dynamic loading ». In: *4th European LS-DYNA Users' Conference*. Ulm (Germany).

Elhagediab, A. and S. Rouhana (1998). « Patterns of Abdominal Injury in Frontal Automotive Crashes ». In: *16th International Technical Conference on the Enhanced Safety of Vehicles (ESV)*. number 98-S1-W-26. Windsor (Canada).

European New Car Assessment Programme (Euro NCAP) (2015a). *2020 Roadmap*.

– (2015b). *Assessment Protocol — Adult Occupant Protection*.

– (2015c). *Full Width Frontal Impact Testing Protocol*.

– (2015d). *Offset Deformable Barrier Frontal Impact Testing Protocol*.

European Transport Safety Council (ETSC) (2003). *Transport Safety Performance in the EU a Statistical Overview*.

– (2015). *Ranking EU Progress on Road Safety*. 9th Road Safety PIN Report.

Foster, C., W. Hardy, K. Yang, A. King, and S. Hashimoto (2006). « High-Speed Seatbelt Pretensioner Loading of the Abdomen ». *Stapp Car Crash Journal* 50. number 2006-22-0002, pp. 27–51.

Foster, J., J. Kortge, and M. Wolanin (1977). « Hybrid III — A Biomechanically-Based Crash Test Dummy ». In: *21st Stapp Car Crash Conference Proceedings*. number 770938. New Orleans (USA).

Frampton, R., J. Lenard, and S. Compigne (2012). « An In-depth Study of Abdominal Injuries Sustained by Car Occupants in Frontal Crashes ». In: *56th Association for the Advancement of Automotive Medicine (AAAM) Annual Conference — Annals of Advances in Automotive Medicine*. Vol. 56. Seattle (USA), pp. 137–149.

Gayzik, F., D. Moreno, N. Vavalle, A. Rhyne, and J. Stitzel (2012). « Development of a Full Human Body Finite Element Model for Blunt Injury Prediction Utilizing a Multi-Modality Medical Imaging Protocol ». In: *12th International LS-DYNA Users' Conference*. Detroit (USA).

GESAC, Inc. (1999). *Test Support for Finite Element Modeling of THOR Crash Test Dummy*. Submitted to Volpe National Transportation System Center.

– (2016). *THOR NT Advanced Frontal Impact Dummy* `http://www.gesacinc.com/thornt.html`.

Haffner, M., M. Kleinberger, R. Eppinger, B. Hennessey, H. Pritz, M. Beebe, A. Hagedorn, K. Klinich, L. Ore anc C. Tanner, and S. Kuppa (1994). « Progress in the Development of New Frontal Dummy Compoenents for the NHTSA Advanced Frontal Protection Program ». In: *14th International Technical Conference on the Enhanced Safety of Vehicles (ESV)*. number 94-S8-O-12. Munich (Germany).

Haffner, M., R. Eppinger, N. Rangarajan, T. Shams, M. Artis, and D. Beach (2001). « Foundations and Elements of the NHTSA THOR Alpha ATD design ». In: *17th International Technical Conference on the Enhanced Safety of Vehicles (ESV)*. number 458. Amsterdam (The Netherlands).

Hallquist, J. (2006). *LS-DYNA®Theory Manual*. ISBN 0-9778540-0-0. Livermore Software Technology Corporation.

Hanen, G., F. Bermond, S. Compigne, and M. Masuda (2011). « Contribution to the Improvement of Crash Test Dummies in Order to Decrease Abdominal Injuries in Road Accidents ». In: *22nd International Technical Conference on the Enhanced Safety of Vehicles (ESV)*. number 11-0218. Washington DC (USA).

Hardy, W., L. Schneider, and S. Rouhana (2001). « Abdominal Impact Response to Rigid-Bar, Seatbelt, and Airbag Loading ». *Stapp Car Crash Journal* 45. number 2001-22-0001, pp. 1–32.

Haug, E., H.-Y. Choi, S. Robin, and M. Beaugonin (2004). « Human Models for Crash and Impact Simulation ». In: *Handbook of Numerical Analysis*. Ed. by P. Ciarlet. Vol. XII, Computational Models for the Human Body. DOI 10.1016/S1570-8659(03)12004-2, ISSN 1570-8659, pp. 231–452.

Hobbs, C. and P. McDonough (1998). « Development of the European New Car Assessment Programme (Euro NCAP) ». In: *16th International Technical Conference on the Enhanced Safety of Vehicles (ESV)*. number 98-S11-O-06. Windsor (Canada).

Howes, M., S. Gregory, W. Hardy, and P. Beillas (2012). « Kinematics of the Thoracoabdominal Contents Under Various Loading Scenarios ». *Stapp Car Crash Journal* 56. number 2012-01, pp. 1–48.

Howes, M., W. Hardy, and P. Beillas (2013). « The Effects of Cadaver Orientation on the Relative Position of the Abdominal Organs ». In: *57th Association for the Advancement of Automotive Medicine (AAAM) Annual Conference — Annals of Advances in Automotive Medicine*. Vol. 57. Quebec City (Canada), pp. 209–224.

Howes, M., W. Hardy, A. Agnew, and J. Hallman (2015). « Evaluation of the Kinematic Responses and Potential Injury Mechanisms of the Jejunum during Seatbelt Loading ». *Stapp Car Crash Journal* 59. number 2015-09, pp. 225–267.

Ishiyama, S.-I., K. Tsukada, H. Nishigaki, Y. Ikeda, S. Sakuma, F. Matsuoka, Y. Kanno, and S. Hayashi (1994). « Development of an Abdominal Deformation Measuring System for Hybrid III Dummy ». In: *38th Stapp Car Crash Conference Proceedings*. number 942223. Fort Lauderdale (USA).

Iwamoto, M., Y. Kisanuki, I. Watanabe, K. Furusu, K. Miki, and J. Hasegawa (2002). « Development of a Finite Element Model of the Totoal Human Model for Safety (THUMS) and Application to Injury Reconstruction ». In: *International Research Council on Biomechanics of Impact (IRCOBI) Conference Proceedings*. Munich (Germany).

Iwamoto, M., K. Omori, H. Kimpara, Y. Nakahira, A. Tamura, I. Watanabe, K. Miki, J. Hasegawa, and F. Oshita (2003). « Recent advances in THUMS: development of individual internal organs, brain, small female, and pedestrian model ». In: *4th European LS-DYNA Users' Conference*. Ulm (Germany).

Johannsen, H., F. Alonzo, and V. Schindler (2007). « Abdominal Sensors for Child Dummies of the Q Family, Injury Criteria and Injury Risk Curves ». In: *International Research Council on Biomechanics of Injury (IRCOBI) Conference Proceedings*. Maastricht (The Netherlands).

Kent, R., J. Funk, and J. Crandall (2003). « How Future Trends in Societal Aging, Air Bag Availability, Seat Belt Use, and Fleet Composition Will Affect Serious Injury Risk and Occurrence in the United States ». *Traffic Injury Prevention* 4, pp. 24–32.

Kent, R., D. Lessley, and C. Sherwood (2004). « Thoracic Response to Dynamic, Non-Impact Loading from a Hub, Distributed Belt, Diagonal Belt, and Double Diagonal Belts ». *Stapp Car Crash Journal* 48. number 2004-22-0022, pp. 495–519.

Kent, R., S. Stacey, M. Kindig, W. Woods, J. Evans, S. Rouhana, K. Higuchi, H. Tanji, S. Lawrence, and K. Arbogast (2008). « Biomechanical Response of the Pediatric Abdomen, Part 2: Injuries and Their Correlation with Engineering Parameters ». *Stapp Car Crash Journal* 52. number 2008-22-0006, pp. 135–166.

Kimpara, H., J. Lee, K. Yang, A. King, M. Iwamoto, I. Watanabe, and K. Miki (2005). « Development of a Three-Dimensional Finite Element Chest Model for the 5th Percentile Female ». *Stapp Car Crash Journal* 49. number 2005-22-0012, pp. 251–269.

Kitagawa, Y. and T. Yasuki (2013). « Correlation among Seatbelt Load, Chest Deflection, Rib Fracture and Internal Organ Strain in Frontal Collisions with Human Body Finite Element Models ». In: *International Research Council on Biomechanics of Injury (IRCOBI) Conference Proceedings*. number IRC-13-36. Lisbon (Portugal).

Klinich, K., C. Flannagan, K. Nicholson, L. Schneider, and J. Rupp (2010). « Factors Associated with Abdominal Injury in Frontal, Farside, and Nearside Crashes ». *Stapp Car Crash Journal* 54. number 2010-22-0005, pp. 73–91.

Kremer, M., H. Gustafson, J. Bolte, J. Stammen, B. Donnelly, and R. Herriott (2011). « Pressure-Based Abdominal Injury Criteria Using Isolated Liver and Full-Body Post-Mortem Human Subject Impact Tests ». *Stapp Car Crash Journal* 55. number 2011-12, pp. 317–350.

Labé, A. (2008). « Étude des mécanismes lésionnels de la région abdomino-pelvienne. Application à la traumatologie virtuelle et à la sécurité routière ». in French. PhD thesis. Université de la Méditerranée Aix-Marseille II.

Lamielle, S. (2008). « Contribution à la compréhension du comportement de l'abdomen lors d'un chargement dynamique frontal par une ceinture de sécurité ». in French. PhD thesis. Université Claude Bernard - Lyon 1.

Lamielle, S., S. Cuny, J.-Y. Foret-Bruno, P. Petit, P. Vezin, J.-P. Verriest, and H. Guillemot (2006). « Abdominal Injury Patterns in Real Frontal Crashes: Influence of Crash Conditions, Occupant Seat and Restraint Sytems ». In: *Annual Proceedings of the Association for the Advancement of Automotive Medicine (AAAM)*. Vol. 50, pp. 109–124.

Lamielle, S., P. Vezin, J.-P. Verriest, P. Petit, X. Trosseille, and G. Vallancien (2008). « 3D Deformation and Dynamics of the Human Cadaver Abdomen under Seatbelt Loading ». *Stapp Car Crash Journal* 52. number 2008-22-0014, pp. 267–294.

Lau, I. and D. Viano (1986). « The Viscous Criterion — Bases and Applications of an Injury Severity Index for Soft Tissues ». In: *30th Stapp Car Crash Conference Proceedings*. number 861882. San Diego (USA).

Lebarbé, M., B. Donnelly, P. Petit, and K. Moorhouse (2015). « A Frontal Response Specification for Assessing the Biofidelity of an Anthropometric Test Dummy Part 1 — Upper Body ». In: *International Research Council on Biomechanics of Injury (IRCOBI) Conference Proceedings*. number IRC-15-58. Lyon (France).

Lee, J. and K. Yang (2001). « Development of a Finite Element Model of the Human Abdomen ». *Stapp Car Crash Journal* 45. number 2001-22-0004, pp. 79–100.

– (2002). « Abdominal Injury Patterns in Motor Vehicle Accidents: A Survey of the NASS Database from 1993 to 1997 ». *Traffic Injury Prevention* 2, pp. 241–246.

Livermore Software Technology Corporation (LSTC) (2015). *LS-DYNA®Keyword User's Manual, Volume II: Material Models*.

Lizee, E., S. Robin, E. Song, N. Bertholon, J.-Y. Le Coz, B. Besnault, and F. Lavaste (1998). « Development of a 3D Finite Element Model of the Human Body ». In: *42nd Stapp Car Crash Conference Proceedings*. number 983152. Tempe (USA).

Lobdell, T., C. Kroell, D. Schneider, W. Hering, and A. Nahum (1973). « Impact Response of the Human Thorax ». In: *Human Impact Response: Measurement and Simulation*. Ed. by W. King and H. Mertz. DOI 10.1007/978-1-4757-1502-6, ISBN 978-1-4757-1504-0. Proceedings of the Symposium on Human Impact Response, Warren (USA), October 2-3, 1972, pp. 201–245.

Luet, C. (2013). « Caractérisation du sous-marinage chez l'occupant de véhicule en choc frontal ». in French. PhD thesis. Université de Valenciennes et du Hainaut-Cambrésis.

Luet, C., X. Trosseille, P. Drazétic, P. Potier, and G. Vallancien (2012). « Kinematics and Dynamics of the Pelvis in the Process of Submarining using PMHS Sled Tests ». *Stapp Car Crash Journal* 56. number 2012-11, pp. 411–442.

Martin, J.-L., A. Lardy, and S. Compigne (2010). « Specificities of Rear Occupant Protection: Analysis of French Accident Data ». In: *International Research Council on Biomechanics of Injury (IRCOBI) Conference Proceedings*. Hanover (Germany).

Mertz, H. (1984). « A Procedure for Normalizing Impact Response Data ». In: *Government / Industry Meeting & Exposition*. number 840884. Washington DC (USA).

National Highway Traffic Safety Administration (NHTSA) (2011). *Occupant crash protection*. Federal Motor Vehicle Safety Standard (FMVSS) — Standard No. 208.

– (2012). *Laboratory Test Procedure for New Car Assessment Program Frontal Impact Testing*. U.S. Department of Transportation.

– (2015). *Request for Comments Notice on the planned upgrade to the New Car Assessment Program*. document 80 FR 78521. U.S. Department of Transportation.

NHTSA / GESAC, Inc. (2005a). *THOR Certification Manual*. Revision 2005.2.

– (2005b). *THOR NT User's Manual*. Revision 2005.1.

Nusholtz, G. and P. Kaiker (1994). « Abdominal Response to Steering Wheel Loading ». In: *14th International Technical Conference on the Enhanced Safety of Vehicles (ESV)*. number 94-S1-O-05. Munich (Germany).

Onda, K., F. Matsuoka, K. Ono, M. Kubota, M. Peter, and Z. Youmei (2006). « Differences in the Dynamic Responses of the Thor-NT and Thor-FT Dummies ». In: *SAE World Congress & Exhibition*. number 2006-01-0676. Detroit (USA).

Panzer, M., S. Giudice, and D. Parent (2015). *THOR 50th Male Finite Element Model User Manual*. Model Version 2.1 for LS-Dyna.

Parent, D., M. Craig, S. Ridella, and J. McFadden (2013). « Thoracic Biofidelity Assessment of the THOR MOD KIT ATD ». In: *23rd International Technical Conference on the Enhanced Safety of Vehicles (ESV)*. number 13-0327. Seoul (Korea).

Rangarajan, N., T. Shams R. White, Y.-M. Zhao, D. Beach, M. Haffner, R. Eppinger, and K. Digges (1996). « Design and Evaluation of an Instrumented Abdomen for the NHTSA Advanced Dummy ». In: *15th International Technical Conference on the Enhanced Safety of Vehicles (ESV)*. number 96-S10-O-06. Melbourne (Australia).

Rangarajan, N., R. White, T. Shams, D. Beach, J. Fullerton, M. Haffner, R. Eppinger, H. Pritz, D. Rhule, D. Dalmotas, and E. Fournier (1998). « Design and Performance of the THOR Advanced Frontal Crash Test Dummy Thorax and Abdomen Assemblies ». In: *16th International Technical Conference on the Enhanced Safety of Vehicles (ESV)*. number 98-S9-O-12. Windsor (Canada).

Ridella, S. and D. Parent (2011). « Modifications to Improve the Durability, Usability and Biofidelity of the THOR-NT Dummy ». In: *22nd International Technical Conference on the Enhanced Safety of Vehicles (ESV)*. number 11-0312. Washington DC (USA).

Robin, S. (2001). « HUMOS: Human Model For Safety - A Joint Effort Towards the Development of Refined Human-Like Car Occupants Models ». In: *17th International Technical Conference on the Enhanced Safety of Vehicles (ESV)*. number 297. Amsterdam (The Netherlands).

Rouhana, S., I. Lau, and S. Ridella (1985). « Influence of Velocity and Forced Compression on the Severity of Abdominal Injury in Blunt, Nonpenetrating Lateral Impact ». *The Journal of Trauma* 25.6, pp. 490–500.

Rouhana, S., D. Viano, E. Jedrzejczak, and J. McCleary (1989). « Assessing Sumbarining and Abdominal Injury Risk in the Hybrid III Family of Dummies ». In: *33rd Stapp Car Crash Conference Proceedings*. number 892440. Washington DC (USA).

Rouhana, S., A. Elhagediab, A. Walbridge, W. Hardy, and L. Schneider (2001). « Development of a Reusable, Rate-Sensitive Abdomen for the Hybrid III Family of Dummies ». *Stapp Car Crash Journal* 45. number 2001-22-0002, pp. 33–60.

Rouhana, S., R. El-Jawahri, and T. Laituri (2010). « Biomechanical Considerations for Abdominal Loading by Seat Belt Pretensioners ». *Stapp Car Crash Journal* 54. number 2010-22-0016, pp. 381–406.

Ruan, J., R. El-Jawahri, L. Chai, S. Barbat, and P. Prasad (2003). « Prediction and Analysis of Human Thoracic Impact Responses and Injuries in Cadaver Impacts Using a Full Human Body Finite Element Model ». *Stapp Car Crash Journal* 47. number 2003-22-0014, pp. 299–321.

Ruan, J., R. El-Jawahri, S. Barbat, and P. Prasad (2005). « Biomechanical Analysis of Human Abdominal Impact Responses and Injuries through Finite Element Simulations of a Full Human Body Model ». *Stapp Car Crash Journal* 49. number 2005-22-0016, pp. 343–366.

Rudd, R., J. Bean, C. Cuentas, C. Kahane, M. Mynatt, and C. Wiacek (2009). « A Study of the Factors Affecting Fatalities or Air Bag and Belt-Restrained Occupants in Frontal Crashes ». In: *21st International Technical Conference on the Enhanced Safety of Vehicles (ESV)*. number 09-0555. Stuttgart (Germany).

Schneider, L., A. King, and M. Beebe (1989). *Design Requirements and Specifications: Thorax-Abdomen Development Task. Interim Report. Trauma Assessment Device Development Program*. DOT HS 807 511.

Schneider, L., M. Haffner, R. Eppinger, M. Salloun, M. Beebe, S. Rouhana, A. King, W. Hardy, and R. Neathery (1992). « Development of an Advanced ATD Thorax System for Improved Injury Assessment in Frontal Crash Environments ». In: *36th Stapp Car Crash Conference Proceedings*. number 922520. Seattle (USA).

Shah, C., J. Lee, W. Hardy, and K. Yang (2004). « A Partially Validated Finite Element Whole-Body Human Model for Organ Level Injury Prediction ». In: *ASME International Mechanical Engineering Congress and Exposition*. number IMECE2004-61844. Anaheim (USA).

Shams, T., N. Rangarajan, J. McDonald, Y. Wang, G. Platten, C. Spade, P. Pope, and M. Haffner (2005). « Development of THOR NT: Enhancement of THOR Alpha — the NHTSA Advanced Frontal Dummy ». In: *19th International Technical Conference on the Enhanced Safety of Vehicles (ESV)*. number 05-0455. Washington DC (USA).

Shaw, G., D. Lessley, J. Bolton, and J. Crandall (2004). « Assessment of the Thor and Hybrid III Crash Dummies: Steering Wheel Rim Impacts to the Upper Abdomen ». In: *SAE World Congress & Exhibition*. number 2004-01-0310. Warrendale (USA).

Shaw, J., R. Herriott, J. McFadden, B. Donnelly, and J. Bolte (2006). « Oblique and Lateral Impact Response of the PMHS Thorax ». *Stapp Car Crash Journal* 50. number 2006-22-0007, pp. 147–167.

Shigeta, K., Y. Kitagawa, and T. Yasuki (2009). « Development of Next Generation Human FE Model Capable of Organ Injury Prediction ». In: *21st International Technical Conference on the Enhanced Safety of Vehicles (ESV)*. number 09-0111. Stuttgart (Germany).

Shin, J., H. Choi, C. Oh, and J. Bae (2015). « Analysis and Simulation of Occupant Injury Risk at NASS / CDS ». In: *24th International Technical Conference on the Enhanced Safety of Vehicles (ESV)*. number 15-0394. Gothenburg (Sweden).

Soni, A. and P. Beillas (2015). « Modelling hollow organs for impact conditions: a simplified case study ». *Computer Methods in Biomechanics and Biomedical Engineering* 18.7, pp. 730–739.

Sparks, J., J. Bolte, R. Dupaix, K. Jones, S. Steinberg, R. Herriott, J. Stammen, and B. Donnelly (2007). « Using Pressure to Predict Liver Injury Risk from Blunt Impact ». *Stapp Car Crash Journal* 51. number 2007-22-0017, pp. 401–432.

Tamura, A., K. Omori, K. Miki, J. Lee, K. Yang, and A. King (2002). « Mechanical Characterization of Porcine Abdominal Organs ». *Stapp Car Crash Journal* 46. number 2002-22-0003, pp. 55–69.

Toyota Motor Corporation (2011). *Documentation — Total Human Model for Safety (THUMS)*.

Trosseille, X., J.-Y. Le-Coz, P. Potier, and J.-P. Lassau (2002). « Abdominal Response to High-Speed Seatbelt Loading ». *Stapp Car Crash Journal* 46. number 2002-22-0004, pp. 71–79.

United Nations Economic Commission for Europe (UNECE) (2013). *Uniform provisions concerning the approval of vehicles with regard to the protection of the occupants in the event of a frontal collision*. Regulation No. 94.

Untaroiu, C., J.-Y. Lim, J. Shin, J. Crandall, D. Malone, and R. Tannous (2009). « Evaluation of a Finite Element Model of the THOR-NT Dummy in Frontal Crash Environment ». In: *21st International Technical Conference on the Enhanced Safety of Vehicles (ESV)*. number 09-0272. Stuttgart (Germany).

Uriot, J., P. Baudrit, P. Potier, X. Trosseille, P. Petit, H. Guillemot, L. Guérin, and G. Vallancien (2006). « Investigations on the Belt-to-Pelvis Interaction in Case of Submarining ». *Stapp Car Crash Journal* 50. number 2006-22-0003, pp. 53–73.

Uriot, J., P. Potier, P. Baudrit, X. Trosseille, O. Richard, and R. Douard (2015a). « Comparison of HII, HIII and THOR dummy responses with respect to PMHS sled tests ». In: *International Research Council on Biomechanics of Injury (IRCOBI) Conference Proceedings*. number IRC-15-55. Lyon (France).

Uriot, J., P. Potier, P. Baudrit, X. Trosseille, P. Petit, O. Richard ans S. Compigne, M. Masuda, and R. Douard (2015b). « Reference PMHS Sled Tests to Assess Submarining ». *Stapp Car Crash Journal* 59. number 2015-08, pp. 203–223.

Vezin, P. and J.-P. Verriest (2005). « Development of a Set of Numerical Human Models for Safety ». In: *19th International Technical Conference on the Enhanced Safety of Vehicles (ESV)*. number 05-0163. Washington DC (USA).

Viano, D. and I. Lau (1985). « Thoracic Impact: A Viscous Tolerance Criterion ». In: *10th International Technical Conference on Experimental Safety vehicles (ESV)*. Oxford (England).

Xu, L., V. Agaram, S. Rouhana, R. Hultman, G. Kostyniuk, J. McCleary, H. Mertz, G. Nusholtz, and R. Scherer (2000). « Repeatability Evaluation of the Pre-Prototype NHTSA Advanced Dummy Compared to the Hybrid III ». In: *SAE World Congress & Exhibition*. number 2000-01-0165. Detroit (USA).

Yaguchi, M., Y. Omoda, K. Ono, M. Masuda, and K. Onda (2011). « Traffic Accident Analysis Towards the Development of an Advanced Frontal Crash Test Dummy Indispensable for Further Improving Vehicle Protection Performance ». In: *22nd International Technical Conference on the Enhanced Safety of Vehicles (ESV)*. number 11-0221. Washington DC (USA).

Yamada, H. (1970). *Stength of Biological Materials*. Ed. by F. Evans. The Williams & Wilkins Company.

Yang, K., J. Hu, N. White, A. King, C. Chou, and P. Prasad (2006). « Development of Numerical Models for Injury Biomechanics Research: A Review of 50 Years of Publications in the Stapp Car Crash Conference ». *Stapp Car Crash Journal* 50. number 2006-22-0017, pp. 429–490.

Yoganandan, N., F. Pintar, T. Gennarelli, and M. Maltese (2000). « Patterns of Abdominal Injuries in Frontal and Side Impacts ». In: *Annual Proceedings of the Association for the Advancement of Automotive Medicine (AAAM)*. Vol. 44, pp. 17–36.

Zhao, J. and G. Narwani (2005). « Development of a Human Body Finite Element Model for Restraint System R&D Applications ». In: *19th International Technical Conference on the Enhanced Safety of Vehicles (ESV)*. number 05-0399. Washington DC (USA).

– (2007). « Biomechanical Analysis of Hard Tissue Responses and Injuries with Finite Element Full Human Body Model ». In: *20th International Technical Conference on the Enhanced Safety of Vehicles (ESV)*. number 07-0354. Lyon (France).

Appendix A

Table of Acronyms

AIS Abbreviated Injury Scale

APTS Abdominal Pressure Twin Sensors

ASIS Anterior Superior Iliac Spine

CFC Channel Frequency Class

DGSP Double Gimbaled String Potentiometer

Euro NCAP European New Car Assessment Programme

FE Finite Element

L1 1st lumbar vertebra

L2 2nd lumbar vertebra

L3 3rd lumbar vertebra

L5 5th lumbar vertebra

MAIS Maximum AIS

NCAP New Car Assessment Programme

NHTSA National Highway Traffic Safety Administration

PMHS Post Mortem Human Subjects

T11 11th thoracic vertebra

T12 12th thoracic vertebra

THOR Test device for Human Occupant Restraint

THUMS Total HUman Model for Safety

VRTC Vehicle Research and Test Center

Appendix B

Injury statements and comparison of PMHS studies

study	impacting device	restrained back	impact level	tests	impact velocity ($m\,s^{-1}$)	peak interaction force (kN)	peak abdomen compression (%)	injury description
Cavanaugh et al. 1986	cylinder 25 mm diameter 32 kg[b]	no	mid-abdomen L3	5	5 to 7	2.4 to 4.5[a]	49 to 67	no organ injuries
				3	11 to 13	7.5 to 10[a]	36 to 72	
	64 kg[b]			2	9 and 10	9 and 12[a]	45 and 55	
Hardy et al. 2001	cylinder 25 mm diameter 48 kg	no	mid-abdomen L3	3	6 to 7	4.1 to 4.3	58 to 68	diaphragm, liver, spleen, intestine, hearth
				3	9 to 10	6.3 to 8.2	61 to 75	liver, spleen
			upper abdomen T11	2	6	4.5 and 4.9	56 and 84	diaphragm, liver, spleen
				1	9	7.4	60	
Shaw et al. 2004	lower steering wheel rim 25 mm diameter 45° inclined 64 kg	yes	upper abdomen T12	4	4	NA	29 to 51	no organ injuries

Table B.1 – Overview of the considered impactor PMHS studies

The numerical values are unscaled values, velocity has been rounded to $1\,m\,s^{-1}$, force to 0.1 kN and compression to 1 %

One unique test per subject has been considered

[a]Normalised values from the original paper

[b]Approximated values as in original paper

[c]Not Applicable

study	re-strained back	loading level	retracting device	sub-jects	peak abdomen penetration velocity ($m\,s^{-1}$)	peak interaction force (kN)	peak abdomen compression (%)	injury description
Hardy et al. 2001	no	mid-abdomen	pneumatic piston	3	3 to 4	3.1 to 4.3	30 to 40	no organ injuries
Trosseille et al. 2002	yes	mid-abdomen	configuration 1 (one pretensioner)	4	8 to 12	6.1 to 10.3	25 to 32	liver, spleen, mesentary, intestine, omentum
			configuration 2 (two pretensioners)	2	11 to 12	7.5 and 7.6	28 and 30	mesentary
Foster et al. 2006	yes	mid-abdomen	A condition (two pretensioners)	4	7 to 13	8.3 to 10.1	43 to 55	liver, kidneys, inferior vena cava
			B condition (one pretensioners)	3	6 to 8	5 to 5.8	27 to 38	no organ injuries
Lamielle et al. 2008	yes	mid-abdomen	MHA series (hydraulic piston)	4	3 to 5	3.5 to 4.1	28 to 41	liver, spleen, pancreas, mesentary, colon, jejunum-ileum, duodenum, omental bag
			PRT series (pretensionners)	4	5 to 6	4.6 to 5.1	30 to 32	liver, spleen, kidneys, mesentary, colon, jejunum-ileum, duodenum

Table B.2 – Overview of the considered seatbelt PMHS studies

The numerical values are unscaled values, velocity has been rounded to $1\,m\,s^{-1}$, force to 0.1 kN and compression to 1 %

One unique test per subject has been considered

condition	study	perfusion fluid	region perfused	pressurisation	lungs inflated
impactor	Cavanaugh et al. 1986	methyl blue dye or heparinized sheep's blood	abdominal aorta	13.3 kPa*	no information
	Hardy et al. 2001	heated, normal saline mixed with methyleneblue stain	arterial system	13.8 kPa	no information
	Shaw et al. 2004	no information	cardiovascular	no information	yes
seatbelt	Hardy et al. 2001	heated, normal saline mixed with methyleneblue stain	arterial system	13.8 kPa	no information
	Trosseille et al. 2002	4 / 5 of alcohol and 1 / 5 of India ink	carotid	15 kPa	2.5 l of air
	Foster et al. 2006	normal saline containing methylene blue dye heated to at least 30 °C	right and left femoral arteries, left common carotid artery, left jugular vein	21 kPa	full breaths (tracheostomy)
	Lamielle et al. 2008	barium sulfate	arteries and organs	no	2.5 l of air (syringe)

Table B.3 – Summary of the perfusion conditions of the considered PMHS studies

*The authors mentioned 100 mmHg

AIS[a]	organ			
2	Bladder (urinary) NFS[b]			
2		contusion (hematoma)		
2		laceration NFS		
3			no perforation (partial thickness)	
4			perforation (full thickness but not complete transection)	
2	Colon (large bowel) NFS			
2		contusion (hematoma)		
2		laceration NFS		
3			no perforation (partial thickness)	
4			perforation (full thickness but not complete transection)	
			massive (avulsion; complex; rupture; tissue loss; gross fecal contamination)	
2	Duodenum NFS			
2		contusion (hematoma)		
3			with obstruction	
3		laceration NFS		
3			no perforation (partial thickness or serosal tear)	
4			perforation (full thickness but not complete transection)	
5				involving pancreatic head, duct, ampulla
5			massive (avulsion; complex; rupture; tissue loss; gross fecal contamination)	
2	Gallbladder NFS			
2		contusion (hematoma)		

Table B.4: AIS coding scale for the main organs of the abdomen according to AAAM 1990

AIS[a]	organ			
2		laceration, (perforation) NFS		
2			minor (superficial)	
3			massive (avulsion; complex; rupture; tissue loss)	
4				with common or hepatic bile duct transection
2	Jejunum-Ileum (small bowel) NFS			
2		contusion (hematoma)		
2		laceration NFS		
2			no perforation (partial thickness)	
3			perforation (full thickness but not complete transection)	
4			massive (avulsion; complex; rupture; tissue loss)	
2	Kidney NFS			
2		contusion (hematoma) NFS		
2			minor (superficial; subcapsular, nonexpanding confined to renal retroperitoneum)	
3			major (large; subcapsular, > 50 % surface area or expanding)	
2		laceration NFS		
2			minor (superficial; < 1 cm, no urinary extravasation)	
3			moderate (> 1 cm but no rupture or urinary extravasation)	
4			major (extending through renal cortex, medulla and collecting system main renal vessel involvement)	
5			hilum avulsion; total destruction of organ and its vascular system	
2	Liver NFS			
2		contusion (hematoma) NFS		
2			minor (supeficial; subcapsular, ≤ 50 % surfaca area, nonexpanding; intraparenchyrnal < 2 cm in diameter)	
3			major (subcapsular, > 50 % surface area or expanding; intraparenchyrnal > 2 cm or expanding; blood loss > 20 % by volume)	
2		laceration NFS		
2			minor (superficial, < 3 cm deep, simple capsular injuries; blood loss ≤ 20 % by volume)	
3			moderate (> 3 cm deep, with major duct involvement; blood loss > 20 % by volume)	
4			major (disruption of < 50 % of hepatic parenchyma; multiple lacerations > 3 cm deep; burst injury)	
5			massive, complex (disruption of > 50 % central hepatic vascular system and involving retrohepatic vena cava / hepatic vein / hepatic artery / portal vein / major duct)	
6			hepatic avulsion (total separation of all vascular attachments)	

Table B.4: AIS coding scale for the main organs of the abdomen according to AAAM 1990

AIS[a]	organ			
2	Mesentery NFS			
2		contusion (hematoma)		
2		laceration NFS		
2			minor (superficial)	
3			major (blood loss > 20 % by volume)	
4			massive (avulsion; complex; rupture; stellate; tissue loss)	
2	Omentum NFS			
2		contusion (hematoma)		
2		laceration NFS		
2			minor (superficial)2 Bladder (urinary) NFS	
2		contusion (hematoma)		
2		laceration NFS		
3			no perforation (partial thickness)	
4			perforation (full thickness but not complete transection)	
2	Pancreas NFS			
2		contusion (hematoma)		
2			minor (superficial; no evidence of duct involvement)	
3			major (large; extensive; duct involvement)	
2		laceration NFS		
2			minor (superficial; no evidence of duct invofvement)	
3			moderate (with major vessel or major duct involvement)	
4				if involving head of pancreas
4			major (multiple lacerations)	
4				if involving head of pancreas
5			massive (avulsion; complex; rupture; stellate; tissue loss)	
2	Spleen NFS			
2		contusion (hematoma) NFS		
2			minor (superficial; ($\leq$ 50 % surface area; intraparenchymal, nonexpanding,< 2 cm in diameter)	
3			major (subcapsular > 50 % surface area or expanding; intraparenchymal > 2 cm in diameter or expanding)	
2		laceration (rupture) NFS		
2			minor (superficial; simple capsular tear $\leq$ 3 cm deep;no major vessel involvement)	
3			moderate (no hilar or segmental parenchymal disruption or destruction;> 3 cm deep)	
4			major (involving segmental parenchymal disruption or destruction with no hilar injury)	
4			massive (with hilar disruption; tissue loss; avulsion; stellate)	
2	Stomach NFS			

Table B.4: AIS coding scale for the main organs of the abdomen according to AAAM 1990

AIS[a]	organ			
2		contusion (hematoma)		
2		laceration NFS		
2			no perforation (partial thickness)	
3			perforation (full thickness)	
4			massive (avulsion; complex; rupture; tissue loss)	
3			major (blood loss > 20 % by volume)	

Table B.4 – AIS coding scale for the main organs of the abdomen according to AAAM 1990

1: minor

2: moderate

3: serious

4: severe

5: critical

6: maximum

[a]Abbreviated Injury Scale

[b]Not Further Specified

test number	gender	age (years)	stature (m)	abdominal depth (mm)	mass (kg)	impactor mass (kg)	impact velocity ($m\,s^{-1}$)	liver AIS	ribs AIS
14	M	56	1.82	283	68	31.24	6.84	4*	0
19	F	43	1.59	231	53	31.24	5	0	0
24	M	57	1.87	257	45	31.24	4.87	0	0
28	F	57	1.63	275	75	31.52	6.66	0	0
33	F	51	1.63	261	68	31.52	7.24	0	0
37	M	50	1.69	332	88	31.3	10.59	0	0
57	M	64	1.84	322	90	31.52	13.01	0	2
61	M	60	1.8	277	79	31.52	11.62	0	2
43	M	66	1.7	245	70	63.56	9.07	0	3
45	M	58	1.76	290	92	63.56	9.79	0	0

Table B.5 – Injury statement from Cavanaugh et al. 1986

*The subject was found during autopsy to have metastatic carcinoma of the liver causing it to be soft and friable

test	impact velocity ($m\,s^{-1}$)	gender	age (years)	stature (m)	mass (kg)	rib fractures	diaphragm injury	liver injury	spleen injury	intestine injury	heart injury	other injury
GI3	6,3	M	87	1.73	73	Bilateral 7, 8, 9	Left lateral tear, 9 cm	Vertical tear of right lobe, 7.5 cm anteriorly, 9 cm posteriorly	/	Tear of cecum, 10 cm	/	/
GI4	6,6	F	93	1.65	58	Bilateral 6, 7, 8, 9, 10	/	— Right capsule tear, 11 cm anteriorly — Tear of left lobe, 3.5 cm posteriorly	/	/	/	/
GI6	6,1	M	85	1.65	91	Bilateral 8, 9 Individual left 6, 7	Left lateral tear, 2.5 cm	Vertical tear of inferior edge, 25 cm	Capsule tear, 12 cm	/	— Vertical tear of anterior right ventricle, 2 cm — Transverse tear of posterior left ventricle, 1.5 cm	Tear of the left R8 / R9 intercostal space, 12 cm
GI7	9,1	M	74	1.81	77	Bilateral 8, 9, 10 Individual left 7	/	/	/	/	/	/
GI8	9	M	71	1.82	64	Bilateral 6, 7, 8, 9, 10 Individual left 5, right 3	/	— Tear of inferior edge, 3 cm — Multiple lacerations of left lobe posteriorly (6 cm by 5.5 cm) — Multiple lacerations of right lobe inferiorly (7.5 cm by 3.5 cm)	/	/	/	/
GI9	9,6	F	85	1.55	51	Bilateral 2, 3, 4, 5, 6, 7, 8, 9, 10	/	— Vertical tear of right lobe of liver, 5 cm — Transverse tear of right lobe of liver, 3.5 cm — Transverse tear of right lobe of liver, 3.2 cm — Multiple irregular tears of right lobe of liver posteriorly (3.5 cm by 2.5 cm)	Transverse tear of anterior edge, 2.2 cm	/	/	/

Table B.6 – Injury statement from Hardy et al. 2001 mid-abdomen impactor tests

test	impact velocity ($m\,s^{-1}$)	gender	age (years)	stature (m)	mass (kg)	rib fractures	diaphragm injury	liver injury	spleen injury	other injury
GI5	6	F	65	1.64	61	Bilateral 2, 6, 7, 8, 9, 10 Individual left 5	/	— Oblique central tear, 5.5 cm — Oblique tear of left lobe, 9 cm	/	/
GI11	6,2	M	74	1.68	75	Bilateral 4, 5, 6, 7, 8, 9 Individual left 3, 11, right 7 Right costal cartilage 7	— Left posterior tear, 4 cm — Left posterior tear, 3.5 cm — Separation from right lobe of liver, 7 cm	Falciform ligament tear	Transfer tear, 7 cm, 1.2 cm deep	Sternum fracture between R2 / R3 above mount
GI10	8,9	M	64	1.80	65	Bilateral 3, 4, 5, 6, 7, 8, 9 Individual left 5, 6, 8, 9, 10 Bilateral costal cartilage 7, 8	— Left posterior tear, 4 cm — Left posterior tear, 3.5 cm — Separation from right lobe of liver, 7 cm	— Horizontal tear, 4.5 cm connecting to vertical tear, 3.5 cm — Capsule tear Falciform ligament tear	Complete tear, 8 cm	Sternum fracture between R3 / R4 under mount

Table B.7 – Injury statement from Hardy et al. 2001 upper abdomen impactor tests

test	gen-der	age (years)	stature (m)	mass (kg)	chest depth (mm)	lateral skin thickness over rib border (mm)	number of rib fractures	number of sternal fractures	MAIS[a]
1	M	63	1.73	69	285	3	3	0	2
2	M	66	1.67	66	251	5	2	0	2
3	M	40	1.58	43	247	2.5	1[b]	0	NA
4	M	61	1.82	66	284	3.5	15	1	5

Table B.8 – Injury statement from Shaw et al. 2004

[a]Maximum AIS

[b]Artefact injury due to stress concentration at sensor location

test	gender	age (years)	stature (m)	mass (kg)	MAIS*	rib fractures*
CB1	F	77	1.68	53	4	Bilateral 7, 8, 9, 10 Individual right 2, 11, left 4, 5, 9, 10
CB3	M	78	1.70	52	3	Bilateral 9, 10, 11 Individual right 8
CB5	M	88	1.56	72	0	/

Table B.9 – Injury statement from Hardy et al. 2001 seatbelt tests

*The subjects face another load condition before injury statement

test	mass (kg)	stature (m)	age (years)	gender	hip breadth (mm)	abdomen depth (mm)	test configuration	MAIS	liver injuries	spleen injuries	mesentery injuries	intestine injury	omentum injuries	right abdominal muscle injury
PRT 034	78	1.75	76	M	360	230	1	2	/	/	/	/	/	incomplete tear of the musculus rectus abdominis on the right
PRT 035	70	1.68	81	M	335	272	1	1	/	/	small very discrete ecchymotic lesion of mesentery	small very discrete ecchymotic lesion of the small intestine	/	/
PRT 036	51	1.65	85	M	335	235	1	5	associated lesions of the lower face of the liver	transverse rupture of spleen	/	/	two tears of the posterior layer of the back cavity of the greater omentum	/
PRT 037*	68	1.62	66	F	360	239	1	NA	NA	NA	NA	NA	NA	NA
PRT 038	45	1.49	64	F	305	206	2	0	/	/	/	/	/	/
PRT 039	50	1.5	86	F	305	207	2	2	/	/	small tear of the left face of the mesentery without significant vascular lesion	/	/	/

Table B.10 – Injury statement from Trosseille et al. 2002

*The subject had pre-existing lesions

test	gender	age (years)	stature (m)	mass (kg)	abdomen depth (mm)	MAIS	liver injury	spleen injury	right kidney	left kidney	inferior vena cava	other injury
A-1	M	24	1.80	96	302	2	— Laceration diaphragmatic surface inferior edge right and left lobes, (crosses midline) forming a "Y" pattern: 9 cm, 7 cm, 3.5 cm — Tear at right edge, 5 cm	Capsular and superficial subcapsular sigmoid tear at diaphragmatic surface inferior left edge, 13 cm long*	/	/	/	Post-mortem contusion at umbilicus
A-2	M	58	1.88	111	356	0	/	/	/	/	/	/
A-3	M	80	1.67	58	252	3	— Right diaphragmatic surface, five parallel transverse lacerations – 5.5 cm (5 mm deep) – 9 cm (5 mm deep) – 5.5 cm (2 mm deep) – 8 cm (5 mm deep) – 11 cm (4 mm deep) — Right lobe visceral surface, four lacerations – Vertical tear 8 cm (7 mm deep) – Diagonal tear 8 cm (10 mm) – Diagonal tear 8 cm (10 mm deep) – Transverse tear 2.5 cm (8 mm deep)	/	Cyst 2.5 cm, inferior pole, not test related	Cyst 3 cm, inferior pole, not test related	— Instrumentation related laceration at L3 – Vessel occluded by strap – No fluid in abdominal cavity	/
A-4	M	83	1.73	82	259	3	— Right diaphragmatic surface – Superficial tear diaphragmatic surface right lobe caudal-lateral to medial-cranial, 4 cm (3 mm deep) – Intermittent superficial tear, 3.5 cm (2 mm deep) – Superficial tear caudal-lateral to medial-cranial, 5 cm — Right visceral surface – Three parallel superficial lacerations; 9 cm, 8.5 cm, 11 cm – Superficial lacerations near tip, 5 cm, 2 cm – Superficial tear inferior edge from midline toward left lobe, 3 cm — Left visceral surface – Two parallel superficial tears visceral side left lobe proximal to tip, 7 cm and 4.5 cm, (2 mm deep) – Transverse superficial tear, 7.5 cm – Two parallel tears edge of lobe, 1.3 cm, 2.5 cm — Complete transection of tip of right lobe, 5.5 cm superior-inferior, 6 cm medial-lateral (3.3 cm deep) — Disruption of right lobe, lateral to falciform ligament, 7 cm medial-lateral, 5 cm superior-inferior	Extensive scarring, not test related	/	/	/	/

Table B.11 – Injury statement from Foster et al. 2006 A condition

*Injury due to leukemia, which causes spleen to enlarge

test	gender	age (years)	stature (m)	mass (kg)	abdomen depth (mm)	MAIS
B-1	M	85	1.69	81	360	0
B-2	M	45	1.74	75	258	0
B-3	M	59	1.69	62	261	0

Table B.12 – Injury statement from Foster et al. 2006 B condition

test	gender	stature (m)	mass (kg)	age (years)	abdomen width (mm)	abdominal depth[a] (mm)	abdominal depth[b] (mm)	liver injuries	spleen injuries	pancreas injuries	mesentery injuries	colon inuries	jejunum-ileum injuries	duodenum inuries	omental bag injuries	MAIS
MHA 111	M	1.75	77	74	340	287	/	/	sub capsular contusion AIS 2	/	small contusion AIS 2	contusion all along the sigmoid AIS 2	/	/	/	2
MHA 115	M	1.8	78	82	317	268	200	simple capsular tear AIS 2	/	extensive contusion (30 cm in length) AIS 3	/	/	contusions AIS 2	contusion located at the 2nd duodenum AIS 2	massive contusion AIS 3	3
MHA 151	M	1.66	69	88	300	249	180	/	/	/	/	/	contusion AIS 2	/	/	2
MHA 155	M	1.69	60	88	290	234	160	/	/	/	small abrasion AIS 0	/	2 contusions AIS 2	/	/	2

Table B.13 – Injury statement from Lamielle et al. 2008 MHA condition

[a] in position

[b] laid down

test	gender	stature (m)	mass (kg)	age (years)	abdomen width (mm)	abdominal depth* (mm)	liver injuries	spleen injuries	kidneys injuries	pancreas injuries	mesentery injuries	colon inuries	jejunum-ileum injuries	duodenum inuries	MAIS
PRT 052	M	1.62	54	72	284	222	/	/	/	/	voluminous contusions AIS 2	/	several laceration with no perforation- contusions AIS 2	/	2
PRT 053	M	1.53	56	85	275	254	/	/	/	moderate laceration at the level of the second duodenum AIS 3	several contusions close to the jejunum-ileum AIS 2	several contusions AIS 2	several contusions - wall totally infiltrated along 20 cm AIS 2	/	3
PRT 065	M	1.72	72	88	284	243	simple capsular tears AIS 2	deep lacerations AIS 4	retroperitoneal contusion - laceration of renal vessel AIS 4	/	several lacerations of inferior and superior faces with no perforation AIS 1	contusion and laceration of the transverse colon AIS 3	laceration and several contusions AIS 2	/	4
PRT 066	M	1.72	77	82	322	258	/	large laceration of the diaphragmic side and deep laceration of the gastric side AIS 2	/	/	/	laceration at the level of the descending colon AIS 3	several contusions AIS 2	considerable laceratations AIS 3	3

Table B.14 – Injury statement from Lamielle et al. 2008 PRT condition

*in position

Appendix C

LS-DYNA hyperelastic material models

The content of this Appendix is taken from LS-DYNA Theory Manual (Hallquist 2006) and Keyword User's Manual (LSTC 2015).

MAT_057: LOW_DENSITY_FOAM

MAT_057 is designed to model highly compressible materials such as foams with a hysteresis on unloading. It is non linear in compression and linear in tension without transverse coupling.

An input load curve is given to define the nominal stress as a function of strain to be use for the compressive response. A Young's modulus is used for tension. In compression, the Cauchy principal stress is computed as in Equation C.1 with σ_{ij}^{f} the hyperelastic term (stress value from load curve) and σ_{ij}^{r} the viscoelastic term defined by Equation C.2. The viscoelastic relaxation function is defined as a one-term Prony series as seen in Equation C.3. E_{d} and β_1 are input parameters of the material model. Additional unloading and damping parameters are also available.

$$\sigma_{ij} = \sigma_{ij}^{f} + \sigma_{ij}^{r} \tag{C.1}$$

$$\sigma_{ij}^{r} = \int_0^t g_{ijkl}\left(t-\tau\right) \cdot \frac{\partial \varepsilon_{kl}}{\partial \tau} \cdot \mathrm{d}\tau \tag{C.2}$$

$$g\left(t\right) = E_{\mathrm{d}} \cdot \mathrm{e}^{-\beta_1 \cdot t} \tag{C.3}$$

MAT_083: FU_CHANG_FOAM

MAT_083 is based on unified constitutive foam equations from Chang et al. 1998. A strain decomposition according to Equation C.4 is postulated where $E^{L}\left(t\right)$ is the linear part and $E^{N}\left(t\right)$ the non linear part. The constitutive equation is given by Equation C.5 where $[X, Y]$ is the Lie derivative of Y along X and S is the state variable. Expanding $E^{N}\left(t-\tau\right)$ in Taylor series leads to express the strain rate $\dot{E}^{N}\left(t-\tau\right)$ as in Equation C.6. The state variable is expressed in Equation C.7. Overall, D_0, a, b, c_0 to c_5 and n_0 to n_3 are material constants. Additional unloading and damping parameters are also available. If a series of nominal stress versus strain data for different strain rates is input, the material model computes the the material constants based on the curves. If no curves are defined for tension, a Young's modulus is used.

$$E(t) = E^L(t) + E^N(t) \tag{C.4}$$

$$\sigma(t) = \int_0^\infty \left[E^N(t-\tau), S(t)\right] \cdot \mathrm{d}\tau \tag{C.5}$$

$$\dot{E}^N(t-\tau) = \frac{\sigma}{\|\sigma\|} \cdot D_0 \cdot \mathrm{e}^{-c_0 \cdot \left(\frac{\mathrm{tr}(\sigma \cdot S)}{\|\sigma\|^2}\right)^{2n_0}} \tag{C.6}$$

$$\dot{S}_{ij} = \left(c_1 \cdot (a \cdot R - c_2 \cdot b) \cdot P + c_3 \cdot W^{n_1} \cdot \|\dot{E}^N\|^{n_2} \cdot I_{ij}\right) \cdot R$$
$$\text{With: } \begin{cases} R = 1 + c_4 \cdot \left(\dfrac{\|\dot{E}^N\|}{c_5} - 1\right)^{n_3} \\ P = \mathrm{tr}\left(\sigma \cdot \dot{E}^N\right) \\ W = \displaystyle\int \mathrm{tr}(\sigma \cdot \mathrm{d}E) \end{cases} \tag{C.7}$$

MAT_181: SIMPLIFIED_RUBBER

MAT_181 is a simplified quasi hyperelastic material model. "quasi" hyperelastic means that no strain energy function is used to determine stress values but the tangent stiffness matrix is derived instead. An uniaxial stress versus strain input curve or a family of curves at different strain rates can be input. Different curves for tension and compression are allowed. The Cauchy principal stresses are computed with Equation C.8 with $f(\lambda_i)$ the stress values from the input load curve and λ_i the principal elongations, K the bulk modulus and J the relative volume change. The material model is nearly incompressible with a Poisson's ratio of 0.495. In practice, the input curves are fitted with polynomial functions so that $f(\lambda) = \sum_{j=1}^{n} \mu_j \cdot \left(\lambda \cdot J^{-1/3}\right)^{\alpha_j}$ (DuBois 2003).

$$\sigma_{ii} = \frac{1}{J} \cdot \left(f(\lambda_i) - \frac{1}{3} \cdot \sum_{k=1}^{3} f(\lambda_k)\right) + K \cdot \frac{J-1}{J} \tag{C.8}$$

Appendix D

Additional results for lumped element model

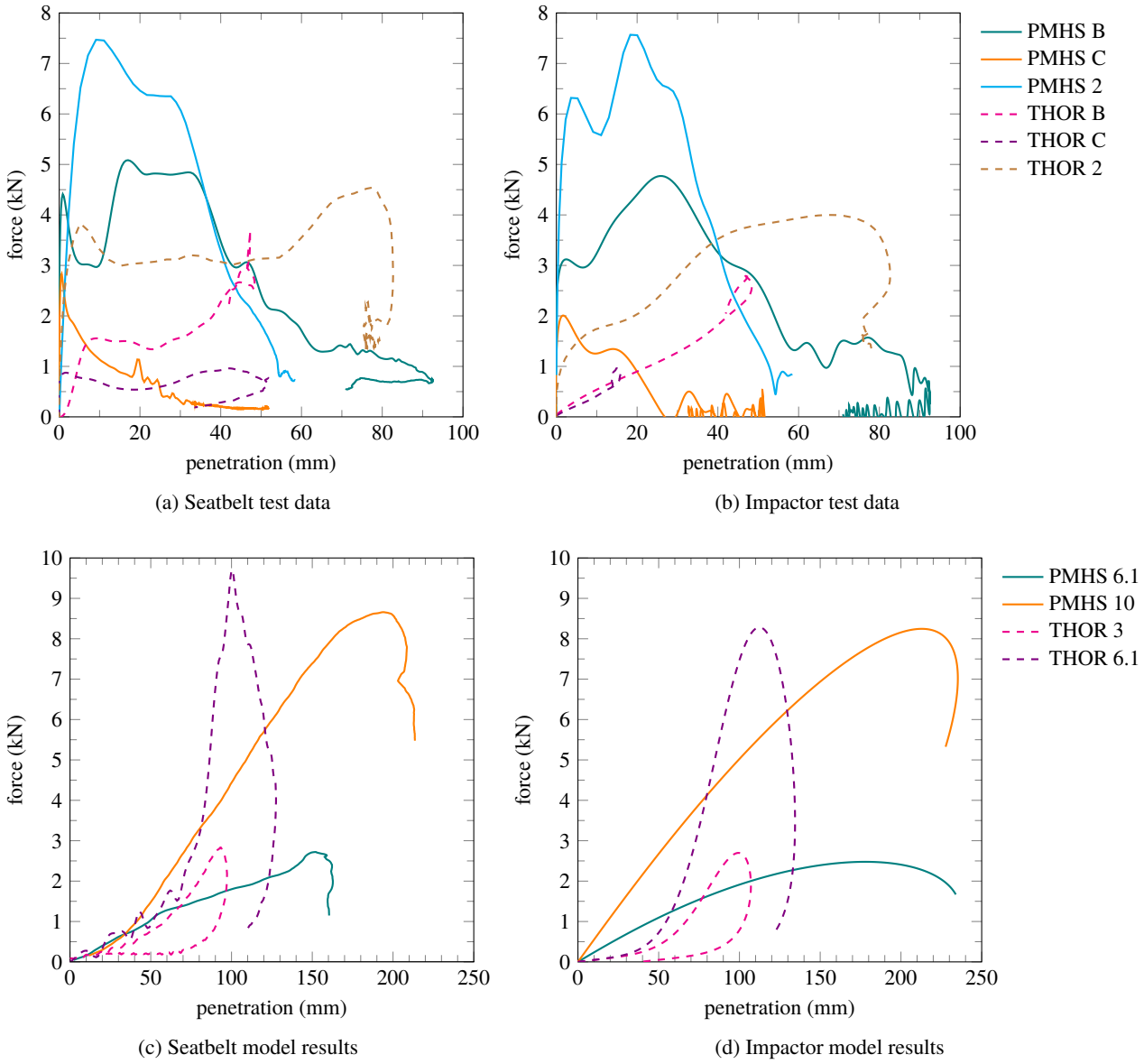

(a) Seatbelt test data

(b) Impactor test data

(c) Seatbelt model results

(d) Impactor model results

Figure D.1 – Force / penetration responses

B: B condition from Foster et al. 2006

C: C condition from Foster et al. 2006

2: configuration 2 from Trosseille et al. 2002

PMHS 6.1: 32 kg 6.1 m s^{-1} condition from Cavanaugh et al. 1986

PMHS 10: 32 kg 10 m s^{-1} condition from Cavanaugh et al. 1986

THOR 3: 32 kg 3 m s^{-1} condition from Compigne et al. 2015

THOR 6.1: 32 kg 6.1 m s^{-1} condition from Compigne et al. 2015

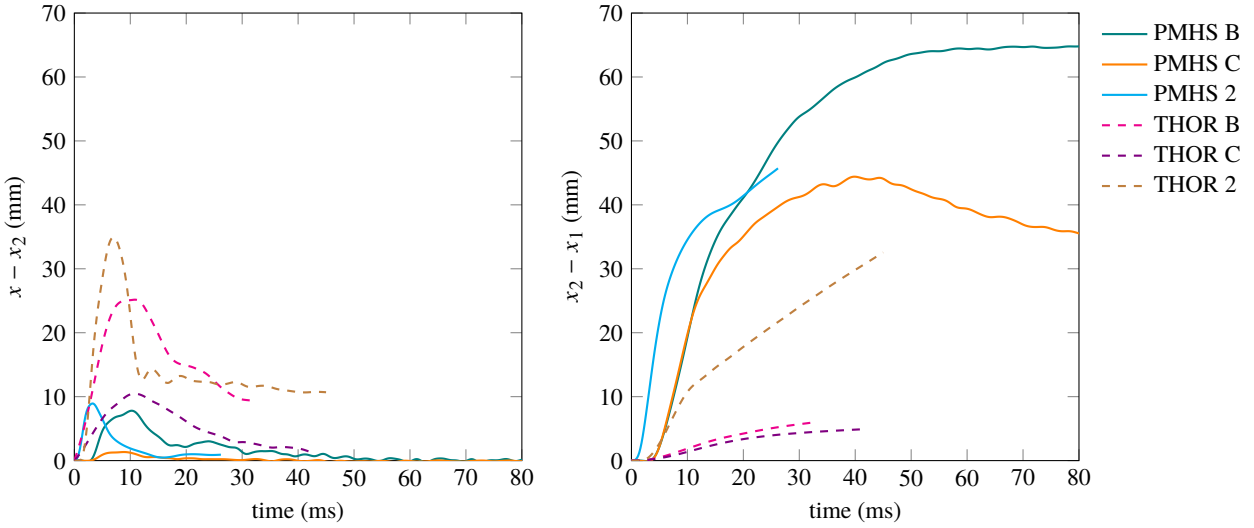

(a) Deformation of K spring

(b) Deformation of C damper

Figure D.2 – Displacement results for seatbelt loading conditions
B: Foster et al. 2006 B condition
C: Foster et al. 2006 C condition
2: Trosseille et al. 2002 configuration 2

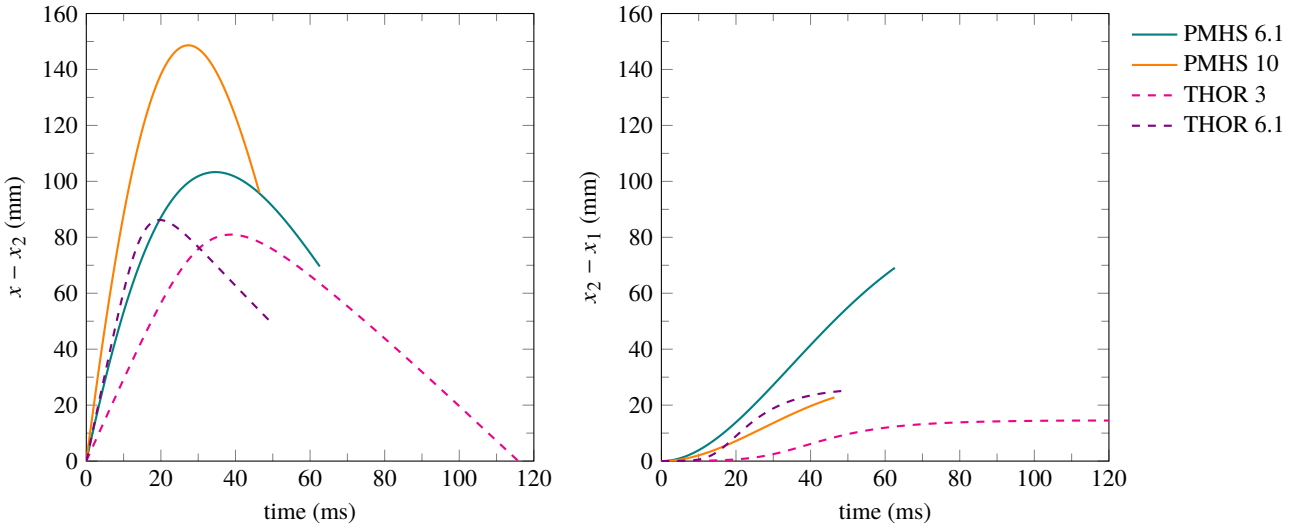

(a) Deformation of K spring

(b) Deformation of C damper

Figure D.3 – Displacement results for impactor loading conditions
PMHS 6.1: Cavanaugh et al. 1986 32 kg 6.1 m s^{-1} condition
PMHS 10: Cavanaugh et al. 1986 32 kg 10 m s^{-1} condition
THOR 3: Compigne et al. 2015 32 kg 3 m s^{-1} condition
THOR 6.1: Compigne et al. 2015 32 kg 6.1 m s^{-1} condition